

1                   Characterisation of Ovarian Cancer  
2           Development, Progression and Treatment  
3           Resistance Through Mass Spectrometry  
4                   Analysis



9                   THE UNIVERSITY  
10                  of ADELAIDE

11  
12           A thesis submitted in fulfillment of the requirements for the  
13                   degree of Doctor of Philosophy

14  
15                   By

16  
17                   Mitchell Acland

18                   B.Sc. (Biomedical Science), B.Sc. (Biomedical Science) (Honours)

19                   School of Biological Science

20                   The University of Adelaide, South Australia

21                   January 2023

1  
2  
3  
4  
5  
6  
7  
8  
9  
10  
11  
12  
13  
14  
15  
16  
17  
18  
19  
20  
21  
22  
23  
24  
25  
26  
27  
28

This page is intentionally left blank

# Table of Contents

---

1		
2		
3	<b>List of Table and Figures</b> .....	VII
4	<b>Declaration</b> .....	VIII
5	<b>Acknowledgements</b> .....	X
6	<b>List of Publications</b> .....	XII
7	<b>Abbreviations</b> .....	XIII
8	<b>Abstract</b> .....	XIX
9	CHAPTER 1: INTRODUCTION .....	1
10	<b>1. Ovarian Cancer Introduction</b> .....	3
11	1.1. Ovarian Cancer Subtypes and Their Precursors.....	3
12	1.1.1. Type 1 Ovarian Cancer .....	3
13	1.1.1.1. Endometrioid Ovarian Cancer (EnOC) .....	4
14	1.1.1.2. Clear Cell Ovarian Cancer (CCOC).....	4
15	1.1.1.3. Mucinous Ovarian Cancer (MOC).....	4
16	1.1.1.4. Low Grade Serous Ovarian Cancer (LGSOC) .....	5
17	1.1.2. Type 2 Ovarian Cancer .....	6
18	1.1.2.1. High Grade Serous Ovarian Cancer (HGSOC) .....	6
19	1.1.2.2. Origins of High Grade Serous Ovarian Cancer.....	7
20	1.2. Ovarian Cancer Risk Factors, Diagnoses, Staging and Screening.....	9
21	1.2.1. Risk Factors .....	9
22	1.2.2. Risk Reducing Interventions.....	12
23	1.2.3. Ovarian Cancer Diagnosis .....	12
24	1.2.4. Ovarian Cancer Staging .....	13
25	1.2.5. Ovarian Cancer Screening .....	15
26	1.3. Treatment of Ovarian Cancer.....	17
27	1.3.1. Action of platinum-based chemotherapy.....	18
28	1.3.2. Molecular Targeted Therapy for Ovarian Cancer.....	18
29	1.3.2.1 CDK4/6 Inhibitors.....	19
30	1.4. Molecular Mechanisms of Chemoresistance to Platinum Based Chemotherapy..	20
31	1.4.1. Altered drug influx and efflux .....	21
32	1.4.2. Intracellular Detoxification of Platinum Compounds.....	22

1	1.4.3.	DNA Repair .....	22
2	1.4.4.	Apoptosis signalling.....	22
3	1.4.5.	Metabolism in Chemoresistance.....	23
4	1.5.	Unique Features of HGSOE Metastatic Progression.....	24
5	1.5.1.	Malignant Ascites .....	24
6	1.5.2.	Multicellular Tumour Spheroids in Ovarian Cancer Progression.....	24
7	1.5.3.	In vitro Multicellular Tumour Spheroids as a Biological Model of Solid Tumours	
8		26	
9	1.6.	Mass Spectrometry Overview .....	27
10	1.6.1.	Mass Spectrometry Proteomics.....	27
11	1.6.2.	Mass Spectrometry Metabolomics.....	27
12	1.6.3.	Utilising Mass Spectrometry for Pan Omics Analysis.....	28
13	1.7.	Our Approach.....	28
14	1.8.	Aims of the Thesis.....	28
15	CHAPTER 2: MATERIALS AND METHODS .....		30
16	2.1.	Summary of Mass Spectrometry (MS) Proteomics Methodology .....	32
17	2.1.1.	Sample Acquisition.....	32
18	2.1.2.	Sample Preparation .....	33
19	2.1.3.	Data Acquisition .....	33
20	2.1.4.	Data Analysis.....	34
21	2.1.5.	Functional Analysis.....	34
22	2.2.	Matrix Assisted Laser Desorption Ionisation (MALDI) Mass Spectrometry Imaging	
23		(MSI).....	34
24	A Protocol for the Acquisition of Comprehensive Proteomics Data from a Single Formalin Fixed		
25	Paraffin Embedded Section.....		35
26	2.3.	Summary .....	37
27	2.4.	Statement of Authorship.....	39
28	2.5.	Supplementary Data.....	41
29	CHAPTER 3: Proteomics Analysis of Serous Lesions of the Endometrium and Fallopian Tube		
30	Reveals Their Metastatic Potential .....		44
31	3.1.	Summary .....	45

1	3.2.	Statement of Authorship.....	47
2	3.3.	Supplementary Data.....	49
3	CHAPTER 4: Chemoresistant Cancer Cell Lines are Characterized by Migratory, Amino Acid		
4	Metabolism Protein Catabolism and IFN1 Signalling Perturbations..... 57		
5	4.1.	Summary .....	58
6	4.2.	Statement of Authorship.....	60
7	4.3.	Supplementary Files.....	63
8	CHAPTER 5: Mass Spectrometry Analyses of Multicellular Tumour Spheroids..... 68		
9	5.1.	Summary .....	69
10	5.2.	Statement of Authorship.....	71
11	CHAPTER 6: Monitoring Penetration and Accumulation of Novel CDK4/6 Inhibitor in an Ovarian		
12	Cancer Multicellular Tumour Spheroid Model with MALDI Mass Spectrometry Imaging..... 74		
13	6.1.	Introduction .....	75
14	6.2.	Methods and Materials .....	76
15	6.3.1.	PolyHEMA Coating.....	76
16	6.3.2.	Culturing OV90 Spheroids: .....	76
17	6.3.3.	CDDD2-94 Treatment.....	77
18	6.3.4.	Gelatine Embedding and Sectioning.....	77
19	6.3.5.	MALDI-MSI Data Acquisition.....	77
20	6.3.6.	MALDI-MSI Data Analysis.....	77
21	6.3.	Results .....	78
22	6.4.	Discussion .....	79
23	6.1.	Supplementary File.....	81
24	CHAPTER 7: DISCUSSION..... 83		
25	<b>7. Discussion</b> ..... 84		
26	7.1.	Technical Limitations.....	84
27	7.1.1	Molecules with Diverse Chemical Properties.....	84
28	7.1.2	Data Acquisition .....	85
29	7.1.3	Identification of Molecules of Interest.....	85
30	7.1.4	Deriving Biological Meaningful Data from Mass Spectrometry Data .....	86

1	7.2. Implications of the Paradigm Shift in the Origin of Ovarian Cancer.....	86
2	7.3. Overcoming Chemoresistance in Ovarian Cancer .....	88
3	7.4. Mass Spectrometry Analyses of <i>in vitro</i> Models of Ovarian Cancer.....	89
4	7.5. Mass Spectrometry Analyses of Ascites Derived MCTS .....	91
5	7.6. Importance of this work and future directions .....	91
6	References.....	95

7  
8  
9  
10  
11  
12  
13  
14  
15  
16  
17  
18  
19  
20  
21  
22

# List of Table and Figures

---

1  
2  
3  
4  
5  
6  
7  
8  
9  
10  
11  
12  
13  
14  
15  
16  
17  
18  
19  
20  
21  
22  
23  
24  
25  
26  
27  
28  
29  
30

**Figure 1:** Risk factors which predict ovarian cancer diagnosis and poor prognosis.

**Figure 2:** Malignant progression of high grade serous ovarian carcinoma (HGSOC) and cellular populations within multicellular tumour spheroids (MCTS).

**Figure 3:** Flow diagram of the standard process for proteomic mass spectrometry analysis of biological samples.

**Figure 4:** Workflow for MALDI MSI analysis of MCTS.

**Figure 5:** MALDI MSI analysis of OV90 spheroids targeting the analyte at 443.24 Da which relates to the small molecule inhibitor of CDK4/6; CDDD2-94.

**Table 1:** Subtypes of epithelial ovarian cancer and their associated histological features, precursor lesions, molecular aberrations, prognosis, and primary chemo response.

**Table 2:** Federation of Gynaecology and Obstetrics (FIGO) staging for ovarian cancer.

# Declaration

I certify that this work contains no material which has been accepted for the award of any other degree or diploma in my name, in any university or other tertiary institution and, to the best of my knowledge and belief, contains no material previously published or written by another person, except where due reference has been made in the text. In addition, I certify that no part of this work will, in the future, be used in a submission in my name, for any other degree or diploma in any university or other tertiary institution without the prior approval of the University of Adelaide and where applicable, any partner institution responsible for the joint award of this degree.

The author acknowledges that copyright of published works contained within the thesis resides with the copyright holder(s) of those works.

I give permission for the digital version of my thesis to be made available on the web, via the University's digital research repository, the Library Search and also through web search engines, unless permission has been granted by the University to restrict access for a period of time.

I acknowledge the support I have received for my research through the provision of an Australian Government Research Training Program Scholarship.

Mitchell Acland



1  
2  
3  
4  
5  
6  
7  
8  
9  
10  
11  
12  
13  
14  
15  
16  
17  
18  
19  
20  
21  
22  
23  
24  
25  
26  
27

This page is intentionally left blank

# Acknowledgements

---

1  
2  
3 The completion of this thesis has been a long and, often difficult, process which  
4 would not have been possible with the contribution of many individuals. Many of  
5 them helped me in practical ways, taught me, or provided advice and guidance.  
6 Others supported me through their unfailing belief in me, their encouragement,  
7 their support, and their love.

8 Firstly, I want to acknowledge all of those in my lab who supported me over the  
9 years. I learnt so much from each and every person who I interacted with across  
10 two universities, several years and many upheavals. Many of you made important  
11 contributions to my publications and this thesis and I truly could not have done it  
12 without your help. Thank you for your patience and understanding when I was  
13 struggling, your encouragement to keep trying and your help in celebrating my  
14 achievements. The PhD experience felt lonely at times but the kind words and  
15 simple day to day conversations with my lab mates gave me a sense of belonging  
16 and drove me forwards.

17 Secondly, I would like to acknowledge my supervisors, particularly my principal  
18 supervisor, Manuela. You continued to believe that I could do this, even when I did  
19 not. You worked tirelessly over many years to provide me practical, strategic, and  
20 emotional support and were always willing to take the time to speak with me and  
21 share my experiences. Without your knowledge, empathy, and support even the  
22 first word of this thesis would not have been possible. I feel great privilege to have  
23 had you as my principal supervisor and am deeply grateful for all that you have  
24 done to support me.

25 I wish to acknowledge all my friends who have been there for me throughout this  
26 experience. You all showed an ongoing interest in my experience and provided me  
27 the space to share my feelings. One of you asked, almost daily, ‘how is the PhD  
28 going?’. It seems a small thing, and at times it was a question I found hard to  
29 answer, but the care that it showed means so much. You all shared the hard  
30 experiences with me and helped me to celebrate my achievements. Just as  
31 importantly, thank you for the fun nights and numerous conversations which did so  
32 much to help me forget about study for a time.

33 I wish to acknowledge my family. Thank you, Mum, Dad and Gemma, for always  
34 sharing my experiences, offering advice and supporting me throughout. I cannot

1 count the number of dinner table conversations, or long phone calls, where you  
2 listened to me talk about my work at length, where you shared your own  
3 experiences and showed that you were proud of me. More than that, thank you for  
4 all you have done in raising me over the last 30 years as the completion of this  
5 thesis is more than a culmination of what I have learnt over my candidature, it is a  
6 culmination of what I have learnt throughout my life.

7 Finally, I would like to acknowledge my partner, Emily. You were by my side for  
8 every step of this journey. Thank you for always being proud of me, for talking me  
9 down when it was all too much, for crying with me and celebrating each and every  
10 step. Most of all, thank you for loving me unconditionally. I never doubted that no  
11 matter what, even if I dropped out of the PhD program the next day, you would  
12 never stop supporting me. It is that knowledge, more than anything, which gave me  
13 the perseverance to complete this PhD and this thesis.

14 Thank you all

15

16

17

18

19

20

21

22

23

24

25

26

27

28

29

30

31

# List of Publications

---

This thesis is based on the following publications, which are referred to in the text.

- I. **Mitchell Acland**, Parul Mittal, Georgia Arentz, Fergus Whitehead, Peter Hoffmann, Manuela Klingler-Hoffmann and Martin K. Oehler. A Protocol for the Acquisition of Comprehensive Proteomics Data from Single Cases Using Formalin-Fixed Parafin Embedded Sections. *Methods and Protocols*, **2022 July**, 5(4), 57; doi: 10.3390/mps5040057
- II. **Mitchell Acland**, Georgia Arentz, Max Mussared, Fergus Whitehead, Peter Hoffmann, Manuela Klingler-Hoffmann and Martin K. Oehler. Proteomics of Pre-Invasive Serous Lesions of the Endometrium and Fallopian Tube Reveals Their Metastatic Potential. *Frontiers In Oncology*, **2020 December**, 15;10:523989. doi: 10.3389/fonc.2020.523989. PMID: 33384952; PMCID: PMC7771701.
- III. **Mitchell Acland**, Parul Mittal, Noor A. Lokman, Manuela Klingler-Hoffmann, Martin K. Oehler and Peter Hoffmann. Mass Spectrometry Analyses of Multicellular Tumour Spheroids. *Proteomics Clinical Applications*, **2018 May**;12(3):e1700124. doi: 10.1002/prca.201700124. Epub 2018 Feb 9. PMID: 29227035.
- IV. **Mitchell Acland**, Noor A. Lokman, Clifford Young, Dovile Anderson, Mark Condina, Chris Desire, Tannith M. Noye, Wanqi Wang, Carmella Ricciardelli, Darren J. Creek, Martin K. Oehler, Peter Hoffmann and Manuela Klingler-Hoffmann. Chemoresistance Cancer Cell Lines are Characterised by Migratory, Amino Acid Metabolism, Protein Catabolism and IFN1 Signalling Perturbations. *Cancers*, **2022 June**, 14(11):2763. doi:10.3390/cancers14112763

# Abbreviations

---

1  
2

2D-DIGE	Two-Dimensional Difference Gel Electrophoresis
2D-PAGE	Two-Dimensional Poly Acrylamide Gel Electrophoresis
Ab	Antibody
ADP	Adenosine Diphosphate
ADS	Ascites Derived Spheroids
Amhr2	Anti-Müllerian Hormone Receptor
AMP	Adenosine Monophosphate
ARG3	Anterior Gradient Homologue 3
ARID1A	AT-Rich Interactive Domain-Containing Protein 1A
ATCC	American Type Culture Collection
ATM	Ataxia Telangiectasia Mutated
ATP	Adenosine Triphosphate
ATP7A	ATPase Copper Transporting Alpha 7A
ATP7B	ATPase Copper Transporting Alpha 7B
ATR	RAD3-Related Protein
Bcl-2	B-Cell Lymphoma 2
Bcl-xL	B-Cell Lymphoma-Extra Large
BRAF	B-Raf Proto-Oncogene, serine/threonine kinase
BRCA1	Breast Cancer Susceptibility Gene 1
BRCA2	Breast Cancer Susceptibility Gene 2
CA	Chloroacetamide
CA125	Carbohydrate Antigen 125
CALHN	Central Adelaide Local Health Network
CAM	Chick Chorioallantoic Membrane
CAN	Acetonitrile
CAPS	Calcyphosin
CBP	Carboplatin
CBPR	Carboplatin Resistant
cCMP	Cytidine 3', 5'-Cyclic Monophosphate
cCMP	Cytidine 3', 5'-Cyclic Monophosphate
CCNE-1	Cyclin E1
CCOC	Clear Cell Ovarian Carcinoma
CD20	B-Lymphocyte Antigen CD20
CDK	Cyclin Dependent Kinase
CDP	Cytidine Diphosphate
CDP-Etn	CDP-Ethanolamine
CHEK1	Checkpoint Kinase 1
CIC	Cortical Inclusion Cyst
CID	Collision Induced Dissociation

CK7	Cytokeratin 7
CLCA1	Calcium Activated Chloride Channel Regulator 1
CM	Cell Matrigel Graft
CMP	Cytidine Monophosphate
CN	Copy Number
CPTAC	Clinical Proteomics Tumour Analysis Consortium
Crt1	Copper Uptake Protein 1
CSC	Cancer Stem Cell
CSPG2	Chondroitin Sulfate Proteoglycan Core Protein 2
CTNN $\beta$ 1	Catenin $\beta$ 1
CXCR4	C-X-C Chemokine Receptor 4
Da	Daltons
DAVID	Data Base for Annotation, Visualisation and Integrated Discovery
DDR	DNA Damage Response
DFS	Disease Free Survival
DHSO	Sorbitol Dehydrogenase
DMSO	Dimethyl Sulfoxide
DNA	Deoxy Ribonucleic Acid
DS	Double Stranded
DTT	Dithiothreitol
EC	Endometrial Cancer
ECT	Ectoderm
EEC	Endometrioid Endometrial Carcinoma
EGFR	Epidermal Growth Factor Receptor
EIC	Endometrial Intraepithelial Carcinoma
EmGD	Endometrial Glandular Dysplasia
END	Endoderm
ENoC	Endometrioid Ovarian Carcinoma
EOC	Epithelial Ovarian Cancer
EPCAM	Epithelial Cell Adhesion Molecule
ER	Estrogen Receptor
ERBB2	Erb-B2 Receptor Tyrosine Kinase
ERK	Extracellular Regulated Kinase
ERO1A	Endoplasmic Reticulum Oxidoreductin-1 Like Protein Alpha
ESI	Electrospray Ionisation
ESTP	Early Serous Tubal Proliferations
EZH	Enhancer of Zeste Homolog
FA	Formic Acid
FAS	Fas Cell Surface Death Receptor
FasL	Fas Ligand
FASP	Filter Assisted Sample Preparation
FBS	Fetal Bovine Serum

FDA	Food and Drug Administration
FDR	False Discovery Rate
FFPE	Formalin Fixed Paraffin Embedded
FIGO	Federation of Gynaecology and Obstetrics
FITC	Fluorescein isothiocyanate
FT-MS	Fourier Transformed Ion Cyclotron Resonance Mass Spectrometry
G-6-P	glucose-6-phosphate
GlcNAc-1-P	N-Acetyl-alpha-D-glucosamine 1-phosphate
GO-BP	Gene Ontology-Biological Processes
GSH	Glutathione
GTP	Guanosine-5'-Triphosphate
H&E	Hematoxylin and Eosin
H3D27	Histone H3 Lysine 27
HCCA	$\alpha$ -cyano-4-hydroxycinnamic acid
HE	Healthy Endometrium
HER2	Human Epithelial Growth Factor Receptor 2
HFT	Healthy Fallopian Tube
HGSOC	High Grade Serous Ovarian Carcinoma
HIF-1 $\alpha$	Hypoxia Inducible Factor 1 $\alpha$
HILIC	Hydrophilic Interaction Liquid Chromatography
HLA-E	Human Leukocyte Antigen E
HNSCC	Head and Neck Squamous Cell Carcinoma
HPLC	High Performance Liquid Chromatography
HR	Homologous Recombination
HRD	Homologous Recombination Deficiency
HSP	Heat Shock Protein
HUVEC	Human Umbilical Vein Endothelial Cells
IAA	Iodoacetamide
IC50	50% Inhibitory Concentration
IDAS	Intensity Dependent Acquisition Speed
IFN1	Type 1 Interferon
IGF-1	Insulin Growth Factor 1
ITH	Intra Tumoural Heterogeneity
ITO	Indium Tin Oxide
iTRAQ	Isobaric Tag for Relative and Absolute Quantification
JAK	Jun N-Terminal Kinase
KEGG	Kyoto Encyclopedia of Genes and Genomes
KM	Kaplan Meier
KRAS	Kirsten Rat Sarcoma Viral Oncogene Homolog
LA-ICP-MS	Laser Ablation Inductively Coupled Plasma Mass Spectrometry
LC	Liquid Chromatography

LCM	Laser Capture Microdissection
LC-MS/MS	Liquid Chromatography Tandem Mass Spectrometry'
LFT	Lactotransferin
LGSOC	Low Grade Serous Ovarian Carcinoma
LSD1	Lysine Specific Histone Demethylase
m/z	Mass to Charge Ratio
MALDI	Matrix Assisted Laser Desorption Ionisation
MAPK	Mitogen Activated Protein Kinase
MCTS	Multicellular Tumour Spheroid
MEK	MAP Kinase Kinase 1
MES	Mesoderm
MIB1	MIB E3 Ubiquitin Ligase
MIEAP	Mitochondrial Eating Protein
miRNA	Micro Ribonucleic Acid
MMR	Mismatch Repair
MOC	Mucinous Ovarian Carcinoma
MPSC	Micropapillary Serous Carcinoma
MRM	Multiple Reaction Monitoring
mRNA	Messenger Ribonucleic Acid
MS	Mass Spectrometry
MS2	Tandem Mass Spectrometry
MSI	Mass Spectrometry Imaging
MT	Metalothionine
MTT	Thiazol Blue Tetrazlium Bromide
mW	Molecular Weight
MYK	Ephrin Type-B Receptor
NCBI	National Centre for Biotechnology Information
NCCN	National Comprehensive Cancer Network
NCRIS	National Collaborative Research Infrastructure Strategy
NER	Nucleotide Excision Repair
NK	Natural Killer Cell
NNMT	N-Methyl Transferase
NSCLC	Non-Small Cell Lung Cancer
OC	Ovarian Cancer
OS	Overall Survival
OS	Organotypic Spheroids
OSE	Ovarian Surface Epithelium
OXPHOS	Oxidative Phosphorylation
PARP	Poly ADP-ribose polymerase
PAX2	Paired Box Gene 2
PBS	Phosphate Buffered Saline
PCA	Principle Component Analysis
PCR	Polymerase Chain Reaction



PDGFR- $\beta$	Platelet Derived Growth Factor $\beta$
PDS	Primary Debulking Surgery
PEN	Polyethylene Naphtholate
PFS	Progression Free Survival
PI3K	Phosphoinositide 3-Kinase
PIP3	Phosphatidylinositol 3, 4, 5-Triphosphate
PKB	Protein Kinase B
PL	Precancerous Lesion
PMT	Photomultiplier
PNGase	Peptide N-Glycosidase F
PNO1	RNA Binding Protein PNO1
POLE	DNA Polymerase Epsilon Catalytic Subunit
PR	Progesterone Receptor
PRC2	Polychrome Repressive Complex 2
PRIDE	Proteomics Identifications Database
PRR	Platinum Resistant Recurrence
PSMB8	Proteosome Subunit Beta 8
PSR	Platinum Sensitive Recurrence
PTEN	Phosphatase Tensin Homolog
PTM	Post Translational Modification
RAH	Royal Adelaide Hospital
Ras	Rat Sarcoma Virus Protein
RB1	Retinoblastoma Protein
RhoA	Ras Homolog Family Member A
RNA	Ribonucleic Acid
ROC	Receiver Operating Characteristic
ROI	Regions of Interest
ROS	Reactive Oxygen Series
RP-LC	Reverse Phase Liquid Chromatography
RSLC	Rapid Separation Liquid Chromatography
RT2	RealTime Re-Think
RTK	Receptor Tyrosine Kinase
RT-PCR	Real Time Polymerase Chain Reaction
SDS	Sodium Dodecyl Sulphate
SEC	Serous Endometrial Cancer
SILAC	Stable Isotopic Labelling of Amino Acids in Culture
siRNA	Small Inhibiting Ribonucleic acid
SLC31A1	High Affinity Copper Uptake Protein
SNP	Single Nucleotide Polymorphism
SORD	Sorbitol Dehydrogenase
SPATA18	Spermiogenesis-Associated Protein 18
SRF	Serum Response Factor
STIC	Serous Tubal Intraepithelial Carcinoma

STR	Short Tandem Repeat
TAM	Tumour Associated Macrophage
TAT	Tumour Associated T-Cell
TCGA	The Cancer Genome Atlas
TDP2	Tyrosyl DNA Phosphodiesterase 2
TFA	Trifluoroacetic acid
TMA	Tissue Microarray
TOF	Time of Flight
TP53	Tumour Protein 53 (gene)
P53	Tumour Protein 53 (protein)
TPPP3	Tubulin Polymerization-Promoting Protein Member 3
TVS	Transvaginal Ultra-Sound
TYK2	Tyrosine Kinase 2
UDP	Uridine Diphosphate
UDP-GlcNAc	Uridine Diphosphate N-acetylglucosamine
UMP	Uridine Monophosphate
UTP	Uridine Triphosphate
VCAN	Veriscan Core Protein
VDAC	Voltage Dependent Anion Channel
VEGF	Vascular Endothelial Growth Factor
Wnt	Wingless Related Integration Site
WT1	Wilm's Tumour protein 1
XPA	DNA Repair Protein Complimenting XP-A
$\gamma$ -H2AX	Phosphorylated Histone Family Member X

1

2

3

4

5

6

7

8

9

10

11

12

13

# Abstract

---

1  
2  
3  
4  
5  
6  
7  
8  
9  
10  
11  
12  
13  
14  
15  
16  
17  
18  
19  
20  
21  
22  
23  
24  
25  
26  
27  
28  
29  
30  
31  
32  
33  
34  
35  
36  
37  
38  
39

Ovarian cancer is the deadliest gynaecological malignancy and impacts thousands of lives each year. High grade serous ovarian carcinoma (HGSOC) represents over 70% of epithelial ovarian cancers, is responsible for more than 80% of ovarian cancer related deaths and is characterised by its aggressiveness and poor prognosis. This results primarily from late detection, often after local metastasis has occurred, and a treatment response trajectory of initial response to surgery and chemotherapy, followed by relapse with chemotherapy resistant disease. Improved clinical outcomes require a detailed understanding of the molecular features which underpin ovarian cancer development, progression, and response to treatment. Through the application of mass spectrometry (MS) techniques, we provide deep and comprehensive molecular characterisation of these important features of ovarian cancer. This serves as a foundation for greater understanding of this disease with the aim of improving clinical outcomes.

In pursuit of a molecular characterisation of precancerous lesions of the endometrium and fallopian tube, we applied LC-MS/MS and MALDI mass spectrometry imaging (MSI) proteomics to a rare case study exhibiting pre-cancerous lesions in the endometrium (endometrial intraepithelial carcinoma (EIC)) and fallopian tube (Serous Tubal Intraepithelial Carcinoma (STIC)) in the absence of developed cancer. Tissue from the fallopian tube was selected as studies have demonstrated that HGSOC does not develop in the ovary, but rather develops as STIC precancerous lesions in the fallopian tube. Through the development of precise sample acquisition and novel sample preparation methods, we were able to delineate between cancers and non-cancerous tissue with MSI and identify proteins in these precancerous samples, and adjacent healthy tissue. Further analysis revealed numerous metastasis associated proteins enriched in precancerous tissues compared to healthy. The development of sample preparation and MS techniques, in conjunction with identification of relevant proteomic drivers of cancer progression, provide a foundation for further molecular investigation of precancerous development of both HGSOC and endometrial cancer.

The major barrier to effective treatment of ovarian cancer remains the acquired resistance to platinum-based chemotherapy, such as carboplatin (CBP). This is known to occur through various mechanisms including, but not limited to, increased drug efflux, altered cellular metabolism, altered apoptotic pathways, and improved DNA repair. However, despite this knowledge, attempts to predict chemotherapy response based on molecular features of the cancer have been unsuccessful. To address this, we applied MS analyses of proteins and metabolites to ovarian cancer cell lines and their CBP resistant pairs. Through unbiased statistical analysis we were able to separate parental from resistant cells based on their molecular profile and identify molecular and metabolic pathways which were perturbed in chemoresistant cells. However, we also identified the challenges of significant molecular heterogeneity between cell lines. This challenge was further emphasised by a proteomic MS analysis of patient derived primary cells from a chemoresistant and chemosensitive patient.

1 The progression of ovarian cancer is facilitated by its immediate access to the peritoneal cavity  
2 which allows for cancer cells to shed from the primary tumour at an early stage and establish  
3 distant metastatic implants. To promote the survival of cancer cells in this cavity, HGSOc forms  
4 cellular aggregates within the peritoneal fluid called multicellular tumour spheroids (MCTS).  
5 These structures are resistant to chemotherapy, avoid cytoreductive surgery and are thought to  
6 represent a niche from which the cancer can re-establish itself after treatment. Further, there is  
7 significant interest in the use of an *in vitro* model of cancer spheroids for replicating both ovarian  
8 cancer MCTS and numerous features of solid tumours. We reviewed MS analyses of both *in*  
9 *vitro* generated MCTS and primary ovarian MCTS with the aim of understanding the molecular  
10 underpinning of their treatment response and metastatic capacity. This is concluded with a  
11 presentation of the first proteomic MALDI MSI analysis of a MCTS derived from primary  
12 patient samples in which we were able to employ spatially defined molecular features to  
13 delineate between different regions of the spheroid.

14 There is growing interest in the use of *in vitro* MCTS as a model to test novel anti-cancer  
15 compounds. These structures have the advantage of replicating numerous features of solid  
16 tumours including barriers to drug penetration. Utilising MCTS, we performed a pilot study  
17 investigating the penetration of a novel CDK4/6 inhibitor (CDDD2-94) with MALDI MSI.  
18 Through this analysis we were able to clearly monitor the accumulation of the drug in different  
19 areas of the MCTS over time representing the first steps in the use of MALDI MSI to monitor  
20 drug penetration in *in vitro* MCTS.

21 Distant origins, complex responses to therapy and the formation of free-floating cancer  
22 aggregates all contribute to the challenges of understanding, detecting and effectively treating  
23 ovarian cancer, and particularly HGSOc. This is reflected in the modest improvements in patient  
24 outcomes in the last 30 years, despite significant efforts by the scientific community. Through  
25 the application of advanced MS based analysis techniques, we provide comprehensive molecular  
26 information about important features in HGSOc development, treatment response and malignant  
27 progression. This sets the foundation for further research which aims to understand the early  
28 molecular events in this disease, characterise and predict chemotherapy response and advise  
29 treatment approaches which account for the molecular heterogeneity and unusual metastatic  
30 progression.

31

32

33

34

35

36

37

1  
2  
3  
4  
5  
6  
7  
8  
9  
10  
11  
12  
13  
14  
15  
16  
17  
18  
19  
20  
21  
22  
23  
24  
25  
26  
27

# CHAPTER 1: INTRODUCTION

---

1  
2  
3  
4  
5  
6  
7  
8  
9  
10  
11  
12  
13  
14  
15  
16  
17  
18  
19  
20  
21  
22  
23  
24  
25  
26  
27

This page is intentionally left blank

# 1. Ovarian Cancer Introduction

Ovarian cancer (OC) is the eighth most common cancer in women and the third most common gynaecological cancer [1]. It has the worst prognosis and highest mortality rate among gynaecological cancers [2] with over 21000 new cases and more than 13000 deaths in the USA alone in 2020 [3]. It represents 3.4% of all cancers and 4.4% of cancer related mortality in women [4] with a five year survival rate of less than 35% [5, 6]. It typically effects women over the age of 65 [7] with risk factors including menstrual related factors [8], family history of breast cancer or ovarian cancer [9], mutations in tumour suppressor genes [10], particularly in breast cancer susceptibility (*BRCA*) genes [11], and obesity [12], while socio economic status is a significant predictor of mortality [13]. Ovarian cancer is commonly diagnosed at an advanced stage, where the primary tumour is no longer confined to the original site which is a major contributor to the high mortality rates from this cancer [14].

## 1.1. Ovarian Cancer Subtypes and Their Precursors

Ovarian cancer is a highly heterogenous disease with diverse risk factors, development, progression, molecular features, and treatment response observed between subtypes. OC is divided into two main subtypes: epithelial and germ cell OC [15]. Germ cell OC is responsible for 20-25% of ovarian neoplasms, but only 3-5% of these are malignant [16]. They account for the majority of OC in premenarchal girls and a high proportion of ovarian neoplasms in women under 20 [17]. These cancers are often diagnosed early and have a generally favourable prognosis [18-20]. Germ cell OC will not be discussed further in this thesis, but their subtypes and prognoses are reviewed here: [21].

Epithelial ovarian tumours (EOC) comprise over 90% of ovarian cancers [22, 23] and have traditionally been separated into type 1 and type 2 based on their pathways of tumorigenesis [24]. Originally, this separation was based on the observation that type 1 ovarian carcinomas are ‘low grade’, being slow to develop and metastasise, and developed in a stepwise manner from well-defined precursor lesions [25]. In contrast, type 2 ovarian carcinomas are ‘high grade’, evolve rapidly and metastasise early, and develop *de novo* from a, at the time, unknown precursor [25].

### 1.1.1. Type 1 Ovarian Cancer

Type 1 EOC are low grade and well differentiated cancers and include low grade serous carcinoma (LGSOC), endometrioid ovarian carcinoma (EnOC), clear cell ovarian carcinoma (CCOC) and mucinous ovarian carcinoma (MOC) [26]. Generally, these cancers exhibit somatic mutations in Kirsten rat sarcoma viral oncogene homolog (*KRAS*), B-Raf Proto-Oncogene, serine/threonine kinase (*BRAF*) or Erb-B2 receptor Tyrosine Kinase (*ERBB2*) and lack Tumour Protein (*TP53*) mutations (Table 1). They are predicted to arise from borderline lesions of the ovary and are typically identified at an early stage and often associated with a good prognosis [27]. However, each of these subtypes are distinct diseases, often with unique histological, genetic, and molecular features, prevalence, disease progression and site of origin. Despite varied responses, all ovarian cancer subtypes currently receive the same standard first line chemotherapy of a platinum agent combined with a taxane [28].

#### 1.1.1.1. Endometrioid Ovarian Cancer (EnOC)

EnOC is a rare subtype of ovarian cancer, representing approximately 10% of all surface ovarian carcinomas [29]. They are commonly detected at an early stage [30] and are associated with endometriosis and synchronous endometrioid endometrial carcinoma (EEC) [31, 32]. Synchronous EnOC and EEC can appear so similar that it is sometimes not possible to determine whether they are two separate carcinomas or one is a metastatic implant from the other [33] however, there is clear genomic and molecular evidence that EnOC can be of endometrial origin [34]. EnOC is histologically characterised by squamous morules, mucinous differentiation, clear cell change, spindle morphology and secretory change [30] (Table 1). EnOC often have somatic mutations in catenin  $\beta$ 1 (CTNNB1) and phosphatase and tensin homolog (PTEN) genes [35]. However, EnOC, in the absence of EEC, have been seen to be heterogenous at a mutational level in a similar manner to EEC [36], albeit with different frequencies of common mutations [37]. While most EnOC patients have a favourable outcome, there is a subset where the outcome is poor [38], potentially reflecting a molecular and genetic subtype of EnOC with differential patient outcomes based on diverse molecular features.

#### 1.1.1.2. Clear Cell Ovarian Cancer (CCOC)

CCOC is a distinct disease from epithelial ovarian cancer in terms of histological and genomic features [39] and is suggested to have a unique biological phenotype compared to other ovarian cancers [40]. It is a rare cancer, with incidence rates below 5% of all ovarian epithelial cancers. However, it is significantly more prevalent in east Asian populations, although the reason for this remains unclear [41].

This cancer is commonly detected at an early stage [42] where it has a good prognosis. In the rare cases that CCOC is detected at a late stage the prognosis is very poor [41]. Both atypical endometriosis and atypical adenofibroma are considered precursor lesions for CCOC [43, 44] and CCOC is histologically characterised by glycogen containing cells with abundant clear cytoplasm [30] combined with tubules, solid areas, and complex papillae [45] (Table 1).

CCOC has molecular features of being cytokeratin 7 (CK7) positive, B-lymphocyte antigen CD20 (CD20) and Wilm's tumour protein 1 (WT1) negative, estrogen receptor (ER) and progesterone receptor (PR) negative [46]. Its genetic features include a lack of TP53 and BRCA1/2 mutations and the presence of AT-Rich Interactive Domain-Containing Protein 1A (ARID1A) and Phosphoinositide 3-Kinase (PI3K) mutations [47]. This ovarian cancer subtype commonly exhibits resistance to treatment with standard platinum/taxane chemotherapy raising questions about the usefulness of this treatment approach for CCOC [48].

#### 1.1.1.3. Mucinous Ovarian Cancer (MOC)

MOC was previously thought to be the second most common ovarian cancer until it was identified that many cases identified as MOC were, in fact, metastatic implants from cancers of the gastrointestinal tract [49]. With advances in our understanding of MOC morphology and immunohistochemical markers, there has been a significant reduction in the reported incidence of MOC [49] which is now believed to represent less than 3% of all epithelial ovarian carcinomas [50]. It has a favourable prognosis when found at an early stage while the prognosis is worse when



1 found late [51-53] and is significantly worse than the prognosis of serous ovarian tumours found  
2 at a similar late stage [54]. MOC can be difficult to identify as it commonly expresses lower levels  
3 of Carbohydrate Antigen 125 (CA125), a commonly utilised blood biomarker for ovarian cancers,  
4 than other ovarian cancers and the correct diagnosis is often only revealed upon surgical  
5 intervention [55, 56].

6 Histologically, MOC is heterogenous, commonly containing benign, borderline, invasive and non-  
7 invasive components in the same tumour [45]. It is characterized by molecular alterations in  
8 KRAS which can be observed in benign, borderline and carcinoma components [57-59]. MOC has  
9 an immunophenotype of CK7 positive, CK20 negative, ER negative, PR negative and WT1  
10 negative (Table 1).

11 Borderline mucinous lesions have been reported as the precursor for MOC [27], however it is also  
12 frequently associated with endometriosis [30].

#### 13 1.1.1.4. Low Grade Serous Ovarian Cancer (LGSOC)

14 Serous ovarian carcinomas represent the majority of epithelial ovarian cancers and are divided into  
15 LGSOC and high grade serous ovarian carcinoma (HGSOC) based on their progression and  
16 treatment response [25]. LGSOC represent 10% of serous ovarian carcinomas [60] and is  
17 diagnosed on average of 7-10 years earlier than HGSOC [61].

18 Major risk factors for LGSOC include the use of ovulation inducing drugs and the presence of  
19 advanced borderline tumours [62]. It is hypothesised that LGSOC develop in a step wise manner  
20 from adenofibridoma to serous borderline tumour to non-invasive micropapillary serous  
21 carcinoma (MPSC) before developing into LGSOC [63]. This is supported by the observation that  
22 invasive LGSOC are associated with non-invasive MPSC in three out of four cases [64], and  
23 through genomic expression analysis, which has demonstrated that LGSOC and borderline  
24 tumours are genomically similar [65]. Further, borderline tumour which relapse after treatment  
25 often do so as LGSOC [66].

26 Genomically, LGSOC differs from HGSOC in their increased expression of ER, PR, paired box  
27 gene 2 (PAX2), anterior gradient homologue 3 (ARG3), insulin growth factor 1 (IGF-1) and  
28 greater chromosomal instability [67, 68]. Further, LGSOC expresses far less P53 mutations  
29 compared to HGSOC [63] and is best characterised by KRAS and BRAF mutations, however the  
30 presence of these mutations appear to be a positive prognostic factor [69].

31 Platinum and taxane chemotherapy remain the standard chemotherapy treatment for LGSOC  
32 despite, similar to other type 1 ovarian cancers, LGSOC being relatively insensitive to this first  
33 line treatment [67]. One study of 58 patients with LGSOC found that only 3.7% of patients  
34 responded to standard first line chemotherapy [70]. Despite this, LGSOC, while often diagnosed  
35 at a similar late stage as HGSOC (Stage 3) [71], has a mean survival time almost twice as long and  
36 a 5 year survival rate of 75% for LGSOC compared to 15% for HGSOC [72]. This is due to slower  
37 growth of LGSOC and the observation that the status of no residual disease after surgery is more  
38 likely to be achieved in LGSOC compared to HGSOC [73].

### 1 *1.1.2. Type 2 Ovarian Cancer*

2 In contrast to type 1 ovarian cancers, type 2 ovarian cancers are generally highly aggressive, high  
3 grade carcinomas characterised by *TP53* mutations [74], chromosomal instability [75] and a  
4 propensity for metastasis. Type 2 ovarian cancers are comprised of undifferentiated carcinoma,  
5 carcinosarcoma and HGSOC. Of these, HGSOC comprises 75-80% of cases [64] are generally  
6 detected at a late stage and are responsible for the majority all ovarian cancer deaths [27]. For this  
7 reason, HGSOC have been the primary focus of medical and scientific research into ovarian cancer  
8 and will be the primary focus of this thesis.

#### 9 *1.1.2.1. High Grade Serous Ovarian Cancer (HGSOC)*

10 HGSOC are characterised by histological characteristics of papillary, glandular, solid, and  
11 transitional patterns [30]. Their immunohistochemistry stain positive for CK7, PAX8 and WT1  
12 and negative for CK20 [27]. They are characterised by high degrees of nuclear atypica and present  
13 with large, hyperchromatic and pleomorphic nuclei with multinucleation in some cases [76]. They  
14 are further separated from LGSOC by a high mitotic index reflecting their accelerated rate of  
15 growth [77].

16 HGSOC are genomically characterised by recurrent mutations in *TP53*, *BRCA1* (96% of cases)  
17 and *BRCA2* (22% of cases) [64]. Additionally, 50% of HGSOC are homologous recombination  
18 (HR) defective [78] and more than 100 recurrent amplifications and deletions have been identified,  
19 representing a high degree of somatic copy number and structural variations [79-81].

20 In recent years, these subtypes have been shown to be inadequate to describe the complexity of  
21 ovarian cancer with HGSOC being divided into further molecular subtypes based on gene  
22 expression profiling, which are associated with different clinical outcomes [82]. The Cancer  
23 Genome Atlas (TCGA) identified four robust HGSOC subtypes: Immunoreactive, Differentiated,  
24 Proliferative and Mesenchymal based on mRNA expression [81]. These subtypes have been  
25 independently validated and shown to have independent prognostic value [82]. They were further  
26 refined to a 100 gene signature which can predict these HGSOC subtypes [83]. More recently, less  
27 common ovarian cancer subtypes, including CCOC, have also been subdivided into further  
28 specific subtypes based on gene expression profiles [84], demonstrating the molecular and  
29 genomic heterogeneity between, and within, different ovarian cancer subtypes.

30 Late detection is a key characteristic of HGSOC and less than 20% of HGSOC are diagnosed in  
31 stage I or II [85]. This is also a key factor in patient prognosis with the 10 year survival rates of  
32 patients diagnosed with late stage HGSOC being around 15% compared to 55% for those  
33 diagnosed with early stage disease [85]. Almost all HGSOC patients undergo the same treatment  
34 regime starting with debulking surgery followed by cytotoxic chemotherapy [86]. The first line  
35 chemotherapy regime for HGSOC is identical to other EOCs [87], is comprised of carboplatin and  
36 paclitaxel and has remained relatively unchanged since the 1990s [88].

37 Unlike other subtypes of EOC, HGSOC respond favourably to first line chemotherapy in 70%  
38 cases [89]. However, it is estimated that more than 80% of those who respond favourably will  
39 eventually relapse [86]. Upon relapse patients are typically re-treated with the standard  
40 chemotherapy regimen of carboplatin and paclitaxel and approximately 50% of patients still

1 respond to this treatment [86]. However, this is not curative, and progression free survival (PFS)  
 2 decreases with each successive platinum therapy [86]. Overall, more than 80% of patients  
 3 diagnosed with advanced disease will develop resistance to treatment which is a major contributing  
 4 factor to the high rates of mortality related to HGSOc [90].

5 **Table 1:** Subtypes of epithelial ovarian cancer: histological features, immuno-histochemical features,  
 6 precursor lesions, molecular aberrations, prognosis, and primary chemo response.

	LGSOC	HGSOC	MOC	EnOC	CCOC
Frequency out of all EOC	10%	70%	<3%	10%	5%
Histology	Small papillae with cells of uniform nuclei and various amounts of hyalinized stroma; psammoma bodies.	Papillary and solid growth; large mononuclear cells; pleomorphic nuclei with prominent nucleoli and mitotic activity.	Heterogeneous; often composed of benign, borderline, non-invasive, and invasive components.	Cystic or predominantly solid. Squamous morules, mucinous differentiation, clear cell change, spindle morphology and secretory change [30]	Mixture of tubules, solid areas, and complex papillae; cells with prominent nucleoli and clear cytoplasm filled with glycogen.
Immunophenotype	CK7+, WT1+, ER+	CK7+, CK20-, PAX8+, WT1+	CK7+, CK20-, ER-, PR-, WT1-	CK7+, PAX8+, CK20-, WT1-	Napsin A+, WT1-, p53-, ER-
Precursor Lesion	Low grade malignant potential lesions	STIC	Borderline Mucinous Lesions	Endometriosis	Endometriosis and adenofibroma
Molecular Aberrations	<i>KRAS</i> , <i>BRAF</i> , MAPK active	<i>TP53</i> , <i>BRCA1/2</i> , HRD	<i>KRAS</i> , <i>HER2</i>	<i>ARID1A</i> , <i>PTEN</i> , <i>KRAS</i> , PI3K, Wnt/ $\beta$ -catenin activation	<i>ARID1A</i> , PI3K/PKB activation, RTK/Ras activation, MMR
Prognosis	Intermediate	Poor	Good	Favourable	Intermediate
Primary Chemo response	Resistant	Sensitive	Resistant	Sensitive	Resistant
Primary chemo response reflects the typical response to first line combination therapy with carboplatin and paclitaxel. Resistant = PFS < 6 months and sensitive = PFS > 6 months. General from [50] and [27], histology from [45], [30] and [39].					

7

#### 8 1.1.2.2. Origins of High Grade Serous Ovarian Cancer

9 As described above, type 2 ovarian carcinomas, which are predominantly HGSOc, were originally  
 10 characterised by the lack of a clear precursor lesion [25]. This is due to HGSOc generally being  
 11 identified at a late stage, after metastatic spread, making clear identification of a precursor lesions  
 12 highly infrequent, hindering the ability to accurately identify the origin of the disease [91]. It was  
 13 initially assumed that the ovary was the disease origin of HGSOc, as most HGSOc patients, even  
 14 those identified at an early stage, featured the cancerous involvement of the ovary [92]. This gave  
 15 rise to the “incessant ovulation theory” [93] which postulated that ovulation gave rise to constant  
 16 repair and regeneration of the ovarian surface epithelium (OSE) which in turn created a pro  
 17 inflammatory and pro-oxidative microenvironment which promotes DNA damage [91, 93, 94]. It  
 18 was postulated that, in cells which have impaired DNA damage repair mechanisms, as is common  
 19 in HGSOc, this would result in carcinogenesis [94], culminating in the development of HGSOc  
 20 in the ovary. This theory was supported by the discovery of cortical inclusion cysts (CICs) which

1 are invaginated sections of the OSE thought to facilitate the neoplastic transition of the OSE  
2 surrounding a CIC [94] representing a potential developmental pathway for ovarian origin  
3 HGSOc.

4 However, some scientific evidence raises questions about this theory of HGSOc origin. For  
5 example, HGSOc cells more closely resemble tissues developmentally derived from the Müllerian  
6 duct [95-97], which includes the uterus and fallopian tubes, but not the ovaries. It has been  
7 postulated that the OSE can undergo metaplasia to resemble Müllerian derived tissue [95, 96], and  
8 this has been mechanistically demonstrated *in vitro* [98]. However, in 1999 it was first argued that  
9 HGSOc in fact originates from a tissue of Müllerian origin as there remained minimal evidence  
10 that the OSE is capable of metaplastic transformation. In addition, there remained a lack of an  
11 observable HGSOc precursor lesion in the ovaries and it was observed that primary peritoneal  
12 carcinoma, which were clinically indistinguishable from HGSOc, could arise without the  
13 involvement of the ovary [99].

14 With the advent of risk reducing salpingo-oophorectomy (surgical removal of both the fallopian  
15 tubes and ovaries) for patients with BRCA mutations, small dysplastic lesions were discovered in  
16 the fallopian tube which morphologically resembled HGSOc [100]. These lesions, classified as  
17 serous tubal intraepithelial carcinoma (STIC), are characterized by high nuclear p53, positive  $\gamma$ -  
18 H2AX staining (indicating DNA damage) and lack of Ki-67 staining (indicating low proliferation)  
19 [101]. They are further characterized by malignant features including enlarged nuclei, dark  
20 staining of the nucleus (hyperchromasia) and coarse chromatin aggregates and prominent nucleoli  
21 [102, 103], which are also characteristics found in HGSC [104]. A recent multi-centre study  
22 demonstrated that, with extensive examination of surgically removed fallopian tubes, STIC, and  
23 their precursors 'p53 signatures', were detected in 10% and 27% of fallopian tubes from BRCA1  
24 and BRCA2 carriers respectively [105].

25 Most STIC lesions have high levels of p53 staining [106] and p53 mutations [107], a defining  
26 characteristic of HGSOc. These lesions share further genomic similarities with HGSOc including  
27 genomic instability [108, 109] and predisposition to BRCA1, BRCA2 and PTEN alterations [109].  
28 In instances where both HGSOc and STIC tissue were available for analysis, many STIC were  
29 identified as having identical TP53 mutations as concurrent HGSOc [107]. This is supported by  
30 STIC and HGSOc sharing similar immunophenotypes [110] and proteomes [111].

31 Further to this, in approximately 60% of HGSOc cases, concurrent STIC is identified in the  
32 fallopian tube [103, 112]. Based on these data, one could hypothesize that STIC either develops  
33 into HGSOc within the fallopian tube before migrating to the ovary, or it sheds from the fallopian  
34 tube at a premalignant stage, imbeds into the ovary and there develops into HGSOc [104, 113].  
35 Further evidence in support of this model is that removal of the fallopian tubes alone reduces the  
36 risk of ovarian cancer across the population by 35-50% [114]. This is not in opposition to the  
37 hypothesis that a greater number of ovulation cycles are associated with a greater risk of HGSOc  
38 development, as the fallopian tube epithelium, especially those near the fimbriated end, where  
39 STIC is most common, are directly exposed to follicular fluids directly after ovulation [115]. These  
40 fluids contain reactive oxygen species and other genotoxic substances which can cause DNA

1 damage [116]. When combined with impaired DNA repair pathways, as in the case of BRCA  
2 deficient individuals [115], this can result in carcinogenesis.

3 Recently a mouse model, utilising *p53*, *Dicer1*, *Pten* and *Anti-Müllerian Hormone Receptor*  
4 (*Amhr2*) mutations, similar mutations as those observed in human HGSOc, was able to replicate  
5 HGSOc development. This included development within the fallopian tube and envelopment of  
6 the ovary followed by aggressive metastasis throughout the peritoneal cavity in a process which  
7 closely resembles the metastatic progression of human HGSOc [117, 118]. In conjunction with  
8 the growing evidence over the past two decades, this has changed how we understand the early  
9 stages of serous ovarian cancer and suggests that, considering HGSOc is often found in the  
10 presence of peritoneal metastasis, serous cancers of the ovary, peritoneum and fallopian tube may  
11 share common origins in the fallopian tube epithelium [119].

12 However, the above mouse model also demonstrated that, even when the fallopian tubes are  
13 removed, HGSOc can still develop within the ovary [118]. There is evidence that HGSOc which  
14 are not related to STIC can arise from concurrent borderline tumours or LGSOc located on the  
15 ovary [120, 121]. These precursors, along with ovarian CICs and endosalpingiosis, are derivatives  
16 of the fallopian epithelium [122]. This is supported by the observation that LGSOc and CICs gene  
17 expression is more closely related to fallopian tube epithelium than they are to OSE [123]. This  
18 represents a second pathway of HGSOc development which is also related to tissue of the fallopian  
19 tube [115]. The existence of two pathways of HGSOc development is supported by the  
20 observation that HGSOc with and without STIC cannot be clearly separated based on their  
21 transcriptome and miRNA profiles [124].

22 The understanding that HGSOc can develop from precursors in the fallopian tube represents a  
23 paradigm shift in how the development of ovarian cancer is understood. This has significant  
24 implications for the early detection and treatment approach and, subsequently, prevention of  
25 ovarian cancer.

## 26 1.2. Ovarian Cancer Risk Factors, Diagnoses, Staging and Screening

27 Despite the diversity of ovarian cancer subtypes, their progression and response to treatment,  
28 early detection and early intervention consistently results in improved patient outcomes.  
29 Specifically, ovarian cancer confined to the ovaries (stage I) can be cured in up to 90% of cases  
30 and disease confined to the pelvis (stage II) is associated with a 5-year survival rate of 70%. In  
31 contrast, disease which has spread beyond the pelvis (stage III-IV) has a long-term survival rate  
32 of less than 20% [125]. However, in EOC early detection is uncommon, with only 20% of  
33 ovarian cancers diagnosed in Stage I-II [126]. This is epitomised by HGSOc which is only rarely  
34 detected before extensive spread throughout the peritoneal cavity. This highlights the importance  
35 of identifying risk factors, early diagnosis, population screening and effective staging of ovarian  
36 cancer to facilitate effective surgical and therapeutic interventions.

### 37 1.2.1. Risk Factors

38 Ovarian cancer is typically a post-menopausal disease [127, 128] and its incidence increases  
39 significantly in women over 65 years of age [7]. Older age at diagnosis is associated with more  
40 advanced disease and lower survival rates [128, 129] with age of onset beyond 64 being a major

1 predictor of mortality [130]. It is expected that this is the result of post-menopausal risk factors,  
2 late detection, and the limitation in aggressive treatment options for this cohort [130].

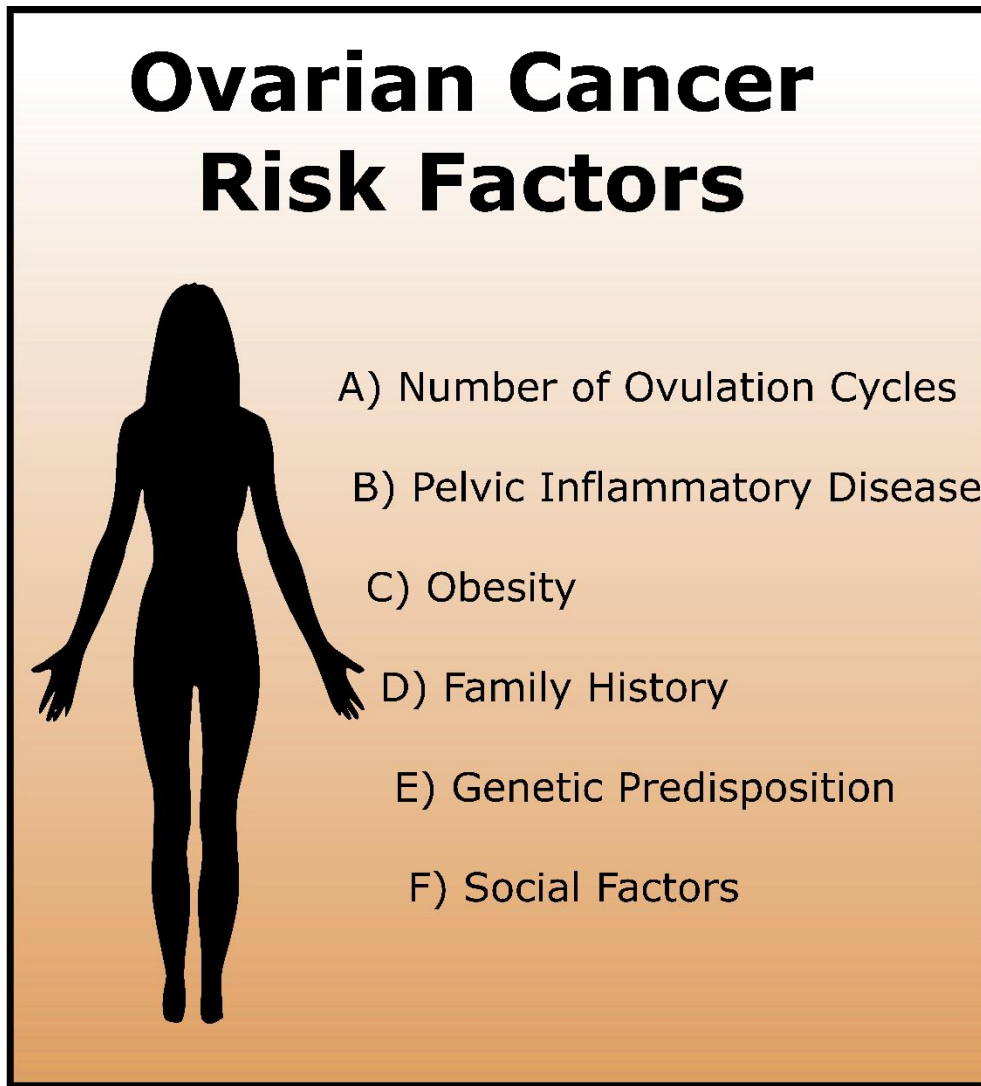
3 An inverse relationship has been observed between the number of ovulation cycles and the risk of  
4 OC [131, 132]. This suggests that anything that lowers the lifetime rate of ovulation, including  
5 early menopause, pregnancy [132-137] and oral contraceptives [8, 138-140], lowers the risk of OC  
6 [93] (Figure 1). This observation gave rise to the ‘incessant ovulation’ theory of OC development,  
7 as described above [141]. However, it has been observed that lack of ovulations due to menstrual  
8 disorders is also associated with increased risk of OC [142], suggesting a more complex  
9 relationship between ovulation and OC.

10 Incessant ovulation results in inflammation in the ovarian epithelium and this inflammation has  
11 been linked to the development of ovarian cancer [143] (Figure 1). Other factors which increase  
12 inflammation, including endometriosis [144], benign ovarian cysts [145] and chronic pelvic  
13 inflammatory disease [146], are linked to the development of ovarian cancer. Further, obesity and  
14 a high fat diet are risk factors for OC occurrence and mortality [12, 132, 147]. It is expected that  
15 this linked to increased levels of oestrogen and progesterone, which are both synthesised from  
16 cholesterol [148], and play an important role in triggering ovulation. Further, leptins, released from  
17 adipose tissue in response to high lipid levels in blood, stimulate the releases luteinising hormone  
18 [149] which, when in high abundance, results in immature release of the ovum and further  
19 increased oestrogen production. Together this gives rise to improper re-epithelisation of the ovary  
20 which can result in abnormal cell growth which can develop into cancer [150].

21 Family history of breast or ovarian cancer is the single most influential risk factor for OC [9]  
22 (Figure 1). A woman with a single first degree relative diagnosed with ovarian cancer has a  
23 threefold greater risk of developing OC in her lifetime [151, 152], primarily due to hereditary  
24 mutations in tumour suppressor genes [10] (Figure 1). The most well characterised of these is  
25 *BRCA1* and *BRCA2* germline mutations which account for 14% of all epithelial OC and 17% of  
26 HGSOC [153]. Further, *BRCA1* and *BRCA2* mutations account for 65-85% of all familial ovarian  
27 cancers [11]. A women with a *BRCA1* mutation has a 40% chance of developing ovarian cancer  
28 in her lifetime while a women with a *BRCA2* mutation has a 11-18% chance [154, 155]. Patients  
29 with *BRCA1* or *BRCA2* mutations are more likely to develop HGSOC than other ovarian cancer  
30 subtypes [156] and are more likely to have ovarian cancer detected at a late stage than non *BRCA1*  
31 or *BRCA2* mutation carrying women [153]. The role of these genes in DNA repair and  
32 transcriptional regulation in response to DNA damage are well characterised and expected to  
33 underpin their contribution to cancer development [157]. The impaired DNA repair response  
34 present in cancer with *BRCA1* and *BRCA2* mutations is expected to contribute to increased  
35 sensitivity to platinum-based chemotherapy, which acts primarily through damaging the DNA  
36 double helix. This is reflected in cancer with *BRCA1* and *BRCA2* mutations having better response  
37 to treatment and patients show longer overall survival (OS) rates [158, 159]. Further, this results  
38 in a sensitivity to treatments which target other DNA repair mechanisms, such as poly ADP-ribose  
39 polymerase (PARP) inhibitors, which are now a standard treatment approach for patients with  
40 *BRCA1/2* mutations, although they are rarely utilised as first line treatments [160].

1 Finally, lower socioeconomic status results in increased incidence of OC and decreased survival  
2 rates [13] (Figure 1). This is believed to result from challenges in accessing healthcare [161], lack  
3 of knowledge of early symptoms, response to symptoms, lifestyle factors and co-morbidities [162].  
4 This is reflected in the observation that high education levels are related to a decreased risk of  
5 ovarian cancer [163] and emphasise the importance of community awareness campaigns and  
6 education programs in reducing the risk of OC mortality.

7



8

9 **Figure 1:** Risk factors which predict ovarian cancer diagnosis and poor prognosis: (A) The number of  
10 ovulation cycles a women has experienced is thought to be directly related to their risk of developing  
11 ovarian cancer. This is reflected in younger age, pregnancy and oral contraceptive use being protective  
12 against ovarian cancer. (B) Chronic inflammatory diseases of the pelvis, including benign ovarian cysts and  
13 endometriosis, have been associated with ovarian cancer development. (C) Obesity is a risk factor for  
14 ovarian cancer diagnosis and poor prognosis which is thought to be mediated primarily through altered  
15 hormone production. (D) Family history of ovarian cancer of breast cancer is the largest single risk factor

1 for the development of ovarian cancer, even in the absence of an identifiable cancer driving genetic  
2 mutation. (E) Genetic predisposition, best characterised in mutations in the *BRCA1* and *BRCA2* genes, is a  
3 major predictor of ovarian cancer development. (F) Social factors including socio economic status and  
4 education levels are closely linked to incidence of ovarian cancer and survival rates of those diagnosed.  
5 This is predicted to result from impacts on access to healthcare, knowledge of early symptoms, lifestyle  
6 factors and co-morbidities.

### 7 **1.2.2. Risk Reducing Interventions**

8 Despite the high mortality rates associated with ovarian cancer, the general incidence in the  
9 population remains low at around 1% [164]. For cancer in general, it has been predicted that  
10 between 1/3 and 2/5 of all cancers could be prevented by eliminating and reducing risk factors [1],  
11 making the reduction of risk factors the most impactful risk reducing intervention for ovarian  
12 cancer in the general population. For the reasons discussed above, the use of oral contraceptives  
13 represents an effective risk reducing intervention for ovarian cancer [165].

14 Patients with *BRCA1* or *BRCA2* mutations are recommended to undergo risk reducing salpingo-  
15 oophorectomy around the age of 40 [166]. While there are side effects related to hormone  
16 imbalances after the removal of the ovaries, this surgical intervention reduces the risk of ovarian  
17 cancer in *BRCA1* or *BRCA2* positive individuals by at least 75% [167, 168]. Further, a meta-  
18 analysis of studies into the use of oral contraceptives by *BRCA* positive women showed that it  
19 reduced their risk of developing ovarian cancer by half [166].

### 20 **1.2.3. Ovarian Cancer Diagnosis**

21 Ovarian cancer is often asymptomatic often resulting in identification at a late stage, after local  
22 metastasis has already occurred [169]. Symptoms often only arise in advanced cancer and are  
23 usually non-specific and not easily recognized as a symptom of cancer [170]. A review of  
24 symptoms associated with ovarian cancer identified the report of abdominal distention, abdominal  
25 or pelvic bloating, abdominal mass, loss of appetite and abdominal or pelvic pain to significantly  
26 increased the likelihood of ovarian cancer being present [171]. However, this review also noted  
27 that none of the above symptoms, when absent, could alone rule out the presence of ovarian cancer.  
28 Further, the authors highlight the challenges with diagnosing ovarian cancer based on these, often  
29 subjective, reports of symptoms.

30 Once certain risk factors are identified, a complete physical examination, including rectovaginal  
31 examination, is recommended for detection of pelvic and abdominal masses [170]. However, this  
32 examination has limited accuracy, particularly in obese patients, and any detected masses are not  
33 easily identifiable as ovarian cancer [172].

34 Upon identification of a suspected case of ovarian cancer, the clinician is advised to perform a  
35 transvaginal ultra-sound (TVS) [172, 173]. This technique is utilised to visualise the ovaries and  
36 fallopian tubes and detect disease through morphological changes or characteristics associated  
37 with ovarian cancer, such as increased ovarian volume [174]. However, it is limited by challenges  
38 in accurately identifying some tumours [175] or missing small tumour masses [176]. There is  
39 ongoing research into improving imaging techniques for identifying ovarian cancer including  
40 improving image resolution [176], utilising immunological markers [177] and the use of nano  
41 probes [178].



1 TVS is accompanied by assessment for blood biomarkers, particularly CA125 [170]. CA125 is a  
2 high molecular weight glycoprotein first described in the 1980s [179] and is the most commonly  
3 used biomarker for diagnosis and monitoring of ovarian cancer [180]. However, the utility of  
4 CA125 is controversial owing to it being elevated in 80% of all epithelial ovarian cancers, but only  
5 50% of early stage epithelial ovarian cancers [173]. This is further complicated by the observation  
6 that CA125 is elevated in benign conditions including endometriosis and fibroids [172, 173, 181].

7 As with any cancer, definitive diagnosis results from a biopsy of sample tissue. In the case of  
8 ovarian cancer, this is generally achieved through the use of a needle core biopsy after which  
9 excised tissue is closely examined for possible malignancy utilising histological, morphological  
10 and immunohistochemical indicators [182].

#### 11 *1.2.4. Ovarian Cancer Staging*

12 Once cancer is identified, cancer staging is an important step for predicting patient outcome and  
13 advising appropriate treatment [183]. It provides description of the characteristics of the cancer,  
14 reproducible metrics to be used within and across tumours, facilitates correlation between tumour  
15 features and prognosis, informs and organizes treatment recommendations and provides a platform  
16 for understanding historical information which can contribute to clinical advances [184].

17 For ovarian cancer this is facilitated through an exploratory laparotomy (open abdominal surgery  
18 for examination of abdominal organs) at the time of presentation [50] and clinical staging is  
19 performed utilising the Federation of Gynaecology and Obstetrics (FIGO) staging system first  
20 published in 1973 and most recently revised in 2014 [185] (Table 2). While each stage has further  
21 substages, they can be broadly separated into the following: Stage I – Cancer is confined to the  
22 fallopian tubes, ovaries, and peritoneal fluid. Stage II – Tumour involves one or both ovaries or  
23 fallopian tubes with pelvic extension or primary peritoneal carcinoma. Stage III – As per stage II  
24 with cytologically or histologically confirmed spread to the peritoneum outside the pelvis and/or  
25 metastasis to the retroperitoneal lymph nodes. Stage IV – Distant metastasis identified excluding  
26 peritoneal metastasis [185].

27 Some oncologists have highlighted shortcomings of the FIGO staging approach highlighting the  
28 one-size-fits-all nature of these classifications, despite the existence of several diverse subtypes of  
29 epithelial ovarian cancer, and the data which informs this staging is dependent on the skill and  
30 aggressiveness of the surgeon performing the surgery [184]. Regardless, this staging approach is  
31 used to advise prognosis and treatment approaches. For example, in women with a Stage III or IV  
32 cancer, and therefore a low likelihood of effective cytoreductive surgery, neo-adjuvant  
33 chemotherapy is advised to reduce the tumour burden before surgery [50]. Regardless of subtype,  
34 detection of ovarian cancer at a late-stage results in significantly reduced 5-year survival rates  
35 [186] highlighting the importance of early detection for effective treatment of ovarian cancer.

36

37

38

39

1

2 **Table 2:** Federation of Gynaecology and Obstetrics (FIGO) staging for ovarian cancer.

FIGO Stage	Clinical Features	Five Year Survival Rate
Stage I	Tumour is confined to the ovaries or fallopian tube(s).	Greater than 80% regardless of EOC subtype
- Stage IA	Growth limited to one ovary (capsule intact) or fallopian tube, no tumour on external surfaces. No malignant cells in peritoneal fluid/washings.	
- Stage IB	Growth limited to both ovaries (capsule intact) or both fallopian tubes, no tumour on external surfaces. No malignant cells in peritoneal fluid/washings.	
- Stage IC	Tumour on surface of one or both ovaries or fallopian tubes; or capsule ruptures; or malignant cells present in peritoneal fluids/washings.	Between 67% (HGSOC) and 84% (endometrioid )
Stage II	Tumour involves one or both ovaries/fallopian tubes with extension to pelvic structures	
- Stage IIA	Extension and/or implants onto the uterus and/or fallopian tubes and/or ovaries.	
- Stage IIB	Extension to other pelvic intraperitoneal tissues	
Stage III	Tumour involves one or both ovaries/fallopian tubes, or primary peritoneal cancer, with confirmed spread to the peritoneum outside the pelvis and/or metastasis to the retroperitoneal lymph nodes	Between 22% (CCOC) and 54% (LGSOC)

- Stage IIIA1	Metastatic implants cytologically or histologically identified in retroperitoneal lymph nodes only.	
- Stage IIIA2	Microscopic extra pelvic peritoneal involvement with or without retroperitoneal lymph node involvement.	
- Stage IIIB	Macroscopic peritoneal metastases beyond the pelvis up to 2 cm in greatest dimension with or without retroperitoneal lymph node involvement.	
- Stage IIIC	As per Stage IIIC with the addition of extension of tumour to capsule of liver and spleen without parenchymal involvement of either organ.	
Stage IV	Distant metastasis beyond peritoneal metastasis	
- Stage IVA	Pleural effusions with positive cytology	
- Stage IVB	Parenchymal metastases and metastases to extra-abdominal organs including inguinal lymph nodes and lymph nodes outside of the abdominal cavity.	
FIGO stages: [187] Survival statistics [186]		

1

2 **1.2.5. Ovarian Cancer Screening**

3 Due to the difficulty in diagnosing ovarian cancer [170], and the significant impact that cancer  
4 stage at time of diagnosis has on patient prognosis [186], effective screening for ovarian cancer is  
5 essential in reducing related mortality. Modelling of HGSOc growth suggests that the tumour has  
6 a median diameter of approximately 3cm when it metastasises as Stage III or Stage IV cancer. To

1 have 50% sensitivity for detection of early HGSOE (Stage I or Stage II) any screening technique  
2 would have to accurately detect and classify tumours which have a median diameter of  
3 approximately 1.3cm [188]. This represents a mammoth challenge, requiring highly sensitive and  
4 specific blood or serum biomarkers, which has not yet been overcome by modern screening  
5 techniques [189].

6 Screening for ovarian cancer has primarily utilised TVS and CA125 surveillance however, its use  
7 remains controversial. This is due to the low prevalence of the disease, relatively low sensitivity  
8 and specificity of screening techniques and the potential for harm if unnecessary surgery is  
9 performed [190]. As discussed above, the identification of at-risk populations has a significant  
10 impact on reducing their likelihood of developing ovarian cancer. Further, improved identification  
11 of at-risk populations improves screening efforts by focussing resources and reducing the  
12 likelihood of inappropriate treatment. Advanced algorithms are beginning to incorporate several  
13 factors, including single nucleotide polymorphisms (SNPs), epidemiological, life style and  
14 reproductive factors to better individualise ovarian cancer risk prediction [191]. One example of a  
15 clinical tool for ovarian cancer risk prediction is: 'CanRisk', an online tool for clinicians which  
16 facilitates ovarian cancer risk prediction based on clinical and genetic factors [192]. This tool came  
17 into use in March 2021 and reported over 3000 registrations and 98000 ovarian and breast cancer  
18 calculations in the first 9 months of launch [192] but it is still too early to see whether this has a  
19 significant impact on patient survival. A second clinical tool is FORECEE, which characterises  
20 methylation and molecular patterns indicative of breast, cervical and ovarian cancer based on  
21 cervical cytology cells [193] and is currently being utilised in several trials throughout Europe.  
22 While the impact of this tool on detection or survival rates is yet to be seen, there is ongoing  
23 recruitment for a large-scale clinical trial at University College London. Further, utilising this tool  
24 has resulted in the observation that the presence of ovarian cancer, or related risk factors for  
25 disease, were significantly associated with specific cervical microbiota potentially representing a  
26 new avenue for research into the causes of ovarian cancer [194].

27 In recent years significant improvements have been observed in blood based screening approaches  
28 through the use of longitudinal CA125 testing [195] and screening for a panel of serum biomarkers  
29 which includes CA125 [196-199]. Further, risk prediction algorithms are beginning to incorporate  
30 several factors including SNPs, epidemiological, life style and reproductive factors to better  
31 individualise ovarian cancer risk prediction [191].

32 Despite these efforts, randomised control trials have not demonstrated any impact on ovarian  
33 cancer mortality resulting from population level screening of women at average risk of developing  
34 ovarian cancer [189]. As a result, routine screening for ovarian cancer is not currently  
35 recommended in either the UK or USA [200, 201].

36 Into the future, the detection of free tumour DNA harbouring a panel of tumour associated  
37 mutations, in combination with a panel of molecular markers including CA125, holds promise for  
38 improving ovarian cancer early detection [202]. Similar approaches to detecting tumour DNA in  
39 the lower genital tract have also been investigated including endocervical liquid cytology samples  
40 [203], tampons [204] and uterine lavage [205].

### 1 1.3. Treatment of Ovarian Cancer

2 Despite the numerous subtypes of ovarian cancer, with their diverse origins, prognosis and  
3 outcomes, all patients receive similar first line treatment [28]. This is typically comprised of  
4 primary debulking surgery (PDS) in combination with chemotherapy [50]. PDS involves full  
5 exploration of the abdominal cavity and pelvis followed by total abdominal hysterectomy (removal  
6 of the uterus), bilateral salpingo-oophorectomy (removal of both fallopian tubes and ovaries), and  
7 omentectomy (removal of the omentum) [50]. Its purpose is to stage the tumour based on its size  
8 and spread to other organs (Table 2) and to therapeutically resect all macroscopic tumour masses  
9 within the peritoneal cavity [86]. There is a clear correlation between the presence of macroscopic  
10 residual disease after PDS and reduced OS [206] highlighting the clinical importance of surgical  
11 intervention.

12 PDS is followed by combination chemotherapy with a platinum agent (carboplatin (CBP) or  
13 cisplatin) and a taxol (paclitaxel) in almost all cases [207]. This has been the standard treatment  
14 for advanced ovarian cancer since the 1980s [208] and the lack of more recent advances in standard  
15 treatment regimens is reflected in modest improvements in OS over recent decades [209]. Cisplatin  
16 is the most commonly used platinum based chemotherapy historically and has been employed  
17 extensively to treat a range of cancers since its approval in 1978 [210]. However, cisplatin has  
18 significant side effects which limit the concentration that can be used for treatment [211]. The  
19 chemical analogue, CBP, has significantly less side effects and similar efficacy when combined  
20 with paclitaxel and is now the preferred first line treatment of ovarian cancer [28].

21 In recent years the combination therapy of CBP and paclitaxel has been demonstrated to be an  
22 effective treatment in combination with optimal debulking surgery for HGSOE and endometrial  
23 subtypes [50]. Taxanes were first developed in the late 1980s and, by inhibiting tubule  
24 depolymerisation and subsequent stabilisation of the cytoskeleton, impairs the process of cell  
25 division, resulting in mitotic failure and cell death [212]. In the 1990s it was demonstrated that  
26 paclitaxel treatment was effective in patients with advanced and platinum resistant ovarian cancer  
27 [213, 214] and in 1996 a clinical trial demonstrated that paclitaxel, in combination with cisplatin,  
28 significantly improved patient response rates compared to the standard treatment at the time of  
29 cisplatin in combination with cyclophosphamide [215]. Subsequent trials demonstrated similar  
30 efficacy of CBP combined with paclitaxel, coupled with fewer side effects [216-218], and this  
31 combination has been the standard first line treatment for ovarian cancer ever since [92].

32 While the standard chemotherapy has remained unchanged since the early 2000s, there has been  
33 significant focus on optimizing the platinum-taxane treatment regimen [92]. This includes changes  
34 to the paclitaxel treatment schedule which has resulted in improved outcomes in some cases [219,  
35 220] and shown no impact in others [221]. Further, intraperitoneal delivery of chemotherapy, as  
36 opposed to standard intravenous deliver, has been shown to improve patient survival [222]  
37 however increased toxicity and decreased patient tolerability has limited its clinical use [223].  
38 Finally, in cases where the patient is too ill to undergo initial PDS, or whose disease is too extensive  
39 for complete resection, neoadjuvant chemotherapy is an option [86]. This involves administration  
40 of the first half of the full chemotherapy regime before PDS which is then followed by the second  
41 half of the regime [86]. This approach has been associated with increased rates of optimal PDS

1 leaving no residual disease and decreased morbidity and mortality compared to patients with non-  
2 optimal PDS [224].

### 3 *1.3.1. Action of platinum-based chemotherapy*

4 CBP and cisplatin act on the DNA through the formation of mono adducts on the N7 of guanidine.  
5 This then forms a secondary bond to nearby guanidine residues resulting in intra or inter-DNA  
6 crosslinks and disturbance of the double helix. This represents a physical barrier to transcription  
7 and DNA replication, resulting in cell cycle arrest and replicative stress response [225]. This  
8 triggers a DNA damage response (DDR) resulting in interruption of DNA synthesis, the activation  
9 of DNA repair pathways, cell cycle arrest and subsequent apoptotic signalling [226].

10 Cell death in response to DNA damage is mediated through activation of ataxia telangiectasia  
11 mutated (ATM) and RAD3-related protein (ATR), which sense DNA damage, followed by signal  
12 transduction through checkpoint kinase 1 (CHEK1), resulting in TP53 phosphorylation and  
13 stabilization [227]. Once activated, TP53 exerts cytotoxic effects via ‘intrinsic’ or ‘extrinsic’  
14 pathways resulting in cell death [228, 229]. The extrinsic pathway is mediated through Fas cell  
15 surface death receptor (FAS) activation and caspase 8 recruitment [230] while the intrinsic  
16 pathway is mediated through release of cytochrome c as a result of mitochondrial membrane  
17 disturbance through activation of the pore stabilizing proteins; B cell lymphoma 2 (Bcl-2) and B  
18 cell lymphoma-extra-large (Bcl-xL) [231].

19 In addition, these chemotherapeutic agents attack the mitochondria [232]. This results in the  
20 production of reactive oxygen series (ROS) [233] contributing to increased oxidative stress which,  
21 in combination with the inherently increased levels of ROS in cancer cells, can trigger apoptosis  
22 [234]. In addition to apoptosis through intrinsic and extrinsic pathways, increased oxidative stress  
23 can also induce cell death through autophagy where cytoplasmic contents are sequestered and  
24 degraded in lysosomes [235].

25 DNA damage and oxidative stress caused by platinum chemotherapy triggers a complex web of  
26 cellular signalling, which both promote and inhibit cell death. This includes signalling through  
27 mitogen activated protein kinase (MAPK), PI3K, Jun N-Terminal kinase (JNK) and other  
28 pathways (reviewed here: [233]). Beyond this, platinum chemotherapies have been seen to destroy  
29 lysosomes releasing lysosomal proteases and to degrade the endoplasmic reticulum resulting in  
30 increased protein misfolding [232]. Furthermore, damage to the mitochondria and endoplasmic  
31 reticulum has the additional impact of dysregulating calcium homeostasis underpinning the  
32 neurotoxicity seen in patients treated with these agents [232]. There are also numerous proteins  
33 which are directly targeted by CBP including DNA polymerase A, via its zing finger domain [236],  
34 potentially resulting in inhibition of DNA replication subsequently triggering apoptotic pathways.  
35 In addition, platinum reacts with guanosine-5'-triphosphate (GTP), depriving the cell of the energy  
36 source required for microtubule formation which inhibits formation of new cells and mitosis [237].

### 37 *1.3.2. Molecular Targeted Therapy for Ovarian Cancer*

38 With the continued advancement in our understanding of cancer and ability to rapidly characterize  
39 its molecular features, the development of targeted therapies has generated great interest. The use  
40 of molecular targeted therapies is based on the concept that, by understanding the physiology and

1 molecular characteristics of a specific cancer, specific agents and strategies can be developed to  
2 inhibit tumour growth and progression [238]. Molecular targeted anti-cancer agents include a wide  
3 range of compounds, such as antibodies (Abs), small molecules, cancer vaccines and gene therapy  
4 [239]. They can target a range of cancer features including cell growth, cell cycle regulation,  
5 triggering cell death [239], activation of the immune system [240], inhibition of tumour invasion  
6 and progression or sensitization of the tumour the other anti-cancer agents [241].

7 The great strength of molecular targeted therapy is that it acts on a specific weak point of the cancer  
8 in question which can be remarkably effective in treating cancer (reviewed here: [238]). However,  
9 this also represents the great weakness of these treatments. Firstly, many targeted therapies are  
10 only effective in the subgroup of patients whose cancer expresses the target molecule, limiting the  
11 broad application of a specific compound [238]. Further, resistance to these compounds is often  
12 observed. Inherent resistance exists in some cancers, even when they express the biomarker target,  
13 potentially owing to the complexity of cross talk between oncogenic pathways which can  
14 compensate for inhibition of the specific target [242]. Acquired resistance is also common in  
15 response to target treatment, either through changes in the molecular target or compensatory  
16 activity of adjacent pathways [238].

17 The treatment for all subtypes of EOC is uniform despite vastly different treatment responses.  
18 LGSOC and CCOC exhibit very low response rates to initial standard treatment which questions  
19 the continued use of standard chemotherapy and highlights the need for novel treatment  
20 approaches for these ovarian cancer subtypes [50]. The application of targeted therapies has seen  
21 some success in HGSOC however it remains challenging in HGSOC as it rarely presenting with  
22 oncogenic alterations which are easily targetable [90].

### 23 1.3.2.1 CDK4/6 Inhibitors

24 Cyclin Dependent Kinase 4/6 (CDK4/6) is a protein complex which is required for the  
25 phosphorylation of retinoblastoma protein 1 (RB1) which subsequently triggers the transcription  
26 of genes required for progression through the S phase of the cell cycle. Therefore, inhibition of  
27 CDK4/6 prevents the transition from G1 to S phase resulting in cell cycle arrest (reviewed here:  
28 [243]). Treatment with CDK4/6 inhibitors have shown promise in several cancer types [244-249],  
29 including successful phase 3 trials in metastatic breast cancer resulting in Food and Drug  
30 Administration (FDA) approval of three CDK4/6 inhibitors, Palbociclib, Ademaciclib and  
31 Ribociclib, for treatment of metastatic breast cancer [250, 251].

32 For HGSOC, CDK4/6 inhibitors have showed some promise in *in vitro* studies, albeit with the  
33 development of resistance mechanisms reported [252]. In combination with cisplatin, CDK4/6  
34 inhibition with Ribociclib has shown growth arrest *in vitro* and significant tumour growth delay in  
35 platinum sensitive tumour xenografts [253]. Importantly, ribociclib treatment demonstrated a  
36 synergistic effect when applied to cell lines after cisplatin treatment [253], potentially owing to the  
37 role of CDK4/6 in DNA damage repair [254] representing a possible combination therapy.

38 Further to this, there have been recent studies into combination therapy with both PARP inhibitors  
39 [255] and CDK4/6 inhibitors [256] which show promising, albeit preliminary, results.  
40 Mechanistically, synergistic activity of PARP and CDK4/6 inhibitors is thought to result from

1 CDK4/6 inhibition impacting MYC-regulated HR repair pathway genes. This is reflected in the  
2 observation that increased growth inhibition, in response to combination PARP inhibitor and  
3 CDK4/6 inhibitor treatment, correlated with increased MYC expression [257]. There is also  
4 interest in the combination of immunotherapy with CDK4/6 inhibitors based on the observation  
5 that CDK4/6 inhibition have significant immunomodulatory effects including increasing cluster of  
6 differentiation 8 positive (CD8+) T-cell infiltration and reduced regulatory T cell proliferation  
7 [258, 259]. Combination treatment with Ademaciclib and anti-programmed cell death protein 1  
8 (PD-1) monoclonal Abs, have shown efficacy in mouse models of ovarian cancer [256] reflecting  
9 the potentially synergistic actions of immune check point inhibition and CDK4/6 inhibitors.

#### 10 1.4. Molecular Mechanisms of Chemoresistance to Platinum Based Chemotherapy

11 The National Comprehensive Cancer Network (NCCN) separates platinum sensitive recurrence  
12 (PSR) from platinum resistant recurrence (PRR) based on the time between first treatment and  
13 patient relapse. If relapse occurs more than 6 months after first chemotherapy treatment then the  
14 patient has PSR while if they relapse less than 6 months after first treatment they have PRR [260].  
15 This information can be combined with other predictors, such as age, disease stage, histology, and  
16 residual disease, to provide a prediction of future treatment sensitivity and patient survival in a  
17 process called a nomogram [261]. A nomogram is a graphical calculating device, a two-  
18 dimensional diagram designed to allow the approximate graphical computation of a mathematical  
19 function. At present, these nomograms do not include genomic or molecular  
20 information/classification, which represents an important gap in the prediction of chemotherapy  
21 response and patient survival.

22 The difference between PSR and PRR is reflected in the observation that HGSOC patients with  
23 PSR typically respond well to a second round of treatment with platinum based chemotherapy  
24 [262]. However, most patients eventually relapse with platinum resistant disease [262]. It is  
25 expected that this outcome reflects acquired resistance to chemotherapy while PRR patients  
26 possess inherent resistance. While these two categories of resistance pathways are sometimes  
27 difficult to distinguish, they are broadly described as follows: Inherent resistance is the innate  
28 ability of cancer cells to survive and persist through their first expose to treatment. In contrast,  
29 acquired resistance represents the evolution of cancer cells in response to exposure to treatment  
30 eventually achieving a state where cells can survive and proliferate despite subsequent therapies  
31 [263-265]. Regardless, resistance can be seen as developing through clonal selection resulting  
32 from survival advantages acquired by the cell, often through environmental or molecular features  
33 which promote survival in response to therapeutic challenge [266, 267]. While there are  
34 environmental factors which can contribute to chemoresistance in ovarian cancer, such as for  
35 example poor vascularisation [268], extracellular matrix interactions and secreted factors [269],  
36 these are beyond the scope of this thesis and are comprehensively reviewed here [270].

37 CBP acts to kill cancer cells through a highly complex interplay of drug with cellular targets and  
38 subsequent pro death signalling. As a result, the molecular features of chemoresistance are equally  
39 complex. In brief they include inhibition of drug influx, increased drug efflux, cytoplasmic  
40 detoxification, alterations in apoptosis pathways, DNA repair and increased response to ROS  
41 production [271].



#### 1 **1.4.1. Altered drug influx and efflux**

2 As described above, platinum-based chemotherapeutics perform their therapeutic activity through  
3 interaction with DNA and cytosolic components of the cell. In platinum resistant cancer cells,  
4 decreased drug accumulation can impair the formation of DNA adducts and low cellular  
5 concentration of platinum is significantly associated with tumour response [272, 273]. As a result,  
6 effective influx, and limited efflux of therapeutics is essential for sufficient drug accumulation and  
7 subsequent anti-cancer activity [274].

8 Inhibition of drug influx has long been recognised as a common feature of platinum resistant cells  
9 [275] and, as early as 2002, high affinity copper uptake protein 1 (Crt1) was identified as a major  
10 mediator of cisplatin uptake in yeast and mouse cells [276]. The expression of this protein is  
11 closely linked to extracellular copper concentrations where excess copper triggers endocytosis and  
12 degradation of Crt1 [277]. This is reflected in the early observation that cellular copper  
13 concentration was associated with cellular cisplatin concentration [278] and that pre-treatment of  
14 cells with copper resulted in cisplatin resistance in a Crt1 dependent manner [276]. In addition,  
15 high Crt1 expression is associated with favourable OS, PFS, disease free survival (DFS) and  
16 treatment response [274] in several cancers, including ovarian [274]. One study demonstrated that  
17 that upregulation of Crt1 expression through administration of the copper chelating agent,  
18 tetrathiomolybdate, enhances the cytotoxic effect of cisplatin on human cervical and ovarian  
19 cancer cells *in vitro* [279]. This was further supported in a clinical trial demonstrating the 20% of  
20 platinum resistant patients responded to platinum after receiving copper chelators [280]. However,  
21 it has been shown that cisplatin can induce rapid degradation of Crt1 through ubiquitin mediated  
22 proteolysis [281] and that, while Crt1 is responsible for 60-70% of cellular uptake of cisplatin, it  
23 is only responsible for 30-40% of cellular uptake of carboplatin [282, 283].

24 Two other copper transporters, ATPase copper transporting alpha 7A (ATP7A) and ATPase  
25 copper transporting alpha 7B (ATP7B), are the primary proteins responsible for platinum efflux  
26 [284] and have been functionally implicated in resistance to both cisplatin and carboplatin [285-  
27 289]. The primary physiological function of these proteins is to transport copper into the lumen of  
28 the trans-Golgi network to facilitate the biosynthesis of copper-dependent enzymes and export of  
29 excess copper out of the cell via sequestration into exocytic vesicles [290]. The analysis of mRNA  
30 expression of 55 transporter genes of 60 ovarian cancer cell lines revealed that ATP7B mRNA  
31 expression level has the highest correlation with cisplatin sensitivity [291]. The silencing of  
32 ATP7B has been demonstrated to increase sensitivity to cisplatin *in vitro* and the silencing of  
33 ATP7A resulted in increased sensitivity to cisplatin in a mouse model of ovarian cancer [292].  
34 Despite this, a meta-analysis did not find a significant relationship between expression of ATP7A  
35 or ATP7B with OS, PFS, DFS or treatment response [274]. The action of these proteins in the  
36 binding and exportation of platinum agents, and their contribution to platinum resistance in ovarian  
37 cancer, is complex and still not well understood but is comprehensively reviewed here [293].

38 While the above-described influx and efflux proteins have a significant impact on intracellular  
39 concentrations of platinum agents, there are several other proteins which contribute to platinum  
40 concentrations within the cell. These are beyond the scope of this thesis but are comprehensively  
41 reviewed here [294].

#### 1 **1.4.2. Intracellular Detoxification of Platinum Compounds**

2 Once in the cell, there are multiple mechanisms which act on platinum-based chemotherapeutic  
3 agents to inhibit their activity and protect the cell. For example, glutathione (GSH) which plays  
4 the physiological role of scavenging free radicals, defending cells against xenobiotics and  
5 maintaining the sulfhydryl groups of many proteins [295]. This metabolite has a high affinity for  
6 platinum [296] competitively inhibiting platinum binding to DNA as reflected in elevated  
7 expression of GSH, and glutathione-S-transferase, often seen in resistant cells [297, 298].  
8 Therapeutic interventions have sought to prevent the interaction between GSH and platinum,  
9 through competitive inhibitors of GSH [299], and interfere with GSH synthesis through inhibition  
10 of enzymes which mediate its synthesis [300]. While inhibition of  $\gamma$ -glutamylcysteine ligase, an  
11 essential enzyme in GSH synthesis, reduces cisplatin resistance in malignant glioma [300], non-  
12 specific GSH depletion can cause significant side effects in normal tissue [294]. Selective GSH  
13 depletion holds great potential in reducing platinum resistance however this remains a significant  
14 challenge [301].

15 Platinum anti-cancer drugs can also be inactivated by interaction with metallothionein (MT)  
16 proteins [294]. The high proportion of cysteine residues in MT results in platinum preferentially  
17 chelating with proteins [302]. Platinum agents have been seen to bind metal transcription inhibitor,  
18 releasing metal transcription factor 1 to bind DNA and trigger the transcription of MT [303].  
19 Studies have suggested that certain isoforms of MT may be valuable prognostic predictors [304]  
20 and that MTs are regulated by miRNAs [305] representing a potential therapeutic strategy.

#### 21 **1.4.3. DNA Repair**

22 There are multiple DNA repair mechanisms involved in the response to platinum mediated DNA  
23 damage (reviewed here: [225]). DNA damage caused by platinum agents is primarily repaired by  
24 nucleotide excision repair (NER) system and facilitated by the related genes DNA repair protein  
25 complementing XP-A (XPA) and BRCA1 [306, 307]. This process recognises areas of DNA  
26 damage, unwinds the DNA helix, and then excises the damaged region. Finally, DNA polymerase  
27 resynthesises the excised region from the complementary DNA strand [308].

28 The cellular status of HR is the strongest predictor of chemoresistance status in ovarian cancer  
29 [78]. This process employs the redundancy of genetic information in sister chromatids in responds  
30 to double stranded (DS) breaks in the DNA [309]. In brief, upon a DS break in one chromatid the  
31 sister chromatid is used as the guide strand for the synthesis of new DNA to repair the break. This  
32 process is complex and multifaceted and is reviewed here: [309]. Most HGSOc are HR deficient,  
33 often mediated through mutations in BRCA1/2 genes [81], facilitating genetic instability which  
34 promotes cancer development but also triggering CBP sensitivity. Restoration of HR, through  
35 reversion of BRCA1/2 mutations, have been seen to give rise to chemoresistance in this context  
36 [310]. The full breadth of DNA repair mechanisms in response to platinum-based insult is complex  
37 and further details are beyond the scope of this thesis. It has been extensively reviewed here: [225]

#### 38 **1.4.4. Apoptosis signalling**

39 P53 plays a tumour suppressive role in healthy cells by promoting apoptosis in response to DNA  
40 damage through both the intrinsic and extrinsic pathways [311]. It triggers the intrinsic,  
41 mitochondrial, apoptotic pathway through triggering the expression of numerous pro apoptotic

1 proteins and inhibiting the expression of anti-apoptotic ones [312, 313]. Furthermore, P53 controls  
2 the expression of proteins involved in numerous steps of the intrinsic, receptor mediated, apoptotic  
3 pathway including the development of Fas ligand (FasL) [311]. Not surprisingly, cells with p53  
4 mutations [314] or deletions [315] are resistant to cisplatin.

5 Apoptosis is controlled by the balance of pro and anti-apoptotic proteins. If this balance is tipped  
6 in favour of pro apoptotic signalling, then pores in the mitochondrial membrane are formed  
7 releasing numerous effector molecules and triggering an apoptotic cascade resulting in cell death  
8 [316, 317]. This balance is influenced by numerous signalling pathways, for example;  
9 overactivation of the PI3K pathway, resulting in increased anti apoptotic protein activation [318],  
10 and up regulation of heat shock proteins (HSPs), which directly inhibit the intrinsic apoptotic  
11 pathway [319], both contribute to chemoresistance.

12 Further drivers of chemoresistance are highly complex and cannot be fully described here  
13 (reviewed here: [320]) but include altered autophagy [321], miRNA expression [322] and  
14 epigenetic alterations [323]. Some of the epigenetic changes which drive CBP resistance include  
15 chromatin remodelling [324], DNA methylation [325] and histone modifications [326]. This  
16 results in the downregulation of genes required for cytotoxicity such as the pro apoptotic signalling  
17 pathways described above and is reviewed here: [323].

#### 18 **1.4.5. Metabolism in Chemoresistance**

19 It is well understood that some cancer cells have altered metabolism compared to healthy tissue  
20 best characterised by the 'Warburg effect', where an increased energy demand in cancer cells is  
21 met through upregulated glycolysis [327]. This contributes to the increased synthesis of  
22 biomolecules and increased proliferation which maintains the tumour in poorly vascularized  
23 microenvironments [328]. This can lead to increased acidity within the microenvironment, due to  
24 increased lactate production, and promotes migration and invasion [329, 330].

25 Increased glycolysis in this context results from altered signalling, such as the stabilization of  
26 hypoxia inducible factor 1 $\alpha$  (HIF-1 $\alpha$ ) [331], activation of PI3K pathways [332] and dysregulated  
27 p53 signalling [333], which have the additional role of promoting cell survival, growth and  
28 metastasis [334]. These pathways can be triggered by reduction in mitochondrial respiration or  
29 mitochondrial dysfunction [335, 336] creating complex feedback mechanisms controlling the  
30 balance between glycolysis and oxidative phosphorylation (OXPHOS).

31 The alterations in these signalling pathways are just one of several avenues through which altered  
32 metabolism contributes to chemoresistance [337, 338], most commonly via an altered redox state  
33 [339-341]. Resistance to ROS mediated apoptosis can be mediated via increased survival  
34 signalling [342], increased detoxification of ROS through glycolytic metabolism intermediaries,  
35 such as glycolytic pyruvate [339, 340], reduced ROS production due to decrease mitochondrial  
36 respiration [343] and increased production of antioxidants [342].

37 An example of a direct connection between glycolysis and increased cell survival is hexokinase, a  
38 glycolytic enzyme which binds voltage dependent anion channel (VDAC) at the mitochondrial  
39 membrane [344]. This process utilises intra-mitochondrial adeno triphosphate (ATP) for the  
40 phosphorylation of glucose facilitating rapid glycolysis [345]. It has the additional effect of

1 stabilising the mitochondrial membrane and preventing pro apoptotic proteins from binding to  
2 VDAC and triggering mitochondrial membrane permeabilization [346] thereby directly inhibiting  
3 the intrinsic apoptotic pathway.

4 OXPHOS and the mitochondria remain essential for effective bioenergetics, biosynthesis and  
5 signalling in cancer cells [347, 348]. Further, chemo resistant ovarian cancer cells have been  
6 observed to have a particular reliance on OXPHOS [349]. This is potentially driven by the reliance  
7 on OXPHOS by quiescent ovarian cancer cells [350] which, due to their reduced DNA synthesis,  
8 are inherently resistant to CBP toxicity [86].

### 9 1.5. Unique Features of HGSOC Metastatic Progression

10 Metastasis is the process by which cancer cells detach from the primary tumour and disseminate  
11 to surrounding tissue and distant organs [351]. This process is the primary cause of cancer related  
12 mortality and is responsible for over 90% of cancer related deaths [352, 353]. Ovarian cancer is  
13 unusual in that it rarely disseminates via the vasculature but instead disseminates to the  
14 peritoneum, via the peritoneal fluid, [354] with tumours detected in the fallopian tubes, uterus and  
15 contralateral adnexa [355].

#### 16 1.5.1. *Malignant Ascites*

17 Under normal physiological conditions, peritoneal fluid is in constant flow, mediated by secretion  
18 via the peritoneal capillaries and drainage through lymphatic vessels. However, in the case of  
19 ovarian cancer, elevated expression of vascular endothelial growth factor (VEGF) results in  
20 increased vascular permeability [356] and lymphatic drainage vessels can be blocked by cancer  
21 cells [355]. This results in the accumulation of peritoneal fluid within the peritoneal cavity creating  
22 malignant ascites. Ascites arises in almost all cases of recurrent ovarian cancer [357] and  
23 represents a microenvironment rich in pro-tumorigenic signals which act to promote cancer  
24 growth, survival, invasion and chemotherapy resistance [358, 359]. Ascites is a hypoxic [360] and  
25 glucose deprived environment [361], promoting altered cellular pathways and metabolism in  
26 HGSOC. In addition to cancer cells, several other cell types, which promote tumour growth and  
27 invasion, have been detected in ascites, such as tumour associated fibroblasts, mesenchymal stem  
28 cells, mesothelial cells and platelets [362, 363]. The presence of ascites in ovarian cancer is a sign  
29 of advanced, high volume disease [173] and is a negative prognostic marker [364] and are routinely  
30 drained to provide relief from debilitating symptoms [365].

#### 31 1.5.2. *Multicellular Tumour Spheroids in Ovarian Cancer Progression*

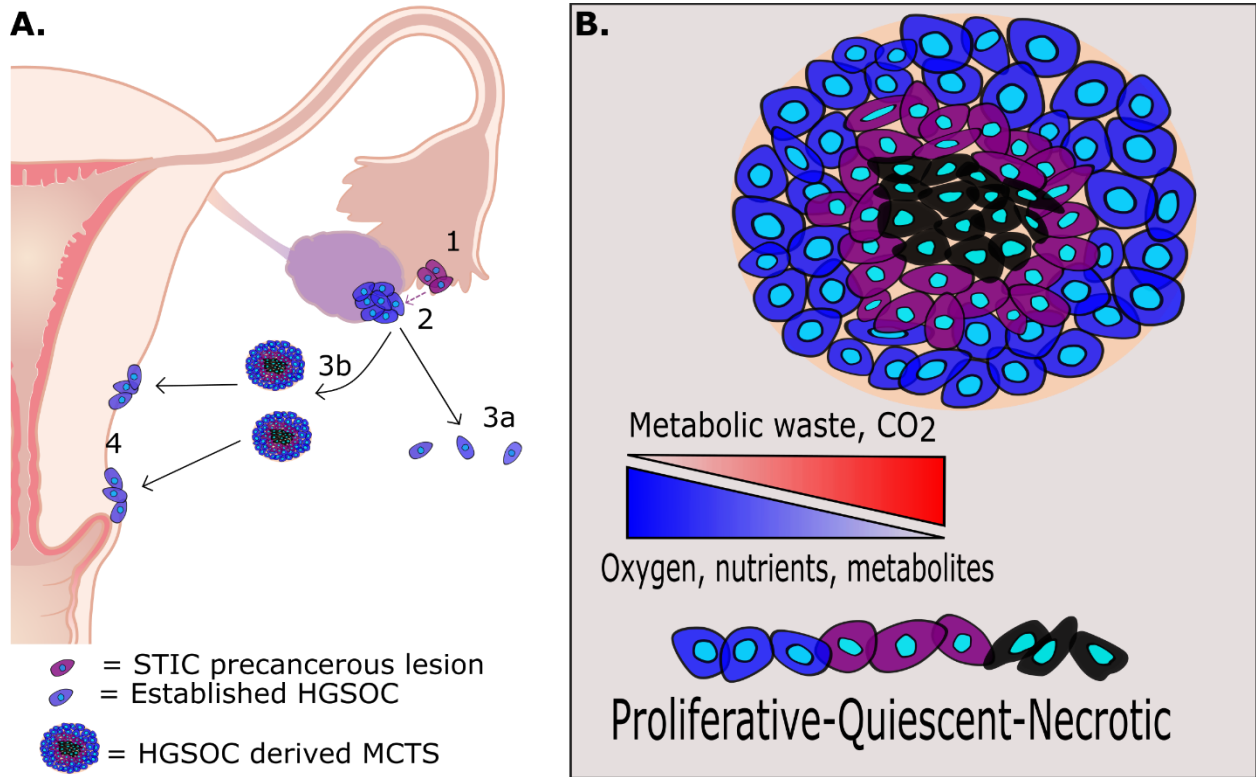
32 Within the ascites EOC cells often exist as multicellular aggregates called ‘ multicellular tumour  
33 spheroids’ (MCTS) [366]. These MCTS have been shown to resist anoikis [367], exhibit increased  
34 chemo resistance *in vitro* [368, 369] and are highly tumorigenic *in vivo* [370]. They have also been  
35 shown to re-attach to adherent surfaces *in vitro* [371, 372] and are predicted to mediate metastasis  
36 to other abdominal organs [373]. It is suggested that initiation of spheroid formation may rely on  
37 chemotactic signals, for example hepatocyte growth factor, which subsequently trigger up-  
38 regulation of cell adhesion molecules, including fibronectin, resulting in increased adhesion  
39 between cells [374].

1 The MCTS structure provides a survival advantage to the cancer cells contained within. For  
2 example, MCTS have been seen to be less sensitive to anti-tumour immune effector molecules  
3 including complement and antibodies [375, 376]. Further, tumour cells within MCTS often lack  
4 FasL, inhibiting the action of FAS-bearing immune cells [377]. In addition, the up regulation of  
5 the anti-apoptotic protein, BCL-xL, has been observed in MCTS and represents another pro-  
6 survival feature of these structures [378].

7 It has been demonstrated that MCTS have three distinct layers; a proliferating outer layer,  
8 quiescent inner layer and a necrotic core [379], which are a result of nutrient, oxygen, pH, CO<sub>2</sub>  
9 and metabolic waste gradients within the structure [379] (Figure 2). It has been estimated that less  
10 than 40% of cells within spheroids are proliferative [380]. Although the exact mechanism by which  
11 MCTS formation protects cells from chemotherapy has not been fully elucidated, inhibited  
12 diffusion of drugs, the maintenance of a quiescent population within the spheroids, expression of  
13 pro survival genes as a result of cell-cell contact and paracrine/autocrine signalling [378] have  
14 been suggested as likely mechanisms. This is supported by studies demonstrating that disruption  
15 of cell-cell contacts sensitises spheroids to chemotherapy treatment *in vitro* [381]. It has been  
16 proposed that MCTS represent a chemotherapy resistant niche which can reseed the tumour after  
17 chemotherapy. This is supported by the observation that the MCTS structure confers several  
18 survival advantages and that they have increased capacity to interact with extracellular matrix  
19 (ECM) components and mesothelial cells [382] facilitating invasion and metastatic implantation  
20 into distant mesothelium. In summary, MCTS are of great clinical interest for the effective  
21 treatment of ovarian cancer due to their predicted role in chemotherapy resistance and mediating  
22 metastasis.

23

24



1 **Figure 2:** Malignant progression of high grade serous ovarian carcinoma (HGSOC) and cellular  
2 populations within multicellular tumour spheroids (MCTS). (A) Malignant progression of HGSOC: 1)  
3 STIC precancerous lesions develop within the fimbriae of the fallopian tube. 2) At an undetermined stage  
4 the STIC lesions translocate to the ovary and establish a neoplastic HGSOC tumour. 3a) Single cells shed  
5 from the primary HGSOC tumour and undergo anoikis in the peritoneal cavity. 3b) Shed HGSOC cells  
6 form together in MCTS to overcome anoikis and remain viable in the peritoneal cavity. 4) MCTS facilitate  
7 the metastatic spread of HGSOC to adjacent organs including the peritoneal wall. (B) The cellular  
8 populations within a MCTS including proliferative out layer (blue), quiescent inner layer (purple) and  
9 necrotic core (black). These populations arise in response to the metabolic waste, gas, and nutrient  
10 gradient present within the MCTS structure. (Adapted from M. Acland, et al. 2018 [383])

### 11 1.5.3. *In vitro* Multicellular Tumour Spheroids as a Biological Model of Solid Tumours

12 Distinct from ascites derived MCTS, which develop *de novo* during the malignant progression of  
13 ovarian cancer, are *in vitro* MCTS. They represent a powerful *in vitro* model which closely  
14 replicate many features of the avascularised tumour [384-387], such as cell-cell and cell-ECM  
15 connections [388, 389], and distinct proliferative layers resulting from gas and nutrient gradients  
16 [379].

17 The relevance of *in vitro* MCTS is supported by the observation that they are more tumorigenic  
18 than single cells when utilised in mouse xenograft models [390], exhibit greater resistance to most  
19 anti-cancer agents [381, 391-393], possess several cancer biomarkers [394, 395] and exhibit gene  
20 expression which more closely replicates solid tumours when compared to the same cells grown  
21 as monolayers [396-399].

1 The simplest form of *in vitro* MCTS is formed from homogeneous cell populations which  
2 spontaneously form MCTS structures when they are prevented from anchoring to tissue culture  
3 plastic and represent a high throughput model which replicates several features of avascularised  
4 tumours. However, these simple models are not capable of replicating several features of solid  
5 tumours including heterogeneous cell populations, paracrine and endocrine signalling, and  
6 immune cell interactions, among others. There are many efforts to overcome these shortcomings  
7 including co-culture MCTS [390] and replication of *in vivo* signalling [400].

## 8 1.6. Mass Spectrometry Overview

9 Mass spectrometry (MS) has established itself as an effective technique for the investigation,  
10 identification and quantification of a diverse range of biological molecules [401]. It holds the  
11 advantageous properties of being able to investigate a particular molecular class within a sample  
12 in an unbiased manner. Further to this, it can provide a deep characterisation of the molecular  
13 features of a sample at a single point in time and provide relative quantification of molecular  
14 abundance. This versatile technique has previously been employed in the investigation of cancer  
15 biomarkers [402-405], prediction of chemotherapy response [406-410], and the biology of cancer  
16 progression [411] among many other areas of research.

17 Most commonly, MS is used to investigate proteins in biological settings, but it is also routinely  
18 used to investigate metabolites and post translational modifications (PTMs) on proteins, primarily  
19 phosphorylation and glycosylation. In this thesis we utilise MS for proteomic and metabolomic  
20 analysis of samples of interest and, for this reason, MS analysis of PTMs will not be discussed  
21 further although they are reviewed here [412].

### 22 1.6.1. Mass Spectrometry Proteomics

23 Proteins are responsible for most cellular processes and their composition, localisation and  
24 interactions underpin the dynamic processes of cellular function [413]. While traditional analyses  
25 of genomics and transcriptomics have greatly contributed to the understanding of cancer biology,  
26 they do not necessarily reflect the cellular phenotype. This is reflected in the, now well established,  
27 observation that the transcriptome does not necessarily correlate with protein abundance [414,  
28 415]. The power of proteomics is demonstrated by the observation that the expression, abundance,  
29 and chemical nature of proteins, as the functional molecule of the cell, represents a highly accurate  
30 reflection of the cellular phenotype.

31 Through specific sample preparation, data acquisition and data analysis methods (as described in  
32 Chapter 2) MS can provide identification and relative quantification of thousands of proteins from  
33 a relatively small amount of cellular material. In recent years, proteomic MS has advanced to allow  
34 large scale, deep proteomic analysis in a short period of time [416], from miniscule amounts of  
35 cellular material [417] and in long stored biological samples such as those from formalin fixed  
36 paraffin embedded (FFPE) tissue [418].

### 37 1.6.2. Mass Spectrometry Metabolomics

38 Metabolites are small molecules which participate in metabolic reactions which are necessary for  
39 cellular function, maintenance and growth [419]. There are more than 100000 predicted,  
40 expected and known human metabolites [420] and, as metabolites are the final response of a

1 biological system to environmental change or gene regulation, the metabolome is highly  
2 predictive of phenotype [419, 421].

3 Unlike proteins, which are all formed from the same building block, the amino acid, metabolites  
4 have a vast range of chemical properties. This diversity means that no single method can capture  
5 and analyse the entire metabolome at once [422]. A range of sample preparation, data acquisition  
6 and data analysis techniques are utilised to investigate a specific metabolite class in each  
7 experiment.

8 MS analysis of the metabolome is an emerging technology which has received great interest in  
9 recent years. This technique can capture the metabolomic profile of a given sample at a defined  
10 point in time to provide phenotypical information about the sample.

### 11 **1.6.3. Utilising Mass Spectrometry for Pan Omics Analysis**

12 MS investigations of proteins and metabolites provide significant insight into the molecular  
13 features of cells and disease states. However, these techniques alone are unable to capture the full  
14 complexity of the molecular features of cancer. In Chapter 4 we combine MS proteomics and  
15 metabolomics in a multiomics approach to characterising the molecular signature of  
16 chemoresistance in ovarian cancer cells. The combination of these omics technologies provides a  
17 deeper and more comprehensive picture of the molecular features of the cell. There is currently  
18 great interest in the combination of multiple omics approaches, including the use of MS based  
19 techniques, to provide truly comprehensive and biologically relevant information about a cellular  
20 state in an approach called ‘panomics’ [418].

## 21 **1.7. Our Approach**

22 For this thesis I have explored mass spectrometry approaches to discover new insights into early  
23 OC development, OC spheroids and drug accumulations, and chemoresistance of immortal and  
24 primary OC cells. Research into these features hold the potential to contribute to early detection,  
25 development of novel anticancer agents and advising personalised treatment regimes.

26 These mass spectrometry-based approaches was performed with a focus on improving techniques  
27 to investigate biologically important features of ovarian cancer, particularly HGSOV, and  
28 improving understanding of the molecular features which underpin the important events in its  
29 progression. This takes the form of developing methods to investigate precancerous lesions,  
30 understanding cancer development through analysis of these lesions, characterising the proteome  
31 and metabolome of chemoresistant ovarian cancer cells, reviewing MS based analyses of MCTS  
32 and utilising *in vitro* MCTS as a biological model to test novel anti-cancer compounds.

## 33 **1.8. Aims of the Thesis**

34 The research presented in this thesis aims to provide a systematic investigation of ovarian cancer  
35 through development, progression, and treatment response. Further, our research explores the  
36 importance of MCTS in ovarian cancer progression and utilises *in vitro* MCTS as a model for  
37 testing anti-cancer compounds. More specifically, the thesis was designed to achieve the  
38 following aims:



1 **Aim 1:** To establish techniques which can provide a molecular insight into the early  
2 development of high grade serous ovarian cancer.

3 This research has been summarized, submitted and presented in chapter 2

4 **Aim 2:** To investigate the molecular features of precancerous lesions of the endometrium and  
5 fallopian tube to characterise their relation to ovarian and endometrial cancer and related  
6 neoplastic or migratory potential.

7 This research has been summarized, published, and presented in chapter 3

8 **Aim 3:** To comprehensively investigate the metabolomic and proteomic features of chemo  
9 resistant high grade serous ovarian cancer.

10 This research has been summarized, published, and presented in chapter 4

11 **Aim 4:** To investigate the proteomic features of MCTS that contribute to progression and  
12 treatment resistance of HGSOE and investigate the spatially defined molecular features of  
13 MCTS.

14 This research has been summarized, published, and presented in chapter 5

15 **Aim 5:** To establish methods of measuring the penetration of novel anti-cancer compounds into  
16 the MCTS model using MALDI MSI.

17 This research has been summarized and presented in chapter 6

18

19

20

21

22

23

24

25

26

27

28

29

30

31

1  
2  
3  
4  
5  
6  
7  
8  
9  
10  
11  
12  
13  
14  
15  
16  
17  
18  
19  
20  
21  
22  
23  
24  
25  
26  
27

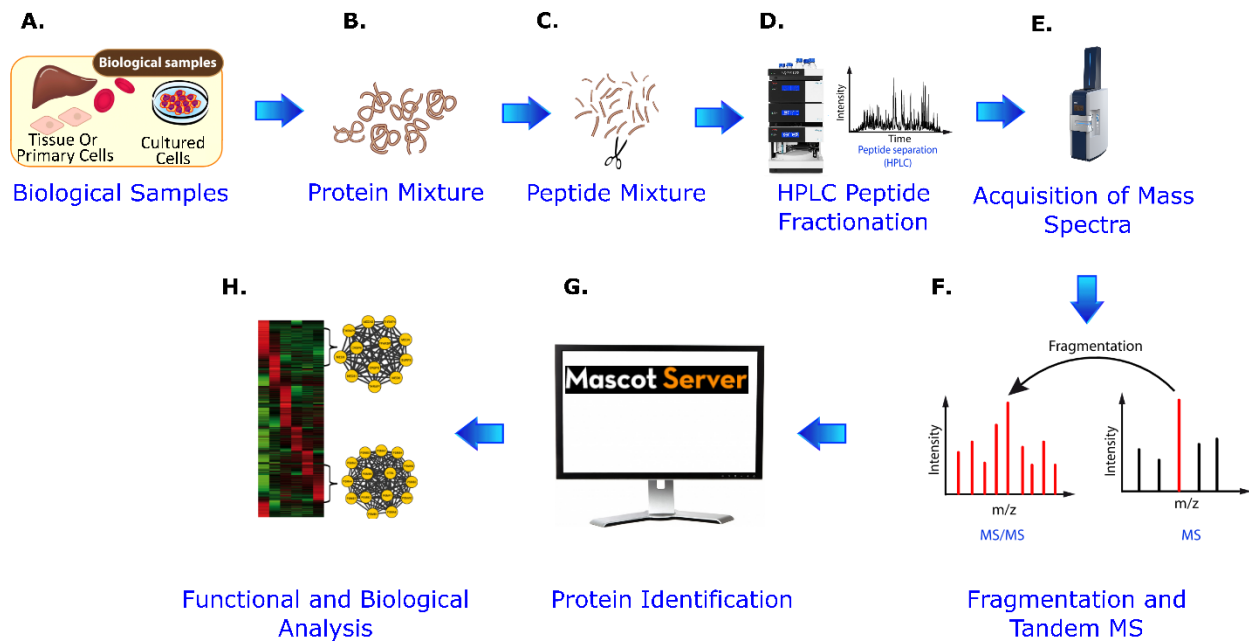
# CHAPTER 2: MATERIALS AND METHODS

---

1  
2  
3  
4  
5  
6  
7  
8  
9  
10  
11  
12  
13  
14  
15  
16  
17  
18  
19  
20  
21  
22  
23  
24  
25  
26  
27  
28

This page is intentionally left blank

1 2.1. Summary of Mass Spectrometry (MS) Proteomics Methodology  
 2 There are numerous methods for MS sample preparation depending on the molecule of interest,  
 3 the sample, and the purpose of the experiment. Below we outline the methodology for a standard  
 4 bottom up (sometimes referred to as ‘shotgun proteomics’) MS proteomic experiment. While these  
 5 steps can be modified to achieve specific outcomes, they generally utilise the following workflow:  
 6 1) sample acquisition, 2) sample preparation, 3) data acquisition, 4) data analysis, 5) functional  
 7 analysis (figure 3).



8  
 9 **Figure 3:** Flow diagram of the standard process for proteomic mass spectrometry analysis of biological  
 10 samples. (A) Samples are collected, typically from cell culture, liquid, or solid biopsies. (B) Biological  
 11 samples are lysed, proteins are isolated and undergo reduction and alkylation. (C) Proteins are digested with  
 12 proteolytic enzymes resulting in a peptide mixture. (D) Samples are fractionated with high performance  
 13 liquid chromatography. (E) Samples are entered into the mass spectrometer providing mass spectra, and  
 14 relative quantification of abundance, for each analyte within the sample. (F) Within the mass spectrometer,  
 15 analytes are selected for fragmentation and tandem MS analysis. (G) Application of data base matching to  
 16 identify proteins within the sample based on the mass spectra acquired. (H) Functional analysis of identified  
 17 proteins of interest to understand altered biological processes or signalling pathways.

18 **2.1.1. Sample Acquisition**

19 One of the advantages of MS based molecular investigations is that it can be applied to a wide  
 20 range of sample types, including those which have been stored for extended periods of time.  
 21 Common sample sources include cell culture, patient derived cells, preserved tissue, blood, and  
 22 plasma. Each of these sample types require specific preparation for MS analysis including cell  
 23 lysis and arrest of biological processes. In the following manuscripts and publications, we utilise  
 24 a range of ovarian cancer samples for MS investigation including FFPE stored ovarian cancer  
 25 tissue, primary ovarian cancer cells maintained in culture and ovarian cancer cell lines.

### 1 **2.1.2. Sample Preparation**

2 Various techniques are employed to isolate the target molecules from the sample of interest, for  
3 example the antigen retrieval from FFPE tissue described in chapter 2 or the laser capture  
4 microdissection method described in chapters 1 and 2. Following this, specific sample preparation  
5 protocols are employed for the molecule of interest.

6 In the case of proteomics this commonly involves reduction (to break disulfide bonds) and  
7 alkylation (to prevent re-establishment of broken disulfide bonds) followed by digestion into  
8 peptides. Digestion typically employs Lys-C and trypsin [423] which specifically cleave proteins  
9 at defined amino acid residues producing a defined set of peptides which can be identified by  
10 search algorithms in subsequent steps.

### 11 **2.1.3. Data Acquisition**

12 There are a wide range of MS equipment and data acquisition approaches, the extent of which are  
13 beyond the scope of this thesis (reviewed in [401], see [424] for the theoretical basis of MS  
14 instruments). One major challenge of investigating proteins is the inability to amplify them, unlike  
15 genomic material which can be amplified via polymerase chain reaction (PCR). As a result, high  
16 abundance analytes mask the presence of low abundance, but potentially biologically relevant,  
17 analytes in the same sample through the process of ‘ion suppression’ [425]. To overcome this,  
18 most MS workflows incorporate a fractionation process, commonly achieved through  
19 chromatography. High performance liquid chromatography (HPLC) is routinely coupled to MS  
20 instruments and, while there are several different types (reviewed in [426]), we will describe  
21 ‘reverse phase chromatography’ as an example. In this process the sample is passed through a  
22 column containing a non-polar material (stationary phase) which binds to the sample. An aqueous,  
23 moderately polar, liquid (mobile phase) is then passed through the column facilitating elution of  
24 molecules off the column. More polar molecules have a lower affinity for the stationary phase and  
25 elute first while less polar molecules elute after resulting in a separation of molecules in the sample  
26 based on their hydrophobicity. Typically, the non-polar content of the mobile phase is increased  
27 gradually over time, facilitating the complete elution of all molecules [426].

28 Once fractionated, molecules are charged through an ionisation source. Commonly utilised  
29 ionisation sources include electrospray ionisation (ESI) and matrix assisted desorption/ionisation  
30 (MALDI) [425, 427], although MALDI ionisation is typically performed without prior  
31 fractionation via LC. They then enter a ‘mass analyser’ where ions are separated based on their  
32 mass to charge ( $m/z$ ) ratio in the presence of an electric or magnetic field. Finally, the amount of  
33 each species with a specific  $m/z$  value are measured [401].

34 After measurement of an analyte at a particular  $m/z$  it can then be isolated for tandem mass  
35 spectrometry analysis ( $MS^2$ ) with the purpose of acquiring structural information about the analyte.  
36 This isolation is achieved through different methods depending on the instrument (reviewed in  
37 [424]) but results in the isolation of all analytes with a defined  $m/z$ . This isolated analyte is then  
38 fragmented, commonly through collision induced dissociation (CID), where an inert gas, typically  
39 helium, is brought into contact with the analyte of interest resulting in fragmentation of the analyte  
40 [424]. These fragments then enter the mass analyser providing a mass spectrum for each fragment  
41 of the selected  $m/z$  facilitating up to amino acid level characterisation of a peptide of interest.

#### 1 2.1.4. *Data Analysis*

2 A typical proteomic LC-MS/MS experiment can provide characterisation and relative  
3 quantification of tens of thousands of peptides. To understand the proteins which these peptides  
4 derive from, data base searching is performed through platforms such as SwissProt (reviewed in  
5 [401]). These data based utilise data from  $m/z$  ratios, LC retention times and fragmentation spectra  
6 which are then matched against the data base of to provide protein identification. The relative  
7 abundance of the measured peptides provides quantitative information about protein abundance in  
8 the sample. Through these techniques modern proteomics techniques can provide identification of  
9 over 5000 proteins from just a few thousand cells and provide relative quantification of differential  
10 protein abundance between samples.

#### 11 2.1.5. *Functional Analysis*

12 To understand the biological importance of observed proteomic differences between samples, a  
13 range of biological and functional analyses can be applied. There are several data bases of proteins  
14 describing their biological processes, cellular location, related pathways, binding partners and  
15 related diseases among others [401].

16 For example, the Kyoto Encyclopedia of Genes and Genomes (KEGG), can be used to provide  
17 comprehensive data regarding metabolism, signalling and interactions within the cell [428]. By  
18 uploading a list of proteins of interest to an online KEGG analysis platform (e.g. Metaboanalyst  
19 [429]) enriched pathways and biological processes can be identified. This provides comprehensive,  
20 data driven, insight into the biological phenotype of a sample based on their molecular features.

#### 21 2.2. Matrix Assisted Laser Desorption Ionisation (MALDI) Mass Spectrometry Imaging 22 (MSI).

23 Spatially defined molecular information is of great value to the investigation of cancer tissues.  
24 This can be achieved through the application of mass spectrometry imaging (MSI) which acts to  
25 capture a molecular profile of small discrete locations which can be combined across a tissue  
26 section. This is commonly employed to trace the localisation of anti-cancer compounds or  
27 differentiate between cancerous and non-cancerous tissue.

28 The most common MSI technology is matrix assisted laser desorption ionisation (MALDI) MSI.  
29 The technique uses a matrix which co-crystallises with the sample before directing a laser at a  
30 discrete region facilitates ionisation and sublimation. This produces a mass spectrum at each laser  
31 point which, when combined across a section, can provide spatially defined detection and relative  
32 quantification of analytes. This technique can be utilised for the investigation of a large range of  
33 analytes including peptides [430], metabolites [431], PTMs [432] and drugs [433] across a tissue  
34 section.

35

36

37

38

1  
2  
3  
4  
5  
6  
7  
8  
9  
10  
11  
12  
13  
14  
15  
16  
17  
18  
19  
20  
21  
22  
23  
24  
25  
26

# A Protocol for the Acquisition of Comprehensive Proteomics Data from Single Cases Using Formalin Fixed Paraffin Embedded Section

---

1  
2  
3  
4  
5  
6  
7  
8  
9  
10  
11  
12  
13  
14  
15  
16  
17  
18  
19  
20  
21  
22  
23  
24  
25  
26  
27

This page is intentionally left blank



1 2.3. Summary

2 HGSOC are characterised by late detection after local metastasis has occurred. This is in part due  
3 to the silent symptoms of this disease and difficulty in detecting it at an early stage. This results  
4 in poor outcomes for patients as standard treatment is rarely curative when HGSOC is detected  
5 after local metastasis.

6 In recent years it has been seen that most cases of HGSOC do not originate from the ovary, but  
7 rather spread from pre-cancerous lesions located in the fallopian tube called STIC. STIC are  
8 predicted to represent the first developmental stage of these cancers which then migrate to the  
9 ovary before establishing the primary tumour.

10 In addition to this, serous endometrial cancers typically metastasis throughout the peritoneal  
11 cavity and endometriosis, where endometrial tissue grows in distant locations, has a clear  
12 connection to CCOC and EnOC. There remains the possibility that, in some cases, pre-cancerous  
13 lesions in the endometrium, endometrial intraepithelial carcinomas (EIC), migrate to the ovary  
14 and establish primary cancers (particularly those of the CCOC or EnOC subtype).

15 While there has been significant research into the origins of these cancers over the past 10 years  
16 there remains disagreement around the prevalence of this precancerous migration, about which  
17 subtypes originate from which tissue and, in the case that ovarian cancer derived from a distant  
18 precancerous lesion, how exactly the cells are able to migrate at this early stage of development.

19 One of the main barriers to these investigations is the small size of the STIC and EIC  
20 precancerous lesions making them difficult to surgically identify and analyse. While much of the  
21 literature in this space has been developed on the back of genetic studies there remains a gap in  
22 proteomics analysis of these sample types.

23 In this chapter we outline a method for effective proteomics analysis of these samples. In brief,  
24 after surgical removal and annotation of the precancerous lesions by an experienced pathologist,  
25 we performed a laser capture microdissection (LCM) to isolate the regions of interest followed  
26 by a proteomics sample preparation method established in our lab for both MALDI mass  
27 spectrometry imaging and LC-MS/MS mass spectrometry analysis.

28 The preliminary results from this technical note identified numerous cancer related proteins  
29 within the STIC and EIC and demonstrated the potential use of MALDI MSI to delineate  
30 between cancerous and healthy tissue based on molecular features. This lays the foundations for  
31 larger scale proteomics analyses of these samples into the future to investigate the potential  
32 metastatic and migratory potential of these precancerous tissues.

33

34

35

36

37

1  
2  
3  
4  
5  
6  
7  
8  
9  
10  
11  
12  
13  
14  
15  
16  
17  
18  
19  
20  
21  
22  
23  
24  
25  
26  
27

This page is intentionally left blank

1 2.4. Statement of Authorship

2

Title of Paper	A Protocol for the Acquisition of Comprehensive Proteomics Data from Single Cases Using Formalin Fixed Paraffin Embedded Section
Publication Status	<input checked="" type="checkbox"/> Published <input type="checkbox"/> Accepted for Publication <input type="checkbox"/> Submitted for Publication <span style="margin-left: 100px;">Unpublished and Unsubmitted work written in manuscript style</span>
Publication Details	M. Acland, P. Mittal, G. Arentz, F. Whitehead, P. Hoffmann, M. Klingler-Hoffmann and M. K. Oehler, (2022), Methods and Protocols.

3

4

### Principal Author

Name of Principal Author (Candidate)	Mitchell Acland		
Contribution to the Paper	Performed data analysis and data interpretation, wrote the first draft of the article and consolidated the final manuscript.		
Overall percentage (%)	60%		
Certification:	This paper reports on original research I conducted during the period of my Higher Degree by Research candidature and is not subject to any obligations or contractual agreements with a third party that would constrain its inclusion in this thesis. I am the primary author of this paper.		
Signature		Date	27/05/2022

5

### 6 Co-Author Contributions

7 By signing the Statement of Authorship, each author certifies that:

8

9

10

- i. the candidate's stated contribution to the publication is accurate (as detailed above);
- ii. permission is granted for the candidate to include the publication in the thesis; and
- iii. the sum of all co-author contributions is equal to 100% less the candidate's stated contribution.

Name of Co-Author	Parul Mittal		
Contribution to the Paper	Performed MALDI mass spectrometry imaging experiments and contributed to method description.		
Signature		Date	23/03/2022

11

Name of Co-Author	Georgia Arentz		
Contribution to the Paper	Contributed to experimental and manuscript design. Performed mass spectrometry analysis and contributed to data analysis and interpretation		
Signature		Date	16/2/2021

1

Name of Co-Author	Fergus Whitehead		
Contribution to the Paper	Performed histological and immunohistochemical analyses.		
Signature		Date	

2

Name of Co-Author	Peter Hoffmann		
Contribution to the Paper	Supervised development of work, data interpretation and manuscript evaluation.		
Signature		Date	24/05/2022

3

Name of Co-Author	Manuela Klingler-Hoffmann		
Contribution to the Paper	Supervised development of work, data interpretation and manuscript evaluation.		
Signature		Date	24/0/2022

4

Name of Co-Author	Martin Oehler		
Contribution to the Paper	Supervised development of work, data interpretation and manuscript evaluation. Provided original samples and acted as corresponding author		
Signature		Date	20 February 2021

5

6

7

8

9

10

11

12

# A protocol for the acquisition of comprehensive proteomics data from single formalin-fixed paraffin embedded sections

Mitchell Acland<sup>1</sup>, Parul Mittal<sup>2</sup>, Georgia Arentz<sup>1</sup>, Fergus Whitehead<sup>3</sup>, Peter Hoffmann<sup>2\*</sup>, Manuela Klingler-Hoffmann<sup>2</sup> and Martin K. Oehler<sup>4,5\*</sup>

1 Adelaide Proteomics Centre, School of Biological Sciences, The University of Adelaide, Adelaide, SA, Australia

2 Clinical & Health Science, Mawson Lakes Campus, University of South Australia, SA, Australia

3 Clinpath Pathology, 21 James Congdon Drive, Mile End, SA, Australia

4 Department of Gynaecological Oncology, Royal Adelaide Hospital, North Terrace, Adelaide, SA, Australia

5 Robinson Research Institute, Discipline of Obstetrics and Gynaecology, Adelaide Medical School, The University of Adelaide, SA, Australia

\* Correspondence: [martin.oehler@adelaide.edu.au](mailto:martin.oehler@adelaide.edu.au) (M.K.O), [Peter.hoffmann@unisa.edu.au](mailto:Peter.hoffmann@unisa.edu.au) (P.H.)

**Abstract:** The molecular analysis of small or rare patient tissue samples is challenging and often limited by available technologies and resources, such as reliable antibodies against a protein of interest. Although targeted approaches provide some insight, here we describe the workflow of two complementary mass spectrometry approaches, which provide a more comprehensive and non-biased analysis of the molecular features of the tissue of interest. Matrix assisted laser desorption/ionization (MALDI) mass spectrometry imaging (MSI) generates spatial intensity maps of molecular features, which can be easily correlated with histology. And liquid chromatography tandem mass spectrometry (LC-MS/MS) can identify and quantify proteins of interest from a consecutive section of the same tissue. Here, we present data from concurrent precancerous lesions from the endometrium and fallopian tube of a single patient. Using this complimentary approach, we monitored the abundance of hundreds of proteins within the precancerous, and neighboring healthy regions. The method described here, represents a useful tool to maximize the amount of molecular data acquired from small sample sizes or even from a single case. Our initial data are indicative of a migratory phenotype in these lesions and warrant further research into their malignant capabilities.

**Keywords:** Serous endometrial carcinoma; high grade serous ovarian carcinoma; endometrial intraepithelial carcinoma; serous tubal intraepithelial carcinoma; proteomics; laser capture microdissection; MALDI mass spectrometry imaging; LC-MS/MS

## 1. Introduction

Matrix assisted laser desorption/ionization (MALDI) mass spectrometry imaging (MSI) is a powerful technique for providing spatial information about the molecular environment of a tissue section without homogenization. This provides greater detail than traditional immunohistochemistry approaches and compliments pathologist annotation of regions of interest within a tissue.

This can be complimented by liquid chromatography tandem mass spectrometry (LC-MS/MS). This technique can be applied to simultaneously identify hundreds of proteins in a single sample providing a temporal snapshot into its molecular features. As proteins represent the functional molecules of the cell, this holds the potential to discover the state of the cell including its malignant and migratory capabilities. This compliments

MALDI-MSI analysis by providing confident protein identification and the potential to provide relative quantification of protein abundance between samples.

Once a tissue has been surgically removed, it is commonly preserved via formalin fixation and paraffin embedding (FFPE) for storage and analysis by a pathologist. This technique holds the advantage of preserving tissues relatively intact for decades, facilitating retrospective studies and the acquisition of large sample numbers for molecular investigations. However, the formalin fixation process induces protein crosslinks which until recently were incompatible with downstream proteomics analyses, including MALDI and LC-MS/MS. We and others, have established an antigen retrieval method which can be used in combination with these techniques to access proteins from FFPE tissues [1].

To demonstrate the potential of these complementary techniques we applied them to the investigation of precancerous lesions (PLs) of the endometrium and fallopian tube derived from a single patient. Recent advances in the understanding of where serous cancers of the ovary and endometrium originate from [2, 3] and the malignant capabilities of their PLs [3, 4] highlights their relevance in cancer progression and merits deeper molecular investigation.

In serous endometrial cancer (SEC) its precursor, endometrial intraepithelial carcinoma (EIC) [5], is often accompanied by distant micro metastases in the absence of developed SEC [3, 4]. While high grade serous ovarian carcinoma (HGSOC) has been identified as originating from serous tubal intraepithelial carcinomas (STIC) located in the fallopian tube [6-10]. These PLs are predicted to migrate to the ovary before they establish a primary tumor. That both PLs hold the potential to migrate to secondary locations before establishing primary tumors suggest that they possess, yet undiscovered, molecular drivers of a migratory phenotype. Genomic studies [11] and mouse models [12, 13] have been instrumental in establishing the connection between STIC and HGSOC. However, they have not revealed the molecular events which underpin the observed migration of these supposedly pre-malignant cells. Mass spectrometry methods, including LC-MS/MS and MALDI MSI, hold the potential to expand our understanding of these early malignant events.

To investigate PLs using our complimentary mass spectrometry approach they were first identified using disease specific antibodies and annotated by an experienced pathologist (Prof. F. Whitehead). We use the pathologist guidance to identify small, precancerous, regions of interest and investigate them with MALDI MSI. In addition, using laser capture microdissection (LCM) we demonstrate how small regions of interest can be isolated for in-depth analysis via LC-MS/MS. We also demonstrate how the use of antigen retrieval and LCM can be used to facilitate MALDI MSI and LC-MS/MS analysis of FFPE tissue to provide complimentary spatial and in-depth proteomic information about small tissue regions of interest.

Here we provide a workflow through which small cancerous samples can be investigated via complimentary MALDI MSI and LC-MS/MS approaches (Figure 1). This is facilitated through antigen retrieval, precise microdissection and well-established sample preparation methods coupled with high sensitivity mass spectrometry. We have successfully performed this protocol on PLs from the fallopian tube and endometrium of a single patient providing spatially defined and detailed proteomics information on these biologically relevant tissues.

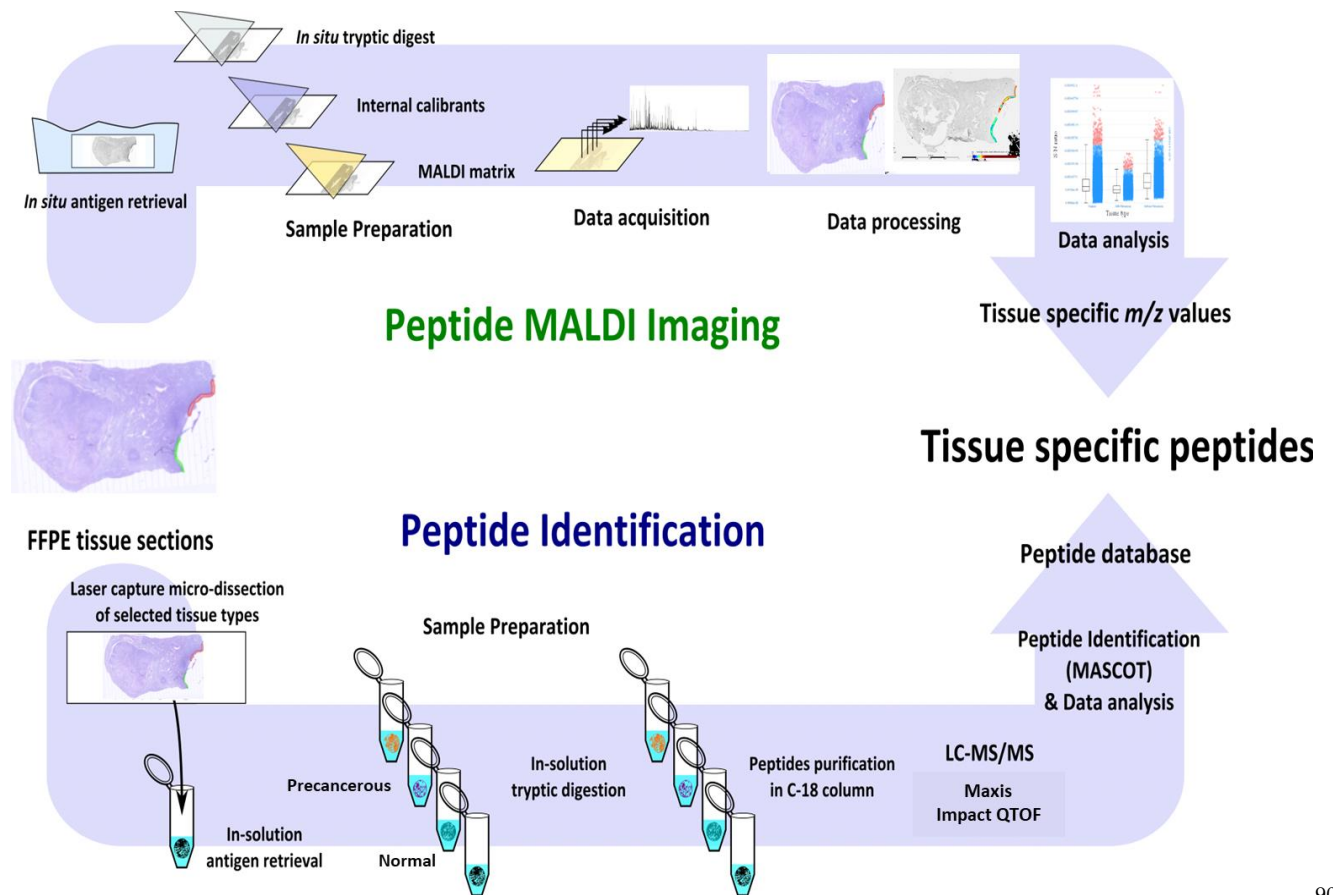


**Figure 1** (adapted from G. Arentz, *et al.* (2017) [14]): Workflow of proteomic analysis of small precancerous regions extracted from FFPE tissue. A) MALDI MSI workflow to acquire spatially defined molecular information. B) LCM extraction of precancerous regions followed by LC-MS/MS analysis for the identification of proteins differentially expressed between healthy and precancerous tissue regions.

## 2. Experimental Design

### 2.1. Materials

1. Acetonitrile, LC-MS/MS grade (1000302500, ACN, Merck, Germany)
2.  $\alpha$ -cyano-4-hydroxycinnamic acid (201344, HCCA, Bruker Daltonics, Germany)
3. Ammonium bicarbonate (103025E, Merck, UK)
4. Citric acid monohydrate (C0706, Sigma-Aldrich, Japan)
5. Dithiothreitol (D9163, DTT, Sigma-Aldrich, USA)
6. Eosin (HT110332, Sigma-Aldrich, Germany)
7. ESI-L low concentration tuning mix (G1969-85000, Agilent, USA)
8. Ethanol AR grade (4.10230.2511, Merck, Australia)
9. Ethanol, LC-MS/MS grade (1117272500, Merck, Australia)
10. Formic acid, LC-MS/MS grade (21909098, FA, Sigma-Aldrich, Germany)
11. Iodoacetamide (RPN6302OL/AG, IAA, GE Healthcare, Sweden)
12. Isopropanol AR grade (8187661000, Merck, Germany)
13. Mayer's hematoxylin (GH5232, Sigma-Aldrich, Germany)
14. Methanol LC-MS/MS grade (1.06018.2500, Merck, Germany)

---

15. Milli-Q® ultrahigh purity water (D11951, ≥18.2 MΩ, Barnstead International, USA)	113
16. Mounting medium (PER40000, Medite, Germany)	114
17. Neutral buffered formalin (HT501, Sigma-Aldrich, Germany)	115
18. Sodium hydroxide (1.06498.0500, NaOH, Merck, Germany)	116
19. Trifluoroacetic acid (1.08262.0100, TFA, Merck, Germany)	117
20. Trypsin Gold (V5280, Promega, USA)	118
21. Trypsin sequencing grade (V51111, Promega, USA)	119
22. Xylene (XA003, Chem-Supply, Australia)	120
23. Urea (1084870500, Merck, Germany)	121
2.2. <i>Equipment</i>	122
• Centrifuge 5810R (Eppendorf, Germany)	123
• CyberScan PC 300 pH Meter (Eutech Instruments, Singapore)	124
• Data analysis software (e.g. MaxQuant 1.5.2.8)	125
• Dry block heater (Ratek, Australia)	126
• Flexcontrol v3.4, fleximaging v4.0 and flexanalysis v4.0 software (Bruker Daltonics, Germany)	127
• Glass coplin Jar (H441, ProSciTech, Australia)	129
• High performance liquid chromatography (HPLC) vials (6820.0029, Dionex, The Netherlands)	130
• ImagePrep (Bruker Daltonics, Germany)	132
• Incubator at 37°C (Boekel Scientific, USA)	133
• Indium-tin-oxide (ITO) slides (237001, Bruker Daltonics, Germany)	134
• Leica EG 114OH embedder (Leica Biosystems, Australia)	135
• Leica TP 1020 processor (Leica Biosystems, Australia)	136
• Leica Zeiss Laser capture microdissection system (Leica Microsystems, Germany)	137
• Mass spectrometer (e.g. Maxis Impact II QTOF (Bruker Daltonics, Germany)	138
• Mass spectrometric data acquisition software [e.g. QTOF control (version 3.4) and hystar (version 3.2)]	139
• Microm HM 325 microtome (Zeiss, Germany)	141
• Microwave (LG 700 W MS19496, LG, China)	142
• MTP slide adaptor II (Bruker Daltonics, Germany)	143
• NanoDrop 2000 (Thermo-Fisher Scientific, USA)	144
• Nanozoomer (Hamamatsu, China)	145
• nano-HPLC Ultimate 3000 RS system (Dionex, The Netherlands)	146
• Polyethylene naphthalate (PEN) membrane slides (11505158, MicroDissect, Germany)	147
• Thermomixer (Eppendorf, Germany)	148
• Tipp-Ex (water-based white out, Winc, Australia).	149
• Scanner (CanoScan 5600 F, Canon, Thailand).	150
• SpeedVac concentrator (Savant SVC 100, Thermo Scientific, USA)	151
• SCiLS lab 2016b (Bruker Daltonics, Germany)	152
• Superfrost Plus microscopic slides (6.700 125, Thermo scientific, Germany)	153
• Ultraflex extreme MALDI TOF TOF (Bruker Daltonics, Germany)	154
• Ultra-low -80°C freezer (SANYO, Japan)	155
• Vivacon ultrafiltration spin columns (VS0101, Sartorius Vivacon 500, 10 000 MWCO HY)	156
• ZipTip C18 (ZTC18M096, Millipore, MA)	157
	159
<b>3. Procedure</b>	160
3.1. <i>Tissue collection</i>	161



Collect the tissue(s) of interest and snap freeze in liquid nitrogen immediately after the surgery.

1. In our study, tissues were collected after total abdominal hysterectomy and bilateral salpingo-oophorectomy was performed on a patient with endometrial hyperplasia at the Royal Adelaide Hospital, Adelaide, Australia with written informed consent from the patient. The study was approved by the Ethics committee of the Royal Adelaide Hospital.
2. Process the tissue(s) using standard procedure [15]. Briefly, fix the tissue(s) in 10% (v/v) neutral buffered formalin overnight at 4°C, followed by washing with milli-Q® water and storing in 70% (v/v) ethanol before processing them with a Leica TP 1020 processor. Embed the tissue in paraffin using a Leica EG 114OH embedder. In our study, tissues were processed and embedded by histology services at the University of Adelaide, Adelaide, Australia. **Critical step:** Formalin fixation time depends on the tissue size, on an average formalin penetrates tissue ~1 mm/h [16].
3. Section the FFPE block(s) using Microm HM 325 microtome at 4µm thickness and water bath mount at 38°C onto PEN membrane slides for LC-MS/MS, ITO slides for MALDI MSI and superfrost slides for staining purposes.
4. Dry the slide(s) at 37°C for 1h, followed by overnight drying at room temperature.
5. For pathological identification, stain the tissue(s) using H&E or antibody using standard protocols [15]. Here, identification of PLs (Figure 2) was performed by an experienced pathologist, Prof. Whitehead, using H&E and antibody stained tissue(s) for P53 and M1B1 (data not shown). Areas of STIC, EIC and adjacent healthy epithelium were annotated as shown in Supplementary Figure 1.

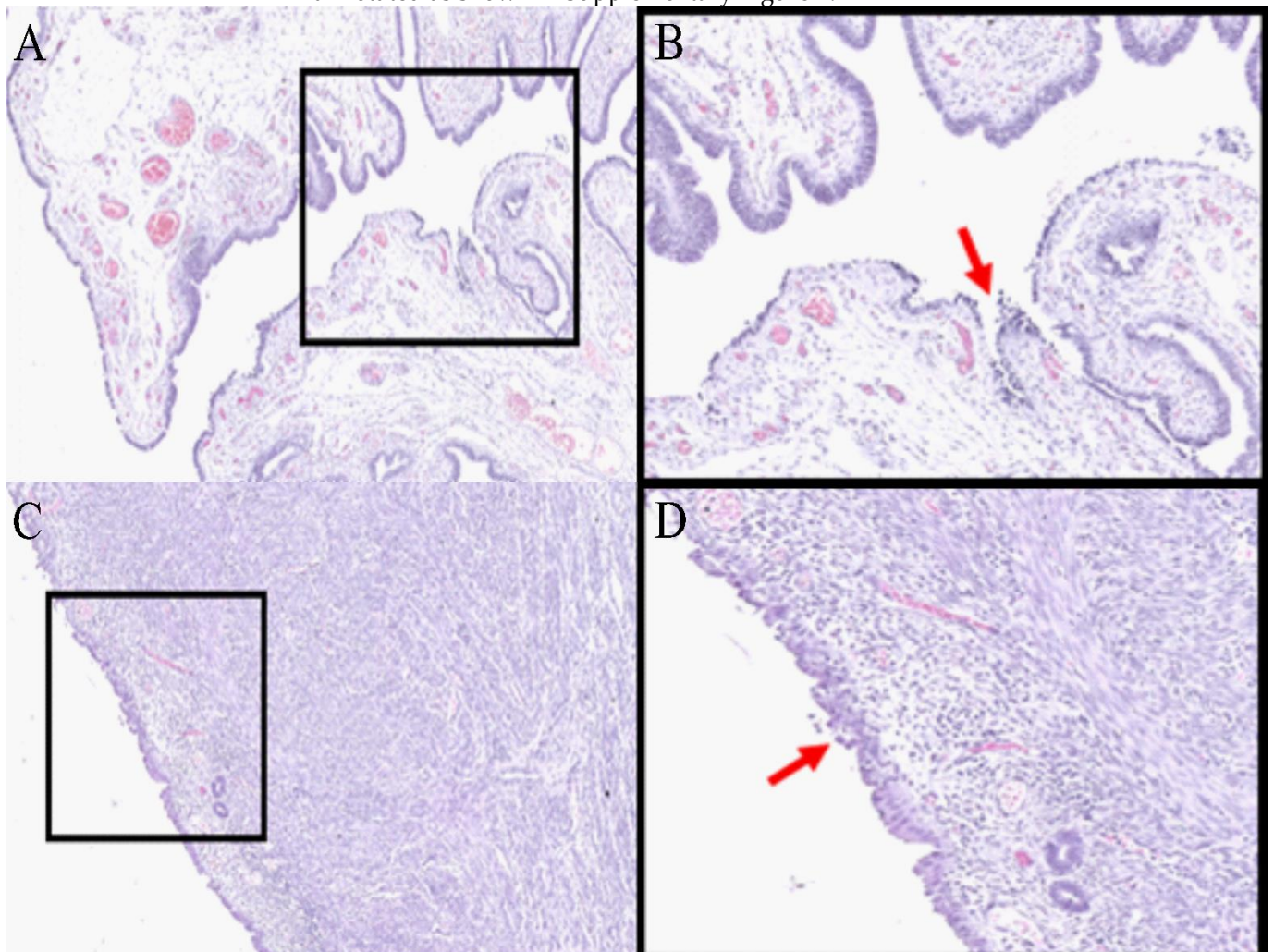


**Figure 2.** Hematoxylin and Eosin-stained fallopian tube (A and B) and endometrium tissue (C and D) at 6x (A and C) and 12x (B and D) magnification. Areas of STIC (B) and EIC (D) are indicated by the red arrows. (Figure adapted from 'Proteomics Analysis of Serous Lesions of the Endometrium and Fallopian Tube Reveals Their Metastatic Potential, Acland, et al. (2020) [17].

### 3.2. Laser capture microdissection and protein extraction for LC-MS/MS

6. Place the PEN membrane slide(s) on a heating block at 60°C for 5 min, tissue facing up.
7. Remove paraffin by dipping the slide(s) in xylene for 90 sec followed by 2 min incubation in 100% ethanol (repeat twice), 5 min incubation in Milli-Q® water (repeat twice) and then stain the slide with hematoxylin for 20 sec or until the tissue appears purple. Critical step: Staining time depends upon the concentration/age of the solution and/or thickness of the tissue section.
8. Destain the slide in Milli-Q® water and then with 70% (v/v) ethanol for 1 min.
9. Let the slide dry at room temperature.
10. Load the stained slide and compatible LCM tubes into the Leica Zeiss LCM system. Critical step: To avoid tissue sticking to the side, 5µL of 10mM citric acid buffer can be added to the cap of an LCM tube
11. Carefully cut out the regions of interest(s) (ROI) and ensure that each ROI have been collected into the cap of separate tubes. The tissue before and after LCM dissection of the tissue is shown in Supplementary Figure 1.
12. Briefly, centrifuge the tubes and make sure that the tissue region(s) are in the buffer and at the bottom of the tube. Pause step: tissue(s) can be stored for months at -80°C
13. To retrieve the proteins, add 200µL of 10mM citric acid and boil the tubes for 100 min at 98°C on a thermomixer.
14. Let the tubes cool at room temperature and centrifuge briefly.
15. Protein concentration can be estimated at this point using Bradford assay, EZQ assay, nanodrop or tryptophan assay. We used NanoDrop 2000 at 280nm.

### 3.3. Trypsin digestion and peptide clean-up for LC-MS/MS

- Our group prepared the samples as per Wisniewski et al. [18] protocol with minor modifications
16. Remove the supernatant and replace with 200µL of lysis buffer (8M urea in 100mM ammonium bicarbonate with final concentration of DTT to 50mM), followed by incubation at 20°C for 1 h.
  17. Put the Vivacon FASP filters into the provided 1.5mL centrifuge tube, rinse the columns three times with 100µL of 100 mM ammonium bicarbonate by centrifuging at 14,000g for 10 mins, followed three times with 100µL of lysis buffer. Critical Step: Once the column gets equilibrated, try not to dry them out. This can be done by retaining a little amount of buffer on top of the column.
  18. Replace the collection tube with a fresh 1.5mL centrifuge tube. Load the tissue samples into the spin columns and centrifuge at 14,000g for 10 min at room temperature. Critical Step: To make sure the proper binding of proteins to the FASP membrane, this step can be repeated twice with the flow-through.
  19. Discard the flow-through and subsequently alkylate the samples with 55mM IAA in 100mM ammonium bicarbonate, followed by incubation in dark at room temperature for 30 min.
  20. Centrifuge the filters as step 17 above and wash the membrane twice with 100µL of 100mM ammonium bicarbonate, followed by one wash with 100µL of 50mM ammonium bicarbonate.
  21. Digest the alkylated proteins at 37°C overnight with sequencing grade trypsin at an enzyme to substrate ratio of 1:50 in 100µL of 5mM ammonium bicarbonate. Critical

- step: To minimize the evaporation and drying of the peptides, bottom of the tubes can be filled with water and must be sealed using paraffin. 237  
238
22. After overnight incubation, add 0.1% FA to stop the digestion. 239
  23. Elute tryptic peptides off the filter by centrifuging the tubes at 14,000g for 10 mins. 240
  24. Dry the samples by vacuum centrifugation without heating. 241
  25. Reconstitute the peptides in 2% (v/v) ACN, sonicate for 5 min, vortex and centrifuge briefly. 242  
243
  26. Estimate the peptide concentration using nanodrop at 205nm wavelength. 244
  27. Samples were then acidified to a final concentration of 0.1% FA and placed in HPLC vials for peptide LC-MS/MS analysis (proceed to step 29). Alternatively, an optional extra clean up step can be done using C18 Zip-tips. This will remove any residual salt that may be remaining. 245  
246  
247  
248
  28. C18 ZipTip preparation: Prepare the ZipTips as per manufacture's protocol. Critical step: Use one tip per sample. 249  
250
    - Equilibrate the tips three times with 100% ACN and followed three times with 0.1% FA (v/v). 251  
252
    - Load the peptide samples ten times by pipetting the digest up and down 253
    - Wash the samples six times with 0.1% FA (v/v). 254
    - Elute the bound peptides six times with 60% (v/v) ACN containing 0.1% (v/v) FA. 255
    - Dry the eluted peptide mixture using a speedVac without heating. 256
    - Resuspend the peptides in 2% (v/v) ACN, sonicate for 5 min, vortex and centrifuge briefly. Pause step: Samples can be stored at -80°C until required. 257  
258
- 3.4. nanoLC-MS/MS analysis 259
- Set up the LC and MS instrument as described under equipment setup 260
29. Prepared peptide samples can now be loaded onto an HPLC system connected online to a mass spectrometry. Our laboratory uses an ultimate 3000 HPLC system (Dionex, Thermo-Fisher Scientific) connected online to a maxis impact II QTOF (Bruker Daltonics). 261  
262  
263  
264
  30. Inject ~1µg of each sample and load for 8 min at a flow rate of 5µL/min in 2% (v/v) ACN, 0.1% (v/v) FA onto a C18 trapping column. Critical step: Based on the flow rate and tubing size, sample loading time and gradient should be optimized for the instrument in use 265  
266  
267  
268
  31. Separate peptides onto a C18 analytical column using 2% (v/v) ACN in 0.1% (v/v) FA (Buffer A) and 80% (v/v) ACN in 0.1% (v/v) FA (Buffer B) at a flow rate of 300nL/min. Gradient used in our laboratory was 5% to 45% buffer B over 130 min, followed by gradual increase of buffer B from 45% to 90% for 1 min and then held at 90% buffer B for 20 min, followed by re-equilibration of the column for 20 min at 5% buffer B, for a total run time of 180 mins. 269  
270  
271  
272  
273  
274
  32. Depending on the selected ion source and the HPLC flow rate, appropriate settings for nebulizer and dry gas must be selected. In our laboratory, the column eluent from the LC connected online to Bruker's CaptiveSpray™ source optimized to capillary voltage of 1300V with capillary temperature of 150°C, at a nebulizing pressure of 3L/min. 275  
276  
277  
278
  33. Data-dependent acquisition can be performed using Bruker's Shotgun InstantExpertise™ method. This is an advanced intelligent method to provide greater coverage and data analysis compatibility. Instead of the typical Top Intensity or Increasing m/z selection, this method uses a simplified acquisition model via an intelligent duty cycle optimizer. In this method 279  
280  
281  
282
    - Depth of sampling is auto optimized 284
    - Acquisition speed for each MS/MS event is auto regulated 285
    - Acquisition exclusion is auto optimized 286
    - Peak depth has been optimized on collision cell recovery using factory settings 287
  34. On the orthogonal TOF systems the mass range for MS and MS/MS mode is the same. For tryptic peptides we recommend setting the mass range to 50 to 2,200 m/z 288  
289

35. Exclude the singly charged precursor ions from acquisition, avoids the selection of singly charged background ions, as well as polymer signals. 290  
291
36. As determined by the m/z of the precursor ion, range the collision energy from 23 to 65%. 292  
293
37. Set-up a sample table in HyStar and select appropriate LC and MS methods for the sample analysis. 294  
295
- 3.5. LC-MS/MS Data analysis 296
- For quantitative label-free proteomics, LC-MS/MS raw files can directly be analyzed using freely available MaxQuant software at [https://www.maxquant.org/download\\_asset/maxquant/latest](https://www.maxquant.org/download_asset/maxquant/latest). 297  
298  
299
- Detailed steps on how to run maxquant with integrated Andromeda search engine is explained by Tyanove, et al. (2016) [19]. Note: MaxQuant version 1.5.2.8 is used in this study 300  
301  
302
38. The standard Bruker QTOF settings can be used with a mass error tolerance of 40ppm, more specific parameters defined as below: 303  
304
- Select appropriate. fasta files, for e.g. UniProt human reviewed database 305
  - Select the digestion enzyme to Trypsin 306
  - Set the maximum number of missed cleavages to 1 307
  - Select fixed modification to carbamidomethyl of cysteines 308
  - Select variable modification of oxidation of methionine 309
  - Set the protein false discovery rate (FDR) and peptide spectrum match FDRs to 1% using a target decoy approach 310  
311
  - Set minimum peptide length of seven amino acids 312
  - Set only unique and razor peptides when reporting protein identifications 313
- The mass spectrometry proteomics data have been deposited to the ProteomeXchange Consortium via the PRIDE partner repository [20] with the data set identifier PXD018538. 314  
315  
316
- 3.6. In-situ tryptic peptide MALDI MSI analysis 317
- Prepare the slide as per Gustafsson et al. [21] 318
39. Place the ITO slide onto a heating block at 60°C for 1 h. 319
40. Wash the slide twice in 100% xylene for 5 min each 320
41. Wash the slide twice in 100% ethanol for 2 min each 321
42. Rinse the slide twice with 10mM ammonium bicarbonate for 5 min each 322
43. Place the slide in an empty cleaned coplin jar and fill the remaining slots with blank super frost slides (to prevent the formation of big air bubbles during the antigen retrieval step). 323  
324  
325
44. Fill the coplin jar with 10mM citric acid monohydrate and microwave it at high power for 1.05 min or until the citric acid starts to boil. 326  
327
45. Once the citric acid reached the boiling point, microwave the slide for 10 min at power 10. 328  
329
46. Following microwave incubation, rapidly transfer the coplin jar to a heating block set at 98°C for 30 min. 330  
331
47. Remove the slide from the coplin jar and allow to cool down at room temperature. 332
48. Rinse the slide twice with 10mM ammonium bicarbonate. 333
49. Dry the slide at room temperature for ~10min. 334
50. Apply teach marks on the 4 sides of the slide using Tipp-Ex (water-based white out). 335
51. Scan the slide at a 2400dpi resolution (CanoScan 5600 F, Canon, Thailand). 336
52. Adjust the spray offset on the ImagePrep station (Bruker Daltonics), such that the spray lasts for at least 54 sec and cover the whole slide slot. Global Power Adjustment set at 38% spray power with 0% modulation. 337  
338  
339
53. Dilute 40µL of the trypsin gold aliquot with 160µL of 25mM ammonium bicarbonate and load directly onto the spray generator of the ImagePrep. 340  
341
54. Spray the trypsin using trypsin deposition method as detailed in 2.4.2. 342

55. After trypsin deposition, incubate the slide at 37°C for 2 h in a humidified chamber. 343
56. After 1.45 h, thaw, vortex and flick centrifuge an aliquot of internal calibrant and spray the internal calibrant using the same method as of trypsin. 344  
345
57. Fill the ImagePrep solution vial with the matrix and adjust the spray offset for the matrix deposition as detailed in 2.4.2 346  
347
58. After matrix deposition, remove the slide from the Imageprep and clean both ends of the slides with 100% methanol 348  
349
59. Load the prepared slide into an MTP slide adapter II and acquire the data using the ultrafleXtreme MALDI TOF/TOF instrument 350  
351
60. Using the flexcontrol, create an autoXecute method with the following required settings: 352  
353
  - Select the optimised and calibrated flexControl method in the general tab 354
  - Turn the fuzzy control off and set the optimized laser power (we used 50% laser power) 355  
356
  - No background list should contain in the evaluation tab 357
  - 500 shots acquired in 500 shot steps with dynamic termination and random walk off 358  
359
  - Choose an appropriate data processing method as of step 61. 360
61. Create a flexAnalysis method with the following defined settings: smoothing by Gaussian (2 cycles with the width of m/z 0.02), TopHat baseline subtraction, Monoisotopic SNAP peak algorithm and the quadratic recalibration using the calibrations masses (1296.685, 1570.677, 2147.199 and 2932.588) with mass tolerance of 500 ppm. 361  
362  
363  
364
62. Open flexImaging and create a new sequence with sample preparation type of uniformly distributed coating and 60µm raster width for this workflow. 365  
366
63. Teach the slide using the scanned slide and check the teaching by moving the sample carrier at various points on the slide 367  
368
64. Create the polygon measurement of region(s) and save the flexImaging sequence. 369
65. Optimize the laser power by shooting the laser outside the tissue region and on the calibrants sprayed. 370  
371
66. Calibrate the flexcontrol method from the calibration tab in the flexcontrol and save the method. Critical Note: Make sure monoisotopic peaks are resolved to baseline. 372  
373
67. Start the data acquisition from the flexImaging checklist menu 374
68. After data acquisition, remove the slide from the instrument and wash the matrix using 70% ethanol (AR grade) and H&E stain using the standard procedure, briefly 375  
376
  - Rinse the slide with 70% ethanol (AR grade) for 5mins or until the matrix is removed 377  
378
  - Dip into deionized water for 30 sec 379
  - Immerse in hematoxylin solution (Mayer's) for 50 sec 380
  - Wash with tap water for 5 min 381
  - Immerse in eosin solution for 30 sec 382
  - Rinse with 70% ethanol (AR grade) for 30 sec 383
  - Rinse with 90% ethanol (AR grade) for 30 sec 384
  - Rinse with 100% ethanol (AR grade) for 30 sec 385
  - Rinse with 100% isopropanol (AR grade) for 30 sec 386
  - Rinse twice with xylene for 1 min each 387
  - Apply the mounting medium onto the cover slide 388
  - Cover the tissue section with the coverslip and gently pressed it onto it 389
  - Let the slide dry overnight at room temperature under the fume hood. 390
69. Scan the slide at 20X objective using a Nanozoomer and co-register the scanned slide using fleximaging edit drop down menu "co-register image" and save the sequence. 391  
392
70. Mark the region(s) of interest as per pathologist's annotation, in our case EIC and normal endometrium. 393  
394

71. Load the raw data into SCiLS lab v2016b and process there by selecting the instrument type "Time-of-flight", Import raw, fallback to reduced spectra and TopHat as the baseline subtraction method.
72. Open the imported dataset, set the denoising as week, baseline removal as TopHat and change the file properties from the file drop down menu to 0.125Da.
73. Using the Peak picked algorithm from the tools drop down menu, create a list of peaks detected and manually go through each  $m/z$  values that are differentially regulated in the region(s) of interest (Figure 3).

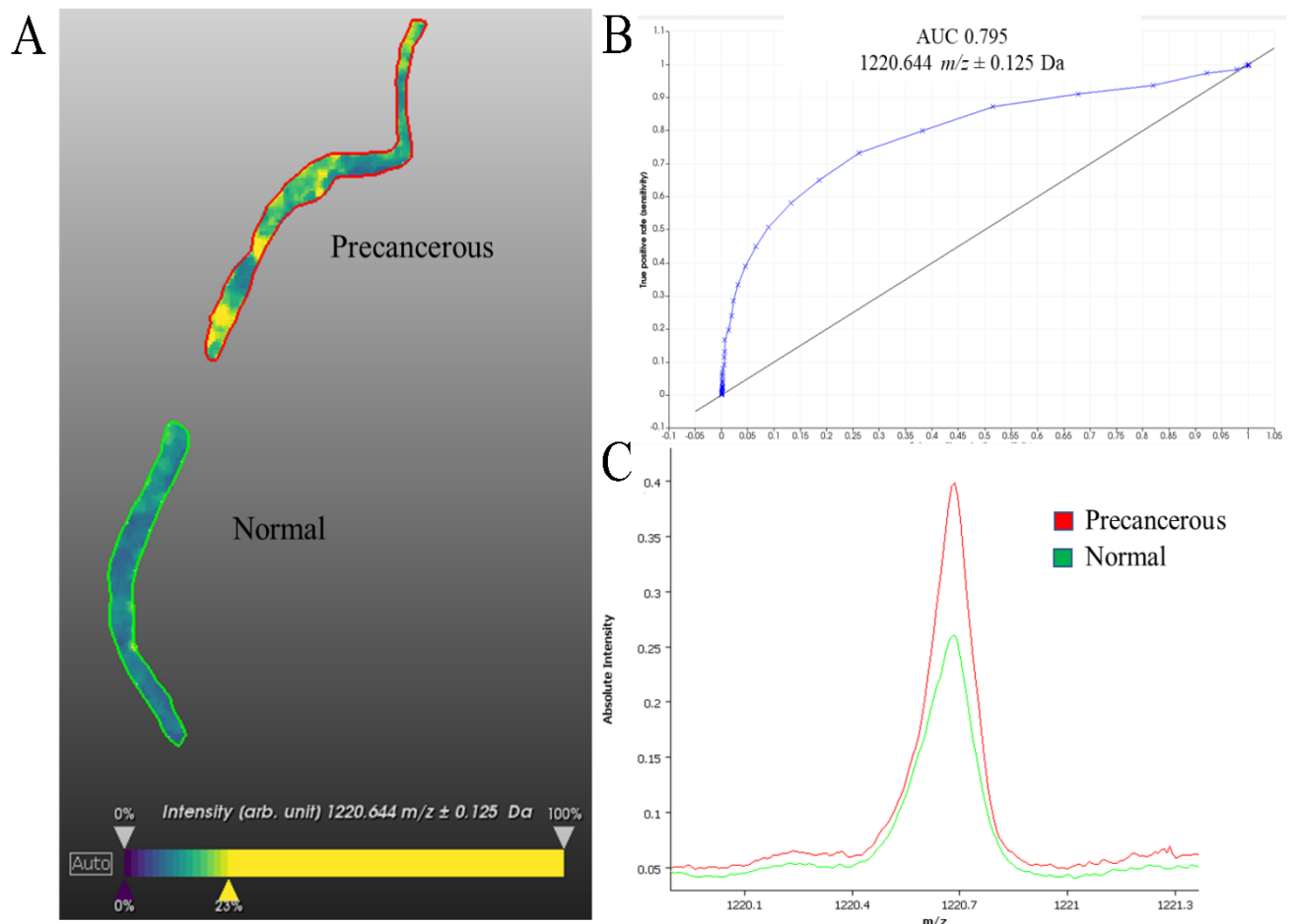


**Figure 3:** MALDI MSI on an endometrial tissue (A) Representative ion intensity image of  $m/z$  1220.644  $\pm$  0.125 Da (B) The ROC curve of  $m/z$  1220.644 (AUC 0.795) for precancerous versus normal region (C) Comparative spectra of  $m/z$  1220.644 Da between precancerous and normal region. Scale bar is 1.4 cm, ion intensity ranges from blue (lowest) to yellow (highest)

#### 4. Expected Results

In this manuscript, we outline two mass spectrometry protocols, which complement each other and provide unique insight into the molecular details of concurrent ovarian and endometrial PLs from a single patient.

The EIC and STIC lesions were found in the endometrium and fallopian tube respectively and tissues were embedded via a standard FFPE protocol [15]. Identification of the PL was achieved through immunoperoxidase staining for p53 and MIB1 (data not shown) which are identifying features of these PLs [5, 22]. In addition, indications of cell

transformation such as hyperchromasia, nuclear atypia and nucleomegaly were utilized to advise an experienced pathologist in the identification of precancerous regions [5, 23] (Figure 2).

Using MALDI MSI, we identified almost 600 hundred molecular features (Supplementary Table 1) of which 72 could be used to distinguish between healthy and precancerous tissue. We chose to display the analyte with mass to charge ratio ( $m/z$ ) of 1220.64 Daltons (Da) (Figure 3) which, as demonstrated in the ROC curve, can be utilized to confidently delineate between cancerous and non-cancerous regions in this sample. While antibody-based techniques are a powerful tool for identifying different regions of tissue, they can be complemented by the MALDI MSI method presented here to gain additional molecular information.

While MALDI MSI is a powerful technique to gather spatially defined molecular information, the lack of peptide fragmentation makes protein identification difficult. To overcome this, we incorporated LC-MS/MS to complement our MALDI MSI analysis (Figure 1).

To excise regions of interest for LC-MS/MS analysis we employed LCM using a Leica Zeiss LCM system. Advised by the annotations of an experienced pathologist and the distribution of analytes visualized through MALDI MSI, we were able to successfully isolate these small, but biologically relevant, regions of tissue.

Proteins were extracted from the isolated regions of tissue using an antigen retrieval protocol [24] and digested using a modified FASP protocol [18] and then analyzed on maxis impact II QTOF connected online to an ultimate 3000 nano-LC before protein identification via MaxQuant. Through isolation of peptides, subsequent fragmentation and analysis of this secondary MS spectra, details of amino acid structures were gathered. Protein identification was achieved using the MaxQuant analysis platform, in combination with the Andromeda data base.

This resulted in a total of 453 proteins detected across the four tissue types [25]. Through the analysis of this data several metastasis related proteins were identified [25]. For example, the protein transketolase was identified here in both the STIC and EIC precancerous lesions. This protein has previously been seen to be upregulated in peritoneal metastasis of ovarian cancer and its expression correlates with reduced over-all survival [26]. The presence of metastasis related proteins in the PLs investigated here merits further investigation into their migratory and metastatic potential and the molecular events which underpin them.

We have previously utilized this approach to investigate spatially defined alterations in protein expression in vulva and endometrial cancer [27, 28]. These techniques have also been utilized to accurately classify endometrial cancers with associated lymph node metastasis [29].

Here, we outline a method for the complementary tissue specific proteomic analysis of ovarian and endometrial PLs. MALDI MSI investigation of these tissues was able to identify an analyte which could successfully delineate between cancerous and non-cancerous tissue (Figure 3). Guided by MALDI MSI ion intensity maps and the annotation of an experienced pathologist, we were able to dissect precancerous areas using LCM (Supplementary Figure 1). We were able to successfully identify hundreds of proteins from each sample using LC-MS/MS. Our lab has previously utilized these techniques [1, 27-36] demonstrating their broad utility.

Depending on sufficient sample material and utilization of the appropriate data acquisition method, LC-MS/MS also has the potential to quantify relative protein abundance between ROIs or between samples. Due to the unique nature of the samples investigated, this was not feasible here. Though small sample size is a limitation, one which could be overcome by the analysis of numerous biological replicates, LC-MS/MS can achieve relative quantification of protein abundance. This could provide further information about molecular perturbations present in PL compared to their neighboring tissue.

## 5. Discussion

In this manuscript we outline a protocol for acquisition of spatially defined proteomic information from small regions of FFPE tissue. This was achieved through the application of MALDI MSI to acquire spectra from across the tissue section in a spatially defined manner. In combination with annotation by an experienced pathologist, the MALDI information was used to advise LCM of regions of interest which were then investigated through a specific sample preparation workflow coupled with high sensitivity label free LC-MS/MS analysis. This analysis resulted in the identification of hundreds of proteins differentially expressed between the different tissues including some which were indicative of a metastatic and migratory potential possessed by these PLs.

Identification and characterization of the PLs investigated here is made difficult through their small size, particularly in relation to the surrounding healthy tissue. Here, we demonstrate that MALDI MSI is a technique which holds great utility for identifying and characterizing small tissue regions from a larger tissue section. This technique utilizes a matrix which is sprayed homogeneously over the tissue facilitating laser induced ionization/desorption of analytes which are then analyzed through a time of flight (TOF) mass spectrometer. This provides spectra at each discrete location which the laser was directed towards. By acquiring data from these locations across the tissue a spatially defined molecular analysis can be achieved.

To demonstrate the utility of MALDI MSI we presented the distribution of a single ion ( $m/z=1220.64\text{Da}$ ) which was able to differentiate between the healthy and precancerous areas of the tissue. In combination with the numerous other analytes present in this analysis (Supplementary Table 1) this shows that the proteomic landscape can be significantly different between adjacent regions of tissue and that PLs represent a significant perturbation in their protein expression compared to the tissue from which they derived. Our lab has previously used MALDI MSI to delineate regions of ovarian cancer tissue [33], to investigate spatially defined alterations in protein expression in vulva and endometrial cancer [27, 28] and to providing predictive information of the metastatic status of endometrial cancer based on a primary cancer biopsy [29] demonstrating the robustness and broad utility of this technique.

Through the application of tailored sample preparation and label free LC-MS/MS analysis, we demonstrate the ability to acquire detailed proteomic information from small formalin fixed tissue sections. This was facilitated through the precise isolation of regions of interest through LCM. This technique is well established and holds great utility for the molecular investigation of small but biologically important tissue regions. In combination with accurate annotation and characterization of different tissue regions, this can facilitate the LC-MS/MS mediated identification of proteins, thereby providing a temporal snapshot into the molecular landscape within these samples.

Further analysis of the proteins identified in this experiment revealed several proteins indicative of a migratory phenotype in these PLs, including transketolase. This was achieved through simple analysis of proteins identified within the cancerous regions which were not present in the healthy tissue. A larger sample set would provide the opportunity to acquire quantitative information regarding relative protein abundance between samples. This has the potential to characterize up and down regulation of proteins which is indicative of oncogenic transformation or migratory potential.

A larger sample set would also facilitate more complex data analysis approaches including, but not limited to, network and pathway analysis. A further advantage of this approach is that it investigates the tissue in an unbiased manner facilitating discovery of new molecular features rather than relying on targeted approaches such as immunohistochemistry.

One of the limitations of proteomics analysis of small sample sizes is that many proteins will be extracted at levels which are below the limit of detection for this technique. However, with improvement of instrumentation this proteome coverage will continue to improve rapidly [37].



While the technology is advancing, we can improve protein coverage by using complementary proteomics approaches. One of the advantages of this protocol is that the antigen retrieval and LCM processes can be coupled with a range of other MS based techniques using method specific sample preparation steps. For example, our lab has investigated spatially defined glycan expression through a combination of MALDI mass spectrometry imaging, LCM, glycan specific sample preparation and LC-MS/MS, in a range of sample types and conditions [31-34, 36]. Into the future this opens the possibility of systematic investigations of precancerous samples, through a range of omics techniques to unlock more molecular details.

PLs located within the endometrium and fallopian tube require more detailed investigation to understand the early stages of their oncogenic development. Barriers to this investigation include acquisition of the PLs in the first instance, accurate identification of precancerous regions and the acquisition of unbiased spatially defined and detailed molecular information. There are several challenges relating to the acquisition of PLs in the first instance, but the method presented here overcomes barriers to the acquisition of spatially defined and detailed molecular information from these samples. This is achieved through MALDI MSI and LCM followed by LC-MS/MS. In this pilot study these complementary techniques provide a detailed picture of the molecular terrain of endometrial and fallopian tube tissue and suggest that the PLs located there possess a migratory phenotype which merit further investigation. In conjunction with other mass spectrometry-based methods, the workflow described here can be used to identify and quantify proteins from small areas of tissue and provide novel insights into the early stages of cancer development, which are complementary to genomics data.

## 6. Reagent and Equipment Set Up

### 6.1. Reagent Set Up

#### 10 mM citric acid monohydrate pH 6

For 500mL of 10mM citric acid, weigh 1.05g of citric acid monohydrate and dissolve in 480mL milli-Q® water. Adjust the pH to 6.0 using 1M NaOH (~16 mL required). Make up the volume to 500mL with milli-Q® water. Note: It can be stored for 30 days at room temperature. It can be stored for 30 days at room temperature.

#### 100 mM ammonium bicarbonate

For 50mL of 10mM ammonium bicarbonate, weigh 394mg into a polypropylene container and make up to 50mL with milli-Q® water. Note: Must be prepared fresh, as the pH of the solution changes over time

#### 10 mM ammonium bicarbonate

For ~500mL of 10mM ammonium bicarbonate, dilute 50ml of 100mM ammonium bicarbonate into 450mL milli-Q® water. Note: Must be prepared fresh, as the pH of the solution changes over time

#### 25 mM ammonium bicarbonate

For ~500µL of 25mM ammonium bicarbonate, dilute 125µL of 100mM ammonium bicarbonate into 475µL milli-Q® water. Note: Must be prepared fresh, as the pH of the solution changes over time

#### 8M urea in 100 mM ammonium bicarbonate

For 10mL of 8M urea in 100mM ammonium bicarbonate, weigh 4.80g urea and 80mg ammonium bicarbonate in a polypropylene container and make up to 10mL with milli-Q® water. Note: Use high quality reagents and make fresh each day.

#### DTT (1,4-Dithiothreitol)

Must be made fresh or from a concentrated solution stored at -80°C. We make it at 1M and store it in 100uL aliquot at -80°C.

#### IAA (Iodoacetamide)

Must be made fresh or from a concentrated, frozen solution. We make it at 550mM and dilute it 1/10 before use with 8M Urea in 100mM ammonium bicarbonate. Note: IAA is light sensitive.

**LC buffer A (2% (v/v) ACN with 0.1% (v/v) FA)**

Dilute 20mL of ACN in 979mL of milli-Q® water and 1ml of FA.

**LC buffer B (80% (v/v) ACN with 0.1% (v/v) FA)**

Dilute 800mL of ACN in 199mL of milli-Q® water and 1ml of FA.

**Trypsin Gold**

Dissolve 100µg lyophilized trypsin gold in 200µL 5mM NH<sub>4</sub>HCO<sub>3</sub> and split it into 40µL aliquots and freeze at -80°C until required

**Internal calibrant solution**

Prepare the calibrant stock solution as per Gustafsson, *et al.* (2012) [38]. Briefly, combine the below calibrants in appropriate amounts, vortex and flick centrifuge. Split into 100µL aliquots & store at -80°C until required

**Table 1:**

Calibrants	Peptide mass [M+H] <sup>+</sup>	Final concentration
Angiotensin I34-43 (C10-00002, BioRad, Hercules, USA)	1296.685	0.4pmol/µL
[Glu1]-fibrinopeptide B (F3261, Sigma-Aldrich, St. Louis, USA)	1570.677	0.4pmol/µL
Dynorphin A 1-17 (2032, Auspep, Australia)	2147.199	2.0pmol/µL
ACTH 1-24 (A0298, Sigma-Aldrich, St. Louis, USA)	2932.588	2.0pmol/µL
TFA (10%)		0.2% (v/v)
Milli-Q® Water (≥18.2 MΩ)		

**7 mg/mL α-cyano-4-hydroxycinnamic acid**

Dissolve 70mg of HCCA in 10mL of 50% ACN, 49.8% milli-Q® water and 0.2% TFA.

**6.2. Equipment Set Up**

**6.2.1. nano-HPLC system**

LC instrument needs to be optimized in advance. Instrument specific settings utilized in our lab is as below

**Analytical column** Acclaim PepMap100 C18 75µm × 50cm, 164568, Thermo-Fisher Scientific

**Trap column** Acclaim PepMap100 C18 75µm × 20mm, 164535, Thermo-Fisher Scientific

**Mobile phases** A: 2% (v/v) ACN with 0.1% (v/v) FA in milli-Q® water,

B: 80% (v/v) ACN with 0.1% (v/v) FA in milli-Q® water

**Loading solvent** 2% (v/v) ACN with 0.1% (v/v) FA in milli-Q® water

**Flow rate** 300nL/min

**Gradient** 5% buffer B for 8 mins

5–45% buffer B over 130 mins

45–90% buffer B in 1 min

90% buffer B for 20 mins

90-5% buffer B for 1min

5% buffer B for 20 mins

**Column temperature** 60°C

**Sample loading** µL pickup

**Injection amount** ~1µg

**ImagePrep**

Adjust the spray offset for trypsin and matrix deposition prior to the spray.

- Deposit the trypsin using Bruker's default method with minor modifications, settings used:

38% Spray Power with 0% Modulation, total number of 30 cycles with spraying time of 1.25 sec and 45 sec of drying.

- Deposit the matrix using Bruker's default HCCA method with minor modifications, settings used:

Phase	Sensor	Nebulization	Incubation	Drying
1	0.65V within 8-20 cycles	20% spray power $\pm$ 35% modulation with fixed spray time of 2.5 sec	10 sec	90 sec
2		30 Sec drying		
3	0.1V within 4-10 cycles	20% spray power $\pm$ 35% modulation with 0.05V sensor-controlled spray time		Complete dry every cycle, safe dry 10 sec
4	0.1V within 8-12 cycles	20% spray power $\pm$ 35% modulation with 0.1V sensor-controlled spray time		Grade 20% $\pm$ 40% complete dry every 2 cycle, safe dry 20 sec
5	0.3V within 12-30 cycles	25% spray power $\pm$ 35% modulation with 0.2V sensor-controlled spray time	30 sec $\pm$ 30 sec	Grade 30% $\pm$ 40% complete dry every 3 cycle, safe dry 30 sec
6	0.6 $\pm$ 0.5V within 20-64 cycles	25% spray power $\pm$ 35% modulation with 0.3V sensor-controlled spray time		Grade 40% $\pm$ 40% complete dry every 4 cycle, safe dry 40 sec
7	0.6 $\pm$ 0.5V within 20-64 cycles	25% spray power $\pm$ 35% modulation with 0.3V sensor-controlled spray time		Grade 40% $\pm$ 40%, complete dry every 4 cycle, safe dry 40 sec

## 6.2.2. Mass spectrometer system

**ESI- maxis Impact II QTOF**

Mass spectrometer (MS) must be calibrated as per the vendor's recommendations. For example, calibration on maxis Impact II QTOF can be performed using Agilent's ESI-L low concentration tuning mix on an enhanced quadratic calibration mode using Bruker's default calibration MS method.

Additionally, optimize the ionizing and spray condition and, if necessary, adjust the MS/MS timing with regards to the chromatographic peak width, mean number of precursor ions, averages in MS & MS/MS as well as active exclusion timing.

**MALDI-ultrafleXtreme TOF/TOF**

On the flexControl, load an appropriate reflectron positive method for the  $m/z$  range of 800-4500.

Optimize the laser power, offset, repetition rate, detector gain and acquisition rate.

**Supplementary Materials:** The following supporting information can be downloaded at: [www.mdpi.com/xxx/s1](http://www.mdpi.com/xxx/s1), Figure S1: Images of fallopian tube and endometrium tissues sections before and after laser capture microdissection. Table S1: List of  $m/z$  values identified from MALDI MSI analysis of endometrium and fallopian tube precancerous lesions and adjacent healthy tissue.

**Author Contributions:** MKO, PH and FW contributed conception and design of the study; GA, PM performed the experiments and together with MA, MKO, PH and MKH interpreted the data; MA wrote the first draft of the manuscript; GA, PM, MKO, MKH, GA, and FG wrote sections of the manuscript. All authors contributed to manuscript revision, read, and approved the submitted version.

**Funding:** M. K. O. and P. H. gratefully acknowledge the support of the Ovarian Cancer Research Foundation (OCRF), Australia and the National Collaborative Research Infrastructure Strategy (NCRIS) node for Tissue Imaging Mass Spectrometry.

**Data Availability Statement:** The mass spectrometry proteomics data have been deposited to the ProteomeXchange Consortium via the PRIDE partner repository [20] with the data set identifier PXD018538.

**Conflicts of Interest:** The authors declare no conflict of interest.

653  
654  
655  
656657  
658  
659  
660

661

662

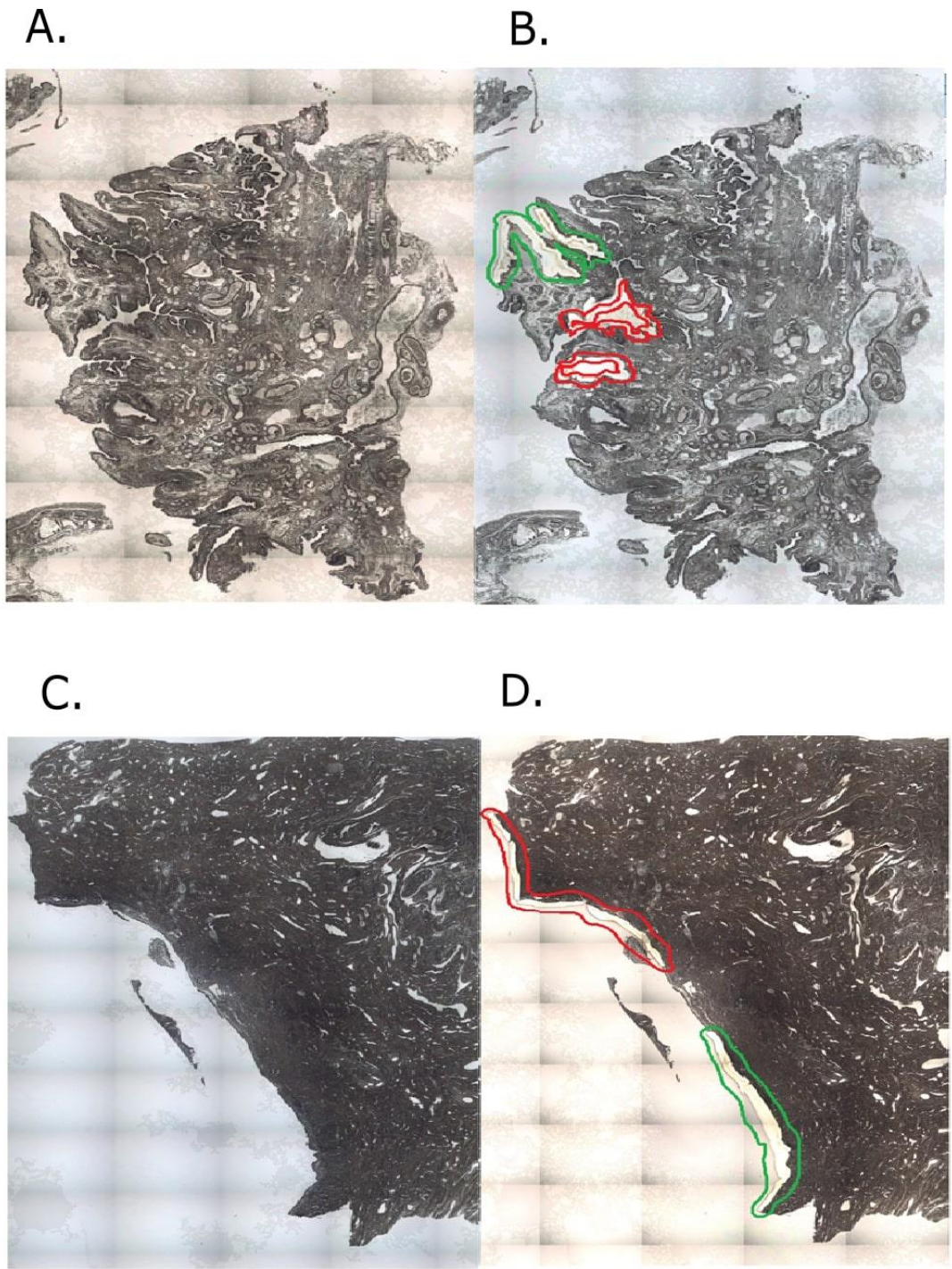
## References

1. Gustafsson, O.J., G. Arentz, and P. Hoffmann, *Proteomic developments in the analysis of formalin-fixed tissue*. *Biochim Biophys Acta*, 2015. **1854**(6): p. 559-80. 663
2. Tolcher, M.C., et al., *Characterization of precursor lesions in the endometrium and fallopian tube epithelium of early-stage uterine serous carcinoma*. *Int J Gynecol Pathol*, 2015. **34**(1): p. 57-64. 664
3. Hui, P., et al., *Minimal uterine serous carcinoma: a clinicopathological study of 40 cases*. *Mod Pathol*, 2005. **18**(1): p. 75-82. 665
4. Wheeler, D.T., et al., *Minimal uterine serous carcinoma: diagnosis and clinicopathologic correlation*. *Am J Surg Pathol*, 2000. **24**(6): p. 797-806. 666
5. Zheng, W., et al., *A proposed model for endometrial serous carcinogenesis*. *Am J Surg Pathol*, 2011. **35**(1): p. e1-e14. 669
6. Bowtell, D.D., *The genesis and evolution of high-grade serous ovarian cancer*. *Nat Rev Cancer*, 2010. **10**(11): p. 803-8. 670
7. George, S.H. and P. Shaw, *BRCA and Early Events in the Development of Serous Ovarian Cancer*. *Front Oncol*, 2014. **4**: p. 5. 671
8. Piek, J.M., et al., *Dysplastic changes in prophylactically removed Fallopian tubes of women predisposed to developing ovarian cancer*. *J Pathol*, 2001. **195**(4): p. 451-6. 672
9. Crum, C.P., et al., *Lessons from BRCA: the tubal fimbria emerges as an origin for pelvic serous cancer*. *Clin Med Res*, 2007. **5**(1): p. 35-44. 673
10. Crum, C.P., et al., *Through the glass darkly: intraepithelial neoplasia, top-down differentiation, and the road to ovarian cancer*. *J Pathol*, 2013. **231**(4): p. 402-12. 674
11. Xiang, L., et al., *Identification of candidate genes associated with tubal origin of high-grade serous ovarian cancer*. *Oncol Lett*, 2018. **15**(5): p. 7769-7775. 675
12. Perets, R., et al., *Transformation of the fallopian tube secretory epithelium leads to high-grade serous ovarian cancer in Brca;Tp53;Pten models*. *Cancer Cell*, 2013. **24**(6): p. 751-65. 676
13. Zhai, Y., et al., *High-grade serous carcinomas arise in the mouse oviduct via defects linked to the human disease*. *J Pathol*, 2017. **243**(1): p. 16-25. 677
14. Arentz, G., et al., *Applications of mass spectrometry imaging to cancer*, in *Advances in cancer research*. 2017, Elsevier. p. 27-66. 678
15. Fischer, A.H., et al., *Hematoxylin and Eosin Staining of Tissue and Cell Sections*. *Cold Spring Harbor Protocols*, 2008. **2008**(5): p. pdb.prot4986. 683
16. Start, R.D., et al., *Reassessment of the rate of fixative diffusion*. *Journal of Clinical Pathology*, 1992. **45**(12): p. 1120-1121. 684
17. Acland, M., et al., *Proteomic Analysis of Pre-Invasive Serous Lesions of the Endometrium and Fallopian Tube Reveals Their Metastatic Potential*. *Front Oncol*, 2020. **10**: p. 523989. 685
18. Wisniewski, J.R., et al., *Universal sample preparation method for proteome analysis*. *Nat Methods*, 2009. **6**(5): p. 359-62. 686
19. Tyanova, S., T. Temu, and J.J.N.p. Cox, *The MaxQuant computational platform for mass spectrometry-based shotgun proteomics*. 2016. **11**(12): p. 2301. 687
20. Perez-Riverol, Y., et al., *The PRIDE database and related tools and resources in 2019: improving support for quantification data*. *Nucleic Acids Res*, 2019. **47**(D1): p. D442-d450. 688
21. Gustafsson, O.J., et al., *Matrix-assisted laser desorption/ionization imaging protocol for in situ characterization of tryptic peptide identity and distribution in formalin-fixed tissue*. *Rapid Commun Mass Spectrom*, 2013. **27**(6): p. 655-70. 689
22. Folkins, A.K., et al., *A candidate precursor to pelvic serous cancer (p53 signature) and its prevalence in ovaries and fallopian tubes from women with BRCA mutations*. *Gynecol Oncol*, 2008. **109**(2): p. 168-73. 690
23. Zheng, W., et al., *Endometrial glandular dysplasia: a newly defined precursor lesion of uterine papillary serous carcinoma. Part I: morphologic features*. *Int J Surg Pathol*, 2004. **12**(3): p. 207-23. 691
24. Gustafsson, O.J.R., et al., *Matrix-assisted laser desorption/ionization imaging protocol for in situ characterization of tryptic peptide identity and distribution in formalin-fixed tissue*. *Rapid Communications in Mass Spectrometry*, 2013. **27**(6): p. 655-670. 692

- 
25. M. Acland, G.A., M. Mussared, F. Whitehead, P. Hoffmann, M. Klingler-Hoffmann and M. K. Oehler, *Proteomics Analysis of Pre-Invasive Serous Lesions of the Endometrium and Fallopian Tube Reveal Their Metastatic Potential* *Frontiers in Oncology*, 2020 (under review)(Proteomics and its Applications in Cancer). 706-708
26. Ricciardelli, C., et al., *Transketolase is upregulated in metastatic peritoneal implants and promotes ovarian cancer cell proliferation*. *Clin Exp Metastasis*, 2015. **32**(5): p. 441-55. 709-710
27. Zhang, C., et al., *MALDI Mass Spectrometry Imaging Reveals Decreased CK5 Levels in Vulvar Squamous Cell Carcinomas Compared to the Precursor Lesion Differentiated Vulvar Intraepithelial Neoplasia*. *Int J Mol Sci*, 2016. **17**(7). 711-712
28. Mittal, P., et al., *Annexin A2 and alpha actinin 4 expression correlates with metastatic potential of primary endometrial cancer*. *Biochim Biophys Acta Proteins Proteom*, 2017. **1865**(7): p. 846-857. 713-714
29. Mittal, P., et al., *Lymph node metastasis of primary endometrial cancers: Associated proteins revealed by MALDI imaging*. *Proteomics*, 2016. **16**(11-12): p. 1793-801. 715-716
30. Mittal, P., et al., *Annexin A2 and alpha actinin 4 expression correlates with metastatic potential of primary endometrial cancer*. *Biochimica et Biophysica Acta (BBA) - Proteins and Proteomics*, 2017. **1865**(7): p. 846-857. 717-718
31. Gustafsson, O.J., et al., *MALDI imaging mass spectrometry of N-linked glycans on formalin-fixed paraffin-embedded murine kidney*. *Anal Bioanal Chem*, 2015. **407**(8): p. 2127-39. 719-720
32. Briggs, M.T., et al., *MALDI mass spectrometry imaging of N-glycans on tibial cartilage and subchondral bone proteins in knee osteoarthritis*. *Proteomics*, 2016. **16**(11-12): p. 1736-41. 721-722
33. Everest-Dass, A.V., et al., *N-glycan MALDI Imaging Mass Spectrometry on Formalin-Fixed Paraffin-Embedded Tissue Enables the Delineation of Ovarian Cancer Tissues*. *Mol Cell Proteomics*, 2016. **15**(9): p. 3003-16. 723-724
34. Briggs, M.T., et al., *MALDI Mass Spectrometry Imaging of Early- and Late-Stage Serous Ovarian Cancer Tissue Reveals Stage-Specific N-Glycans*. *Proteomics*, 2019. **19**(21-22): p. e1800482. 725-726
35. Arentz, G., et al., *Applications of Mass Spectrometry Imaging to Cancer*. *Adv Cancer Res*, 2017. **134**: p. 27-66. 727
36. Briggs, M.T., et al., *N-Glycan matrix-assisted laser desorption/ionization mass spectrometry imaging protocol for formalin-fixed paraffin-embedded tissues*. *Rapid Commun Mass Spectrom*, 2017. **31**(10): p. 825-841. 728-729
37. Li, X., W. Wang, and J. Chen, *Recent progress in mass spectrometry proteomics for biomedical research*. *Sci China Life Sci*, 2017. **60**(10): p. 1093-1113. 730-731
38. Gustafsson, J.O., et al., *Internal calibrants allow high accuracy peptide matching between MALDI imaging MS and LC-MS/MS*. *J Proteomics*, 2012. **75**(16): p. 5093-105. 732-733-734

1 2.5. Supplementary Data

2



3

4 **Supplementary Figure 1:** Endometrial and fallopian tube tissue sections before and after laser  
5 capture microdissection (LCM). A) Endometrial tissue section before LCM. B) Endometrial  
6 tissue section after EIC is extracted via LCM. C) Fallopian tube tissue section before LCM. D)  
7 Fallopian tube tissue section after STIC is extracted via LCM.



1 **Supplementary Table 1:**

2 Full list of molecular features identified in EIC and STIC via MALDI Mass Spectrometry.

3 (Can be found online – pending publication)

4

5

6

7

8

9

10

11

12

13

14

15

16

17

18

19

20

21

22

23

24

25

26

27

28

29

1  
2  
3  
4  
5  
6  
7  
8  
9  
10  
11  
12  
13  
14  
15  
16  
17  
18  
19  
20  
21  
22  
23  
24  
25  
26  
27  
28  
29

This page is intentionally left blank

1  
2  
3  
4  
5  
6  
7  
8  
9  
10  
11  
12  
13  
14  
15  
16  
17  
18  
19  
20  
21  
22  
23  
24  
25  
26

# CHAPTER 3: Proteomics Analysis of Serous Lesions of the Endometrium and Fallopian Tube Reveals Their Metastatic Potential

---

1 3.1. Summary

2 Having established the method for proteomic analysis of precancerous lesions located within the  
3 endometrium and fallopian tube, as outlined in the previous chapter, additional LC-MS/MS  
4 analysis was performed. Samples from a single patient, who displayed both EIC and STIC in the  
5 absence of synchronous gynaecological malignancy, were investigated. We utilise gene  
6 expression data bases to compare proteins of interest to gene expression in numerous subtypes of  
7 ovarian and endometrial cancer to further elucidate a connection between these precancerous  
8 lesions and subsequent invasive carcinoma.

9 In addition to providing an insight into the connection between these precancerous lesions and  
10 subsequent invasive carcinoma, we identified numerous migration and metastasis related  
11 proteins in the precancerous lesions. Together, this suggests that these lesions may possess more  
12 metastatic potential than previously thought and may establish tumours in the ovary,  
13 endometrium, or peritoneum at an early stage in their development.

14 While our findings are restricted by the single case study nature of the sample, it represents the  
15 first proteomic analysis of these precancerous lesions in a patient which does not have  
16 synchronous cancer. This is of great importance in the investigation of lesions which are truly  
17 precancerous and not simply metastatic implants from a more developed primary tumour. This  
18 establishes the foundation for further proteomics analyses of precancerous lesions of the ovary  
19 and endometrium to better understand the early steps in their neoplastic development.

20  
21  
22  
23  
24  
25  
26  
27  
28  
29  
30  
31  
32  
33  
34

1  
2  
3  
4  
5  
6  
7  
8  
9  
10  
11  
12  
13  
14  
15  
16  
17  
18  
19  
20  
21  
22  
23  
24  
25  
26  
27

This page is intentionally left blank

1 3.2. Statement of Authorship

2

Title of Paper	Proteomic Analysis of Pre-Invasive Lesions of the Endometrium and Fallopian Tube Reveals Their Metastatic Potential
Publication Status	<input checked="" type="checkbox"/> Published <input type="checkbox"/> Accepted for Publication <input type="checkbox"/> Submitted for Publication <span style="float: right;">Unpublished and Unsubmitted work written in manuscript style</span>
Publication Details	M. Acland, G. Arentz, M. Mussared F. Whitehead, P. Hoffmann, M. Klingler-Hoffmann and M. K. Oehler, <u>Frontiers in Oncology</u> , 15; 10:523989 (2020)

3

4 **Principal Author**

Name of Principal Author (Candidate)	Mitchell Acland			
Contribution to the Paper	Performed data analysis and data interpretation, wrote the first draft of the article and consolidated the final manuscript.			
Overall percentage (%)	70%			
Certification:	This paper reports on original research I conducted during the period of my Higher Degree by Research candidature and is not subject to any obligations or contractual agreements with a third party that would constrain its inclusion in this thesis. I am the primary author of this paper.			
Signature	<table border="1" style="width: 100%;"> <tr> <td style="width: 60%;"></td> <td style="width: 10%;">Date</td> <td style="width: 30%;">27/05/2022</td> </tr> </table>		Date	27/05/2022
	Date	27/05/2022		

5

6 **Co-Author Contributions**

7 By signing the Statement of Authorship, each author certifies that:

- 8 i. the candidate's stated contribution to the publication is accurate (as detailed above);
- 9 ii. permission is granted for the candidate to include the publication in the thesis; and
- 10 iii. the sum of all co-author contributions is equal to 100% less the candidate's stated contribution.

11

Name of Co-Author	Georgia Arentz			
Contribution to the Paper	Contributed to experimental and manuscript design. Performed mass spectrometry analysis and contributed to data analysis and interpretation			
Signature	<table border="1" style="width: 100%;"> <tr> <td style="width: 60%;"></td> <td style="width: 10%;">Date</td> <td style="width: 30%;">16/2/2021</td> </tr> </table>		Date	16/2/2021
	Date	16/2/2021		

12

13

Name of Co-Author	Max Mussared		
Contribution to the Paper	Performed statistical analyses		
Signature		Date	15/02/2021

1

Name of Co-Author	Fergus Whitehead		
Contribution to the Paper	Performed histological and immunohistochemical analyses.		
Signature		Date	

2

Name of Co-Author	Peter Hoffmann		
Contribution to the Paper	Supervised development of work, data interpretation and manuscript evaluation.		
Signature		Date	24/05/2022

3

Name of Co-Author	Manuela Klingler-Hoffmann		
Contribution to the Paper	Supervised development of work, data interpretation and manuscript evaluation.		
Signature		Date	24/05/22

4

Name of Co-Author	Martin Oehler		
Contribution to the Paper	Supervised development of work, data interpretation and manuscript evaluation. Provided original samples and acted as corresponding author		
Signature		Date	20 February 2021

5

6

7

8

9



# Proteomic Analysis of Pre-Invasive Serous Lesions of the Endometrium and Fallopian Tube Reveals Their Metastatic Potential

Mitchell Acland<sup>1</sup>, Georgia Arentz<sup>1</sup>, Max Mussared<sup>2</sup>, Fergus Whitehead<sup>3</sup>, Peter Hoffmann<sup>4\*</sup>, Manuela Klingler-Hoffmann<sup>4\*</sup> and Martin K. Oehler<sup>4,5,6\*</sup>

## OPEN ACCESS

### Edited by:

Harsha Gowda,  
The University of Queensland,  
Australia

### Reviewed by:

Wa Xian,  
University of Connecticut,  
United States  
Jian-Jun Wei,  
Northwestern University,  
United States

### \*Correspondence:

Martin K. Oehler  
martin.oehler@adelaide.edu.au  
Peter Hoffmann  
peter.hoffmann@unisa.edu.au  
Manuela Klingler-Hoffmann  
Manuela.Klingler-Hoffmann@unisa.edu.au

### Specialty section:

This article was submitted to  
Molecular and Cellular Oncology,  
a section of the journal  
Frontiers in Oncology

**Received:** 17 January 2020

**Accepted:** 28 October 2020

**Published:** 15 December 2020

### Citation:

Acland M, Arentz G, Mussared M,  
Whitehead F, Hoffmann P,  
Klingler-Hoffmann M and Oehler MK  
(2020) Proteomic Analysis of Pre-  
Invasive Serous Lesions of the  
Endometrium and Fallopian Tube  
Reveals Their Metastatic Potential.  
*Front. Oncol.* 10:523989.  
doi: 10.3389/fonc.2020.523989

<sup>1</sup> Adelaide Proteomics Centre, School of Biological Sciences, The University of Adelaide, Adelaide, SA, Australia, <sup>2</sup> School of Mathematical Sciences, The University of Adelaide, Adelaide, SA, Australia, <sup>3</sup> Cytopathology Department, Clinpath Pathology, Adelaide, SA, Australia, <sup>4</sup> Future Industries Institute, Mawson Lakes Campus, University of South Australia, Adelaide, SA, Australia, <sup>5</sup> Department of Gynaecological Oncology, Royal Adelaide Hospital, North Terrace, Adelaide, SA, Australia, <sup>6</sup> Robinson Research Institute, Discipline of Obstetrics and Gynaecology, Adelaide Medical School, The University of Adelaide, SA, Australia

Serous endometrial cancer (SEC) and high grade serous ovarian cancer (HGSOC) are aggressive gynecological malignancies with high rates of metastasis and poor prognosis. Endometrial intraepithelial carcinoma (EIC), the precursor for SEC, and serous tubal intraepithelial carcinoma (STIC), believed to be the precursor lesion for HGSOC, can also be associated with intraabdominal spread. To provide insight into the etiology of these precancerous lesions and to explore the potential molecular mechanisms underlying their metastatic behavior, we performed a proteomic mass spectrometry analysis in a patient with synchronous EIC and STIC. Through histological and molecular identification of precancerous lesions followed by laser capture microdissection, we were able to identify over 450 proteins within the precancerous lesions and adjacent healthy tissue. The proteomic analysis of STIC and EIC showed remarkable overlap in the proteomic patterns, reflecting early neoplastic changes in proliferation, loss of polarity and attachment. Our proteomic analysis showed that both EIC and STIC, despite being regarded as premalignant lesions, have metastatic potential, which correlates with the common presentation of invasive serous gynecological malignancies at advanced stage.

**Keywords:** proteomics, serous tubal intraepithelial carcinoma, endometrial intraepithelial carcinoma, serous endometrial carcinoma, high grade serous ovarian carcinoma

## INTRODUCTION

Endometrial cancer (EC) is the 6<sup>th</sup> most common cancer in women worldwide and is the most common gynecological malignancy (1). Despite significant advances in early detection (2), molecular subtyping (3, 4), and new or improved treatment regimens (5), the relative survival of patients with EC has declined in recent times (6, 7).



Serous endometrial carcinoma (SEC) is a highly aggressive malignancy (8). It represents only 10% of EC cases (9, 10) but is responsible for 39% of EC related deaths (11) and is frequently diagnosed at late stage when prognosis is poor (9, 10). The current model of SEC development suggests that it evolves from a pre-neoplastic lesion in atrophic endometrium called endometrial glandular dysplasia (EmGD) (12, 13). This lesion then progresses further into endometrial intraepithelial carcinoma (EIC) and, finally, into SEC (14).

EmGD is characterized by loss of cell polarity, nuclear atypia, and nuclear hyperchromasia (12). It has a marked loss of heterozygosity in TP53 and chromosome p1; however, this is to a lesser extent than that seen in EIC and SEC (12). Although quite difficult to identify, nucleomegaly and staining for p53, MIB-1 as well as IMP3 are characteristics of EmGD (14). The connection between EmGD and SEC has been confirmed through identical mutations observed in EmGD and subsequent SEC (15).

EIC was first described in the 1990s (16) and seen to arise almost exclusively in atrophic endometrium and in the context of SEC in a majority of cases (17). EIC exhibit similar features as EmGD but with further nucleomegaly, nuclear irregularity and hyperchromasia (14). However, cases of EIC associated with extrauterine metastasis suggest that EIC may more closely resemble SEC (18, 19). This early peritoneal spread is in stark contrast to non-serous endometrial cancers which usually do not show early peritoneal spread but preferentially invade the myometrium and spread to the lymph nodes (18, 19).

SEC closely resembles other serous cancers of the female genital tract, such as high grade serous ovarian cancer (HGSOC) (4). Both diseases share similar molecular features and clinical properties (20) and, consequently, are treated in a similar way (21, 22).

In recent years the fallopian tube has been identified as the precursor site of HGSOC, specifically serous tubal intraepithelial carcinoma (STIC) (23–27). These lesions are identified histopathologically by a “p53 signature” comprised of strong p53 staining (28), p53 mutations (29), positive  $\gamma$ -H2AX staining (indicating DNA damage) and lack of Ki-67 staining (indicating low proliferation) (30) (Table 1). STICs share many genomic features with HGSOC, such as genomic instability (31, 32), and HGSOC has a gene expression profile more similar to the fallopian epithelium than the ovarian surface epithelium (33).

Results from studies using mouse models have established a connection between STIC and subsequent HGSOC (34, 35). Inactivation of PTEN, p53 and BRCA1/2 in the fallopian tubes of mice resulted in STIC and concurrent HGSOC with ovarian

and peritoneal spread (34, 35). However, in the absence of BRCA1/2 inactivation, STIC developed but did not progress to metastatic HGSOC in this mouse model (34).

Cases of HGSOC arising in the absence of STIC (35–37) have also been reported suggesting that other, as yet unidentified, precursor lesions might exist (38). “Early Serous Tubal Proliferations” (ESTP) have been identified as a potential HGSOC precursor. They are found in the fimbria (30), demonstrate DNA damage (30), and are found in non-ciliated cells, which also give rise to STIC (39). A physical and lineage continuity has been demonstrated between ESTP and STIC suggesting that some ESTP give rise to STIC and subsequently to HGSOC (30, 32).

The understanding that HGSOC arises from the fallopian tube in many cases has changed the understanding of serous ovarian cancer. Now serous cancers of the fallopian tube, peritoneum and ovary are thought to share a common origin in the fallopian tube (20). While it is well established that many HGSOC arise from the fallopian tube, it has not been excluded that some serous cancers of the endometrium and ovary may share common origins. For example, Roelofsen et al. (40) suggested that some serous ovarian cancers (SOC) may arise from EIC by showing that they shared TP53 mutations, similar expression of p53, Ki67, estrogen, and progesterone receptors (40). Additionally, Tolcher et al. (20) analyzed 38 patients with SEC and investigated their fallopian tubes. They found STIC, without evidence of tubal metastasis, in 2 of these cases (20).

To better understand the potential link between serous preinvasive lesions of the female genital tract and serous gynaecological cancer, molecular investigations of the precursor lesions of the endometrium and fallopian tube are required. Here, we present the first proteomic analysis of synchronous precancerous lesions of the endometrium and fallopian tubes in a patient without invasive malignancy, by means of mass spectrometry. This precludes the possibility of these premalignant lesions representing metastases from established primary tumors. The analysis of EIC and STIC in this context provides insight into the temporal and mechanistic features of their development and dissemination.

## MATERIALS AND METHODS

### Sample

Archived formalin-fixed paraffin-embedded (FFPE) fallopian tube and endometrial tissues from a 67-year-old female who

**TABLE 1** | Morphological and molecular features of precancerous lesions of the gynecological tract.

Location	Precancerous lesion	Morphological features	Molecular features
Endometrium	EmGD	Some nuclear atypia, some nucleomegaly.	Low rates of loss of heterozygosity in TP53 and chromosome P1. p53 mutations in 50% of cells. Staining for P53, MIB1, and IMP3.
	EIC	Extensive nuclear atypia, extensive nucleomegaly, hyperchromasia.	High rates of loss of heterozygosity in TP53 and chromosome P1. p53 mutations in 75% of cells. Strong staining for P53, MIB1, and IMP3.
Fallopian tube	ESTP	No visible morphological features.	TP53 mutations, p53 staining, DNA damage.
	STIC	Hyperchromasia, nucleomegaly.	TP53 mutations, p53 and MIB1 staining, DNA damage, Chromosomal instability.

had undergone a total abdominal hysterectomy and bilateral salpingo-oophorectomy for endometrial hyperplasia was retrieved for analysis with approval of the Research Ethics Committee of the Royal Adelaide Hospital. The fallopian tube and endometrial tissues were processed using standard procedures, stained with hematoxylin and eosin, and annotated by a pathologist. P53 and MIB1 immunostaining was also performed to confirm the location of precancerous lesions.

## Laser Microdissection and Sample Preparation

FFPE tissues were sectioned at 4- $\mu$ m thickness, water bath mounted onto PEN membrane slides (Micro-Dissect, Herborn, Germany), and deparaffinized by submersion in xylene for 5 min, following by two 2-min incubations in 100% ethanol, and two 5-min incubations in water. Areas of STIC, EIC and adjacent healthy epithelium were dissected using a Leica AS LCM microscope (Leica Microsystems, Wetzlar, Germany) into 20  $\mu$ l of 10 mM citric acid buffer (pH = 6) and subjected to heat induced antigen retrieval by incubation at 100°C for 90 min. The solution containing the protein extracts were digested with trypsin gold (Promega, Madison, WI, USA) as described in Mittal et al. (41) using a modified FASP method (42). In brief, protein extracts were mixed with 0.2 ml of 8M urea in 0.1M Tris/HCl, pH 8.5 before being loaded into a 30k Microcon filtration device (Millipore) and centrifuged at 14,000g for 15 min. This step was repeated to ensure the removal of any residual contaminants. Samples were reduced with 5 mM DTT (Roche) for 45 min at room temperature and alkylated with 10mM iodoacetamide (IAA) (GE Healthcare, Little Chalfont, UK) for 30 min at room temperature in the dark followed by centrifugation at 14,000g for 15 min. The protein concentrate was diluted with 0.2mL of 8M urea in 0.1M Tris/HCl, pH 8.5, and spun again at 14,000g for 15 min. This step was repeated twice. Samples were buffered with 10mM  $\text{NH}_4\text{HCO}_3$  and digested with 100ng trypsin gold overnight at 37°C. Peptides were collected by centrifugation of the filter unit at 14,000g for 20 min.

## Nanoflow Liquid Chromatography Tandem Mass Spectrometry

Nanoflow liquid chromatography tandem mass spectrometry (Nano-LC-MS/MS) was performed on each sample in duplicate using an Ultimate 3000 RSLC system (Thermo-Fisher Scientific, Waltham, USA) coupled to an Impact HD<sup>TM</sup> QTOF mass spectrometer (Bruker Daltonics, Bremen, Germany) *via* an Advance CaptiveSpray source (Bruker Daltonics). Peptide samples were pre-concentrated onto a C18 trapping column (Acclaim PepMap100 C18 75  $\mu$ m  $\times$  20 mm, Thermo-Fisher Scientific) at a flow rate of 5  $\mu$ l/min in 2% (v/v) ACN 0.1% (v/v) TFA for 10 min. Peptide separation was performed using a 75  $\mu$ m ID C18 column (Acclaim PepMap100 C18 75  $\mu$ m  $\times$  50 cm, Thermo-Fisher Scientific) at a flow rate of 0.2  $\mu$ l/min using a linear gradient from 5 to 45% B (A: 5% (v/v) ACN 0.1% (v/v) FA, B: 80% (v/v) ACN 0.1% (v/v) FA) over 130 min, followed by a 20-min wash with 90% B, and a 20-min equilibration with 5% A. MS

scans were acquired in the mass range of 300 to 2,200 m/z in a data-dependent fashion using Bruker's Shotgun Instant Expertise<sup>TM</sup> method. This method uses IDAS (intensity dependent acquisition speed) to adapt the speed of acquisition depending on the intensity of precursor ions (fixed cycle time), and RT<sup>2</sup> (RealTime Re-Think) to exclude previously selected precursor ions from undergoing re-fragmentation unless the chromatographic peak intensity of the ion has increased by a factor of 5. Singly charged precursor ions were excluded from acquisition. Collision energy ranged from 23% to 65% as determined by the m/z of the precursor ion.

## Data Analysis

Spectra were analyzed using the MaxQuant software (version 1.5.2.8) with the Andromeda search engine (43) against the UniProt non-redundant human database. The standard Bruker QTOF settings in MaxQuant were used with a mass error tolerance of 40 ppm. The variable modifications of oxidation of methionine and the fixed modification of carbamidomethyl of cysteines were specified, with the digestion enzyme specified as trypsin. The protein false discovery rate (FDR) and peptide spectrum match FDRs were both set to 1% using a target decoy approach, with a minimum peptide length of 7 amino acids (43). Only unique and razor peptides were used when reporting protein identifications.

## Gene Expression Analysis

In order to assess the gene expression levels of the corresponding proteins of interest in early stage I ovarian carcinoma tissues, the dataset of Yoshihara et al. (44) [Gene Expression Omnibus (GEO) Accession GSE12470, <http://www.ncbi.nlm.nih.gov/geo/>] was considered. From this dataset the expression of EPCAM and CAPS was considered in 8 in early stage I patients compared to 10 healthy peritoneum control tissues. The results were natural log transformed and compared using paired T-tests and p-values < 0.05 were considered significant. Full patient details are available in the Yoshihara et al. (44) manuscript.

To assess the gene expression levels of the corresponding proteins of interest in differing subtypes of EOC, the dataset of Hendrix et al. (45) (GEO Accession GSE6008, <http://www.ncbi.nlm.nih.gov/geo/>) was considered. From this dataset the expression of TPPP3, SORD and VCAN was investigated in 37 endometrioid, 41 serous, 13 mucinous, and 8 clear cell ovarian carcinoma tissues, and 4 normal control tissues. Transformation of the data and full patient details are available from the Hendrix et al. (45) manuscript. Groups were compared using paired T-tests and p-values < 0.05 were considered significant.

With the aim to assess the gene expression levels of corresponding proteins in early stage I endometrial carcinoma tissue, R was used to investigate the data set of Days et al. (46) (GEO Accession GDS4589, <http://www.ncbi.nlm.nih.gov/geo/>). This dataset the expression of EPCAM and CAPS were investigated in 79 endometrioid and 12 serous papillary endometrial carcinoma tissues, and in 12 normal control tissues. The results were natural log transformed and compared using paired T-tests. P-values < 0.05 were considered significant. Full patient details are available through the Day's et al. (46) manuscript.

To evaluate the gene expression levels of corresponding proteins in different subtypes of endometrial carcinoma tissue, R was used to investigate the data set of Kandolph et al. (4) (<https://gdc.cancer.gov/node/875>). From this data set the expression of TPPP3, SPATA18, ERO1A, SORD and VCAN were investigated in 13 CN high, 15 CN low, 16 MSI hypermutated, and 4 POLE ultra-mutated carcinoma tissues. Transformation of the data set is detailed in Kandolph et al. (4). Groups were compared using paired T-tests and p-values < 0.05 were considered significant. Full patient details are available in the Kandolph et al. (4) manuscript.

## RESULTS

### Histological Analysis Identifying STIC and EIC

Upon analysis of the H&E stained tissue sections, atypical intraepithelial proliferation involving a small population of cells in the endometrium were identified. These changes were consistent with early stages of EIC (**Table 1**). Similarly, atypical changes involving a small population of cells in the fimbriated tube (**Table 1**), consistent with early stages of STIC, were detected and both EIC and STIC are represented in **Figure 1**. Immunoperoxidase staining for p53 and MIB1 revealed atypical intraepithelial epithelial proliferations in both the fimbriated tube and endometrial lining, confirming the presence of STIC and EIC (data not shown).

### Proteomic Comparison of Healthy Epithelia to STIC and EIC

Regions of STIC, EIC, and adjacent healthy epithelium were laser microdissected (LMD) from sectioned tubal and endometrial specimens and analyzed by Nano-LC-MS/MS. In total, 453 proteins were detected across the 4 tissue types (369 proteins in the STIC, 110 proteins in healthy tubal epithelium, 428 proteins in EIC, and 162 proteins in healthy endometrial epithelium (**Supplementary Table 1**).

When comparing the numbers of identified proteins, the greatest overlap occurred between STIC and EIC with 348 identical proteins identified in both samples. Across all tissue types 73 proteins were detectable, with 96 identical proteins identified in both the STIC and healthy tubal tissue, 157 identical proteins detected in both the EIC and healthy endometrial tissue, and 85 identical proteins were detected in both healthy tissues (**Figure 2**).

### Proteins Relevant to STIC, EIC, and the Development of Gynecological Cancer

In analyzing potential links between STIC and EIC cells and their respective invasive carcinomas, two of the identified proteins were of particular interest based on their involvement in gynecological cancer development: Epithelial cell adhesion molecule (EPCAM) and Calcyphosin (CAPS) (47–49). EPCAM was identified in both the STIC and EIC tissue samples but was not detected in either of the healthy tissues while CAPS was only detected in the healthy tube and in STIC.

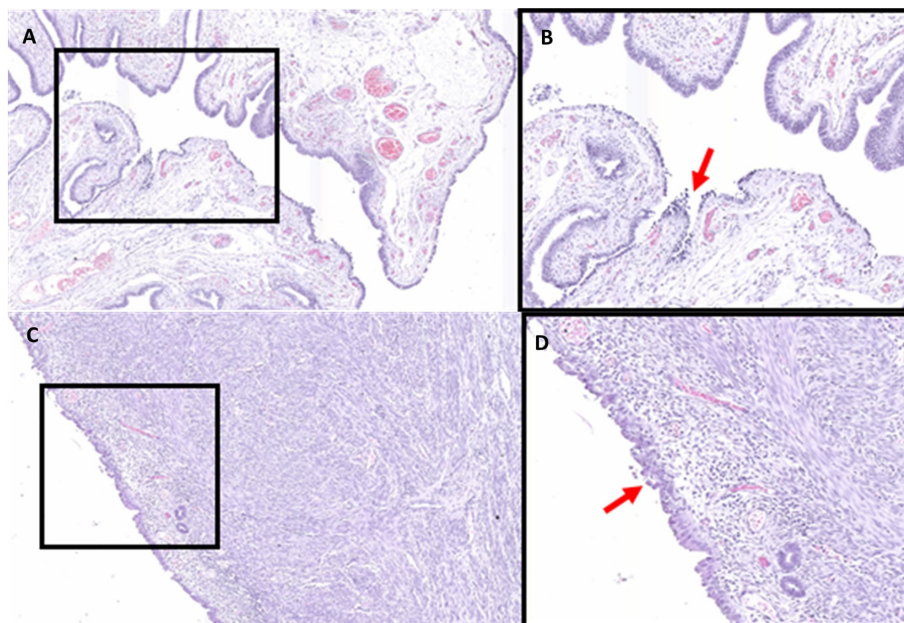


**FIGURE 1** | Hematoxylin and Eosin stained fallopian tube (**A, B**) and endometrium tissue (**C, D**) at 6× (**A, C**) and 12× (**B, D**) magnification. Areas of STIC (**B**) and EIC (**D**) are indicated by the red arrows.

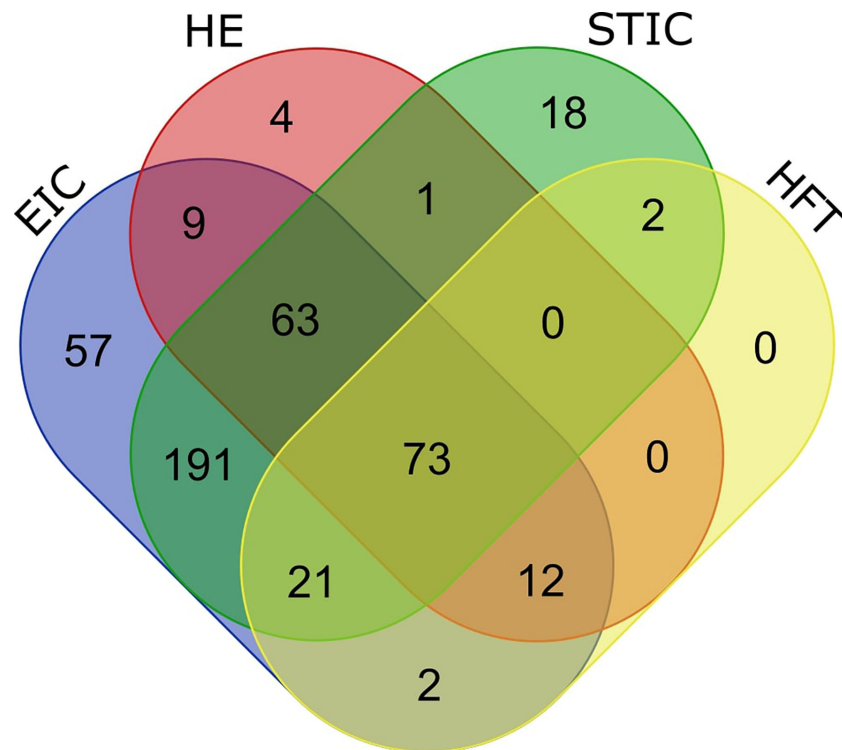


**FIGURE 2** | Venn diagram describing overlapping protein identifications in endometrial intraepithelial carcinoma (EIC), healthy endometrium (HE), serous tubal intraepithelial carcinoma (STIC) and healthy fallopian tube (HFT). A significant overlap of (348 proteins) is observed between EIC and STIC (diagram generated at <http://bioinformatics.psb.ugent.be/webtools/Venn/>).

### Expression of EPCAM and CAPS in Early Stage Serous Ovarian Carcinomas Compared to Healthy Peritoneal Tissue

To evaluate the expression of *EPCAM* and *CAPS* in early stage I serous ovarian carcinoma tissues, oligonucleotide microarray data was considered from the GEO data set GSE12470 (44). We chose to investigate the expression of these genes in early stage ovarian cancer as this is expected to be the stage following STIC in the development of serous ovarian cancer. STIC lesions were not deemed an appropriate comparison samples as they are often taken in the context of metastatic disease and potentially represent metastatic implants, and therefore more developed cancer, rather than true precursor lesions.

The gene expression levels were analyzed in 10 healthy peritoneal control tissues compared to 8 Stage I serous EOC tissues. The median expression levels of both *CAPS* and *EPCAM* were found to be significantly increased in the Stage I serous OC tissues compared to healthy peritoneal controls ( $p = 0.00014$  and  $p = 3.3 \times 10^{-7}$ , respectively) (**Figure 3**).

Healthy OSE is infrequently available for research purposes given healthy ovaries are rarely removed during any type of medical procedure. Healthy peritoneum is an effective control because the lining of the ovaries is comprised of a single-cell mesothelial layer of poorly differentiated epithelium derived from the coelomic epithelium and extended to the serosa

peritoneal cavity (50). In addition, it has been reported that peritoneal mesothelium and OSE are structurally very similar (51) and are both negative for *EPCAM* and *CAPS* expression (52, 53).

### Expression of EPCAM and CAPS in Early Stage Endometrial Carcinoma Compared to Healthy Endometrial Tissue

To assess the expression of *EPCAM* and *CAPS* in early stage endometrial cancer, oligonucleotide microarray data was considered from the GEO data set GDS4589. The gene expression levels were analyzed from 79 endometrioid and 12 serous papillary endometrial carcinomas as well as 12 healthy controls. The median expression of *CAPS* was increased significantly in EEC ( $p = 0.00066$ ), while it was significantly decreased in SEC ( $p = 0.023$ ) compared to healthy endometrium. The median expression of *EPCAM* was significantly increased in EEC ( $p = 0.02$ ) and further increased in SEC ( $p = 0.0007$ ) compared to healthy controls (**Figure 4**).

### Expression of Proteins Identified Exclusively in the STIC or EIC Across Ovarian Cancer Subtypes

Proteins detected exclusively in either the STIC or EIC tissues were analyzed to determine if their expression is specific to

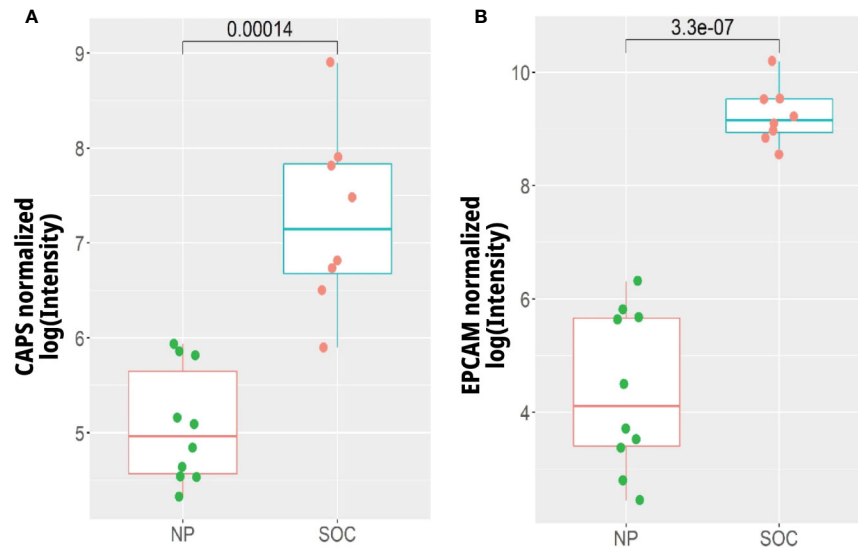


**FIGURE 3** | Gene expression of **(A)** CAPS and **(B)** EPCAM in early stage I serous ovarian cancer tissues (SOC) ( $n = 8$ ) compared to normal peritoneum (NP) ( $n = 10$ ). Expression levels were extracted from the data of Yoshihara et al. (44) (GEO Accession GSE12470) via the R package CuratedOvarianData (<http://www.ncbi.nlm.nih.gov/geo/>).

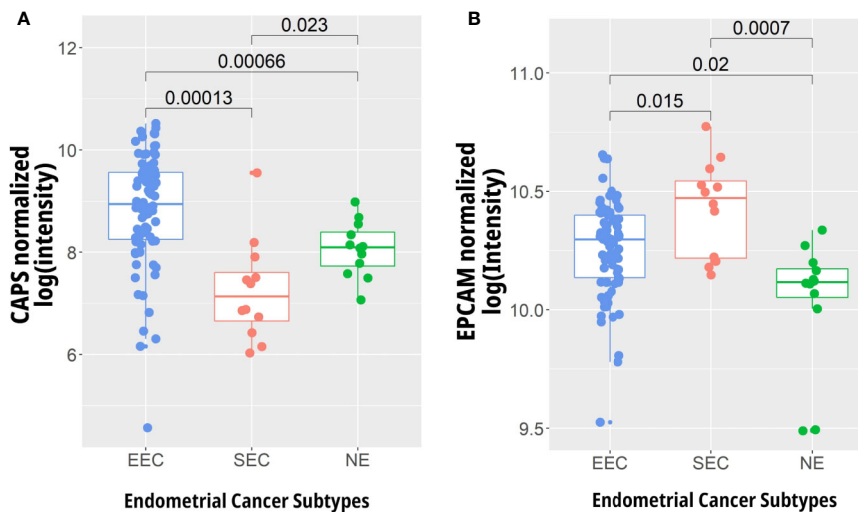


**FIGURE 4** | Gene expression analysis of **(A)** CAPS and **(B)** EPCAM in early stage endometrioid (EEC) ( $n = 79$ ) and serous (SEC) endometrial carcinoma ( $n = 12$ ) compared to normal endometrium (NE) ( $n = 12$ ). Expression levels were extracted from the data of Days et al. (46) (GEO Accession GDS4589, <http://www.ncbi.nlm.nih.gov/geo/>) using R.

certain gynecological tissues. Marker proteins expressed exclusively by the precancerous cells of either the tube or endometrium, which are also expressed by ovarian carcinomas, may aid in determining the tissue specific origin of HGSOE. Eighteen proteins were detected exclusively in the STIC tissue and 57 proteins in the EIC tissue. Of these proteins a small number appear to be specific to certain gynecological tissues according to Protein Atlas; 2 identified from STIC (MIEAP,

TPPP3), and 3 identified from EIC (ERO1A, DHSO, CSPG2/VCAN). These proteins and their tissue specificities across all gynecological tissues are listed in **Table 2**. The remaining proteins appeared to be more homogeneously expressed and hence were not analyzed further.

The gene expression levels corresponding to the proteins listed in **Table 2** were compared using oligonucleotide microarray data from the GEO data set GSE6008 (**Figure 5**).

**TABLE 2** | Proteins identified exclusively in the STIC or EIC that appear to be specific to certain gynaecological tissues.

Protein	Detected In	Protein abundance levels in healthy tissues *	Protein abundance in ovarian cancer *	Protein abundance in endometrial cancer *
Mitochondrial eating protein (MIEAP), <i>SPATA18</i> <sup>#</sup>	STIC	High in fallopian tube, low in endometrium and breast. Not expressed in the ovary.	Low	Low
Tubulin polymerization-promoting protein member 3 (TPPP3), <i>TPPP3</i>	STIC	Medium in glandular cells of the endometrium and cervix. Highly enriched in tube, negative in ovaries.	Medium	Medium to high
Endoplasmic reticulum oxidoreductin1-like protein alpha (ERO1A), <i>ERO1A</i> <sup>#</sup>	EIC	High in cervix and medium in endometrium. No expression in tube or ovary.	Low	Low
Sorbitol dehydrogenase (DHSO), <i>SORD</i>	EIC	High in endometrium, cervix/uterus, and low in breast. Negative in tube and ovaries.	Low	Medium
Versican core protein (CSPG2), <i>VCAN</i>	EIC	High in placenta. Medium in cervix/uterus, and endometrium. Low in tube and ovaries.	Low to medium	Low to Medium

\*According to Protein Atlas (<http://www.proteinatlas.org/>).

<sup>#</sup>Not present in the Hendrix et al. data set. (45).

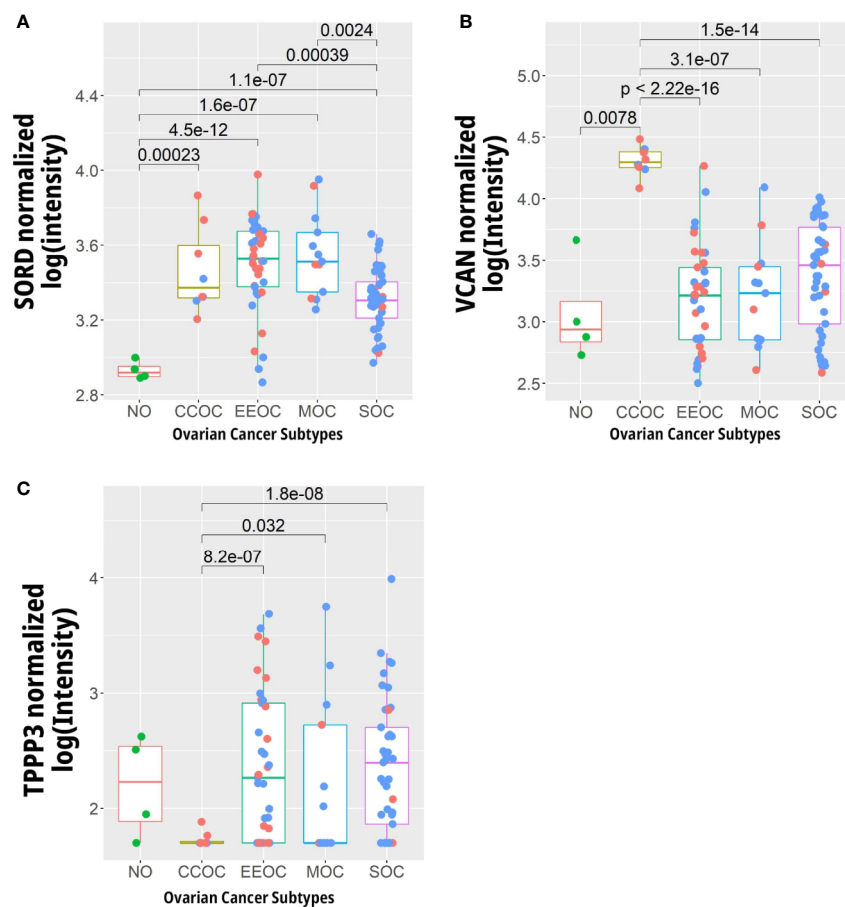


**FIGURE 5** | Expression levels of genes whose protein abundance is specific to certain to gynaecological tissues. **(A)** SORD, **(B)** TPP3, and **(C)** VCAN in 4 normal ovarian (NO), 8 clear cell (CCOC), 37 endometrial (EEOC), 13 mucinous (MOC), and 41 serous (SOC) ovarian carcinomas. Blue dots represent data points from late stage patients while the red represent early stage. Data gathered from Hendrix et al. (45) (GEO Accession GSE6008, <http://www.ncbi.nlm.nih.gov/geo/>).

For the gene *TPPP3* there was reduced expression in ovarian clear cell carcinoma compared to healthy tissue and other ovarian cancer subtypes. *SORD* showed significantly lower expression levels in the normal control tissues, and to a smaller extent, in serous ovarian carcinoma compared to the other

subtypes. The high expression of *SORD*, whose related protein was detected only in EIC in our data set, in non-SOC was unexpected as the protein atlas reports low expression of *SORD* in ovarian cancer. *CSPG2/VCAN* expression, which was detected at the protein level in EIC only, was increased in CCOC when

compared to the normal tissue and other EOC subtypes (Figure 5).

## Expression of Proteins Identified Exclusively in STIC or EIC Across Endometrial Cancer Subtypes

By investigating the gene expression corresponding to proteins in our data set which are enriched in specific gynecological tissues,

we aimed to investigate the connection between preneoplastic lesions of the endometrium and tube with subtypes of endometrial cancer as defined by the TCGA. The expression levels of the genes corresponding to the proteins listed in Table 1 were compared using oligonucleotide microarray data from Kandolph et al. (4) (<https://gdc.cancer.gov/node/875>) (Figure 6).

They were selected as their related proteins were found exclusively in a precancerous lesion and their abundance

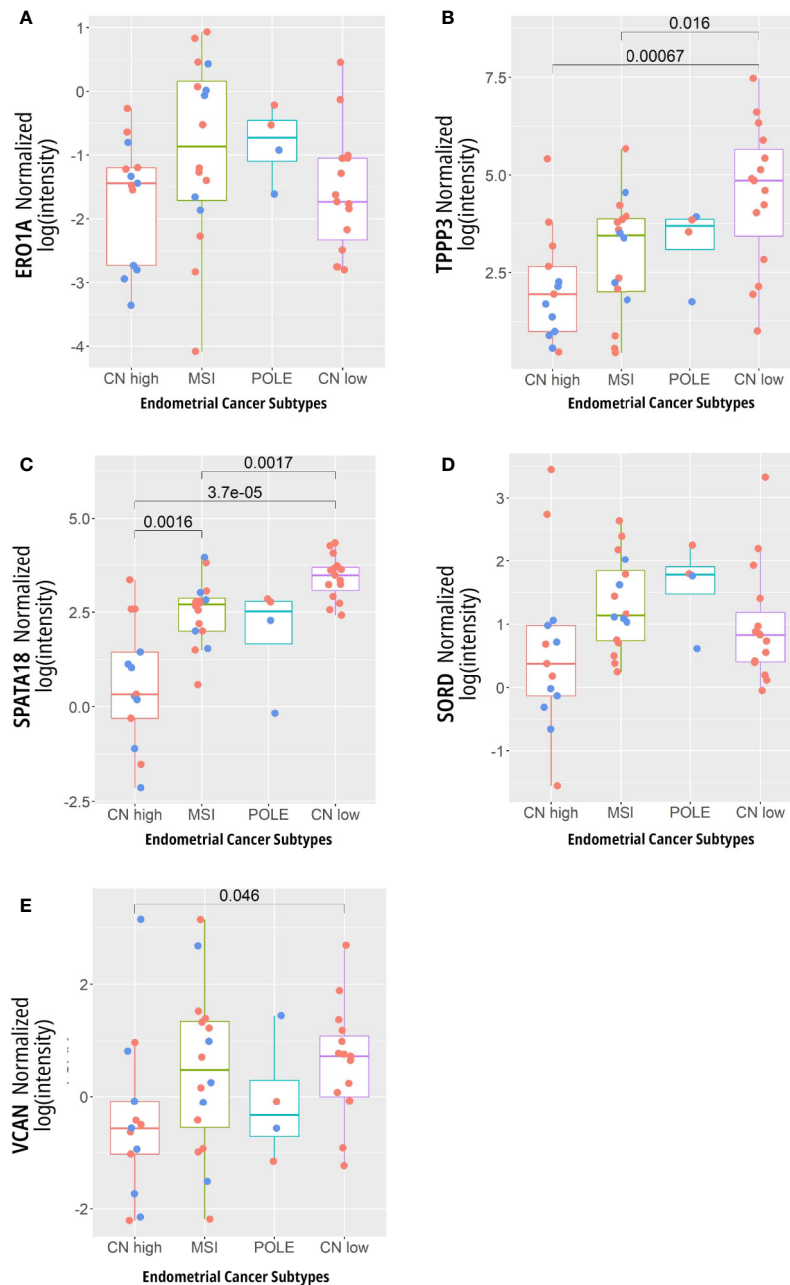


**FIGURE 6** | Expression levels of genes whose proteins are associated with specific gynecological tissues. **(A)** ERO1A, **(B)** TPPP3, **(C)** SPATA18, **(D)** SORD, and **(E)** VCAN in 13 copy number (CN) high, 16 micro satellite instability (MSI) hypermutated, 4 POLE ultra-mutated, and 15 CN low. Here, the blue dots represent data points from late stage patients while the red represent early stage cancers. Data from Kandolph et al. (4) (<https://gdc.cancer.gov/node/875>).

(according to protein atlas) was unique to specific gynecological tissue. However, most did not show different gene expression between the TCGA defined subtypes, except for *TPPP3* and *SPATA18*, which both showed decreased expression in the CN high (serous) subgroup compared to other subtypes (**Figure 6**). These proteins were detected exclusively in STIC in our analysis and their expression was seen to be decreased in SEC compared to healthy controls (**Supplementary Figure 2**).

## Proteins Associated With Metastasis Identified in STIC or EIC

The 34 identified proteins expressed exclusively in STIC and/or EIC which are known to be involved in metastasis or migration were listed in **Supplementary Table 2**. Most of these proteins are implicated in the promotion of metastasis, with the exceptions of Galectin-9 (54, 55), Mimecan (56, 57), and Catenin alpha-1 (58, 59) which have been implicated in the inhibition of metastasis.

## DISCUSSION

The application of proteomic techniques, particularly that of mass spectrometry, hold the potential to provide a temporal snapshot of the molecular features within a given sample. Here, we provide what is, to the best of our knowledge, the first proteomic analyses of synchronous precursor lesions of serous endometrial and high-grade ovarian cancer. Through histological and molecular identification of precancerous lesions, followed by laser-capture microdissection and mass spectrometry analysis, we were able to identify over 450 proteins within the precancerous lesions and adjacent healthy tissue. The proteomic profiles of the precancerous lesions showed striking similarity (**Figure 1**) and shared a molecular profile indicative of metastatic transformation (**Supplementary Table 2**). To investigate the connection between these precancerous lesions and serous gynecological malignancies we investigated the gene expression of several proteins of interest in serous endometrial and ovarian cancer data sets (**Figures 3–6**).

EPCAM and CAPS were selected for further investigation based on their implication in the development of ovarian and endometrial cancer (47–49). Genomic analysis of their expression in Stage I SOC compared to peritoneal control tissue revealed significantly increased levels in the cancerous specimens (**Figure 3**). It is well recognized that EPCAM expression has a complex relationship to SOC development (60); however, it has not previously been identified in STIC or other gynecological precancerous lesions. This transmembrane adhesion molecule plays a role in migration and proliferation in wound healing (61) as well as the maintenance of pluripotency in stem cells (62).

The exact function of CAPS is unknown, but it is a suggested target of cAMP-dependent protein kinase and has been implicated in the cAMP and calcium-phosphatidylinositol signaling cascades (63). According to protein atlas, CAPS has high expression in the fallopian tube but is not expressed in healthy OSE (<http://www.proteinatlas.org/ENSG00000152611-CAPSL/tissue>) which is in agreement with our identification of this protein in both the healthy fallopian tissue and STIC.

Interestingly, CAPS gene expression was seen to be increased in SOC compared to control tissue (**Figure 3**). Furthermore, EPCAM is not expressed in healthy ovarian surface epithelium (OSE) (53) but is frequently up regulated in ovarian cancer (60). The single case study presented here is insufficient to draw broader conclusions about potential markers of tissues of origin, but we believe that expression of EPCAM and CAPS merit further investigation in a larger cohort.

To further investigate proteins which may act as markers of tissue of origin in SEC or SOC, we investigated proteins identified exclusively in either the STIC or EIC which were unique to specific gynecological tissues according to protein atlas. CSGP/VCAN was identified exclusively in EIC, was seen to have increased expression in COCC compared to other ovarian cancer cell types (**Figure 5**) and had increased expression in SEC compared to healthy control tissue (**Supplementary Figure 2**). This protein has been previously seen to be increased in COCC (64, 65) and represents a potential link between EIC and COCC. COCC has been suggested to arise from endometriosis lesions (66) potentially representing a pathway for endometrial origin of COCC.

A previous mass spectrometry-based analysis of ovarian cancer precursor lesions was performed by Levenon et al. (67) and investigated *ex vivo* culture derived cells from fallopian tube fimbria (67). Their proteomic analysis identified 11 different ovarian cancer biomarkers present in this *ex vivo* model. A larger study by M. Eckart et al. (68) investigated both tumor and stroma tissue from STIC, invasive fallopian tube lesions, invasive ovarian lesions and omental metastasis (68). In addition to identifying N-methyltransferase (NNMT) as a metabolic regulator of cancer associated fibroblasts, they also showed that the molecular profiles of primary cancers and metastatic implants were remarkably similar within the same patient while the microenvironment showed site specific differences. The STIC lesion they investigated showed lower expression compared to normal tube in 4 of our proteins of interest (CAPS, ERO1A, TPPP3, and SPATA18) and similar expression in 2 (EPCAM and SORD). Only VCAN showed marginally increased expression in STIC compared to normal fallopian tube epithelium in this analysis. The authors' focus on stromal tissue, a lack of normal epithelial ovarian or omental controls and the potential that STIC represents metastatic lesions from a primary ovarian tumor limits further comparison to this data set.

The traditional understanding of cancer development is that it acquires metastatic capacities over time within the primary lesion (69). However, the identification of STIC as the origin site of HGSOC implicates that these pre-invasive lesions can leave their site of origin and establish themselves in distant locations. In addition, EIC is often identified with extrauterine spread (18, 19) which can take the form of EIC like growths on the ovaries, peritoneum and fallopian tube in the absence of obvious disease in these locations (16, 18). Together, this suggests that these premalignant lesions possess some migratory or metastatic ability facilitating their translocation to distant sites within the gynecological system. Here, we identified numerous metastasis and migration related proteins in precancerous lesions in the absence of malignant disease (**Supplementary Table 2**).



A major limitation of this study is that the data is derived from a single patient case study which makes generalized interpretation of biological implication of this data difficult. Furthermore, only a modest number of proteins was identified from these small tissue regions. As highly abundant proteins are identified preferentially in mass spectrometry analysis (70), the low number of proteins identified potentially masks differences in lower abundance proteins. The analysis of a larger cohort, coupled with the utilization of advanced sample preparation and mass spectrometry techniques to improve proteome coverage, holds the potential to build upon the data presented here and paint a clearer picture of the molecular landscape of precancerous lesions of serous cancers of the ovary and endometrium.

## CONCLUSION

Here, we present the first proteomic investigation of precancerous lesions of the gynecological tract in a patient without advanced gynecological malignancy. Interpretation of the data is limited by the single case study and the modest number of proteins identified; however, we provide a foundation for further analysis of the molecular links between precancerous lesions and subsequent cancer. In addition, we identified several metastasis-related proteins in precancerous tissues. The understanding that precancerous lesions of the female genital tract potentially possess metastatic potential raises many questions about when, where, and how these cancers develop. Though the early steps are not well understood, further proteomic analyses of gynecological precancerous lesions hold the potential to unravel the early temporal and molecular events underlying the development of these malignancies which, in turn, holds the potential to improve detection and treatment.

## DATA AVAILABILITY STATEMENT

Publicly available datasets were analyzed in this study. These can be found in the NCBI Gene Expression Omnibus. The mass spectrometry proteomics data have been deposited to the

ProteomeXchange Consortium via the PRIDE partner repository (71) with the data set identifier PXD018538.

## ETHICS STATEMENT

The studies involving human participants were reviewed and approved by Research Ethics Committee of the Royal Adelaide Hospital. The patients/participants provided their written informed consent to participate in this study.

## AUTHOR CONTRIBUTIONS

Design of the work: MO, PH, GA, and MA. Acquisition, analysis, and interpretation of data: all authors. Drafting the work or revising it critically: all authors. All authors contributed to the article and approved the submitted version.

## FUNDING

PH gratefully acknowledges the support of the National Collaborative Research Infrastructure Strategy (NCRIS) Bioplatforms Australia Node for Tissue Imaging Mass Spectrometry.

## ACKNOWLEDGMENTS

We acknowledge the contribution of Lyron Winderbaum in analyzing the preliminary proteomics and genomics data gathered.

## SUPPLEMENTARY MATERIAL

The Supplementary Material for this article can be found online at: <https://www.frontiersin.org/articles/10.3389/fonc.2020.523989/full#supplementary-material>

## REFERENCES

- Amant F, Mirza MR, Koskas M, Creutzberg CL. Cancer of the corpus uteri. *Int J Gynaecol Obstet* (2015) 131(Suppl 2):S96–104. doi: 10.1016/j.ijgo.2015.06.005
- Costas L, Frias-Gomez J, Guardiola M, Benavente Y, Pineda M, Pavon MA, et al. New perspectives on screening and early detection of endometrial cancer. *Int J Cancer* (2019) 145(12):3194–206. doi: 10.1002/ijc.32514
- Urick ME, Bell DW. Clinical actionability of molecular targets in endometrial cancer. *Nat Rev Cancer* (2019) 19(9):510–21. doi: 10.1038/s41568-019-0177-x
- Kandath C, Schultz N, Cherniack AD, Akbani R, Liu Y, Shen H, et al. Integrated genomic characterization of endometrial carcinoma. *Nature* (2013) 497(7447):67–73. doi: 10.1038/nature12113
- Charo LM, Plaxe SC. Recent advances in endometrial cancer: a review of key clinical trials from 2015 to 2019. *F1000Res* (2019) 8. doi: 10.12688/f1000research.17408.1
- Ferlay J, Soerjomataram I, Dikshit R, Eser S, Mathers C, Rebelo M, et al. Cancer incidence and mortality worldwide: sources, methods and major patterns in GLOBOCAN 2012. *Int J Cancer* (2015) 136(5):E359–86. doi: 10.1002/ijc.29210
- Arnold M, Pandeya N, Byrnes G, Renehan PAG, Stevens GA, Ezzati PM, et al. Global burden of cancer attributable to high body-mass index in 2012: a population-based study. *Lancet Oncol* (2015) 16(1):36–46. doi: 10.1016/S1470-2045(14)71123-4
- Soslow RA, Bissonnette JP, Wilton A, Ferguson SE, Alektiar KM, Duska LR, et al. Clinicopathologic analysis of 187 high-grade endometrial carcinomas of different histologic subtypes: similar outcomes belie distinctive biologic differences. *Am J Surg Pathol* (2007) 31(7):979–87. doi: 10.1097/PAS.0b013e31802ee494
- Kelly MG, O'Malley D, Hui P, McAlpine J, Dziura J, Rutherford TJ, et al. Patients with uterine papillary serous cancers may benefit from adjuvant platinum-based chemoradiation. *Gynecol Oncol* (2004) 95(3):469–73. doi: 10.1016/j.ygyno.2004.08.030
- Olwaiye AB, Rauh-Hain JA, Withiam-Leitch M, Rueda B, Goodman A, del Carmen MG. Utility of pre-operative serum CA-125 in the management of uterine papillary serous carcinoma. *Gynecol Oncol* (2008) 110(3):293–8. doi: 10.1016/j.ygyno.2008.05.027

11. Hamilton CA, Cheung MK, Osann K, Chen L, Teng NN, Longacre TA, et al. Uterine papillary serous and clear cell carcinomas predict for poorer survival compared to grade 3 endometrioid corpus cancers. *Br J Cancer* (2006) 94 (5):642–6. doi: 10.1038/sj.bjc.6603012
12. Zheng W, Liang SX, Yu H, Rutherford T, Chambers SK, Schwartz PE. Endometrial glandular dysplasia: a newly defined precursor lesion of uterine papillary serous carcinoma. Part I: morphologic features. *Int J Surg Pathol* (2004) 12(3):207–23. doi: 10.1177/106689690401200302
13. Liang SX, Chambers SK, Cheng L, Zhang S, Zhou Y, Zheng W. Endometrial glandular dysplasia: a putative precursor lesion of uterine papillary serous carcinoma. Part II: molecular features. *Int J Surg Pathol* (2004) 12(4):319–31. doi: 10.1177/106689690401200405
14. Zheng W, Xiang L, Fadare O, Kong B. A proposed model for endometrial serous carcinogenesis. *Am J Surg Pathol* (2011) 35(1):e1–14. doi: 10.1097/PAS.0b013e318202772e
15. Jia L, Liu Y, Yi X, Miron A, Crum CP, Kong B, et al. Endometrial glandular dysplasia with frequent p53 gene mutation: a genetic evidence supporting its precancer nature for endometrial serous carcinoma. *Clin Cancer Res* (2008) 14 (8):2263–9. doi: 10.1158/1078-0432.CCR-07-4837
16. Sherman ME, Bitterman P, Rosenshein NB, Delgado G, Kurman RJ. Uterine serous carcinoma. A morphologically diverse neoplasm with unifying clinicopathologic features. *Am J Surg Pathol* (1992) 16(6):600–10. doi: 10.1097/00000478-199206000-00008
17. Sherman ME, Bur ME, Kurman RJ. p53 in endometrial cancer and its putative precursors: evidence for diverse pathways of tumorigenesis. *Hum Pathol* (1995) 26(11):1268–74. doi: 10.1016/0046-8177(95)90204-X
18. Wheeler DT, Bell KA, Kurman RJ, Sherman ME. Minimal uterine serous carcinoma: diagnosis and clinicopathologic correlation. *Am J Surg Pathol* (2000) 24(6):797–806. doi: 10.1097/00000478-200006000-00004
19. Hui P, Kelly M, O'Malley DM, Tavassoli F, Schwartz PE. Minimal uterine serous carcinoma: a clinicopathological study of 40 cases. *Mod Pathol* (2005) 18(1):75–82. doi: 10.1038/modpathol.3800271
20. Tolcher MC, Swisher EM, Medeiros F, Lima JF, Hilderbrand JL, Donovan JL, et al. Characterization of precursor lesions in the endometrium and fallopian tube epithelium of early-stage uterine serous carcinoma. *Int J Gynecol Pathol* (2015) 34(1):57–64. doi: 10.1097/PGP.0000000000000109
21. Fader AN, Boruta D, Olawaiye AB, Gehrig PA. Uterine papillary serous carcinoma: epidemiology, pathogenesis and management. *Curr Opin Obstet Gynecol* (2010) 22(1):21–9. doi: 10.1097/GCO.0b013e328334d8a3
22. Sovak MA, Hensley ML, Dupont J, Ishill N, Alektiar KM, Abu-Rustum N, et al. Paclitaxel and carboplatin in the adjuvant treatment of patients with high-risk stage III and IV endometrial cancer: a retrospective study. *Gynecol Oncol* (2006) 103(2):451–7. doi: 10.1016/j.ygyno.2006.03.019
23. Bowtell DD. The genesis and evolution of high-grade serous ovarian cancer. *Nat Rev Cancer* (2010) 10(11):803–8. doi: 10.1038/nrc2946
24. George SH, Shaw P. BRCA and Early Events in the Development of Serous Ovarian Cancer. *Front Oncol* (2014) 4:5. doi: 10.3389/fonc.2014.00005
25. Piek JM, van Diest PJ, Zweemer RP, Jansen JW, Poort-Keesom RJ, Menko FH, et al. Dysplastic changes in prophylactically removed Fallopian tubes of women predisposed to developing ovarian cancer. *J Pathol* (2001) 195 (4):451–6. doi: 10.1002/path.1000
26. Crum CP, Drapkin R, Kindelberger D, Medeiros F, Miron A, Lee Y. Lessons from BRCA: the tubal fimbria emerges as an origin for pelvic serous cancer. *Clin Med Res* (2007) 5(1):35–44. doi: 10.3121/cm.2007.702
27. Crum CP, Herfs M, Ning G, Bijron JG, Howitt BE, Jimenez CA, et al. Through the glass darkly: intraepithelial neoplasia, top-down differentiation, and the road to ovarian cancer. *J Pathol* (2013) 231 (4):402–12. doi: 10.1002/path.4263
28. Folkins AK, Jarboe EA, Saleemuddin A, Lee Y, Callahan MJ, Drapkin R, et al. A candidate precursor to pelvic serous cancer (p53 signature) and its prevalence in ovaries and fallopian tubes from women with BRCA mutations. *Gynecol Oncol* (2008) 109(2):168–73. doi: 10.1016/j.ygyno.2008.01.012
29. Kuhn E, Kurman RJ, Vang R, Sehdev AS, Han G, Soslow R, et al. TP53 mutations in serous tubal intraepithelial carcinoma and concurrent pelvic high-grade serous carcinoma—evidence supporting the clonal relationship of the two lesions. *J Pathol* (2012) 226(3):421–6. doi: 10.1002/path.3023
30. Lee Y, Miron A, Drapkin R, Nucci MR, Medeiros F, Saleemuddin A, et al. A candidate precursor to serous carcinoma that originates in the distal fallopian tube. *J Pathol* (2007) 211(1):26–35. doi: 10.1002/path.2091
31. Salvador S, Rempel A, Soslow RA, Gilks B, Huntsman D, Miller D. Chromosomal instability in fallopian tube precursor lesions of serous carcinoma and frequent monoclonality of synchronous ovarian and fallopian tube mucosal serous carcinoma. *Gynecol Oncol* (2008) 110(3):408–17. doi: 10.1016/j.ygyno.2008.05.010
32. Labidi-Galy SI, Papp E, Hallberg D, Niknafs N, Adloff V, Noe M, et al. High grade serous ovarian carcinomas originate in the fallopian tube. *Nat Commun* (2017) 8(1):1093. doi: 10.1038/s41467-017-00962-1
33. Xiang L, Rong G, Zhao J, Wang Z, Shi F. Identification of candidate genes associated with tubal origin of high-grade serous ovarian cancer. *Oncol Lett* (2018) 15(5):7769–75. doi: 10.3892/ol.2018.8346
34. Perets R, Wyant GA, Muto KW, Bijron JG, Poole BB, Chin KT, et al. Transformation of the fallopian tube secretory epithelium leads to high-grade serous ovarian cancer in Brca;Tp53;Pten models. *Cancer Cell* (2013) 24 (6):751–65. doi: 10.1016/j.ccr.2013.10.013
35. Zhai Y, Wu R, Kuick R, Sessine MS, Schulman S, Green M, et al. High-grade serous carcinomas arise in the mouse oviduct via defects linked to the human disease. *J Pathol* (2017) 243(1):16–25. doi: 10.1002/path.4927
36. Bijron JG, Seldenrijk CA, Zweemer RP, Lange JG, Verheijen RH, van Diest PJ. Fallopian tube intraluminal tumor spread from noninvasive precursor lesions: a novel metastatic route in early pelvic carcinogenesis. *Am J Surg Pathol* (2013) 37(8):1123–30. doi: 10.1097/PAS.0b013e318282da7f
37. Kim J, Coffey DM, Creighton CJ, Yu Z, Hawkins SM, Matzuk MM. High-grade serous ovarian cancer arises from fallopian tube in a mouse model. *Proc Natl Acad Sci USA* (2012) 109(10):3921–6. doi: 10.1073/pnas.1117135109
38. Lim D, Oliva E. Precursors and pathogenesis of ovarian carcinoma. *Pathology* (2013) 45(3):229–42. doi: 10.1097/PAT.0b013e32835f2264
39. Marquez RT, Baggerly KA, Patterson AP, Liu J, Broaddus R, Frumovitz M, et al. Patterns of gene expression in different histotypes of epithelial ovarian cancer correlate with those in normal fallopian tube, endometrium, and colon. *Clin Cancer Res* (2005) 11(17):6116–26. doi: 10.1158/1078-0432.CCR-04-2509
40. Roelofsens T, van Kempen LC, van der Laak JA, van Ham MA, Bulten J, Massuger LF. Concurrent endometrial intraepithelial carcinoma (EIC) and serous ovarian cancer: can EIC be seen as the precursor lesion? *Int J Gynecol Cancer* (2012) 22(3):457–64. doi: 10.1097/IGC.0b013e3182434a81
41. Mittal P, Klingler-Hoffmann M, Arentz G, Winderbaum L, Kaur G, Anderson L, et al. Annexin A2 and alpha actinin 4 expression correlates with metastatic potential of primary endometrial cancer. *Biochim Biophys Acta Proteins Proteom* (2017) 1865(7):846–57. doi: 10.1016/j.bbapap.2016.10.010
42. Wisniewski JR, Zougman A, Nagaraj N, Mann M. Universal sample preparation method for proteome analysis. *Nat Methods* (2009) 6(5):359–62. doi: 10.1038/nmeth.1322
43. Cox J, Neuhauser N, Michalski A, Scheltema RA, Olsen JV, Mann M. Andromeda: a peptide search engine integrated into the MaxQuant environment. *J Proteome Res* (2011) 10(4):1794–805. doi: 10.1021/pr101065j
44. Yoshihara K, Tajima A, Komata D, Yamamoto T, Kodama S, Fujiwara H, et al. Gene expression profiling of advanced-stage serous ovarian cancers distinguishes novel subclasses and implicates ZEB2 in tumor progression and prognosis. *Cancer Sci* (2009) 100(8):1421–8. doi: 10.1111/j.1349-7006.2009.01204.x
45. Hendrix ND, Wu R, Kuick R, Schwartz DR, Fearon ER, Cho KR. Fibroblast growth factor 9 has oncogenic activity and is a downstream target of Wnt signaling in ovarian endometrioid adenocarcinomas. *Cancer Res* (2006) 66 (3):1354–62. doi: 10.1158/0008-5472.CAN-05-3694
46. Day RS, McDade KK, Chandran UR, Lisovich A, Conrads TP, Hood BL, et al. Identifier mapping performance for integrating transcriptomics and proteomics experimental results. *BMC Bioinf* (2011) 12:213. doi: 10.1186/1471-2105-12-213
47. Li Z, Huang C, Bai S, Pan X, Zhou R, Wei Y, et al. Prognostic evaluation of epidermal fatty acid-binding protein and calyphosine, two proteins implicated in endometrial cancer using a proteomic approach. *Int J Cancer* (2008) 123(10):2377–83. doi: 10.1002/ijc.23808
48. Wen KC, Sung PL, Chou YT, Pan CM, Wang PH, Lee OK, et al. The role of EpCAM in tumor progression and the clinical prognosis of endometrial

- carcinoma. *Gynecol Oncol* (2018) 148(2):383–92. doi: 10.1016/j.ygyno.2017.11.033
49. Tayama S, Motohara T, Narantuya D, Li C, Fujimoto K, Sakaguchi I, et al. The impact of EpCAM expression on response to chemotherapy and clinical outcomes in patients with epithelial ovarian cancer. *Oncotarget* (2017) 8(27):44312–25. doi: 10.18632/oncotarget.17871
  50. Erickson BK, Conner MG, Landen CN Jr. The role of the fallopian tube in the origin of ovarian cancer. *Am J Obstet Gynecol* (2013) 209(5):409–14. doi: 10.1016/j.ajog.2013.04.019
  51. Blaustein A. Peritoneal mesothelium and ovarian surface cells—shared characteristics. *Int J Gynecol Pathol* (1984) 3(4):361–75.
  52. Reece-Smith AM, Parsons SL, Watson SA. Oesophago-Gastric Cancer. In: Bologna M, editor. *Biotargets of Cancer in Current Clinical Practice. Current Clinical Pathology*. Humana Press (2012). p. 221–44. doi: 10.1007/978-1-61779-615-9\_8
  53. Szotek PP, Chang HL, Brennand K, Fujino A, Pieretti-Vanmarcke R, Lo Celso C, et al. Normal ovarian surface epithelial label-retaining cells exhibit stem/progenitor cell characteristics. *Proc Natl Acad Sci USA* (2008) 105(34):12469–73. doi: 10.1073/pnas.0805012105
  54. Nobumoto A, Nagahara K, Oomizu S, Katoh S, Nishi N, Takeshita K, et al. Galectin-9 suppresses tumor metastasis by blocking adhesion to endothelium and extracellular matrices. *Glycobiology* (2008) 18(9):735–44. doi: 10.1093/glycob/cwn062
  55. Fujihara S, Mori H, Kobara H, Rafiq K, Niki T, Hirashima M, et al. Galectin-9 in cancer therapy. *Recent Pat Endocr Metab Immune Drug Discovery* (2013) 7(2):130–7. doi: 10.2174/1872214811307020006
  56. Cui X, Song B, Hou L, Wei Z, Tang J. High expression of osteoglycin decreases the metastatic capability of mouse hepatocarcinoma Hca-F cells to lymph nodes. *Acta Biochim Biophys Sin (Shanghai)* (2008) 40(4):349–55. doi: 10.1111/j.1745-7270.2008.00392.x
  57. Wang L, Zhang F, Cui JY, Chen L, Chen YT, Liu BW. CAFs enhance paclitaxel resistance by inducing EMT through the IL6/JAK2/STAT3 pathway. *Oncol Rep* (2018) 39(5):2081–90. doi: 10.3892/or.2018.6311
  58. Yoshida R, Kimura N, Harada Y, Ohuchi N. The loss of E-cadherin, alpha- and beta-catenin expression is associated with metastasis and poor prognosis in invasive breast cancer. *Int J Oncol* (2001) 18(3):513–20. doi: 10.3892/ijo.18.3.513
  59. Beavon IR. The E-cadherin-catenin complex in tumour metastasis: structure, function and regulation. *Eur J Cancer* (2000) 36(13 Spec No):1607–20. doi: 10.1016/S0959-8049(00)00158-1
  60. Kobel M, Kalloger S, Boyd NJPM. Ovarian carcinoma subtypes are different diseases: implications for biomarker studies. *PLoS Med* (2008) 5(12):e232. doi: 10.1371/journal.pmed.0050232
  61. Kuechlin S, Schoels M, Slanchev K, Lassmann S, Walz G, Yakulov TA. EpCAM controls morphogenetic programs during zebrafish pronephros development. *Biochem Biophys Res Commun* (2017) 487(2):209–15. doi: 10.1016/j.bbrc.2017.04.035
  62. Lu TY, Lu RM, Liao MY, Yu J, Chung CH, Kao CF, et al. Epithelial cell adhesion molecule regulation is associated with the maintenance of the undifferentiated phenotype of human embryonic stem cells. *J Biol Chem* (2010) 285(12):8719–32. doi: 10.1074/jbc.M109.077081
  63. Clement S, Dumont JE, Schurmans S. Loss of calyphosine gene expression in mouse and other rodents. *Biochem Biophys Res Commun* (1997) 232(2):407–13. doi: 10.1006/bbrc.1997.6297
  64. Kusumoto T, Kodama J, Seki N, Nakamura K, Hongo A, Hiramatsu Y. Clinical significance of syndecan-1 and versican expression in human epithelial ovarian cancer. *Oncol Rep* (2010) 23(4):917–25. doi: 10.3892/or\_00000715
  65. Yamaguchi K, Mandai M, Oura T, Matsumura N, Hamanishi J, Baba T, et al. Identification of an ovarian clear cell carcinoma gene signature that reflects inherent disease biology and the carcinogenic processes. *Oncogene* (2010) 29(12):1741–52. doi: 10.1038/onc.2009.470
  66. Yamamoto S, Tsuda H, Takano M, Iwaya K, Tamai S, Matsubara O. PIK3CA mutation is an early event in the development of endometriosis-associated ovarian clear cell adenocarcinoma. *J Pathol* (2011) 225(2):189–94. doi: 10.1002/path.2940
  67. Levanon K, Ng V, Piao HY, Zhang Y, Chang MC, Roh MH, et al. Primary ex vivo cultures of human fallopian tube epithelium as a model for serous ovarian carcinogenesis. *Oncogene* (2010) 29(8):1103–13. doi: 10.1038/onc.2009.402
  68. Eckert MA, Coscia F, Chryplewicz A, Chang JW, Hernandez KM, Pan S, et al. Proteomics reveals NNMT as a master metabolic regulator of cancer-associated fibroblasts. *Nature* (2019) 569(7758):723–8. doi: 10.1038/s41586-019-1173-8
  69. Koscielny S, Tubiana M, Le MG, Valleron AJ, Mouriessé H, Contesso G, et al. Breast cancer: relationship between the size of the primary tumour and the probability of metastatic dissemination. *Br J Cancer* (1984) 49(6):709–15. doi: 10.1038/bjc.1984.112
  70. Aebersold R, Mann M. Mass spectrometry-based proteomics. *Nature* (2003) 422(6928):198–207. doi: 10.1038/nature01511
  71. Perez-Riverol Y, Csordas A, Bai J, Bernal-Llinares M, Hewapathirana S, Kundu DJ, et al. The PRIDE database and related tools and resources in 2019: improving support for quantification data. *Nucleic Acids Res* (2019) 47(D1):D442–50. doi: 10.1093/nar/gky1106

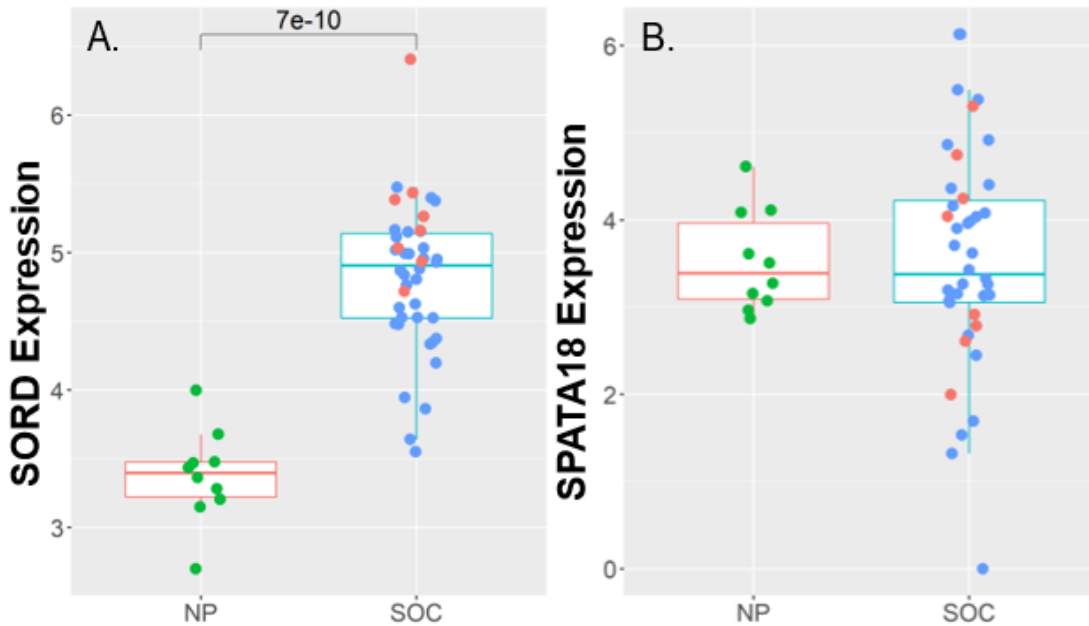
**Conflict of Interest:** Author FW was employed by the company Clinpath.

The remaining authors declare that the research was conducted in the absence of any commercial or financial relationships that could be construed as a potential conflict of interest.

Copyright © 2020 Acland, Arentz, Mussared, Whitehead, Hoffmann, Klingler-Hoffmann and Oehler. This is an open-access article distributed under the terms of the Creative Commons Attribution License (CC BY). The use, distribution or reproduction in other forums is permitted, provided the original author(s) and the copyright owner(s) are credited and that the original publication in this journal is cited, in accordance with accepted academic practice. No use, distribution or reproduction is permitted which does not comply with these terms.

1 3.3. Supplementary Data

2



**Supplementary Figure 1:** Gene expression of proteins exclusive to particular gynaecological tissues; A) SORD and B) SPATA18 in serous ovarian cancer tissues (SOC) (n=42) compared to normal peritoneum (NP) (n=10). Expression levels were extracted from the data of Yoshihara et.al. 2009 (GEO Accession GSE12470) via the R package CuratedOvarianData (<http://www.ncbi.nlm.nih.gov/geo/>). Red dots represent data points from early stage patients while blue dots represent late stage data points. The other proteins whose expression was exclusive to particular gynaecological tissue (ERO1A, TPPP3 and VCAN) were not present in this data set.

3

4

5

6

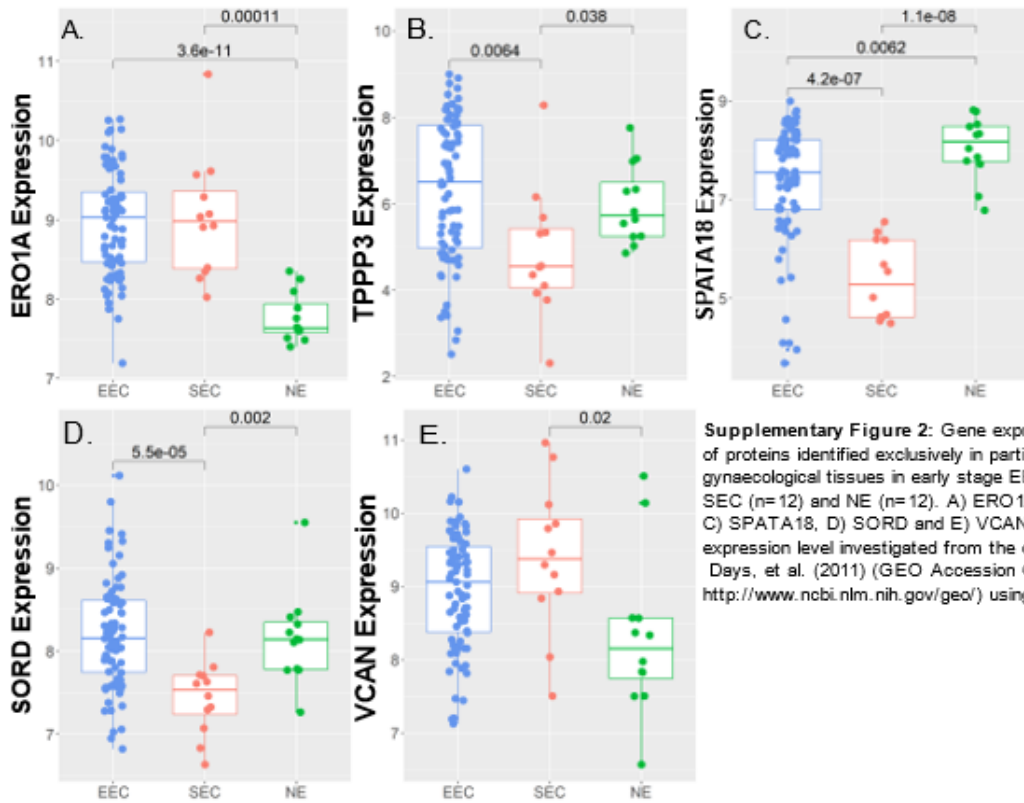
7

8

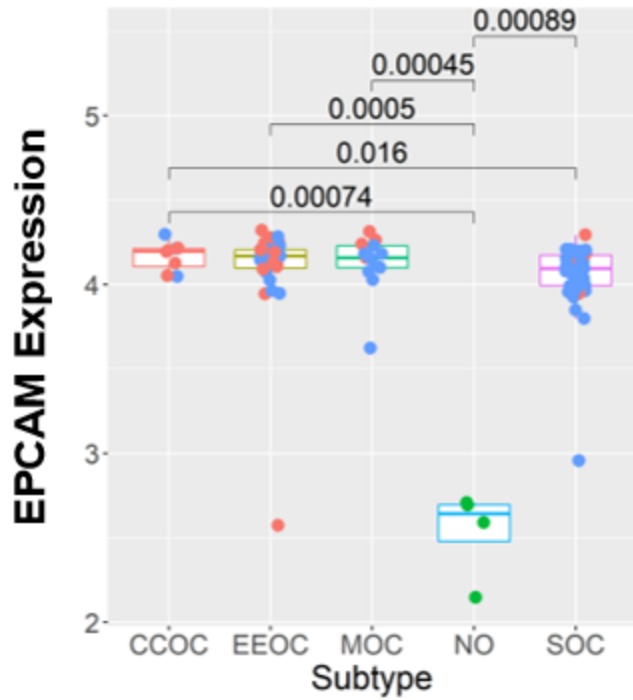
9

10

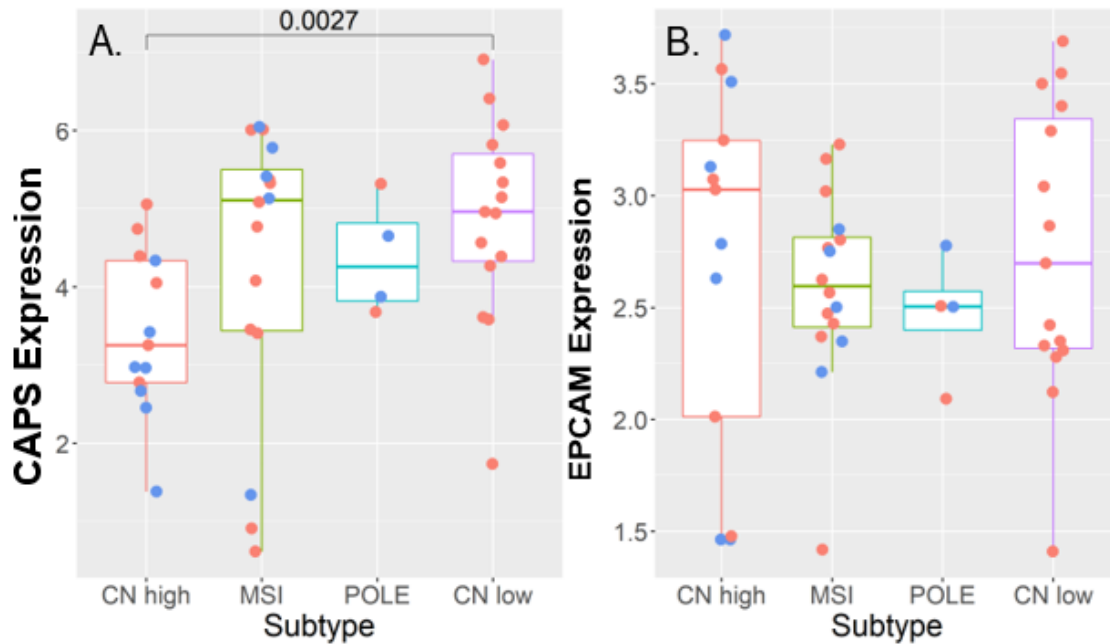
11



**Supplementary Figure 2:** Gene expression of proteins identified exclusively in particular gynaecological tissues in early stage EEC (n=79), SEC (n=12) and NE (n=12). A) ERO1A, B) TPPP3, C) SPATA18, D) SORD and E) VCAN had their expression level investigated from the data of Days, et al. (2011) (GEO Accession GDS4589, <http://www.ncbi.nlm.nih.gov/geo/>) using R.



**Supplementary figure 3:** Expression of cancer related protein, EPCAM, in ovarian cancer subtypes. In CCOC (n=8), EEOC (n=37), MOC (n=13), NO (n=4) and SOC (n=41) from the Hendrix, et. al. (2006) data set (GEO Accession GSE6008, <http://www.ncbi.nlm.nih.gov/geo/>). Red dots represent data points from early stage cancer while blue dots represent late stage cancer samples. CAPS was not present in this data set.



**Supplementary figure 4:** Gene expression of proteins of interest in gynaecological cancer in endometrial cancer subtypes. A) CAPS and B) EPCAM in 13 copy number (CN) high, 16 micro satellite instability (MSI) hypermutated, 4 POLE ultra-mutated and 15 CN low. Here the blue dots represent data points from late stage patients while the red represent early stage cancers. Data from Kandath, et.al. (2013) (<https://gdc.cancer.gov/node/875>).

1  
2  
3  
4  
5  
6  
7  
8  
9  
10  
11  
12

1 Supplementary Table 1:

2 Can be found online – <https://www.ncbi.nlm.nih.gov/pmc/articles/PMC7771701/>

3 Supplementary Table 2:

4

5 **Supplementary Table 2.** Proteins associated with metastasis, identified exclusively in the STIC and/or EIC

<b>Protein</b>	<b>Detected In</b>	<b>Biological Significance</b>
Adenylyl cyclase-associated protein 1 (CAP1)	STIC and EIC	Associated with metastasis in lung and breast cancers [434, 435]
Poly r(C) binding protein-1 (PCBP1)	STIC and EIC	Integral to the maintenance of stem-cell-like prostate cancer cells [436]
Lamina associated polypeptide 2 (LAP2A)	STIC and EIC	Increased in abundance in digestive tract cancers and has been linked to metastasis via the regulation of cell motility [437]
Protein disulfide isomerase A (PDIA)	STIC and EIC	Linked to metastasis in hepatocellular carcinoma [438]
Transketolase (TKT)	STIC and EIC	Identified as a promoter of ovarian cancer cell proliferation and is up-regulated in peritoneal metastases [439]
Annexin A11 (ANX11)	STIC and EIC	Promotes tumourigenesis, metastasis, and chemosensitivity in hepatocarcinoma [440, 441]
Cytoskeleton-associated protein 4 (CKAP4)	STIC and EIC	Expression associated with metastasis in intrahepatic cholangiocellular carcinoma [442]
Myoferlin (MYOF)	STIC and EIC	Influences the invasive capacity of breast cancer cells [443]
Glutamate dehydrogenase 2 (DHE3)	STIC and EIC	Over-expression of glutamate dehydrogenase promotes cell proliferation, migration and invasion <i>in vivo</i> in colorectal cancer [444]
Transcription factor A (TFAM)	STIC and EIC	Shown potential in predicting the clinical outcome of metastatic colorectal cancer patients treated with chemotherapies [445]
Elongation factor 1-delta (EF1D)	STIC and EIC	Increased expression correlates with lymph node metastasis in oesophageal cancer [446]
Agrin (AGRIN)	STIC and EIC	Associated with cell migration and adhesion in oral squamous cell carcinoma [447]
Moesin (MOES)	STIC and EIC	Involved in the metastatic spread of several tumours [448]
Kinectin (KTN1)	STIC and EIC	Supports the development of focal adhesions [449]



Biliverdin reductase A (BIEA)	STIC and EIC	Biliverdin reductase shown to promote epithelial-mesenchymal transition in breast cancer [450]
Chloride intracellular channel protein 1 (CLIC1)	STIC and EIC	Regulates invasion and migration in colon cancer [451], and is correlates with poorer prognosis in gliomas [452]
Zyxin (ZYG)	STIC and EIC	Involved in the reorganisation of actin fibres to enhance cell motility [453]
Claudin-3 (CLD3)	STIC and EIC	Over expression linked to enhanced cellular motility in breast cancer cell lines [454]
Mimecan (MIME)	STIC and EIC	Expression decreased metastatic capacity of mouse hepatocarcinoma cells [455, 456]
Annexin A4 (ANXA4)	STIC and EIC	Associated with poor prognosis and metastasis of hepatocellular carcinoma [457]
Far upstream element binding protein 1 (FUBP1)	STIC and EIC	Promotes carcinoma progression and migration [458, 459]
Galectin-9 (LEG9)	STIC and EIC	Shown to suppress tumour metastasis [460, 461]
Rho GDP-dissociation inhibitor 1 (GDIR1)	STIC and EIC	Associated with metastasis in colorectal cancer [462]
PDZ and LIM domain protein 1 (PDLI1)	STIC and EIC	Promotes migration, invasion and metastasis through interaction with $\alpha$ -actinin in breast cancer [463]
ADP-ribosylation factor-like 4C (ARF4)	STIC and EIC	Associated with suppression of metastasis in ovarian cancer [464]
Glucose-6-phosphate dehydrogenase (G6PD)	STIC and EIC	Implicated in the survival, proliferation, and metastasis of cancer cells [465]
Aldehyde dehydrogenase (ALDH2)	STIC and EIC	Mediator of metastasis in several solid tumours [466]
Cathepsin B (CATB)	STIC and EIC	Shown to mediate tumour metastasis [467]
Dimethylarginine dimethylaminohydrolase 2 (DDAH2)	STIC and EIC	Associated with invasiveness and angiogenesis in lung adenocarcinoma [468]
Ceruloplasmin (CERU)	STIC and EIC	Plasma levels elevated in metastatic breast cancer patients [469]
Microtubule associated protein-4 (MAP4)	STIC and EIC	Regulator of invasion and migration in esophageal squamous cell carcinoma [470]
Catenin alpha-1 (CTNA1)	STIC and EIC	Suppressor of metastasis [471, 472]
	STIC	Knock down suppresses tumour proliferation and metastasis in lung cancer [473] [474]

Tubulin polymerisation promoting proteins (TPPP3)		
Membrane-associated progesterone receptor component 1 (PGRC1)	EIC	Promotes tumour growth by binding to and stabilising EGFR at the plasma membrane [475]. Found to promote tumor cell viability during chemotherapeutic stress in endometrial cancer [476].
Myristoylated alanine-rich C-kinase substrate (MARCS)	EIC	Enhances the migration and metastasis of lung and biliary carcinoma [477-479].
Prolactin-inducible protein (PIP)	EIC	Suggested marker of breast and prostate cancer metastasis [480-482].
Superoxide dismutase [Mn] (SODM)	EIC	Involved in redox-responsive signaling events that drive invasion, migration, and tumor cell survival [483].
F-actin-capping protein subunit alpha-1 (CAZA1)	EIC	Inhibition of CapG protein reduces breast cancer metastasis [484].
Retinal dehydrogenase 1 (AL1A1)	EIC	Implicated in breast cancer metastasis [485, 486].
Thioredoxin domain-containing protein 5 (TXND5)	EIC	Highly expressed in metastatic gastric adenocarcinoma [487].
Suprabasin (SBSN)	EIC	Involved in salivary adenoid carcinoma metastasis [488] and in oesophageal squamous cell carcinoma proliferation and tumourigenesis [489].
Carnitine palmitoyltransferase 1A (CPT1A)	EIC	Promotes cell motility in alveolar rhabdomyosarcoma cells [490].
Tenascin (TENA)	EIC	Reported to play an important role in the metastasis of several cancers [491].
Palladin (PALLD)	EIC	Regulates actin cytoskeleton organisation and cell adhesion [492], promotes pancreatic and breast cancer invasion [493, 494].
Tight junction protein ZO-1 (ZO1)	EIC	Differential expression in metastatic pancreatic and liver cancer [495, 496].

1  
2  
3

1  
2  
3  
4  
5  
6  
7  
8  
9  
10  
11  
12  
13  
14  
15  
16  
17  
18  
19  
20  
21  
22  
23  
24  
25  
26  
27  
28  
29

This page is intentionally left blank

1  
2  
3  
4  
5  
6  
7  
8  
9  
10  
11  
12  
13  
14  
15  
16  
17  
18  
19  
20  
21  
22  
23  
24  
25

**CHAPTER 4: Chemoresistant Cancer  
Cell Lines are Characterized by  
Migratory, Amino Acid Metabolism  
Protein Catabolism and IFN1 Signalling  
Perturbations.**

---

#### 1 4.1. Summary

2 In addition to being detected at a late stage, HGSOC is characterised by initial response to  
3 platinum and taxane based chemotherapy followed by relapse and chemoresistance in most  
4 cases. It is this relapse which is the major cause of death in HGSOC patients. Despite numerous  
5 modern and targeted drugs being developed over the last 30 years, this platinum and taxane  
6 based treatment regime remains the first line approach. The slow progress in drug development  
7 is reflected in the modest improvement in survival rates for HGSOC patients over the last 30  
8 years. This highlights chemoresistance to platinum and taxane chemotherapy as the single largest  
9 barrier to improved patient outcome and makes the understanding of the molecular  
10 underpinnings of this chemoresistance of great clinical importance.

11 Chemoresistance to platinum-based chemotherapy agents (such as cisplatin and CBP) is  
12 predicted to arise through a range of molecular processes including drug efflux, drug  
13 detoxification, DNA repair and impaired apoptosis signalling. Despite several of these  
14 mechanisms being well described, there remains a gap in the ability to predict chemoresistance  
15 in patients before the application of chemotherapy. We approached this publication in the search  
16 for a molecular pattern which described chemoresistance in this context.

17 To achieve this, we applied global proteomic and metabolomic MS analyses to two ovarian  
18 cancer cell lines and their platinum resistant pairs. The platinum resistant pairs were generated  
19 through prolonged exposure to CBP, and we observed increased migratory ability in one of the  
20 resistant lines compared to its parent. Through global metabolomic and proteomic analyses,  
21 coupled with principal component analysis (PCA) and hierarchical clustering analysis, we were  
22 also able to separate sensitive from resistant cell lines based on both their metabolome and  
23 proteome. However, our conclusions were limited by the observation that the parental cell lines,  
24 despite both being HGSOC derived, had significantly different proteomes and metabolomes and  
25 that there were few identifiable common changes upon acquisition of CBP resistance.

26 Despite this, we identified several enriched metabolomic and proteomic pathways in the CBP  
27 cell lines which are of interest and warrant further investigation. Finally, we applied the  
28 proteomic analysis to primary cells derived from one patient with chemo resistant disease and  
29 one with chemo sensitive disease. As expected, these cells showed vastly different proteomic  
30 profiles but, when compared to the cell line analysis, we were unable to identify a proteomic  
31 pattern indicative of CBP resistance. Together this highlights the challenges in characterising, or  
32 predicting, the molecular pattern related to CBP resistance due to the heterogeneity between  
33 different cell line models, between *in vitro* and *in vivo* based studies and between patients.  
34 Despite this, we provide deep metabolomic and proteomic characterisation of these cell lines and  
35 their CBP resistant pairs providing the foundation for further molecular investigation of  
36 chemoresistant ovarian cancer.

37

38

39

1  
2  
3  
4  
5  
6  
7  
8  
9  
10  
11  
12  
13  
14  
15  
16  
17  
18  
19  
20  
21  
22  
23  
24  
25  
26  
27  
28

This page is intentionally left blank

1 **4.2. Statement of Authorship**

Title of Paper	Chemoresistant Cancer Cell Lines are Characterized by Migratory, Amino Acid Metabolism, Protein Catabolism and IFN1 Signalling Perturbations.
Publication Status	<input checked="" type="checkbox"/> Published <input type="checkbox"/> Accepted for Publication <input type="checkbox"/> Submitted for Publication <span style="float: right;">Unpublished and Unsubmitted work written in manuscript style</span>
Publication Details	<u>M. Acland</u> , N. A. Lokman, C. Young, D. Anderson M. Condina, C. Desire, T. M. Noye, W. Wang, C. Ricciardelli, D. J. Creek, M. K. Oehler, P. Hoffmann and M. Klingler-Hoffmann, (2022) Cancers,

2

3

**Principal Author**

Name of Principal Author (Candidate)	Mitchell Acland		
Contribution to the Paper	Performed experiments, data analysis and data interpretation. Wrote the first draft of the article and consolidated the final manuscript.		
Overall percentage (%)	80%		
Certification:	This paper reports on original research I conducted during the period of my Higher Degree by Research candidature and is not subject to any obligations or contractual agreements with a third party that would constrain its inclusion in this thesis. I am the primary author of this paper.		
Signature		Date	27/05/2022

4

5 **Co-Author Contributions**

6 By signing the Statement of Authorship, each author certifies that:

- 7 i. the candidate's stated contribution to the publication is accurate (as detailed above);
- 8 ii. permission is granted for the candidate to include the publication in the thesis; and
- 9 iii. the sum of all co-author contributions is equal to 100% less the candidate's stated contribution.

Name of Co-Author	Noor Alia Lokman		
Contribution to the Paper	Contributed to conceptualization, experimental design, experimentation, data analysis and manuscript evaluation.		
Signature		Date	30/6/2021

Name of Co-Author	Clifford Young		
Contribution to the Paper	Contributed to data acquisition and data analysis. Provided expert advice on data interpretation and contributed to manuscript evaluation.		
Signature		Date	03/05/2022

Name of Co-Author	Dovile Anderson		
Contribution to the Paper	Performed metabolomics data acquisition and analysis. Contributed to manuscript evaluation.		
Signature		Date	22 03 2022

Name of Co-Author	Mark Condina		
Contribution to the Paper	Contributed to data acquisition and data analysis. Provided expert advice on data interpretation and contributed to manuscript evaluation.		
Signature		Date	01/07/2021

Name of Co-Author	Chris Desire		
Contribution to the Paper	Contributed to data acquisition and data analysis. Provided expert advice on data interpretation and contributed to manuscript evaluation.		
Signature		Date	29/06/2021

1

Name of Co-Author	Tannith M. Noye		
Contribution to the Paper	Performed experiments and data analysis.		
Signature		Date	29.6.21

Name of Co-Author	Wanqi Want		
Contribution to the Paper	Performed experiments and data analysis.		
Signature		Date	30.6.21

Name of Co-Author	Carmella Ricciardelli		
Contribution to the Paper	Contributed to conceptualization and experimental design. Supervised experimentation, data interpretation and manuscript evaluation.		
Signature		Date	29.6.21



Name of Co-Author	Darren J. Creek		
Contribution to the Paper	Oversaw the metabolomics analysis, provided expert advice on data interpretation and contributed to manuscript evaluation		
Signature		Date	22/3/2022

Name of Co-Author	Martin Oehler		
Contribution to the Paper	Contributed to conceptualization and experimental design. Supervised development of work, data interpretation and manuscript evaluation. Provided original samples.		
Signature		Date	02 May 2022

1

Name of Co-Author	Peter Hoffmann		
Contribution to the Paper	Contributed to conceptualization and experimental design. Supervised development of work, data interpretation and manuscript evaluation.		
Signature		Date	24/05/2022

2

Name of Co-Author	Manuela Klingler-Hoffmann		
Contribution to the Paper	Contributed to conceptualization and experimental design. Supervised development of work, data interpretation and manuscript evaluation. Acted as corresponding author		
Signature		Date	24/05/2022

3

4

5

6

7

## Article

# Chemoresistant Cancer Cell Lines Are Characterized by Migratory, Amino Acid Metabolism, Protein Catabolism and IFN1 Signalling Perturbations

Mitchell Acland <sup>1,2</sup>, Noor A. Lokman <sup>3</sup> , Clifford Young <sup>1</sup>, Dovile Anderson <sup>4</sup>, Mark Condina <sup>1</sup>, Chris Desire <sup>1</sup>, Tannith M. Noye <sup>3</sup> , Wanqi Wang <sup>3</sup>, Carmela Ricciardelli <sup>3</sup> , Darren J. Creek <sup>4</sup> , Martin K. Oehler <sup>1,3,5</sup>, Peter Hoffmann <sup>1</sup> and Manuela Klingler-Hoffmann <sup>1,\*</sup>

- <sup>1</sup> Clinical & Health Sciences, University of South Australia, Adelaide, SA 5095, Australia; mitch.acland@gmail.com (M.A.); clifford.young@unisa.edu.au (C.Y.); mark@massdynamics.com (M.C.); chris.desire@unisa.edu.au (C.D.); oehler.mk@gmail.com (M.K.O.); peter.hoffmann@unisa.edu.au (P.H.)
- <sup>2</sup> Adelaide Proteomics Centre, School of Biological Sciences, The University of Adelaide, Adelaide, SA 5000, Australia
- <sup>3</sup> Discipline of Obstetrics and Gynaecology, Adelaide Medical School, Robinson Research Institute, The University of Adelaide, Adelaide, SA 5005, Australia; noor.lokman@adelaide.edu.au (N.A.L.); tannith.noye@adelaide.edu.au (T.M.N.); wanqi.wang@adelaide.edu.au (W.W.); carmela.ricciardelli@adelaide.edu.au (C.R.)
- <sup>4</sup> Monash Institute of Pharmaceutical Sciences, Monash University, Parkville, VIC 3052, Australia; dovile.anderson@monash.edu (D.A.); darren.creek@monash.edu (D.J.C.)
- <sup>5</sup> Department of Gynaecological Oncology, Royal Adelaide Hospital, Adelaide, SA 5005, Australia
- \* Correspondence: manuela.klingler-hoffmann@unisa.edu.au



**Citation:** Acland, M.; Lokman, N.A.; Young, C.; Anderson, D.; Condina, M.; Desire, C.; Noye, T.M.; Wang, W.; Ricciardelli, C.; Creek, D.J.; et al. Chemoresistant Cancer Cell Lines Are Characterized by Migratory, Amino Acid Metabolism, Protein Catabolism and IFN1 Signalling Perturbations. *Cancers* **2022**, *14*, 2763. <https://doi.org/10.3390/cancers14112763>

Academic Editor: Simon Langdon

Received: 22 April 2022

Accepted: 27 May 2022

Published: 2 June 2022

**Publisher's Note:** MDPI stays neutral with regard to jurisdictional claims in published maps and institutional affiliations.



**Copyright:** © 2022 by the authors. Licensee MDPI, Basel, Switzerland. This article is an open access article distributed under the terms and conditions of the Creative Commons Attribution (CC BY) license (<https://creativecommons.org/licenses/by/4.0/>).

**Simple Summary:** While chemoresistance remains a major barrier to improving the outcomes for patients with ovarian cancer, the molecular features, and associated biological functions, which underpin chemoresistance in ovarian cancer remain poorly understood. In this study we aimed to provide insight into the proteins and metabolites, and their associated biological pathways, which play a role in conferring chemoresistance to ovarian cancer. Through mass spectrometry analysis comparing the proteome and metabolome of chemosensitive vs chemoresistant ovarian cancer cell lines we revealed numerous perturbations in signalling and metabolic pathways in chemoresistant cells. Further comparison to primary cells taken from patients with chemoresistant or chemosensitive disease identified a shared dysregulation in cytokine and type 1 interferon signalling. Our research sets the foundation for a deeper understanding of the proteomic and metabolomic features of chemoresistance and identifies type 1 interferon signalling as a common feature of chemoresistance.

**Abstract:** Chemoresistance remains the major barrier to effective ovarian cancer treatment. The molecular features and associated biological functions of this phenotype remain poorly understood. We developed carboplatin-resistant cell line models using OVCAR5 and CaOV3 cell lines with the aim of identifying chemoresistance-specific molecular features. Chemotaxis and CAM invasion assays revealed enhanced migratory and invasive potential in OVCAR5-resistant, compared to parental cell lines. Mass spectrometry analysis was used to analyse the metabolome and proteome of these cell lines, and was able to separate these populations based on their molecular features. It revealed signalling and metabolic perturbations in the chemoresistant cell lines. A comparison with the proteome of patient-derived primary ovarian cancer cells grown in culture showed a shared dysregulation of cytokine and type 1 interferon signalling, potentially revealing a common molecular feature of chemoresistance. A comprehensive analysis of a larger patient cohort, including advanced in vitro and in vivo models, promises to assist with better understanding the molecular mechanisms of chemoresistance and the associated enhancement of migration and invasion.

**Keywords:** ovarian cancer; chemoresistance; cancer cell lines; proteomics; metabolomics

## 1. Introduction

Ovarian cancer (OC) is the deadliest gynaecological malignancy, with survival rates of below 30% when detected at a late stage [1]. Owing to its often asymptomatic progression, 70% of ovarian cancers are diagnosed at a late stage [2]. The 5-year survival rate for a patient diagnosed with advanced ovarian cancer is approximately 35% [1], and this has not increased substantially over the last 30 years [3].

The typical treatment regime for ovarian cancer consists of debulking surgery, followed by platinum-based chemotherapy with carboplatin (CBP) [4]. It is estimated that 20% of patients do not respond to chemotherapy due to the innate chemoresistance of their OC, while 70% of patients experience acquired chemoresistance [5]. High-grade serous ovarian carcinoma (HGSOC) represents the majority of advanced OC, and is characterized by an initial response to treatment, followed by recurrence and the development of chemoresistance [6,7], and is responsible for the majority of ovarian cancer-associated fatalities [8]. This highlights chemoresistance as being the main barrier to improving survival rates for this deadly cancer.

Despite the development of numerous novel anti-cancer agents against OC [9], platinum-based chemotherapy drugs remain the first-line treatment of choice [4]. They are the National Comprehensive Cancer Network-recommended treatment following surgery for all Stage II, III, and IV ovarian cancers [10]. These drugs act primarily through the formation of intra- and inter-strand DNA cross-links, which induce cell cycle arrest, typically at the G2/M checkpoint [11].

In addition, platinum-based chemotherapeutics also contribute to increased oxidative stress within the cell, through the production of reactive oxygen species (ROS) [12]. In cancer cells, where greater oxidative stress is exhibited in comparison with normal cells, carboplatin-induced oxidative stress can result in apoptosis [13].

The DNA damage and oxidative stress induced by platinum chemotherapy triggers a complex web of signalling, which both promotes and inhibits cell death. This includes signalling through MAPK, PI3K, JNK and other pathways (reviewed in [12]). In addition, platinum chemotherapies have broader impacts on protein folding [14] and calcium homeostasis [14], and they inhibit the function of certain proteins, influencing transcription [15] and microtubule formation [16].

Cisplatin has historically been the most commonly used platinum-based chemotherapy, and it has been employed extensively to treat a range of cancers since its approval in 1978 [17]. However, cisplatin has significant side effects that limit the concentration that can be used for treatment [18]. The chemical analogue, carboplatin, has significantly less side effects and a similar efficacy when combined with paclitaxel, and it is now the preferred first-line treatment of ovarian cancer [19].

There are several mechanisms through which resistance to platinum-based chemotherapy can occur, including the impaired influx of the compound, increased drug efflux, cytoplasmic detoxification, increased DNA repair and alterations in apoptosis signalling pathways [20]. The DNA crosslinks formed by carboplatin give rise to incomplete DNA repair, resulting in single- and double-stranded breaks giving rise to apoptotic signalling [21]. DNA repair mechanisms and apoptosis signalling pathways are of great importance in the resistance to platinum-based chemotherapy.

There has been significant research into the genetic and molecular underpinnings of HGSOC, which has provided a deeper understanding of this cancer and its progression. Though these efforts have revealed the deep complexity and heterogeneity of HGSOC, they have failed to translate into improved clinical outcomes. It has been long understood that altered metabolism is a key feature of cancer cells that is best characterised by the Warburg effect, where cancer cells favour glycolysis over oxidative phosphorylation [22]. Metabolism contributes to a vast array of cancer biological features, including oncogenic transformation, growth, stress response and the detoxification of damaging chemical agents [23]. It has been demonstrated that the downregulation of glycolytic enzymes has the potential to overcome chemoresistance [24,25]; however, the mechanisms are not well understood.

One way to investigate the molecules that underpin chemoresistance is through the application of mass spectrometry (MS) coupled with high-performance chromatography techniques. This approach can be applied to identify a range of molecules including metabolites and proteins. Through the application of this technique, hundreds of metabolites and thousands of proteins can be routinely identified and relatively quantified from very small amounts of material.

To provide a comprehensive molecular characterisation of chemoresistant HGSOC, we combined MS-based metabolomic and proteomic analyses of these cell lines. Together, this holds the potential to provide a deep characterisation of these cell lines, and to reveal alterations in proteomic and metabolomic pathways that underpin chemoresistance in this model.

## 2. Materials and Methods

### 2.1. Cell Culture

The human OC cell line CaOV3 was purchased from the American Type Culture Collection (ATCC, Manassas, VA, USA), and the OVCAR-5 cell line was obtained from Dr. Thomas Hamilton (Fox Chase Cancer Centre, Philadelphia, PA, USA). Both cell lines were authenticated via a short tandem repeat (STR) DNA profile in 2020. The OVCAR-5 cells were grown in RPMI 1640 media (Sigma Aldrich, St. Louis, MO, USA). Recent reports have indicated that OVCAR-5 might originate from metastatic gastrointestinal cancer, and were potentially wrongfully labelled as being ovarian cancer [26]. CaOV3 cells were grown in DMEM media (Sigma Aldrich, St. Louis, MO, USA). Both cell lines were cultured with the addition of 10% foetal bovine serum (Bovogen Biologicals, East Keilor, VIC, Australia) supplemented with 1% penicillin/streptomycin (Sigma Aldrich, St. Louis, MO, USA) and 1% L-glutamine (Sigma Aldrich, St. Louis, MO, USA). OVCAR-5 and CaOV3 cells were made resistant to CBP after treatment with 6–8 cycles of CBP (50  $\mu$ M, Hospira Australia, Pty Ltd., Mulgrave, VIC, Australia) [27,28]. Resistance to CBP was measured regularly, and CBPR cell lines were seen to be at least two-fold more resistant to CBP than their parental partners through the following experiments.

### 2.2. Primary HGSOC Culture

Primary cells were isolated from the ascites of advanced stage HGSOC patients ( $n = 2$ ), with patient consent and approval, by the Royal Adelaide Hospital RAH and Central Adelaide Local Health Network Human Ethics Committees (RAH # 140201) (CALHN # R20181215). All primary cells were grown in Advanced RPMI 1640 medium (Life Technologies, Mulgrave, VIC, Australia) supplemented with 4 mM L-glutamine, 10% FBS (Sigma Aldrich, St. Louis, MO, USA), and antibiotics (100 U penicillin G, 100  $\mu$ g/mL streptomycin sulphate, and 100  $\mu$ g/mL amphotericin B, Sigma Aldrich). Patients that experienced a recurrence within six months after finishing first-line CBP+paclitaxel chemotherapy were classified as being chemoresistant. Patients that remained in full remission for longer than 6 months were classified as being chemosensitive. Here, we investigated the proteome of cells derived from one patient who was deemed chemoresistant and one who was deemed chemosensitive using the above-mentioned classifications. Patient diagnoses and chemotherapy responses are outlined in Supplementary Figure S1.

### 2.3. In Vitro Motility Assay

OVCAR-5 cell motility was assessed using a ChemoTx<sup>®</sup> 96-well plate (Neuroprobe, Gaithersburg, MD, USA), as previously described [29]. Briefly, cells were labelled with calcein AM (1  $\mu$ g/mL, Life Technologies, Mulgrave, VIC, Australia) for 30 min in the dark on a nutator. Excess calcein AM was removed by washing with media (RPMI1640 + 0.1% BSA). A concentration of 40,000 cells/50  $\mu$ L were loaded onto uncoated 12  $\mu$ m filter inserts. The cells were allowed to migrate for 6 h to the bottom well with chemoattractant (10% FBS) and media (RPMI 1640 + 0.1% BSA). Migrated cells were measured using the Triad series

multimode detector (Dyner Technologies, Chantilly, VA, USA) at 485–520 nm. Assays were carried out in biological quadruplicate in 2–3 independent experiments.

#### 2.4. Chick Chorioallantoic Membrane (CAM) Assay

The CAM assay was performed as previously described [30]. In brief, 90,000 OVCAR-5 cells were mixed with Matrigel (8.9 mg/mL, BD Biosciences, Melbourne, VIC, Australia) and placed on top of the CAM of Day 11 chick embryos. Matrigel grafts with adjacent CAM were harvested from each embryo ( $n = 6–9$ /treatment group) after 3 days (day 14), fixed with 10% formalin for 24 h, processed, and embedded in paraffin. Serial sections (6  $\mu$ m) were stained with haematoxylin and eosin, or immunostained with the monoclonal mouse anti-human cytokeratin clone AE1/AE3 (1:50 Dako-Agilent Santa Clara, CA, USA). Immunohistochemistry was performed as described previously, using citrate buffer antigen retrieval [29]. Slides were digitally scanned using the NanoZoomer (Hamamatsu Photonics). A quantitative analysis for assessing OVCAR-5 cancer cell invasion was performed on 8 to 12 CAM images for each embryo, as previously described [30].

#### 2.5. Cell Survival Assay

Ovarian cancer cells were plated at 5000 cells/well in 96-well plates in the respective growth media. After 24 h, cells were treated with varying concentrations of CBP (0–200  $\mu$ M) for 72 h. Then, the conditioned media was removed and thiazolyl blue tetrazolium bromide (MTT) (0.5 mg/mL, Sigma Aldrich) was added for 4.5 h, followed by MTT solvent (0.1 N HCl in isopropanol) for 10 min, before absorbance readings were measured at 595 nm using a Triad series multimode detector plate reader (Dyner technologies, Chantilly, VA, USA). The CBP IC<sub>50</sub> values were calculated using a non-linear fit from the variable slope of log (inhibitor), using GraphPad Prism.

#### 2.6. Metabolomics Sample Preparation

Cells were maintained at 60–80% confluence for 3 passages before being plated in 10 cm dishes. Cell numbers were estimated from an additional dish with the same number of cells at seeding. The media was aspirated and the cells were washed 3 times with 3 mL warmed PBS. Metabolic arrest was achieved through the addition of approximately 2 mL of liquid nitrogen directly to cells ensuring that the surface of the plate was covered before plates were placed onto dry ice. Metabolite extraction was achieved through the addition of 1 mL 100% ice-cold methanol. Cells were lifted off the plate using an ice-cold cell scraper and transferred to a 2 mL Eppendorf. An additional 1 mL of 100% ice-cold methanol was added before snap freezing via immersion in liquid nitrogen for 3 min. This was followed by thawing on dry ice and vortexing to resuspend the contents. The freeze/thaw process was repeated 5 times to ensure the full extraction of the metabolites. The samples were centrifuged at  $16,000 \times g$  at  $-9^\circ\text{C}$  for 5 min, and the supernatant was retained. The pellet was resuspended in 500  $\mu$ L of 100% ice-cold methanol and freeze/thawed 5 times in liquid nitrogen. This sample was centrifuged at  $16,000 \times g$  at  $-9^\circ\text{C}$  for 5 min, and the supernatant was retained and combined with the previously retained supernatant. The samples were then dried in a SpeedVac Vacuum Concentrator (John Morris Scientific, RVC 2-18) at room temperature, with a vacuum of 40 mbar and a rotor speed of  $1000 \text{ min}^{-1}$ . Before data acquisition, the samples were resuspended in volumes of 20 mM ammonium carbonate and acetonitrile to achieve an identical concentration of biological material based on the cell number estimate.

#### 2.7. Metabolomics Data Acquisition

LCMS data was acquired on a Q-Exactive Orbitrap mass spectrometer (Thermo Fisher) coupled with a Dionex Ultimate<sup>®</sup> 3000 RS high-performance liquid chromatography (HPLC) system (Thermo Fisher). Chromatographic separation was performed on a ZIC-pHILIC column (5  $\mu$ m, polymeric,  $150 \times 4.6 \text{ mm}$ , SeQuant<sup>®</sup>, Merck, Darmstadt, Germany). The mobile phase was (A) 20 mM ammonium carbonate and (B) acetonitrile. The gradient

program started at 80% B and was reduced to 50% B over 15 min, then this reduced from 50% B to 5% B over 3 min, followed by a wash with 5% B for another 3 min, and finally an 8 min re-equilibration with 80% B. The flow rate was 0.3 mL/min and the column compartment temperature was 25 °C. The total run time was 32 min with an injection sample volume of 10 µL. The mass spectrometer operated in full scan mode with positive and negative polarity switching at 35,000 resolution and 200 *m/z*, with detection range of 85 to 1, 275 *m/z* in full scan mode. The electro-spray ionisation source (HESI) was set to 3.5 kV for the positive mode and 4.0 kV for the negative mode, the sheath gas was set to 50 and the aux gas to 20 arbitrary units, the capillary temperature was 300 °C and the probe heater temperature was 120 °C.

Mixtures of pure authentic standards containing over 320 metabolites were acquired as separate injections and used to confirm the retention times. The metabolites confirmed with the authentic standards were given the highest confidence MSI level 1.

The metabolomics data were deposited in the data repository Metabolomics Workbench [31] under the study ID ST002010 (DOI: <http://dx.doi.org/10.21228/M81Q4Z>, accessed on 21 April 2022).

### 2.8. Metabolomics Data Analysis

The acquired LCMS data was processed in an untargeted fashion using the open-source software IDEOM [32,33]. Default IDEOM parameters were used to eliminate unwanted noise and artefact peaks. The putative identification of metabolites was achieved using accurate mass (within 3 ppm mass error) searching against the Kyoto Encyclopedia of Genes and Genomes (KEGG), MetaCyc, and LIPIDMAPS databases and others.

Despite the washing steps performed in sample preparation, it is expected that some metabolites that were present in the cell culture media may influence the metabolite abundances observed in our cell samples. To avoid their influence on our results, we utilized a media-only blank performing the same sample preparation steps on a plate with no cells and only 10 mL of cell culture media. To exclude the media components from our analysis, we excluded all metabolites where the media blank/control ratio was greater than 0.5, for the downstream analysis.

### 2.9. Metabolomic Functional Pathway Analysis

To understand the functional pathways associated with dysregulated metabolites, we utilized the Enrichment Analysis function on the Metaboanalyst platform [34,35] using the default settings, and comparing them to the SMPDB metabolomics database.

### 2.10. Cell Lysis and Acetone Precipitation

Cells pellets containing up to  $1 \times 10^7$  cells were collected and washed three times with PBS before being stored at  $-80$  °C for lysis. Pellets were lysed on ice via resuspension in 200 µL RIPA buffer (Reference Number: 20-188, Millipore) supplemented with 1% (*v/v*) protease inhibitor cocktail (Reference Number: P8340, Sigma Aldrich, St. Louis, MO, USA). The solution was then passed through a 26.5 G needle (reference number: NN+2613R, Terumo) 5 times before being spun at 20,000 G for 30 min in a centrifuge pre-cooled to 4 °C. The supernatant was transferred to a second tube and 4 volumes of ice-cold acetone were added. The tube was then gently mixed and incubated overnight at  $-20$  °C. Using a centrifuge pre-cooled to  $-9$  °C, samples were spun at 20,000 G for 10 min and the supernatant was carefully removed. The pellet was then washed twice with 200 µL of ice-cold acetone to ensure the removal of any remaining contaminants. Finally, the pellet was air dried on ice for 20 min or until all liquid had evaporated. The pellet was then dissolved in 8 M urea with 50 mM ammonium bicarbonate before the protein content was estimated using a tryptophan fluorescence assay.

### 2.11. Tryptophan Fluorescence Assay for Protein Estimation

Protein quantification was performed using tryptophan fluorescence [36]. Briefly, 10  $\mu\text{L}$  of sample was diluted in 90  $\mu\text{L}$  of 8 M urea (1:10) before 50  $\mu\text{L}$  was added to a 40  $\mu\text{L}$  fluorescence cell (Agilent Technologies, P.N. 6610021600). The fluorescence was read using an Agilent Carry Eclipse Fluorescence Spectrophotometer G9800A (Agilent Technologies, S.N. MY13260001) with software version 1.2 (146), applying the following settings: excitation = 295 nm (bandwidth = 5 nm), emission = 350 nm (bandwidth = 20 nm), average time = 0.1 s and PMT starting voltage = 560 V. The cell was washed with water and 8 M urea before measuring the next sample. Fluorescence readings were compared to a 9-point L-tryptophan (Sigma-Aldrich,  $\geq 98\%$ , P.N. T0254) standard curve ( $9.15 \times 10^{-5}$  to 0.0117 mg/mL) and multiplied by a conversion factor (85.47) determined for the average number of tryptophan residues in mammalian proteins.

### 2.12. Protein Digestion and Clean Up

A total of 100  $\mu\text{g}$  of purified protein in 100  $\mu\text{L}$  of 8 M urea (Merck, Kenilworth, NJ, USA) with 50 mM ammonium bicarbonate (pH 8.0) (Fluka Analytical, P.N. 09830) was reduced via the addition of 10 mM DTT (Sigma-Aldrich) and incubated at room temperature for 1 h. Samples were then reduced via the addition of 15 mM chloroacetamide (CA) and incubated in the dark at room temperature for 30 min. Samples were diluted with 900  $\mu\text{L}$  of 50 mM (pH 8.0) before the addition of 2  $\mu\text{g}$  of trypsin/Lys-C (Promega) (1:50 trypsin: protein) and incubation for 8 h at 37  $^{\circ}\text{C}$ .

Samples were then cleaned up using a C18 Sep-Pak (Waters) equipped to a vacuum manifold. The Sep-Pak was washed with 1 mL methanol before being equilibrated via the addition of 1 mL 80% acetonitrile with 0.1% formic acid (FA) 3 times, followed by the addition of 1 mL of 0.1% FA, 4 times. The collection tube was replaced, and the sample was run through the Sep-Pak twice. The Sep-Pak was then washed 3 times with 1 mL of 0.1% FA before the peptides were eluted into a new collection tube via the addition of 500  $\mu\text{L}$  50% acetonitrile with 0.1% FA. This step was repeated to ensure that all peptides were eluted. The samples were then dried in a SpeedVac vacuum concentrator (John Morris Scientific, RVC 2-18) at 40  $^{\circ}\text{C}$ , with a vacuum of 40 mbar and a rotor speed of 1000  $\text{min}^{-1}$ . Finally, the samples were resuspended in 5  $\mu\text{L}$  of 0.1% FA and used for subsequent MS data acquisition.

### 2.13. Proteomics Data Acquisition

LC-MS analysis was performed using an Ultimate 3000 RSLC nanosystem connected to an Orbitrap Exploris 480 mass spectrometer (Thermo Fisher Scientific, Bremen, Germany). Peptides (1  $\mu\text{g}$ ) were resuspended in 0.1% formic acid and loaded onto a 25 cm fused silica column heated to 50  $^{\circ}\text{C}$ . The internal diameter (75  $\mu\text{m}$ ) of the column was packed with 1.9  $\mu\text{m}$  C18 particles. Peptide separation occurred over a 70 min linear gradient (3 to 20% acetonitrile in 0.1% formic acid) at a flow rate of 300 nL/min. The compensation voltages (−50 and −70 V) were applied from a FAIMS Pro interface (Thermo Fisher Scientific) to regulate the entry of ionised peptides into the mass spectrometer. The MS scans ( $m/z$  300 to 1500) were acquired at a resolution of 60,000 ( $m/z$  200) in positive ion mode. The MS/MS scans of fragment ions were measured at 15,000 resolution after the application of 27.5% HCD collision energy. A dynamic exclusion period of 40 s was specified. The mass spectrometry proteomics data have been deposited to the ProteomeXchange Consortium via the PRIDE [37] partner repository with the dataset identifier PXD034246.

### 2.14. Proteomics Data Analysis

The raw data was processed using the proteome discoverer platform (v2.4). The fragmentation Spectra were searched against the FASTA human database using the Sequest search engine with the precursor and fragment mass tolerance set to 10 ppm and 0.02 Da. Two missed cleavage sites were allowed, and the minimum peptide length was

6 amino acids. Oxidation and acetylation were included as variable modifications and carbamidomethylation was included as a fixed modification.

Principle component analysis (PCA) was performed through the proteome discoverer platform using unscaled protein abundances. Hierarchical clustering was performed through the Proteome Discoverer platform using Euclidian distance function, and scaled before clustering.

#### 2.15. Functional Annotation of Biological Process

Biological Process analysis was performed using the DAVID database [38]. The list of differentially abundant proteins was compared against the Gene Ontology-Biological Process (GO-BP) database, with a count threshold of 2 and EASE threshold of 0.1.

#### 2.16. KEGG Global Metabolomic Network Analysis of Metabolites and Proteins of Interest

Network analysis was performed using the Metaboanalyst platform [34,35]. Proteins and metabolites with a differential abundance of at least 1.5-fold in CBPR vs. parental cell lines were investigated for related metabolomic networks in the KEGG Global Metabolomic Network, using the default settings.

#### 2.17. Kaplan Meier Analysis

Proteins with a differential abundance of at least 1.5-fold in CBPR vs. parental cells in both OVCAR-5 and CaOV3 were selected for further investigation. The progression-free survival related to the selected genes was investigated in serous ovarian cancer, using the online Kaplan Meier (KM) plotter for the gene chip data of ovarian cancer [39,40]. The default settings were used, except for a restriction of analysis to patients with high-grade (grades 2 and 3) serous ovarian cancer who had received platinum-based chemotherapy, and the significance was deemed to be a  $p$ -value of less than 0.05.

### 3. Results

#### 3.1. Generation and Growth Rate of CBPR Cells

Through the exposure of OVCAR-5 and CaOV3 cell lines to 6–8 cycles of CBP, we successfully generated two CBPR cell lines. The MTT viability assay was used to measure the growth rates of the cell lines over 72 h, and it showed no significant difference in growth rates between the parental and CBPR cell lines (Unpaired  $t$ -test, OVCAR-5:  $p = 0.331$  and CaOV3:  $p = 0.818$ ) (Figure 1A,B). MTT viability assays showed that the CBPR cells were significantly more resistant to CBP than the parental cell lines (OVCAR-5 parental IC<sub>50</sub> = 88.6  $\mu$ M, OVCAR-5 CBPR IC<sub>50</sub> = 197.0  $\mu$ M,  $p = 0.001$ ; CaOV3 parental IC<sub>50</sub> = 41.9  $\mu$ M, CaOV3 CBPR IC<sub>50</sub> = 124.0  $\mu$ M,  $p = 0.02$ ) (Figure 1C).

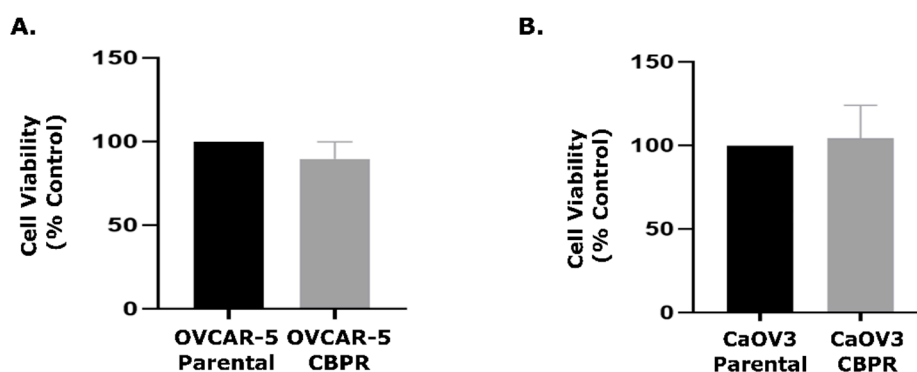
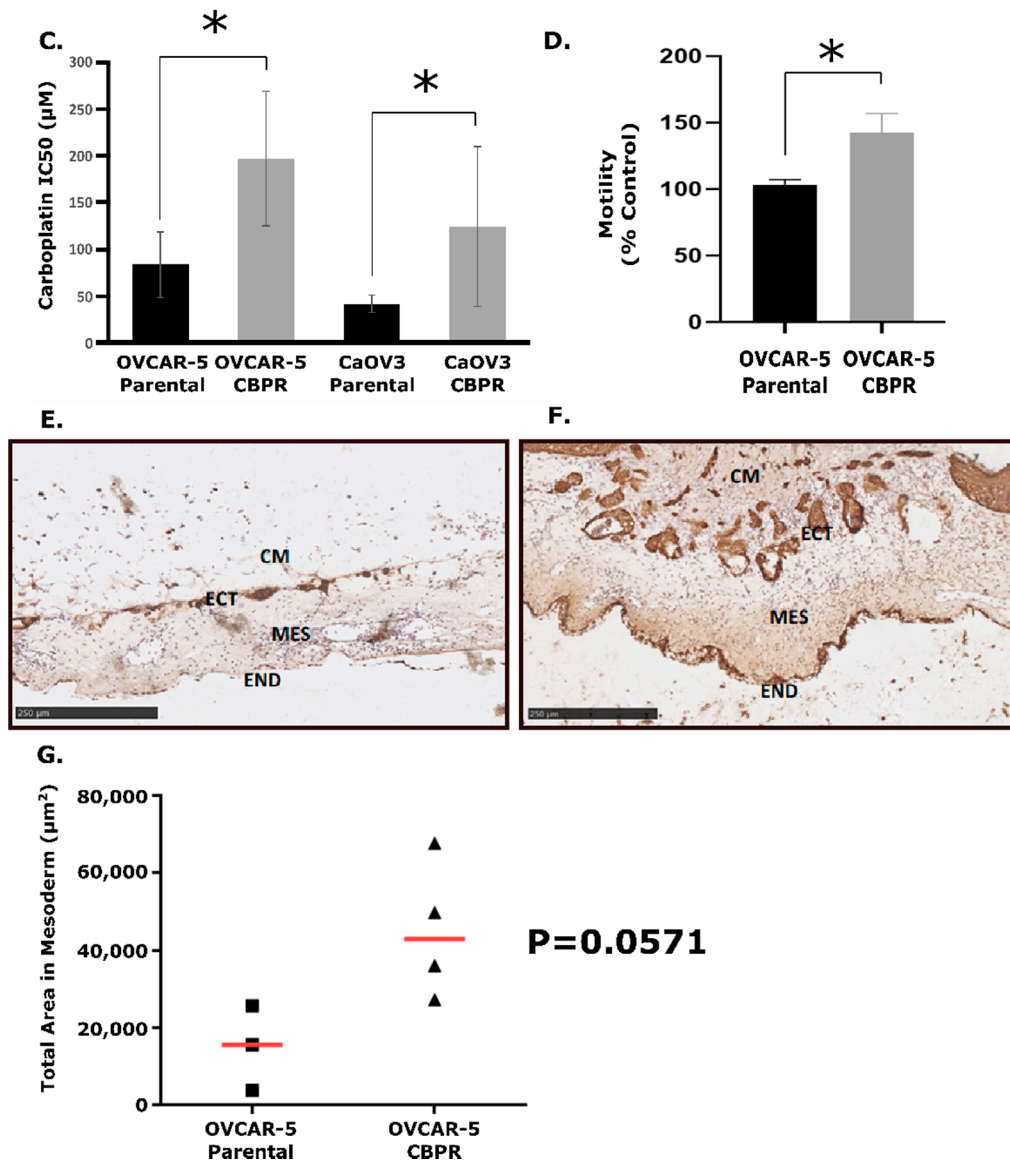


Figure 1. Cont.





**Figure 1.** Biological data for carboplatin-resistant cancer cell lines. Growth rates determined using an MTT assay of (A) OVCAR-5 parental vs. CBPR and (B) CaOV3 parental vs. CBPR show no significant difference (unpaired *t*-test, OVCAR-5:  $p = 0.331$  and CaOV3:  $p = 0.818$ ). (C) Dose response of OVCAR-5 and CaOV3 resistant and parental pairs to carboplatin. OVCAR-5 parental IC<sub>50</sub> = 83.6 ( $n = 8$ ), OVCAR-5 CBPR IC<sub>50</sub> = 1967.0 ( $n = 8$ ); CaOV3 parental IC<sub>50</sub> = 41.9 ( $n = 7$ ), CaOV3 CBPR IC<sub>50</sub> = 124.0 ( $n = 7$ ). Unpaired T test showed IC<sub>50</sub> to be significantly higher in CBPR cell lines compared to their parental cells (OVCAR-5  $p = 0.001$ , CaOV3  $p = 0.02$ ). (D) In vitro motility assay of OVCAR-5 parental compared to OVCAR-5 CBPR cell lines showed that OVCAR-5 CBPR is significantly more motile than its parental pair (unpaired *t*-test,  $p = 0.037$ ). In vivo CAM invasion assay with OVCAR-5 parental (E) and OVCAR-5 CBPR (F). OVCAR-5 cell Matrigel grafts (CM) were placed in the top of the ectoderm (ECT) layer and cancer cell invasion into the CAM mesoderm (MES) layers was assessed on Day 14 of chick embryo development. END = endoderm CAM paraffin sections (6 µm) were immunostained with pan-cytokeratin antibody. Scale bar = 250 µm. (G) Quantification of OVCAR-5 parental ( $n = 3$ ) and OVCAR-5 CBPR ( $n = 4$ ) invasion into the CAM mesoderm. Data represents the total pan-cytokeratin positive area (µm<sup>2</sup>) in the mesoderm area from 5 to 6 images per embryo. Mann–Whitney U test showed greater invasion in OVCAR-5 CBPR compared to parental cells ( $p = 0.0571$ ) (\* = statistical significance,  $p < 0.05$ ).

### 3.2. OVCAR-5 CBPR Cells Are More Motile than OVCAR-5 Parental In Vitro

An in vitro motility assay investigating the rate at which OVCAR-5 parental and CBPR cells move towards a chemoattractant (10% FBS) showed that the OVCAR-5 CBPR cells migrated at a significantly higher rate than the parental cell line ( $p = 0.037$ ) (Figure 1D).

### 3.3. OVCAR-5 Cells Are More Invasive in the In Vivo CAM Assay

The CAM assay was performed with OVCAR-5 parental and OVCAR-5 CBPR cell lines to investigate their ability to invade the mesothelial layer in chicken embryos (Figure 1E,F). This model of cancer invasion replicates numerous aspects of the in vivo barriers to cancer cell metastasis, specifically the extracellular matrix (ECM). The CAM onplants were sectioned and stained to visualize OVCAR-5 cancer cell invasion, and the degree of invasion was measured as the total area of cancer cells ( $\mu\text{m}^2$ ) within the mesoderm of the CAM layer, using pan-cytokeratin immunohistochemistry. We observed that the OVCAR-5 CBPR cells were more invasive in vivo than the OVCAR-5 parental cells (Figure 1G,  $p = 0.0571$ ).

### 3.4. LC-MSMS Analysis of Metabolites in Resistant vs. Parental Ovarian Cancer Cell Lines

The metabolomic profiles of the parental and CBPR pairs for both the OVCAR-5 and CaOV3 cell lines were analysed via LC-MS using a Thermo Scientific QExactive in biological triplicate. Analysis through the Metaboanalyst platform [34] putatively identified 380 metabolites in the OVCAR-5 samples (66 confirmed with reference standards) and 436 metabolites in the CaOV3 cell line samples (65 confirmed with reference standards) (OVCAR-5 parental: 369, OVCAR-5 CBPR: 370; CaOV3 parental: 436, CaOV3 CBPR: 428). The Venn diagrams show an almost complete overlap in the metabolites identified between the parental cell lines and their chemoresistant equivalents (Figure 2A,C). Volcano plots, calculated after filtering to remove cell culture media-related metabolites, show numerous metabolites that were differentially abundant between the parental and CBPR cells (1.5-fold,  $p < 0.05$ ; more abundant in the OVCAR-5 parental:  $n = 29$ , less abundant in the OVCAR-5 parental:  $n = 7$ , more abundant in the CaOV3 parental:  $n = 29$ , less abundant in the CaOV3 parental:  $n = 11$ ) (Figure 2B,D) (full details in Supplementary Tables S1 and S3). Furthermore, the metabolic classes identified in these analyses favoured those that are related to amino acid metabolism and lipid metabolism (Figure 2E,F).

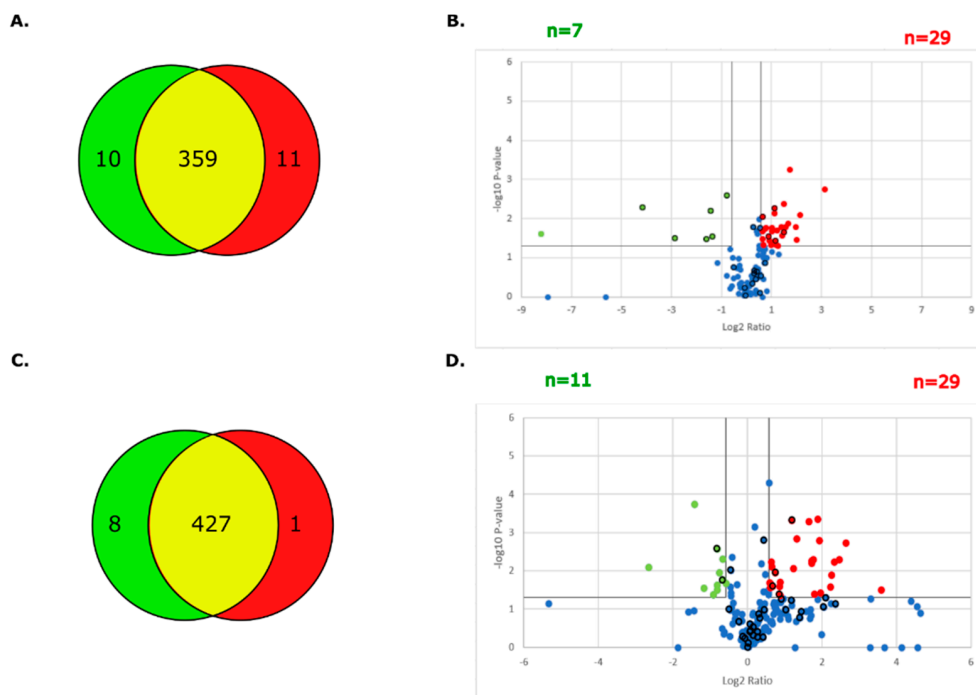
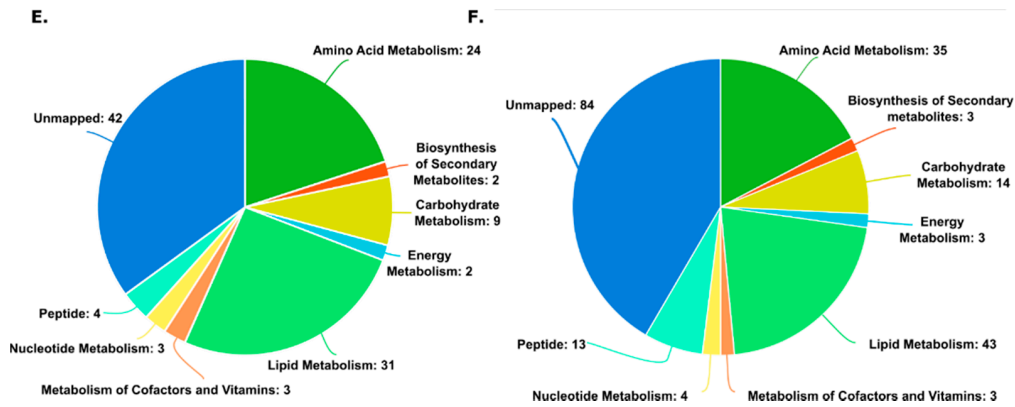


Figure 2. Cont.



**Figure 2.** Summary of metabolites identified in parental and CBPR cell lines. (A) Metabolites putatively identified in OVCAR-5 cell line pair. OVCAR-5 parental total= 369, OVCAR-5 CBPR total= 370, unique to OVCAR-5 parental= 10, unique to OVCAR-5 CBPR= 1, in both OVCAR-5 parental and CBPR= 359. (B) Volcano plot showing metabolites with 1.5-fold ( $=0.58 \log_2$ ) differential abundance in OVCAR-5 parental compared to CBPR. Twenty-nine metabolites (5 identified with reference standards indicated by bold outline) were upregulated, and 7 metabolites (6 identified with reference standards indicated by bold outline) were downregulated in parental OVCAR-5 cells. (C) Metabolites identified in CaOV3 cell line pair before filtering: CaOV3 parental total= 435, CaOV3 CBPR total= 428, unique to CaOV3 parental = 8, unique to CaOV3 CBPR= 1, in both CaOV3 parental and CBPR= 436. (D) Volcano plot showing metabolites with 1.5-fold ( $=0.58 \log_2$ ) differential abundance in CaOV3 parental compared to CBPR. Twenty-nine metabolites were seen to be upregulated (4 identified with reference standards indicated by bold outline) and 11 metabolites (2 identified with reference standards indicated by bold outline) were downregulated in parental CaOV3 cells. (E) Pie chart of metabolite classes identified in OVCAR-5 parental and CBPR cell lines. (F) Pie chart of metabolite classes identified in CaOV3 parental and CBPR cell lines.

3.5. Classification of Ovarian Cancer Cell Lines Based on Metabolomic Profiles

The online platform, Metaboanalyst [34], was used to generate PCA plots and heat maps to investigate the separation of the parental and CBPR cell lines based on their molecular features. The PCA plots demonstrated a robust separation between the parental and CBPR cell lines based on their metabolomic profile (Figure 3A,C). This was further supported by hierarchical clustering and visualised in the heat maps (Figure 3B,D).

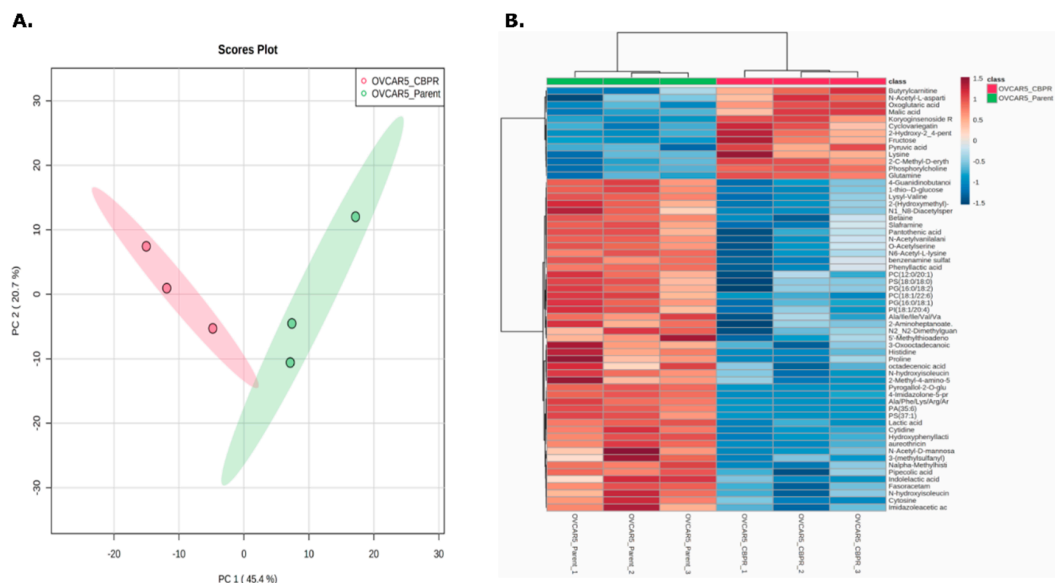


**Figure 3.** Cont.

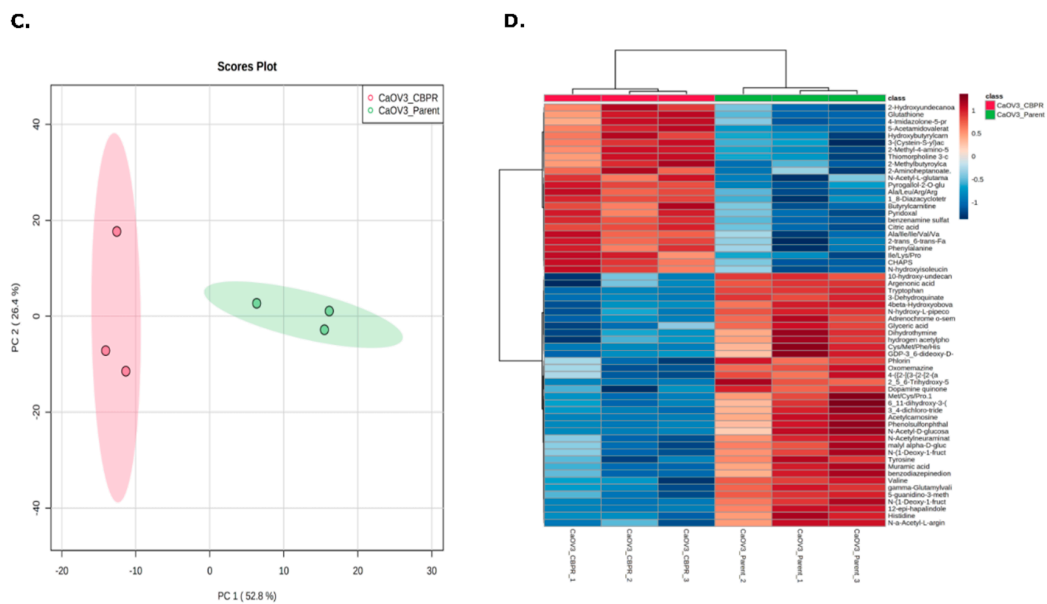


**Figure 3.** Principle component analysis (PCA) and hierarchical clustering of top 50 differentially abundant metabolites (identified through *t*-test) between parental (green) and the CBPR (red) cancer cell lines (A,B) OVCAR-5 and (C,D) CaOV3. Analysis was performed with Metaboanalyst.

3.6. LC-MSMS Analysis of Proteins in Resistant vs. Parental Ovarian Cancer Cell Lines

The proteomic profiles of parental and CBPR pairs for both OVCAR-5 and CaOV3 cell lines were generated and analysed via LC-MSMS using the Exploris480 in biological triplicate, each of which was run as technical triplicates. An analysis with Proteome Discoverer resulted in over 5000 proteins being identified in each group (OVCAR-5 parental: 6423, OVCAR-5 CBPR: 6439; CaOV3 parental: 5395, CaOV3 CBPR: 5380). The Venn diagrams showed significant overlap in the proteins identified between both the parental cell lines and their chemoresistant equivalents (Figure 4A,C), while the volcano plots showed numerous proteins that were differentially abundant between the parental and CBPR cells (1.5-fold,  $p < 0.05$ ; more abundant in OVCAR-5 parental:  $n = 154$ , more abundant in OVCAR-5 CBPR:  $n = 125$ , more abundant in CaOV3 parental:  $n = 124$ , more abundant in CaOV3 CBPR:  $n = 63$ ) (Figure 4B,D). The full details of the proteomics results can be found in Supplementary Table S3.

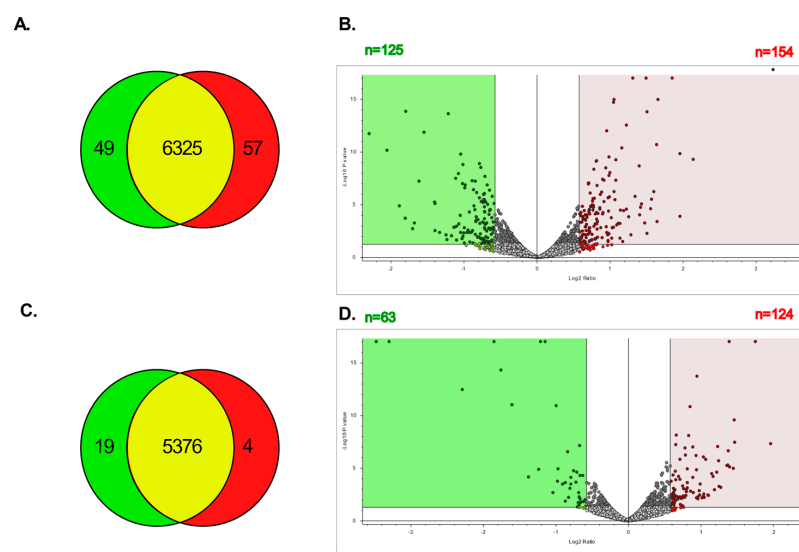


**Figure 4.** Total number of proteins identified in parental and CBPR cell lines. (A) Proteins identified

in OVCAR-5 cell line pair: OVCAR-5 parental total = 6374, OVCAR-5 CBPR total = 6382, OVCAR-5 parental exclusive = 49, OVCAR-5 CBPR exclusive = 57, in both OVCAR-5 parental and CBPR = 6325. (B) Volcano plot showing proteins with 1.5-fold ( $=0.58 \log_2$ ) differential abundance in OVCAR-5 parental compared to CBPR. A total of 154 proteins were upregulated and 125 proteins were downregulated in parental OVCAR-5 cells. (C) Proteins identified in CaOV3 cell line pair: CaOV3 parental total = 5395, CaOV3 CBPR total = 5380, CaOV3 parental exclusive = 19, CaOV3 CBPR exclusive = 4, in both CaOV3 parental and CBPR: 5399. (D) Volcano plot showing proteins 1.5-fold ( $=0.58 \log_2$ ) differentially abundant in CaOV3 parental compared to CBPR. A total of 124 proteins were seen to be upregulated and 63 proteins were downregulated in parental CaOV3 cells.

### 3.7. Separation of Ovarian Cancer Cell Lines Based on Proteomic Profiles

The Proteome discoverer software was used to generate PCA plots and heat maps to investigate the separation of parental and CBPR cell lines based on their molecular features. The PCA plots demonstrated a robust separation between the parental and CBPR cell lines based on their proteomic profiles (Figure 5A,C). This was further supported by hierarchical clustering and was visualised in the heat maps (Figure 5B,D).

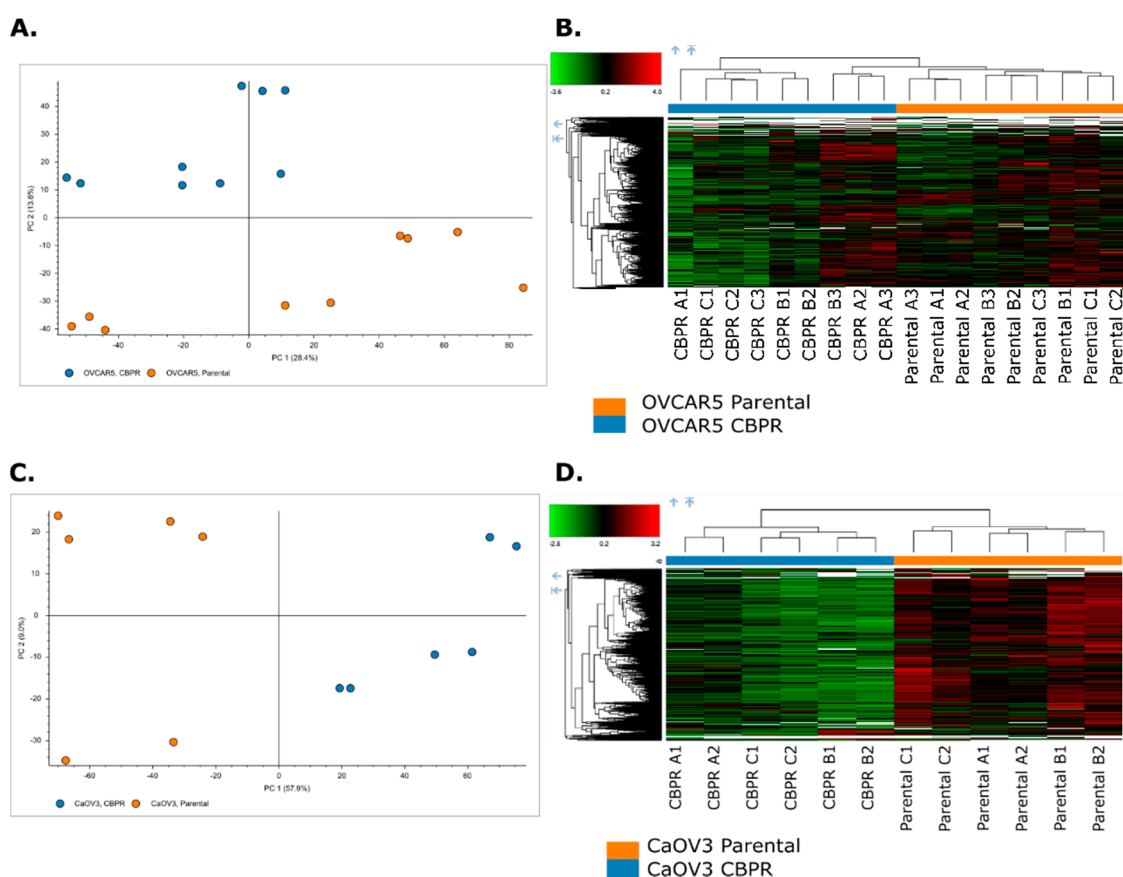


**Figure 5.** Principle component analysis (PCA) and hierarchical clustering of proteomic features of parental (orange) and the CBPR (blue) cancer cell lines (A,B) OVCAR-5, (C,D) CaOV3. Analysis was performed with Proteome Discoverer (Thermo) inbuilt data visualisation tools.

### 3.8. Functional Analysis of Differentially Abundant Proteins between Parental and CBPR Cancer Cell Lines

To assess the altered pathways observed between the parental and CBPR cell lines, we performed functional analysis on differentially abundant proteins using the Gene Ontology Biological Process database through DAVID. In the OVCAR-5 cells, there was a significant enrichment of structural biological processes (Table 1). In the CaOV3 cells, there was an enrichment of catabolic, survival and cell structure biological processes (Table 2).

**Table 1.** Top 10 gene ontology biological functions for proteins with decreased or increased abundance in OVCAR-5 cells. Terms in bold represent those which are represented in both OVCAR-5 and CaOV3 cells.

Rank	Term	Count	Involved Genes/Total Genes (%)	p-Value
1	cytoskeleton organisation	29	13.1	$3.2 \times 10^{-0.4}$
2	antigen processing and presentation of peptide antigen	10	4.5	$3.5 \times 10^{-0.4}$
3	cellular component assembly	51	23	$6.3 \times 10^{-0.4}$
4	<b>response to cytokine</b>	22	9.9	$8.1 \times 10^{-0.4}$
5	cell junction organisation	11	5	$9.8 \times 10^{-0.4}$
6	cytokine-mediated signalling pathway	17	7.7	$1.3 \times 10^{-0.3}$
7	<b>intermediate filament cytoskeleton organisation</b>	5	2.3	$1.7 \times 10^{-0.3}$
8	regulation of cellular component organisation	45	20.3	$1.7 \times 10^{-0.3}$
9	<b>type I interferon signalling pathway</b>	6	2.7	$2.1 \times 10^{-0.3}$
10	cell junction assembly	9	4.1	$2.5 \times 10^{-0.3}$

**Table 2.** Top 10 gene ontology biological functions for proteins with decreased or increased abundances in CaOV3 cells. Terms in bold represent those which are represented in both OVCAR-5 and CaOV3 cells.

Rank	Term	Count	Involved Genes/Total Genes (%)	p-Value
1	negative regulation of necroptotic process	3	2.2	$1.8 \times 10^{-0.3}$
2	<b>response to type I interferon</b>	5	3.7	$2.5 \times 10^{-0.3}$
3	cellular macromolecule catabolic process	16	11.9	$4.8 \times 10^{-0.3}$
4	negative regulation of cellular protein metabolic process	16	11.9	$5.5 \times 10^{-0.3}$
5	protein catabolic process	14	10.4	$6.1 \times 10^{-0.3}$
6	positive regulation of extrinsic apoptotic signalling pathway	4	3	$7.1 \times 10^{-0.3}$
7	<b>intermediate filament organisation</b>	3	2.2	$1.0 \times 10^{-0.2}$
8	<b>response to cytokine</b>	13	9.7	$1.4 \times 10^{-0.2}$
9	regulation of protein ubiquitination	7	5.2	$1.0 \times 10^{-0.2}$
10	positive regulation of proteolysis	8	6	$1.60 \times 10^{-0.2}$

Both OVCAR-5 and CaOV3 cell lines showed an enrichment of proteins with functions related to IFN1 signalling, response to cytokine and intermediate filament cytoskeletal organisation. There were no common differentially abundant proteins in the cell lines related to IFN1 signalling and response to cytokines, while keratin 2 and keratin 9 were both more abundant in OVCAR5 parental cells and less abundant in CaOV3 parental cells, and related to intermediate filament cytoskeletal organisation (Supplementary Table S4).

### 3.9. KEGG Global Metabolomic Network Analysis of Differentially Abundant Proteins and Metabolites between Parental and CBPR Cell Lines

To investigate how dysregulated proteins and metabolites contribute to altered metabolomic pathways in CBPR compared to parental ovarian cancer cell lines, we performed a KEGG Global Metabolomic Network analysis on differentially abundant proteins and metabolites using the Metaboanalyst platform [34]. In both cell lines, there was an enrichment of proteins with functions related to amino acid metabolism and energy metabolism-related pathways (Tables 3 and 4).

**Table 3.** Top 10 KEGG Global Metabolic Pathways for proteins and metabolites with decreased or increased abundances in OVCAR-5 cells. Terms in bold represent those which are represented in both OVCAR-5 and CaOV3 cells.

Rank	Metabolite Set	Count (Metabolites)	Count (Proteins)	Count (Total)	p-Value
1	<b>Alanine, aspartate and glutamate metabolism</b>	4	2	6	0.000817
2	Glycolysis/Gluconeogenesis	2	3	5	0.000717
3	Pyruvate metabolism	2	3	5	0.00419
4	Inositol phosphate metabolism	0	4	4	0.0053
5	<b>Arginine and proline metabolism</b>	3	1	4	0.0189
6	Citrate cycle (TCA cycle)	2	1	3	0.0208
7	Limonene and pinene degradation	1	0	1	0.03
8	Chloroalkane and chloroalkene degradation	1	1	2	0.0348
9	Valine, leucine and isoleucine degradation	2	1	3	0.0445
10	Fatty acid biosynthesis	0	2	2	0.0452

**Table 4.** Top 10 KEGG Global Metabolic Pathways for proteins and metabolites with decreased or increased abundances in CaOV3 cells. Terms in bold represent those which are represented in both OVCAR-5 and CaOV3 cells.

Rank	Metabolite Set	Count (Metabolites)	Count (Proteins)	Count (Total)	p-Value
1	<b>Alanine, aspartate and glutamate metabolism</b>	2	1	3	0.00692
2	<b>Arginine and proline metabolism</b>	1	2	3	0.0148
3	Folate biosynthesis	0	2	2	0.045
4	Linoleic acid metabolism	0	1	1	0.0858
5	Vitamin B6 metabolism	1	0	1	0.0893
6	Glycine, serine and threonine metabolism	2	0	2	0.0895
7	Glycosylphosphatidylinositol (GPI)-anchor biosynthesis	0	1	1	0.134
8	Thiamine metabolism	0	1	1	0.145
9	Amino sugar and nucleotide sugar metabolism	0	2	2	0.145
10	Sphingolipid metabolism	0	1	1	0.181

Both the OVCAR-5 and CaOV3 cell lines showed significant enrichment in alanine, aspartate and glutamate metabolism, and in arginine and proline metabolism. One protein (glutamin-fructose-6-phosphate transaminase (isomerizing) 2 (GFPT2)) related to alanine, aspartate and glutamate metabolism was common to both the OVCAR-5 and CaOV3 cells. It was more abundant in the OVCAR-5 parental cells compared to the CBPR pair, and less abundant in the CaOV3 parental cells compared to the CBPR pair (Supplementary Table S5). GFPT2 was also seen to be more abundant in chemosensitive primary cells compared to chemoresistant cells (Supplementary Table S5).

### 3.10. Kaplan Meier Analysis of Proteins of Interest in Chemoresistance

To investigate whether the result of proteins that were differentially expressed in parental and CBPR cells was reflected in patients, we examined the relationship with PFS, and the gene expression of differentially abundant proteins present in both CaOV3 and OVCAR-5 CBPR cells compared to their chemosensitive counterparts, using the Kaplan Meier plotter (Supplementary Table S3). Further, we investigated proteins with differential abundances between the parental and CBPR cell lines that contributed to commonly identified metabolic pathways (Supplementary Table S5). We identified several proteins with differential expression between the CBPR and chemosensitive cell lines that were associated with patient survival (Figure 6).

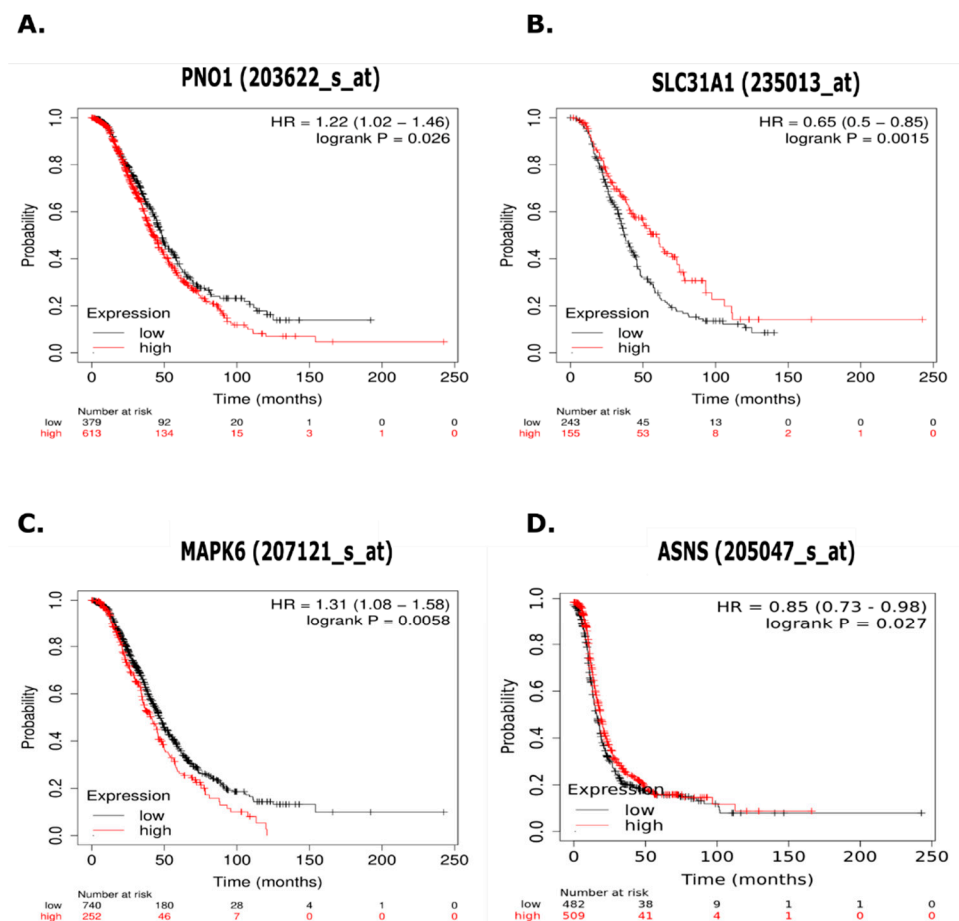


**Figure 6.** Kaplan Meier (KM) plots measuring progression free survival (PFS) in serous ovarian cancer patients treated with platinum-based chemotherapy ( $n = 979$ ) related to selected proteins. (A) RNA binding protein *PNO1* (*PNO1*) showed abundance at least 1.5-fold lower in parental cell lines and is associated with significantly decreased PFS. (B) High affinity copper uptake protein (*SLC31A1*) showed abundance at least 1.5-fold higher in parental cell lines and is associated with significantly increased PFS. (C) Mitogen-activated protein kinase 6 (*MAPK6*) showed abundance at least 1.5-fold lower in parental cell lines and is associated with significantly decreased PFS. (D) Asparagine synthase (*ASNS*) showed abundance at least 1.5-fold higher in OVCAR-5 parental cells, is part of the enriched Alanine, Aspartate and Glutamate Metabolism pathway, and is associated with significantly increased PFS.

RNA binding protein (*PNO1*) and mitogen-activated protein kinase 6 (*MAPK6*) both showed at least 1.5-fold expression in CBPR cells, and this increased expression was associated with significantly decreased PFS. High affinity copper uptake protein (*SLC31A1*) showed 1.5-fold higher expression in both OVCAR-5 and CaOV3 parental cells, and this increased expression was associated with significantly increased PFS. Asparagine synthase (*ASNS*) showed 1.5-fold higher expression in OVCAR-5 parental cells, is associated with alanine, aspartate and glutamate metabolism (Supplementary Table S5), and its increased expression was associated with significantly increased PFS in HGSOV patients.

#### 4. Discussion

The molecular mechanisms defining chemosensitivity and chemoresistance remain poorly understood. A detailed understanding might enable us to predict treatment responses and may potentially lead to the identification of novel drug targets that aid therapy. The unbiased, comprehensive molecular characterisation that is achievable through mass spectrometry analysis has great potential for meeting this need and for providing deep insight into the molecular basis of chemoresistance. Here, we present a mass spectrometry



analysis of cancer cell lines that were selected to exhibit resistance to treatment with the primary chemotherapeutic agent used for this disease, CBP. Mass spectrometry-based metabolomic and proteomic analysis of these samples allowed us to separate resistant cells from parental cells based on these respective molecular characteristics through unbiased statistical analysis. Further, dysregulated proteins and metabolites between resistant cells and their parental pairs were related to cancer-associated pathways.

There has been speculation regarding the cellular origins of the OVCAR5 cell line [26], and we include this information for transparency. However, it is speculative as to whether the differences observed in the phenotypical or molecular features reflect potentially different organs of origin.

While metabolomics has been widely employed in the search of HGSOC biomarkers (reviewed in [41]), there are relatively few studies utilising mass spectrometry-based metabolomics for the investigation of chemoresistance in HGSOC. One study investigated the metabolomic profiles of one ovarian cancer cell line, and its platinum-resistant derivative, and identified the impacts on methionine metabolism and glutathione synthesis pathways [42]. Here, we expanded on these findings, investigating two additional ovarian cancer cell lines and putatively identifying almost twice as many metabolites.

Furthermore, numerous proteomics investigations into chemoresistant ovarian cancer have been previously performed with the aim of understanding the molecular basis of chemoresistance and identifying biomarkers of chemoresistance to advise on treatment approaches [43]. These have employed multiple mass spectrometry techniques, including iTRAQ [44], ICAT [45,46], 2D DIGE coupled with MALDI-TOF-MS [47–49] or LC-MSMS [50], and label-free LC-MSMS [51]. In addition, mitochondrial fractionation has been employed to provide a deeper coverage of chemoresistance-associated proteins [48,51].

Previous analyses have identified pathways that correlate with a chemoresistant phenotype, such as glycolysis [44,50], ubiquitination [50], redox states [44], and PI3K signalling [45]. Furthermore, a broad panel of proteins has been highlighted for their potential as biomarkers of chemoresistant ovarian cancer (reviewed in [52]).

G. Fan, et al. (2015) [44] employed eight-plex iTRAQ MS to investigate 10 ovarian cancer cell lines, and identified several dysregulated proteins related to redox states and homologous repair in resistant cells. Interestingly, they were able to separate resistant from sensitive cell lines based on a panel of 300 differentially abundant proteins. Here, we demonstrate that a similar and potentially more robust separation can be achieved using over 6000 proteins when comparing directly between a cancer cell line and its resistant counterpart. Interestingly, Fan et al. were unable to achieve such a degree of separation with the DNA methylation and RNA data. A similar pattern has been observed previously [47], affirming the strength of proteomics-based approaches for the characterisation of chemoresistant phenotypes.

Exposure to chemotherapeutic agents has extreme impacts on the molecular and functional state of the affected cell. Chemoresistance is a major barrier to improving patient survival, not only because it prevents the clearance of the cancer, but because it often results in a more aggressive cancer upon relapse [53]. This could be a result of the evolutionary pressures which are placed upon cancer cells that are exposed to treatment, resulting in the development of adaptive survival and migration capabilities in response to these stressors. Our results show that repeated exposure to small doses of carboplatin is sufficient to produce an OVCAR-5 population that more readily migrates and invades, compared with its parent cell line, with very little difference in growth rates.

Molecular changes that occur in response to CBP treatment can be monitored in differentially abundant metabolites and proteins, and the biological function and pathways that they regulate. We applied SMPDB enrichment and Gene Ontology-Biological Process analysis to our metabolomic and proteomic data sets, respectively.

Most of the metabolites identified were not differentially abundant between the parental and chemoresistant cells. While the differences were sufficient to correctly clus-

ter biological replicates, pathways analysis of dysregulated metabolites did not result in significant insights, and are summarised in Supplementary Table S6.

A manual analysis of dysregulated metabolites between parental and chemoresistant OVCAR-5 cells identified perturbations in glutaminolysis, the TCA cycle and glycolysis. The enrichment of glutaminolysis and the TCA cycle, was reflected by significant increases in glutamine (14-fold), oxoglutaric acid (2.7-fold), succinic acid (1.6-fold), malate (2.6-fold) and aspartic acid (1.9-fold), observed in OVCAR-5 CBPR cells compared to OVCAR-5 parental. Furthermore, we observed an increase in glycolysis-related metabolites in OVCAR-5 CBPR, including pyruvic acid (7.2-fold) and glucose (3.4-fold). (Note that glutamine, aspartic acid and glucose were excluded from our above analysis (Table 3) due to their high abundances in the media-only control).

In contrast, a manual analysis of metabolites that were dysregulated between parental and chemoresistant CaOV3 cells did not show any clear trends. This could be attributed to very few of the dysregulated metabolites being confidently identified in this analysis (six metabolites were identified with reference standards out of 40 differentially abundant putative metabolites between the CaOV3 parental and CaOV3 CBPR cells (Figure 2)). Although it was difficult to interpret, the observation that several short peptides and some putatively identified glycosylated amino acids showed lower abundances in the CaOV3 CBPR cells (Supplementary Table S2), coupled with the observation from our proteomics data of enriched catabolic pathways in the CaOV3 CBPR cells (Table 1) potentially reflect alterations in protein turnover. Protein turnover and autophagy are well known to play complex roles in tumorigenesis and chemoresistance [54], although further studies are required to address their role in the development of CBPR resistance.

Our manual analysis revealed only one metabolite that was similarly dysregulated in chemoresistance between the OVCAR5 and CaOV3 cell line pairs (Supplementary Tables S1 and S2). Alanine was 2.8-fold higher in OVCAR5 parental and 2-fold higher in CaOV3 parental, compared to their CBPR pairs. While alanine is involved in several important metabolic pathways, including lactose metabolism [55], glycolysis and gluconeogenesis [56] and the alanine–glucose cycle [57], it is not clear how the increase in this metabolite contributes to the resistance phenotype in the absence of broader alterations in these related pathways.

No other metabolites were similarly dysregulated in chemoresistance between OVCAR5 and CaOV3 cell line pairs, suggesting that these cell lines possess distinct metabolomes. This could be due to differences in the metabolomes of the parental cells, as seen in Supplementary Figure S1, or in differences in how the metabolism of each cell type responds to treatment, or a combination of the two.

Proteomic analysis of both cell line models revealed enriched biological processes that were related to response to cytokines and cellular response to IFN1 (Tables 1 and 2). IFN1 production and signalling has been previously implicated in the chemotherapy response of neoplastic cells [58]. However, chemoresistance has previously been associated with a decreased expression of IFN1 genes in ovarian cancer, contributing to an immunosuppressed microenvironment [59]. Moreover, A. Sistigu, et al. (2014) [60] showed that cisplatin treatment of a panel of cell lines was unable to stimulate IFN1 gene expression. However, they demonstrated that supplying exogenous IFN1 enhanced the anti-neoplastic effects of carboplatin in a mice model of melanoma [60]. The role of IFN signalling in ovarian cancer chemoresistance merits further investigation. Combination therapy with IFN-gamma, Carboplatin and Paclitaxel for the treatment of ovarian cancer has previously been investigated in a phase III clinical trial [61]. Combining diverse immunotherapy approaches with standard chemotherapy has also shown promise in treating ovarian cancer [62]. Our findings merit further investigation into combination therapy with cytokines and carboplatin, with the express aim of overcoming chemoresistance. Further investigations will be necessary to better understand the molecular details and biological relevance of these findings.

Additional proteins are implicated in the regulation of IFN signalling. For example, our results showed a decreased abundance of tyrosine kinase 2 (TYK2) in CaOV3 CBPR cells, which plays a key role in the promotion of IFN1 signalling in response to cytokines

(Supplementary Table S3). Moreover, we observed an increased abundance of proteasome subunit beta 8 (PSMB8) in OVCAR-5 CBPR cells (Supplementary Table S3). This protein can be activated by IFN signalling to form the ‘immunoproteasome’ [63]. In addition to antigen processing, this complex promotes cell survival, and its inhibition has been shown to sensitize drug-resistant stomach and colon cancer cell lines to cisplatin [64]. Interestingly, the stimulation of IFN1 genes is currently under investigation as a potential therapeutic in a range of contexts and cancers [59,65].

The metabolic network analysis of dysregulated metabolites and proteins, using the KEGG Global Metabolomic Pathways database, identified ‘alanine, aspartate and glutamate metabolism’ and ‘arginine and proline’ metabolism as enriched pathways in both OVCAR-5 and CaOV3 cells. Auxotrophy, where the cell relies on external sources for a specific molecule, for alanine and glutamate, have both been observed in cancer [66,67], and it is theorized that this can promote growth and survival through exogenous amino acid importation pathways [66]. In our results, we observed an increased abundance of alanine in CBPR for both cell lines, while glutamate showed an increased abundance in OVCAR5 CBPR, but a decreased abundance in CaOV3 CBPR (Supplementary Tables S1 and S2). There is a significant demand for glutamate in proliferating cells for transamination reactions, and for the use of its carbon backbone for the synthesis of other anabolic metabolites and antioxidants [68]. Further, glutamate contributes to the TCA cycle (it was enriched according to a KEGG global metabolomic pathway analysis for OVCAR-5 (Table 3)) through the process of ‘glutaminolysis’, which contributes to energy production and cell survival [69]. However, due to the differences between our cell line pairs, it is difficult to draw broad and consistent conclusions regarding how the metabolome changes in response to acquired resistance to CBP.

A deeper investigation into the enrichment of the ‘arginine and proline’ pathway revealed the contribution of proteins and metabolites involved in the creatine (creatine kinase (CK) and guanidoacetic acid) and urea cycle (arginase and 4-guanidinobutanoic acid) (Supplementary Table S5). The creatine pathway is responsible for maintaining energy homeostasis through the reversible biosynthesis of phosphocreatine (PCr) from ATP [70]. The presence of a pool of PCr facilitates the rapid generation of ATP at sites with high energy demands without the need for transporting ATP across cellular membranes [71]. As cell division is regulated in an energy-dependent manner [72], CK-regulated ATP homeostasis is important for the progression of the G1 and G2 phases into S phase and M phase, respectively [73]. The urea cycle is often dysregulated in cancer to maximize the available nitrogen and carbon for the anabolic synthesis of macromolecules that are required for rapid tumour proliferation and growth [74]. Further, the urea cycle is essential for the detoxification of ammonia, through its conversion to urea [75], which accumulates primarily as a byproduct of the glutaminolysis reaction [74], which was seen to be enriched in OVCAR5 CBPR cells, as discussed above. These altered pathways potentially represent perturbations in energy homeostasis, cell cycle control, anabolic pathways, and the detoxification of anabolic waste products. However, the relatively small number of metabolites and proteins that were observed to contribute to these pathways in this study means that these results must be interpreted with caution. Further, the observation that the two cell lines employed in this study have distinct metabolic pathways, both at base line and after acquired resistance to CBP, limit the broader conclusions that can be drawn from this data.

To expand on the proteins identified as being differentially abundant between both the CBPR and chemosensitive cancer cell lines, we investigated the relationship between their expression and patient survival, using a KM plotter [39]. We identified two proteins (RNA binding protein PNO1 (PNO1) and mitogen-activated protein kinase 6 (MAPK6)) that exhibited increased abundance in CBPR cells and decreased PFS in HGSOC patients when their related gene expression was high.

PNO1 is involved in ribosomal biogenesis, and its knockdown has been seen to increase p53 and p21 signalling, resulting in apoptosis in colon cancer cell lines [76]. In addition, its expression has been related to lung adenocarcinoma progression mediated

by amplified Notch signalling pathways [77]. Downregulation of the Notch signalling pathway sensitizes lung cancer cells to cisplatin [78], potentially representing a pathway through which PNO1 expression promotes resistance to platinum-based chemotherapy.

MAPK6 is a multifunctional signalling protein that is involved in inflammatory responses, and cell growth and differentiation [79]. It has been reported to promote metastasis in lung cancer [80] and inhibit apoptosis in HUVEC cells [81]. It also phosphorylates tyrosyl DNA phosphodiesterase 2 (TDP2), promoting its topoisomerase 2-linked DNA repair mechanism, which has been shown to confer resistance to topoisomerase inhibitors [82].

We also identified the high affinity copper transporter protein (SLC31A1), which showed decreased abundance in CBPR cell lines and increased PFS related to high *SLC31A1* expression. SLC31A1 is the main import channel for platinum-based antineoplastic drugs into the cell [83], and its increased expression confers platinum sensitivity in several contexts [84,85]. Increased SLC31A1 expression, in combination with platinum-based chemotherapy, correlates with increased survival in ovarian [86] and lung cancer [87]. As SLC31A1 expression increases in response to limited copper availability, there have been numerous clinical trials investigating the use of copper-chelating agents to increase SLC31A1 expression and to subsequently sensitize cells to platinum-based chemotherapy [88–90].

Further, we identified a protein (asparagine synthase (ASNS)) that was upregulated in OVCAR-5 parental cells, related to the enriched ‘alanine, aspartate and glutamate metabolism’ metabolic network, and whose high expression related to increased PFS in HGSOC patients. This protein catalyses the synthesis of asparagine from aspartate and glutamate [91], playing a role in tumour initiation and growth under amino acid-limiting conditions [92]. Silencing ASNS in nasopharyngeal carcinoma has been demonstrated to sensitize cells to cisplatin treatment through impaired DNA repair and cell survival mechanisms [93]. Interestingly, supplementation with exogenous asparagine improved the growth rates of the tumour cells, but did not impact on resistance to cisplatin [93]. In contrast, increased ASNS expression in response to glucose starvation was seen to enhance cisplatin resistance in pancreatic cancer [94]. Further work is required to understand how ASNS contributes to platinum resistance in ovarian cancer, but in acute lymphoblastic leukaemia, in which the *ASNS* gene is silenced, asparaginase treatment is effective at limiting tumour growth, representing a metabolism-targeted treatment in ASNS deficient cells [95].

It is important to note that we showed these KM curves to demonstrate that these proteins of interest may play a role in disease progression in a larger cohort. However, as these were only a small portion of the up- and downregulated proteins identified, we do not imply that these are the main regulators of chemoresistance in this setting. While the roles of these proteins in chemoresistance do merit further investigation, we have not pursued further validation experiments (such as Western blots, knockdown, or overexpression experiments).

We have been successful in identifying numerous pathways that are altered in chemotherapy-resistant cells lines. However, it is difficult to draw broader conclusions, due to our relatively small sample size and the observation that PCA and the hierarchical clustering of metabolomic and proteomic data favour clustering that is based on cell type rather than chemoresistance status (Supplementary Figures S2 and S3). Furthermore, we accept that the *in vitro* exposure of these cells to chemotherapy, in the absence of an *in vivo* microenvironment, results in a chemotherapy-resistant phenotype that does not accurately reflect the *in vivo* situation. Our model also does not replicate chemoresistance mechanisms that exist outside of the cell, such as extracellular signalling, drug exclusion and the influence of other features, including hypoxia and nutrient deprivation.

A proteomic analysis of patient-derived samples is required in order to better understand the molecular features of chemoresistance *in vivo*. Here, we performed a pilot proteomic analysis on two patient samples taken from the ascites of one patient with a chemosensitive disease and one with a chemoresistant disease (Supplementary Figure S1). Our findings highlight that there is a striking difference in the molecular profiles of the

cell lines and primary cells that is far more significant than the differences attributed to chemosensitivity status (Supplementary Figure S3). Of interest is the observed enrichment of responses to cytokines and cellular responses to IFN1 biological processes in relation to differentially abundant proteins between sensitive and resistant primary cells (Supplementary Figure S1), which is also observed in the cell line proteomics data. Currently, we have access to only two well-characterized and matched primary samples for analysis, but these findings provide a foundation to expand upon this study using a larger cohort of primary samples in the future.

A previous study investigated the molecular profiles of ascites-derived ovarian cancer cells in a larger cohort [96]. They were able to identify approximately 2800 proteins across four sensitive and four resistant samples, using SDS-PAGE protein separation followed by mass spectrometry analysis using an Orbitrap Elite mass spectrometer (Thermo Fisher Scientific, Adelaide, SA, Australia). From these proteins, they identified a total of 353 differentially abundant proteins between the resistant and sensitive groups, and observed enriched metabolic, DNA repair and host immune response pathways in resistant cells. Interestingly, they identified the ‘spheroid’ structures as being essential in ovarian cancer chemoresistance, representing a structural feature of ovarian cancer that is not captured in traditional cell culture.

With the application of the modern mass spectrometry approaches outlined here to a larger cohort of patient-derived samples, there is the potential to further develop our understanding of chemoresistance. Furthermore, the application of advanced in vitro cell culturing techniques, including ovarian cancer spheroids, promises to help bridge the gap between the in vitro and in vivo settings. Finally, combining multiple molecular analyses beyond metabolomics and proteomics, in a ‘panomics’ approach [97] promises to provide a deeper understanding of the molecular underpinnings of chemoresistance, as has recently been demonstrated in a study of low-grade serous ovarian cancer [98]. Together, these advances hold the potential to provide a holistic molecular snapshot of chemoresistance in a biologically and clinically relevant manner, to improve patient outcomes.

## 5. Conclusions

Our analysis was able to separate chemoresistant cells from their parental cells based on their metabolomic and proteomic features, and we identified altered biological processes and pathways that are of further interest. A preliminary investigation of patient-derived cells highlighted the need to perform broad biological and molecular analyses, and comprehensive in vitro and in vivo studies using a larger patient cohort, to achieve a deeper and more clinically relevant characterisation of the molecular drivers of chemoresistance.

**Supplementary Materials:** The following supporting information can be downloaded at: <https://www.mdpi.com/article/10.3390/cancers14112763/s1>, Figure S1: Proteomics summary data for primary cells; Figure S2: PCA and hierarchical clustering analysis of cell line metabolomic data; Figure S3: PCA and hierarchical clustering analysis of cell line and primary cell proteomics; Table S1: OVCA9-5 metabolomic data; Table S2: CaOV3 metabolomic data; Table S3: Full list of proteins identified; Table S4: List of proteins related to GOBP terms; Table S5: List of metabolites and proteins related to KEGG global metabolomic network terms; Table S6: List of metabolites related to SMPDBT terms.

**Author Contributions:** Conceptualisation, M.K.-H., P.H., M.K.O. and C.R.; methodology, M.A., N.A.L., C.Y., M.C., C.D., T.M.N. and W.W.; cell work, M.A., N.A.L., T.M.N. and W.W.; mass spectrometry analysis, M.A., C.Y., M.C. and C.D.; writing—original draft preparation, M.A.; writing—review and editing, all authors; supervision, M.K.-H., P.H., M.K.O., C.R. and D.A.; project administration, M.K.-H., P.H., M.K.O., C.R. and D.J.C. All authors have read and agreed to the published version of the manuscript.

**Funding:** P.H. gratefully acknowledges the support of the National Collaborative Research Infrastructure Strategy (NCRIS) node for Tissue Imaging Mass Spectrometry.

**Institutional Review Board Statement:** The study was conducted according to the guidelines of the Declaration of Helsinki and approved by the Human Research Ethics Committee of Central Adelaide Local Health Network (CALHN). (HREC/18/CALHN/811, approved 14/02/2019).

**Informed Consent Statement:** Informed consent was obtained from all subjects involved in the study.

**Data Availability Statement:** The data presented in this study are available in this article, referenced online data depositories and Supplementary Materials.

**Conflicts of Interest:** The authors declare no conflict of interest.

## References

1. Siegel, R.L.; Miller, K.D.; Jemal, A. Cancer statistics, 2020. *CA Cancer J. Clin.* **2020**, *70*, 7–30. [\[CrossRef\]](#) [\[PubMed\]](#)
2. Koukoura, O.; Spandidos, D.A.; Daponte, A.; Sifakis, S. DNA methylation profiles in ovarian cancer: Implication in diagnosis and therapy. *Mol. Med. Rep.* **2014**, *10*, 3–9. [\[CrossRef\]](#) [\[PubMed\]](#)
3. Vaughan, S.; Coward, J.I.; Bast, R.C., Jr.; Berchuck, A.; Berek, J.S.; Brenton, J.D.; Coukos, G.; Crum, C.C.; Drapkin, R.; Etemadmoghadam, D.; et al. Rethinking ovarian cancer: Recommendations for improving outcomes. *Nat. Rev. Cancer* **2011**, *11*, 719–725. [\[CrossRef\]](#) [\[PubMed\]](#)
4. Karam, A.; Ledermann, J.; Kim, J.-W.; Sehouli, J.; Lu, K.; Gourley, C.; Katsumata, N.; Burger, R.; Nam, B.-H.; Bacon, M. Fifth ovarian Cancer consensus conference of the gynecologic Cancer InterGroup: First-line interventions. *Ann. Oncol.* **2017**, *28*, 711–717. [\[CrossRef\]](#)
5. Assis, J.; Pereira, C.; Nogueira, A.; Pereira, D.; Carreira, R.; Medeiros, R. Genetic variants as ovarian cancer first-line treatment hallmarks: A systematic review and meta-analysis. *Cancer Treat. Rev.* **2017**, *61*, 35–52. [\[CrossRef\]](#)
6. Bowtell, D.D.; Bohm, S.; Ahmed, A.A.; Aspuria, P.J.; Bast, R.C., Jr.; Beral, V.; Berek, J.S.; Birrer, M.J.; Blagden, S.; Bookman, M.A.; et al. Rethinking ovarian cancer II: Reducing mortality from high-grade serous ovarian cancer. *Nat. Rev. Cancer* **2015**, *15*, 668–679. [\[CrossRef\]](#)
7. Kroeger, P.T., Jr.; Drapkin, R. Pathogenesis and heterogeneity of ovarian cancer. *Curr. Opin. Obstet. Gynecol.* **2017**, *29*, 26–34. [\[CrossRef\]](#)
8. Anglesio, M.S.; Wiegand, K.C.; Melnyk, N.; Chow, C.; Salamanca, C.; Prentice, L.M.; Senz, J.; Yang, W.; Spillman, M.A.; Cochrane, D.R.; et al. Type-specific cell line models for type-specific ovarian cancer research. *PLoS ONE* **2013**, *8*, e72162. [\[CrossRef\]](#)
9. Lee, J.M.; Minasian, L.; Kohn, E.C. New strategies in ovarian cancer treatment. *Cancer* **2019**, *125* (Suppl. S24), 4623–4629. [\[CrossRef\]](#)
10. National Comprehensive Cancer Network. *Ovarian Cancer: NCCN Guideline for Patients*; National Comprehensive Cancer Network: Washington, DC, USA, 2021.
11. Yuan, L.; Yu, W.-M.; Qu, C.-K. DNA damage-induced G2/M checkpoint in SV40 large T antigen-immortalized embryonic fibroblast cells requires SHP-2 tyrosine phosphatase. *J. Biol. Chem.* **2003**, *278*, 42812–42820. [\[CrossRef\]](#)
12. Dasari, S.; Tchounwou, P.B. Cisplatin in cancer therapy: Molecular mechanisms of action. *Eur. J. Pharmacol.* **2014**, *740*, 364–378. [\[CrossRef\]](#) [\[PubMed\]](#)
13. Ozben, T. Oxidative stress and apoptosis: Impact on cancer therapy. *J. Pharm. Sci.* **2007**, *96*, 2181–2196. [\[CrossRef\]](#) [\[PubMed\]](#)
14. Joybari, A.Y.; Sarbaz, S.; Azadeh, P.; Mirafsharieh, S.A.; Rahbari, A.; Farasatinasab, M.; Mokhtari, M. Oxaliplatin-induced renal tubular vacuolization. *Ann. Pharmacother.* **2014**, *48*, 796–800. [\[CrossRef\]](#)
15. Hosnedlova, B.; Kepinska, M.; Skalickova, S.; Fernandez, C.; Ruttkay-Nedecky, B.; Peng, Q.; Baron, M.; Melcova, M.; Opatrilova, R.; Zidkova, J.; et al. Nano-selenium and its nanomedicine applications: A critical review. *Int. J. Nanomed.* **2018**, *13*, 2107–2128. [\[CrossRef\]](#) [\[PubMed\]](#)
16. Boulikas, T.; Stathopoulos, G.P.; Volakakis, N.; Vougiouka, M. Systemic Lipoplatin infusion results in preferential tumor uptake in human studies. *Anticancer Res.* **2005**, *25*, 3031–3039. [\[PubMed\]](#)
17. Trzaska, S. Cisplatin. *Chem. Eng. News* **2005**, *83*, 52. [\[CrossRef\]](#)
18. Karasawa, T.; Steyger, P.S. An integrated view of cisplatin-induced nephrotoxicity and ototoxicity. *Toxicol. Lett.* **2015**, *237*, 219–227. [\[CrossRef\]](#)
19. The Medical Letter. Drugs of Choice for Cancer. In *Treatment Guidelines from the Medical Letter*; The Medical Letter: New Rochelle, NY, USA, 2003; Volume 1, pp. 41–52.
20. Freimund, A.E.; Beach, J.A.; Christie, E.L.; Bowtell, D.D.L. Mechanisms of Drug Resistance in High-Grade Serous Ovarian Cancer. *Hematol./Oncol. Clin. N. Am.* **2018**, *32*, 983–996. [\[CrossRef\]](#)
21. Dilruba, S.; Kalayda, G.V. Platinum-based drugs: Past, present and future. *Cancer Chemother. Pharmacol.* **2016**, *77*, 1103–1124. [\[CrossRef\]](#)
22. Warburg, O. The metabolism of carcinoma cells. *J. Cancer Res.* **1925**, *9*, 148–163. [\[CrossRef\]](#)
23. Vander Heiden, M.G.; DeBerardinis, R.J. Understanding the Intersections between Metabolism and Cancer Biology. *Cell* **2017**, *168*, 657–669. [\[CrossRef\]](#) [\[PubMed\]](#)

24. Taniguchi, K.; Sakai, M.; Sugito, N.; Kuranaga, Y.; Kumazaki, M.; Shinohara, H.; Ueda, H.; Futamura, M.; Yoshida, K.; Uchiyama, K.; et al. PKM1 is involved in resistance to anti-cancer drugs. *Biochem. Biophys. Res. Commun.* **2016**, *473*, 174–180. [[CrossRef](#)] [[PubMed](#)]
25. Roh, J.L.; Park, J.Y.; Kim, E.H.; Jang, H.J.; Kwon, M. Activation of mitochondrial oxidation by PDK2 inhibition reverses cisplatin resistance in head and neck cancer. *Cancer Lett.* **2016**, *371*, 20–29. [[CrossRef](#)] [[PubMed](#)]
26. Blayney, J.K.; Davison, T.; McCabe, N.; Walker, S.; Keating, K.; Delaney, T.; Greenan, C.; Williams, A.R.; McCluggage, W.G.; Capes-Davis, A.; et al. Prior knowledge transfer across transcriptional data sets and technologies using compositional statistics yields new mislabelled ovarian cell line. *Nucleic Acids Res.* **2016**, *44*, e137. [[CrossRef](#)]
27. Weiland, F.; Arentz, G.; Klingler-Hoffmann, M.; McCarthy, P.; Lokman, N.A.; Kaur, G.; Oehler, M.K.; Hoffmann, P. Novel IEF Peptide Fractionation Method Reveals a Detailed Profile of N-Terminal Acetylation in Chemotherapy-Responsive and -Resistant Ovarian Cancer Cells. *J. Proteome Res.* **2016**, *15*, 4073–4081. [[CrossRef](#)]
28. Wang, W.; Lokman, N.A.; Noye, T.M.; Macpherson, A.M.; Oehler, M.K.; Ricciardelli, C. ABCA1 is associated with the development of acquired chemotherapy resistance and predicts poor ovarian cancer outcome. *Cancer Drug Resist.* **2021**, *4*, 485–502. [[CrossRef](#)]
29. Ricciardelli, C.; Lokman, N.A.; Cheruvu, S.; Tan, I.A.; Ween, M.P.; Pyragius, C.E.; Ruskiewicz, A.; Hoffmann, P.; Oehler, M.K. Transketolase is upregulated in metastatic peritoneal implants and promotes ovarian cancer cell proliferation. *Clin. Exp. Metastasis* **2015**, *32*, 441–455. [[CrossRef](#)]
30. Lokman, N.A.; Elder, A.S.; Ricciardelli, C.; Oehler, M.K. Chick chorioallantoic membrane (CAM) assay as an in vivo model to study the effect of newly identified molecules on ovarian cancer invasion and metastasis. *Int. J. Mol. Sci.* **2012**, *13*, 9959–9970. [[CrossRef](#)]
31. Sud, M.; Fahy, E.; Cotter, D.; Azam, K.; Vadivelu, I.; Burant, C.; Edison, A.; Fiehn, O.; Higashi, R.; Nair, K.S.; et al. Metabolomics Workbench: An international repository for metabolomics data and metadata, metabolite standards, protocols, tutorials and training, and analysis tools. *Nucleic Acids Res.* **2016**, *44*, D463–D470. [[CrossRef](#)]
32. Kim, S.J.; Rosen, B.; Fan, I.; Ivanova, A.; McLaughlin, J.R.; Risch, H.; Narod, S.A.; Kotsopoulos, J. Epidemiologic factors that predict long-term survival following a diagnosis of epithelial ovarian cancer. *Br. J. Cancer* **2017**, *116*, 964–971. [[CrossRef](#)]
33. Creek, D.J.; Jankevics, A.; Burgess, K.E.; Breitling, R.; Barrett, M.P. IDEOM: An Excel interface for analysis of LC-MS-based metabolomics data. *Bioinformatics* **2012**, *28*, 1048–1049. [[CrossRef](#)] [[PubMed](#)]
34. Pang, Z.; Chong, J.; Zhou, G.; de Lima Morais, D.A.; Chang, L.; Barrette, M.; Gauthier, C.; Jacques, P.; Li, S.; Xia, J. MetaboAnalyst 5.0: Narrowing the gap between raw spectra and functional insights. *Nucleic Acids Res.* **2021**, *49*, W388–W396. [[CrossRef](#)] [[PubMed](#)]
35. Metaboanalyst. Available online: <https://www.metaboanalyst.ca/> (accessed on 1 October 2021).
36. Wiśniewski, J.R.; Gaugaz, F.Z. Fast and sensitive total protein and Peptide assays for proteomic analysis. *Anal. Chem.* **2015**, *87*, 4110–4116. [[CrossRef](#)] [[PubMed](#)]
37. Perez-Riverol, Y.; Bai, J.; Bandla, C.; Hewapathirana, S.; García-Seisdedos, D.; Kamatchinathan, S.; Kundu, D.; Prakash, A.; Frericks-Zipper, A.; Eisenacher, M.; et al. The PRIDE database resources in 2022: A Hub for mass spectrometry-based proteomics evidences. *Nucleic Acids Res.* **2022**, *50*, D543–D552. [[CrossRef](#)] [[PubMed](#)]
38. DAVID. Available online: <https://david.ncifcrf.gov/> (accessed on 1 June 2021).
39. Kaplan Meier Plotter. Available online: <http://kmplot.com/analysis/index.php?qp=service&cancer=ovar#> (accessed on 10 August 2021).
40. Györfy, B.; Lánckzy, A.; Szállási, Z. Implementing an online tool for genome-wide validation of survival-associated biomarkers in ovarian-cancer using microarray data from 1287 patients. *Endocr. Relat. Cancer* **2012**, *19*, 197–208. [[CrossRef](#)]
41. Saorin, A.; Di Gregorio, E.; Miolo, G.; Steffan, A.; Corona, G. Emerging Role of Metabolomics in Ovarian Cancer Diagnosis. *Metabolites* **2020**, *10*, 419. [[CrossRef](#)]
42. Poisson, L.M.; Munkarah, A.; Madi, H.; Datta, I.; Hensley-Alford, S.; Tebbe, C.; Buekers, T.; Giri, S.; Rattan, R. A metabolomic approach to identifying platinum resistance in ovarian cancer. *J. Ovarian Res.* **2015**, *8*, 13. [[CrossRef](#)]
43. Elzek, M.A.; Rodland, K.D. Proteomics of ovarian cancer: Functional insights and clinical applications. *Cancer Metastasis Rev.* **2015**, *34*, 83–96. [[CrossRef](#)]
44. Fan, G.; Wrzeszczynski, K.O.; Fu, C.; Su, G.; Pappin, D.J.; Lucito, R.; Tonks, N.K. A quantitative proteomics-based signature of platinum sensitivity in ovarian cancer cell lines. *Biochem. J.* **2015**, *465*, 433–442. [[CrossRef](#)]
45. Stewart, J.J.; White, J.T.; Yan, X.; Collins, S.; Drescher, C.W.; Urban, N.D.; Hood, L.; Lin, B. Proteins associated with Cisplatin resistance in ovarian cancer cells identified by quantitative proteomic technology and integrated with mRNA expression levels. *Mol. Cell. Proteom.* **2006**, *5*, 433–443. [[CrossRef](#)]
46. Pan, S.; Cheng, L.; White, J.T.; Lu, W.; Utleg, A.G.; Yan, X.; Urban, N.D.; Drescher, C.W.; Hood, L.; Lin, B. Quantitative proteomics analysis integrated with microarray data reveals that extracellular matrix proteins, catenins, and p53 binding protein 1 are important for chemotherapy response in ovarian cancers. *Omics J. Integr. Biol.* **2009**, *13*, 345–354. [[CrossRef](#)] [[PubMed](#)]
47. Yan, X.D.; Pan, L.Y.; Yuan, Y.; Lang, J.H.; Mao, N. Identification of platinum-resistance associated proteins through proteomic analysis of human ovarian cancer cells and their platinum-resistant sublines. *J. Proteome Res.* **2007**, *6*, 772–780. [[CrossRef](#)] [[PubMed](#)]
48. Dai, Z.; Yin, J.; He, H.; Li, W.; Hou, C.; Qian, X.; Mao, N.; Pan, L. Mitochondrial comparative proteomics of human ovarian cancer cells and their platinum-resistant sublines. *Proteomics* **2010**, *10*, 3789–3799. [[CrossRef](#)]

49. Gong, F.; Peng, X.; Zeng, Z.; Yu, M.; Zhao, Y.; Tong, A. Proteomic analysis of cisplatin resistance in human ovarian cancer using 2-DE method. *Mol. Cell. Biochem.* **2011**, *348*, 141–147. [[CrossRef](#)] [[PubMed](#)]
50. Cruz, I.N.; Coley, H.M.; Kramer, H.B.; Madhuri, T.K.; Safuwani, N.A.; Angelino, A.R.; Yang, M. Proteomics analysis of ovarian cancer cell lines and tissues reveals drug resistance-associated proteins. *Cancer Genom.-Proteom.* **2017**, *14*, 35–51. [[CrossRef](#)] [[PubMed](#)]
51. Chappell, N.P.; Teng, P.N.; Hood, B.L.; Wang, G.; Darcy, K.M.; Hamilton, C.A.; Maxwell, G.L.; Conrads, T.P. Mitochondrial proteomic analysis of cisplatin resistance in ovarian cancer. *J. Proteome Res.* **2012**, *11*, 4605–4614. [[CrossRef](#)]
52. Swiatly, A.; Plewa, S.; Matysiak, J.; Kokot, Z.J. Mass spectrometry-based proteomics techniques and their application in ovarian cancer research. *J. Ovarian Res.* **2018**, *11*, 88. [[CrossRef](#)]
53. D’Alterio, C.; Scala, S.; Sozzi, G.; Roz, L.; Bertolini, G. Paradoxical effects of chemotherapy on tumor relapse and metastasis promotion. *Semin. Cancer Biol.* **2020**, *60*, 351–361. [[CrossRef](#)]
54. Chen, N.; Karantza, V. Autophagy as a therapeutic target in cancer. *Cancer Biol. Ther.* **2011**, *11*, 157–168. [[CrossRef](#)]
55. Adeva-Andany, M.; López-Ojén, M.; Funcasta-Calderón, R.; Ameneiros-Rodríguez, E.; Donapetry-García, C.; Vila-Altesor, M.; Rodríguez-Seijas, J. Comprehensive review on lactate metabolism in human health. *Mitochondrion* **2014**, *17*, 76–100. [[CrossRef](#)]
56. Da Graça Lütz, M.; Feksa, L.R.; de Souza Wyse, A.T.; Dutra-Filho, C.S.; Wajner, M.; Wannmacher, C.M.D. Alanine prevents the in vitro inhibition of glycolysis caused by phenylalanine in brain cortex of rats. *Metab. Brain Dis.* **2003**, *18*, 87–94. [[CrossRef](#)] [[PubMed](#)]
57. Perriello, G.; Jorde, R.; Nurjhan, N.; Stumvoll, M.; Dailey, G.; Jenssen, T.; Bier, D.; Gerich, J.E. Estimation of glucose-alanine-lactate-glutamine cycles in postabsorptive humans: Role of skeletal muscle. *Am. J. Physiol.-Endocrinol. Metab.* **1995**, *269*, E443–E450. [[CrossRef](#)] [[PubMed](#)]
58. Zitvogel, L.; Kepp, O.; Kroemer, G. Immune parameters affecting the efficacy of chemotherapeutic regimens. *Nat. Rev. Clin. Oncol.* **2011**, *8*, 151–160. [[CrossRef](#)] [[PubMed](#)]
59. Ghaffari, A.; Peterson, N.; Khalaj, K.; Vitkin, N.; Robinson, A.; Francis, J.A.; Koti, M. STING agonist therapy in combination with PD-1 immune checkpoint blockade enhances response to carboplatin chemotherapy in high-grade serous ovarian cancer. *Br. J. Cancer* **2018**, *119*, 440–449. [[CrossRef](#)] [[PubMed](#)]
60. Sistigu, A.; Yamazaki, T.; Vacchelli, E.; Chaba, K.; Enot, D.P.; Adam, J.; Vitale, I.; Goubar, A.; Baracco, E.E.; Remédios, C.; et al. Cancer cell-autonomous contribution of type I interferon signaling to the efficacy of chemotherapy. *Nat. Med.* **2014**, *20*, 1301–1309. [[CrossRef](#)]
61. Alberts, D.S.; Marth, C.; Alvarez, R.D.; Johnson, G.; Bidzinski, M.; Kardatzke, D.R.; Bradford, W.Z.; Loutit, J.; Kirn, D.H.; Clouser, M.C.; et al. Randomized phase 3 trial of interferon gamma-1b plus standard carboplatin/paclitaxel versus carboplatin/paclitaxel alone for first-line treatment of advanced ovarian and primary peritoneal carcinomas: Results from a prospectively designed analysis of progression-free survival. *Gynecol. Oncol.* **2008**, *109*, 174–181. [[CrossRef](#)]
62. Wang, W.; Liu, J.R.; Zou, W. Immunotherapy in Ovarian Cancer. *Surg. Oncol. Clin. N. Am.* **2019**, *28*, 447–464. [[CrossRef](#)]
63. Basler, M.; Kirk, C.J.; Groettrup, M. The immunoproteasome in antigen processing and other immunological functions. *Curr. Opin. Immunol.* **2013**, *25*, 74–80. [[CrossRef](#)]
64. Matsunaga, T.; Tsuchimura, S.; Azuma, N.; Endo, S.; Ichihara, K.; Ikari, A. Caffeic acid phenethyl ester potentiates gastric cancer cell sensitivity to doxorubicin and cisplatin by decreasing proteasome function. *Anticancer. Drugs* **2019**, *30*, 251–259. [[CrossRef](#)]
65. George, P.M.; Badiger, R.; Alazawi, W.; Foster, G.R.; Mitchell, J.A. Pharmacology and therapeutic potential of interferons. *Pharmacol. Ther.* **2012**, *135*, 44–53. [[CrossRef](#)]
66. Furusawa, A.; Miyamoto, M.; Takano, M.; Tsuda, H.; Song, Y.S.; Aoki, D.; Miyasaka, N.; Inazawa, J.; Inoue, J. Ovarian cancer therapeutic potential of glutamine depletion based on GS expression. *Carcinogenesis* **2018**, *39*, 758–766. [[CrossRef](#)]
67. Richards, N.G.; Kilberg, M.S. Asparagine synthetase chemotherapy. *Annu. Rev. Biochem.* **2006**, *75*, 629–654. [[CrossRef](#)] [[PubMed](#)]
68. Spinelli, J.B.; Yoon, H.; Ringel, A.E.; Jeanfavre, S.; Clish, C.B.; Haigis, M.C. Metabolic recycling of ammonia via glutamate dehydrogenase supports breast cancer biomass. *Science* **2017**, *358*, 941–946. [[CrossRef](#)] [[PubMed](#)]
69. Altman, B.J.; Stine, Z.E.; Dang, C.V. From Krebs to clinic: Glutamine metabolism to cancer therapy. *Nat. Rev. Cancer* **2016**, *16*, 749. [[CrossRef](#)] [[PubMed](#)]
70. Wallimann, T.; Tokarska-Schlattner, M.; Schlattner, U. The creatine kinase system and pleiotropic effects of creatine. *Amino Acids* **2011**, *40*, 1271–1296. [[CrossRef](#)]
71. Kemp, G.J.; Meyerspeer, M.; Moser, E. Absolute quantification of phosphorus metabolite concentrations in human muscle in vivo by 31P MRS: A quantitative review. *NMR Biomed.* **2007**, *20*, 555–565. [[CrossRef](#)]
72. Pederson, T. Historical review: An energy reservoir for mitosis, and its productive wake. *Trends Biochem. Sci.* **2003**, *28*, 125–129. [[CrossRef](#)]
73. Yan, Y.B. Creatine kinase in cell cycle regulation and cancer. *Amino Acids* **2016**, *48*, 1775–1784. [[CrossRef](#)]
74. Keshet, R.; Szlosarek, P.; Carracedo, A.; Erez, A. Rewiring urea cycle metabolism in cancer to support anabolism. *Nat. Rev. Cancer* **2018**, *18*, 634–645. [[CrossRef](#)]
75. Erez, A. Argininosuccinic aciduria: From a monogenic to a complex disorder. *Genet. Med. Off. J. Am. Coll. Med. Genet.* **2013**, *15*, 251–257. [[CrossRef](#)]



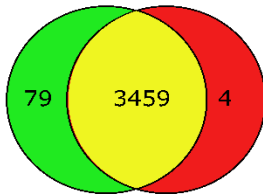
76. Shen, A.; Chen, Y.; Liu, L.; Huang, Y.; Chen, H.; Qi, F.; Lin, J.; Shen, Z.; Wu, X.; Wu, M.; et al. EBF1-Mediated Upregulation of Ribosome Assembly Factor PNO1 Contributes to Cancer Progression by Negatively Regulating the p53 Signaling Pathway. *Cancer Res.* **2019**, *79*, 2257–2270. [[CrossRef](#)] [[PubMed](#)]
77. Liu, D.; Lin, L.; Wang, Y.; Chen, L.; He, Y.; Luo, Y.; Qi, L.; Guo, Y.; Chen, L.; Han, Z.; et al. PNO1, which is negatively regulated by miR-340-5p, promotes lung adenocarcinoma progression through Notch signaling pathway. *Oncogenesis* **2020**, *9*, 58. [[CrossRef](#)] [[PubMed](#)]
78. Wang, X.; Meng, Q.; Qiao, W.; Ma, R.; Ju, W.; Hu, J.; Lu, H.; Cui, J.; Jin, Z.; Zhao, Y.; et al. miR-181b/Notch2 overcome chemoresistance by regulating cancer stem cell-like properties in NSCLC. *Stem Cell Res. Ther.* **2018**, *9*, 327. [[CrossRef](#)] [[PubMed](#)]
79. Brand, F.; Schumacher, S.; Kant, S.; Menon, M.B.; Simon, R.; Turgeon, B.; Britsch, S.; Meloche, S.; Gaestel, M.; Kotlyarov, A. The extracellular signal-regulated kinase 3 (mitogen-activated protein kinase 6 [MAPK6])-MAPK-activated protein kinase 5 signaling complex regulates septin function and dendrite morphology. *Mol. Cell. Biol.* **2012**, *32*, 2467–2478. [[CrossRef](#)]
80. Long, W.; Foulds, C.E.; Qin, J.; Liu, J.; Ding, C.; Lonard, D.M.; Solis, L.M.; Wistuba, I.I.; Qin, J.; Tsai, S.Y.; et al. ERK3 signals through SRC-3 coactivator to promote human lung cancer cell invasion. *J. Clin. Investig.* **2012**, *122*, 1869–1880. [[CrossRef](#)]
81. Hu, C.; Huang, S.; Wu, F.; Ding, H. miR-98 inhibits cell proliferation and induces cell apoptosis by targeting MAPK6 in HUVECs. *Exp. Ther. Med.* **2018**, *15*, 2755–2760. [[CrossRef](#)]
82. Bian, K.; Muppani, N.R.; Elkhadragey, L.; Wang, W.; Zhang, C.; Chen, T.; Jung, S.; Seternes, O.M.; Long, W. ERK3 regulates TDP2-mediated DNA damage response and chemoresistance in lung cancer cells. *Oncotarget* **2016**, *7*, 6665–6675. [[CrossRef](#)]
83. Ishida, S.; Lee, J.; Thiele, D.J.; Herskowitz, I. Uptake of the anticancer drug cisplatin mediated by the copper transporter Ctr1 in yeast and mammals. *Proc. Natl. Acad. Sci. USA* **2002**, *99*, 14298–14302. [[CrossRef](#)]
84. Kuo, M.T.; Chen, H.H.; Song, I.S.; Savaraj, N.; Ishikawa, T. The roles of copper transporters in cisplatin resistance. *Cancer Metastasis Rev.* **2007**, *26*, 71–83. [[CrossRef](#)]
85. Howell, S.B.; Safaei, R.; Larson, C.A.; Sailor, M.J. Copper transporters and the cellular pharmacology of the platinum-containing cancer drugs. *Mol. Pharmacol.* **2010**, *77*, 887–894. [[CrossRef](#)]
86. Ishida, S.; McCormick, F.; Smith-McCune, K.; Hanahan, D. Enhancing tumor-specific uptake of the anticancer drug cisplatin with a copper chelator. *Cancer Cell.* **2010**, *17*, 574–583. [[CrossRef](#)] [[PubMed](#)]
87. Chen, H.H.; Yan, J.J.; Chen, W.C.; Kuo, M.T.; Lai, Y.H.; Lai, W.W.; Liu, H.S.; Su, W.C. Predictive and prognostic value of human copper transporter 1 (hCtr1) in patients with stage III non-small-cell lung cancer receiving first-line platinum-based doublet chemotherapy. *Lung Cancer* **2012**, *75*, 228–234. [[CrossRef](#)] [[PubMed](#)]
88. Huang, Y.-F.; Kuo, M.T.; Liu, Y.-S.; Cheng, Y.-M.; Wu, P.-Y.; Chou, C.-Y. A dose escalation study of trientine plus carboplatin and pegylated liposomal doxorubicin in women with a first relapse of epithelial ovarian, tubal, and peritoneal cancer within 12 months after platinum-based chemotherapy. *Front. Oncol.* **2019**, *9*, 437. [[CrossRef](#)] [[PubMed](#)]
89. Fu, S.; Hou, M.-M.; Wheler, J.; Hong, D.; Naing, A.; Tsimberidou, A.; Janku, F.; Zinner, R.; Piha-Paul, S.; Falchook, G. Exploratory study of carboplatin plus the copper-lowering agent trientine in patients with advanced malignancies. *Investig. New Drugs* **2014**, *32*, 465–472. [[CrossRef](#)]
90. Fu, S.; Naing, A.; Fu, C.; Kuo, M.T.; Kurzrock, R. Overcoming platinum resistance through the use of a copper-lowering agent. *Mol. Cancer Ther.* **2012**, *11*, 1221–1225. [[CrossRef](#)] [[PubMed](#)]
91. Chiu, M.; Taurino, G.; Bianchi, M.G.; Kilberg, M.S.; Bussolati, O. Asparagine Synthetase in Cancer: Beyond Acute Lymphoblastic Leukemia. *Front. Oncol.* **2019**, *9*, 1480. [[CrossRef](#)]
92. Ye, J.; Kumanova, M.; Hart, L.S.; Sloane, K.; Zhang, H.; De Panis, D.N.; Bobrovnikova-Marjon, E.; Diehl, J.A.; Ron, D.; Koumenis, C. The GCN2-ATF4 pathway is critical for tumour cell survival and proliferation in response to nutrient deprivation. *EMBO J.* **2010**, *29*, 2082–2096. [[CrossRef](#)]
93. Liu, R.Y.; Dong, Z.; Liu, J.; Zhou, L.; Huang, W.; Khoo, S.K.; Zhang, Z.; Petillo, D.; Teh, B.T.; Qian, C.N.; et al. Overexpression of asparagine synthetase and matrix metalloproteinase 19 confers cisplatin sensitivity in nasopharyngeal carcinoma cells. *Mol. Cancer Ther.* **2013**, *12*, 2157–2166. [[CrossRef](#)]
94. Cui, H.; Darmanin, S.; Natsuisaka, M.; Kondo, T.; Asaka, M.; Shindoh, M.; Higashino, F.; Hamuro, J.; Okada, F.; Kobayashi, M.; et al. Enhanced expression of asparagine synthetase under glucose-deprived conditions protects pancreatic cancer cells from apoptosis induced by glucose deprivation and cisplatin. *Cancer Res.* **2007**, *67*, 3345–3355. [[CrossRef](#)]
95. Pieters, R.; Hunger, S.P.; Boos, J.; Rizzari, C.; Silverman, L.; Baruchel, A.; Goekbuget, N.; Schrappe, M.; Pui, C.H. L-asparaginase treatment in acute lymphoblastic leukemia: A focus on Erwinia asparaginase. *Cancer* **2011**, *117*, 238–249. [[CrossRef](#)]
96. Ahmed, N.; Greening, D.; Samardzija, C.; Escalona, R.M.; Chen, M.; Findlay, J.K.; Kannourakis, G. Unique proteome signature of post-chemotherapy ovarian cancer ascites-derived tumor cells. *Sci. Rep.* **2016**, *6*, 30061. [[CrossRef](#)] [[PubMed](#)]
97. Doll, S.; Gnad, F.; Mann, M. The Case for Proteomics and Phospho-Proteomics in Personalized Cancer Medicine. *Proteom. Clin. Appl.* **2019**, *13*, e1800113. [[CrossRef](#)] [[PubMed](#)]
98. Shrestha, R.; Llauro Fernandez, M.; Dawson, A.; Hoenisch, J.; Volik, S.; Lin, Y.Y.; Anderson, S.; Kim, H.; Haegert, A.M.; Colborne, S.; et al. Multiomics Characterization of Low-Grade Serous Ovarian Carcinoma Identifies Potential Biomarkers of MEK Inhibitor Sensitivity and Therapeutic Vulnerability. *Cancer Res.* **2021**, *81*, 1681–1694. [[CrossRef](#)] [[PubMed](#)]

1 4.3. Supplementary Files

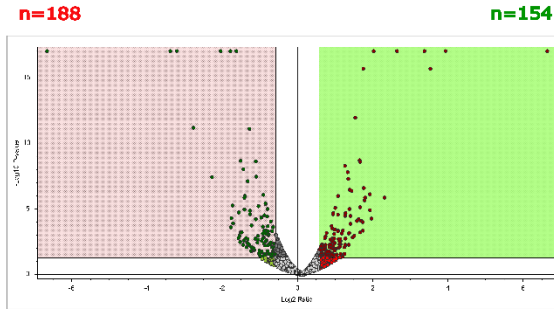
A.

Patient	Age at diagnosis	Stage at diagnosis	Diagnosis	Chemo resistant Status
P1	61	3c	Serous carcinoma of the ovary	Sensitive
P2	43	?	Recurrent chemotherapy resistant ovarian carcinoma	Resistant

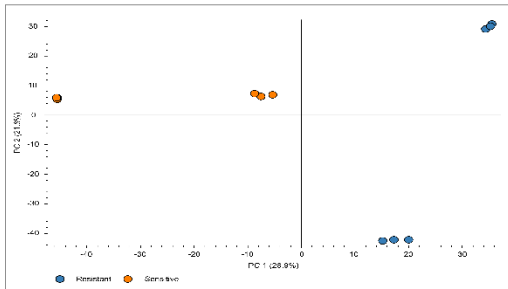
B.



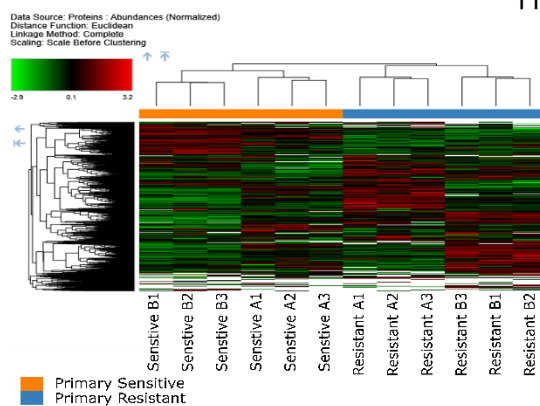
C.



D.



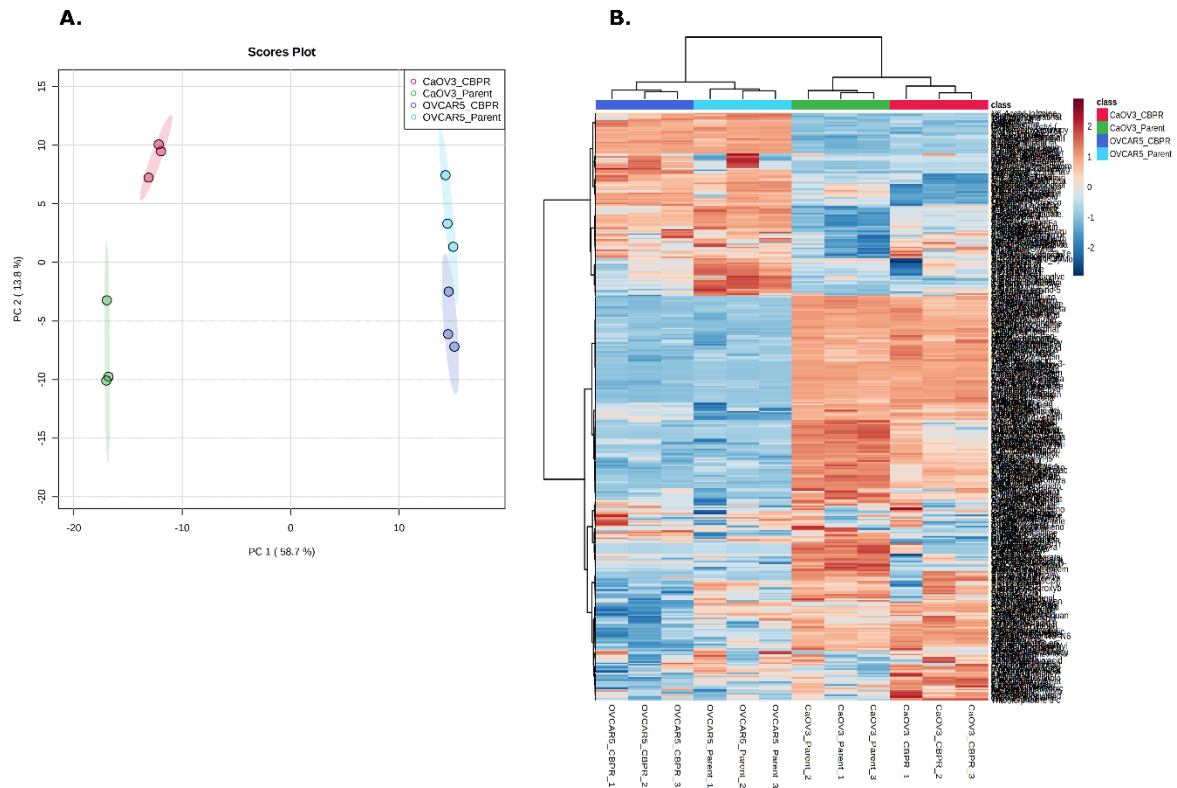
E.



F.

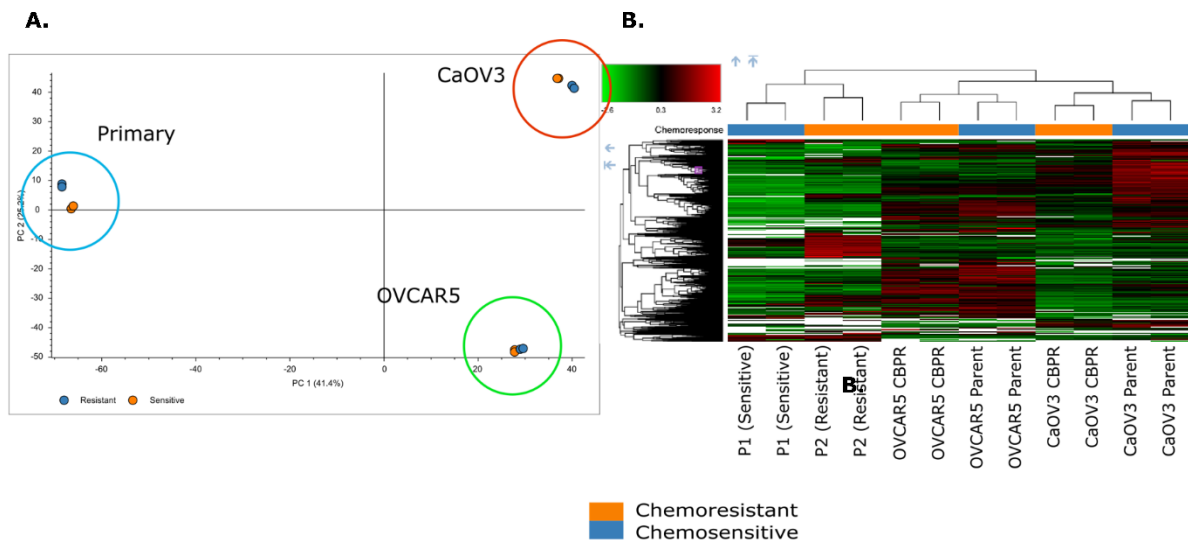
Rank	Term	Count	Involved genes/total genes (%)	P-value
1	type I interferon signaling pathway	10	3.1	7.40E-06
2	mitochondrial translation	12	12	1.10E-05
3	oxidation-reduction process	38	38	2.10E-05
4	response to oxidative stress	21	21	3.60E-05
5	cellular component disassembly	23	23	1.30E-04
6	Generation of precursor metabolites and energy	19	5.8	7.60E-02
7	carboxylic acid metabolic process	31	9.5	7.60E-02
8	protein complex subunit organization	51	15.7	7.60E-02
9	single-organism catabolic process	31	9.5	7.60E-02
10	NAD metabolic process	7	2.2	1.60E-01

25  
**Supplementary Figure 1:** Proteomics investigation of primary ovarian cancer samples taken from chemosensitive (n=1) and chemoresistant (n=1). A) Table of patient details for P1 (chemosensitive) and P2 (chemoresistant) primary cell samples. B) Venn diagram of proteins identified in primary samples showing 3459 proteins identified in common between primary samples (P1 total=3538, P1 exclusive=79, P2 total=3463, P2 exclusive=4, total proteins identified=3542). C) Volcano plot of abundance ratios (resistant/sensitive) using a 1.5-fold cut off (0.58 log<sub>2</sub>, p<0.05) shows 188 proteins more abundant in P2 (resistant) and 154 proteins more abundant in P1 (sensitive). D) Principle component analysis shows clear separation of primary cells based on their origin. E) Heirarchical clustering shows clear separation of primary cells based on their cell origin. F) Table of the top 10 gene ontology biological functions related to 1.5 fold differentially abundant proteins between P1 and P2. Analysis performed via the DAVID functional gene annotation platform and duplicate categories and sub categories removed.



**Supplementary Figure 2:** PCA and hierarchical clustering of all metabolites across both OVCAR-5 and CaOV3 Parental and CBPR cell lines. A) PCA scores plot shows separation based on chemoresistant status within cell lines but significantly larger separation between cell lines. B) Hierarchical clustering of all metabolites across all cell lines shows clear separation based on chemoresistant status within cell lines. Shows a larger separation between different cell lines regardless of chemoresistance status.

- 1
- 2
- 3



**Supplementary Figure 3:** PCA and hierarchical clustering of all proteins across Parental and CBPR cell lines and chemoresensitive and chemoresistant primary cells. A) PCA plot shows clear separation of proteomic features based on sample origin. B) Hierarchical clustering of all proteomes shows clear clustering of each sample type. Further clustering is observed based on cell origin.

1  
2

**Supplementary Table 1:** Full metabolomics data for OVCAR-5 Parental and CBPR Cell Line Analysis

This table can be found online – ([https://www.mdpi.com/2072-6694/14/11/2763?utm\\_campaign=releaseissue\\_cancersutm\\_medium=emailutm\\_source=releaseissueutm\\_term=doilink61](https://www.mdpi.com/2072-6694/14/11/2763?utm_campaign=releaseissue_cancersutm_medium=emailutm_source=releaseissueutm_term=doilink61))

**Supplementary Table 2:** Full metabolomics data for CaOV3 Parental and CBPR Cell Line Analysis

This table can be found online – ([https://www.mdpi.com/2072-6694/14/11/2763?utm\\_campaign=releaseissue\\_cancersutm\\_medium=emailutm\\_source=releaseissueutm\\_term=doilink61](https://www.mdpi.com/2072-6694/14/11/2763?utm_campaign=releaseissue_cancersutm_medium=emailutm_source=releaseissueutm_term=doilink61))

**Supplementary Table 3:** Full list of proteins identified for Parental vs CBPR Cell Lines and Sensitive vs Resistant Primary Cells.

This table can be found online – ([https://www.mdpi.com/2072-6694/14/11/2763?utm\\_campaign=releaseissue\\_cancersutm\\_medium=emailutm\\_source=releaseissueutm\\_term=doilink61](https://www.mdpi.com/2072-6694/14/11/2763?utm_campaign=releaseissue_cancersutm_medium=emailutm_source=releaseissueutm_term=doilink61))

**Supplementary Table 4:** List of Proteins Identified Related to Enriched Gene Ontology – Biological Processes as Identified Through the DAVID Software Tool.

This table can be found online – ([https://www.mdpi.com/2072-6694/14/11/2763?utm\\_campaign=releaseissue\\_cancersutm\\_medium=emailutm\\_source=releaseissueutm\\_term=doilink61](https://www.mdpi.com/2072-6694/14/11/2763?utm_campaign=releaseissue_cancersutm_medium=emailutm_source=releaseissueutm_term=doilink61))

**Supplementary Table 5:** List of Metabolites and Proteins Related to KEGG Global Metabolic Networks

1 This table can be found online – ([https://www.mdpi.com/2072-6694/14/11/2763?utm\\_campaign=releaseissue\\_cancersutm\\_medium=emailutm\\_source=releaseissueutm\\_term=doilink61](https://www.mdpi.com/2072-6694/14/11/2763?utm_campaign=releaseissue_cancersutm_medium=emailutm_source=releaseissueutm_term=doilink61))

4 **Supplementary Table 6:** List of Metabolites Found to be Related to SMPDBT Terms.

5 This table can be found online – ([https://www.mdpi.com/2072-6694/14/11/2763?utm\\_campaign=releaseissue\\_cancersutm\\_medium=emailutm\\_source=releaseissueutm\\_term=doilink61](https://www.mdpi.com/2072-6694/14/11/2763?utm_campaign=releaseissue_cancersutm_medium=emailutm_source=releaseissueutm_term=doilink61))

8  
9  
10  
11  
12  
13  
14  
15  
16  
17  
18  
19  
20  
21  
22  
23  
24  
25  
26  
27  
28  
29  
30

1  
2  
3  
4  
5  
6  
7  
8  
9  
10  
11  
12  
13  
14  
15  
16  
17  
18  
19  
20  
21  
22  
23  
24  
25  
26  
27  
28  
29

This page is intentionally left blank

1  
2  
3  
4  
5  
6  
7  
8  
9  
10  
11  
12  
13  
14  
15  
16  
17  
18  
19  
20  
21  
22  
23  
24  
25  
26

# CHAPTER 5: Mass Spectrometry Analyses of Multicellular Tumour Spheroids

---

## 1 5.1. Summary

2 Standard biological and pharmaceutical analyses of cancer cell lines and cells have traditionally  
3 been performed in two-dimensional cell culture systems. These have the advantage of ease of  
4 use, relative cost effectiveness and the capacity to upscale into high throughput platforms.  
5 However, they come with several shortcomings in how they replicate the *in vivo* situation. This  
6 goes some way to explain the striking discrepancies between the number of anti-cancer drugs  
7 which are seen to be effective in tissue culture and the number which show efficacy in the clinic.  
8 This is particularly evident in ovarian cancer where there have not been significant changes in  
9 the first line chemotherapy treatment over the last 30 years.

10 One way to begin to overcome this is through the development of *in vitro* models which better  
11 replicate the *in vivo* situation. One of these models are multicellular tumour spheroids (MCTS).  
12 These are cellular aggregates form spontaneously, or with the assistance of extracellular matrix,  
13 when cells are prevented from adhering to tissue culture surfaces. While they do not replicate all  
14 features of the *in vivo* situation they go some way to bridge the gap by replicating cell-cell  
15 connections and waste and gas gradients observed in solid tumours. Through this they represent  
16 a middle ground between cell lines (easy to use but not biologically relevant) and animal studies  
17 (biologically relevant but expensive and time consuming).

18 Ovarian cancer, and other cancers of the female pelvic region, hold the unusual characteristic of  
19 existing within an open system where cells can and do move between organs as part of healthy  
20 reproductive processes. This provides unique advantages to the cancers which develop in these  
21 regions. This primarily includes metastasis, where, in the case of ovarian cancer, cancer cells can  
22 shed from the ovary and implant into the peritoneum without the need to invade through tissue.  
23 For cancer cells to perform this migration they are required to live in an anchorage free  
24 environment and develop resistance to anoikis. In the case of HGSOC, this is performed through  
25 the formation of spherical cellular aggregates similar to MCTS described above, which can exist,  
26 free floating, in the peritoneal cavity. While the ascites derived MCTS are distinct from the *in*  
27 *vitro* MCTS described above, they both possess a gradient of cellular proliferative activity  
28 resulting from the gas, nutrient and waste gradients which are inherent to this spherical structure.

29 The metastasis and survival of ovarian cancer is further supported through the cancer driven  
30 accumulation of fluid in the peritoneal cavity called ascites. The ascites are a cancer promoting  
31 niche within which ovarian cancer exists primarily as MCTS and demonstrate increased  
32 chemoresistance in this setting. The exact reasons why MCTS are more resistant to primary  
33 chemotherapy is not entirely understood but is thought to be the result of reduced penetration of  
34 the drugs into the spheroid structure, protective paracrine signalling between the cells and the  
35 formation of a quiescent population with the spheroid which are inherently resistant to  
36 proliferation targeted chemotherapy such as CBP.

37 Together, this makes the role of MCTS in the progression of HGSOC of great importance. In the  
38 below publication we review the mass spectrometry-based approaches to investigating MCTS,  
39 both in the context of an *in vitro* model for solid tumours and ascites derived ovarian cancer  
40 MCTS. Further, we present the first MALDI MSI analysis of an ascites derived MCTS and  
41 identify analytes which relate to the different layers of the MCTS structure.



1  
2  
3  
4  
5  
6  
7  
8  
9  
10  
11  
12  
13  
14  
15  
16  
17  
18  
19  
20  
21  
22  
23  
24  
25  
26  
27  
28

This page is intentionally left blank

1 **5.2. Statement of Authorship**

Title of Paper	Mass Spectrometry Analyses of Multicellular Tumor Spheroids
Publication Status	<input checked="" type="checkbox"/> Published <input type="checkbox"/> Accepted for Publication <input type="checkbox"/> Submitted for Publication <span style="float: right;">Unpublished and Unsubmitted work written in manuscript style</span>
Publication Details	<u>M. Acland, P. Mittal, N. A. Lokman, M. Klingler-Hoffmann, M. K. Oehler and P. Hoffmann, Mass Spectrometry Analyses of Multicellular Tumor Spheroids, <i>Proteomics Clinical Applications</i>, 12 (3) (2018)</u>

2

3

**Principal Author**

Name of Principal Author (Candidate)	Mitchell Acland				
Contribution to the Paper	Performed literature search, wrote the first draft of the article and consolidated the final version of the manuscript.				
Overall percentage (%)	70%				
Certification:	This paper reports on original research I conducted during the period of my Higher Degree by Research candidature and is not subject to any obligations or contractual agreements with a third party that would constrain its inclusion in this thesis. I am the primary author of this paper.				
Signature	<table border="1" style="width: 100%;"> <tr> <td style="width: 60%;"></td> <td style="width: 40%;">Date</td> </tr> <tr> <td></td> <td>27/05/2022</td> </tr> </table>		Date		27/05/2022
	Date				
	27/05/2022				

4

5 **Co-Author Contributions**

6 By signing the Statement of Authorship, each author certifies that:

- 7 i. the candidate's stated contribution to the publication is accurate (as detailed above);
- 8 ii. permission is granted for the candidate to include the publication in the thesis; and
- 9 iii. the sum of all co-author contributions is equal to 100% less the candidate's stated contribution.

10

11

Name of Co-Author	Parul Mittal				
Contribution to the Paper	Performed the MALDI-MSI analysis of sectioned ovarian cancer spheroids.				
Signature	<table border="1" style="width: 100%;"> <tr> <td style="width: 60%;"></td> <td style="width: 40%;">Date</td> </tr> <tr> <td></td> <td>23/03/2022</td> </tr> </table>		Date		23/03/2022
	Date				
	23/03/2022				

12

Name of Co-Author	Noor Alia Lokman		
Contribution to the Paper	Developed and performed sample preparation of ovarian cancer spheroid for MALDI MSI analysis		
Signature		Date	15/2/2021

1

Name of Co-Author	Manuela Klingler Hoffmann		
Contribution to the Paper	Supervised development of work, data interpretation and manuscript evaluation.		
Signature		Date	24/05/2022

2

Name of Co-Author	Martin K. Oehler		
Contribution to the Paper	Supervised development of work, provided sample material and manuscript evaluation.		
Signature		Date	20 February 2021

3

Name of Co-Author	Peter Hoffmann		
Contribution to the Paper	Supervised development of work, data interpretation, manuscript evaluation and acted as corresponding author.		
Signature		Date	24/05/2022

4

5

6

7

8

9

10

11

12

13

14

# Mass Spectrometry Analyses of Multicellular Tumor Spheroids

Mitchell Acland, Parul Mittal, Noor A. Lokman, Manuela Klingler-Hoffmann, Martin K. Oehler, and Peter Hoffmann\*

Multicellular tumor spheroids (MCTS) are a powerful biological *in vitro* model, which closely mimics the 3D structure of primary avascularized tumors. Mass spectrometry (MS) has established itself as a powerful analytical tool, not only to better understand and describe the complex structure of MCTS, but also to monitor their response to cancer therapeutics. The first part of this review focuses on traditional mass spectrometry approaches with an emphasis on elucidating the molecular characteristics of these structures. Then the mass spectrometry imaging (MSI) approaches used to obtain spatially defined information from MCTS is described. Finally the analysis of primary spheroids, such as those present in ovarian cancer, and the great potential that mass spectrometry analysis of these structures has for improved understanding of cancer progression and for personalized *in vitro* therapeutic testing is discussed.

## 1. Introduction

Since the establishment of HeLa cells in 1953,<sup>[1]</sup> cell lines have provided researchers with an almost unlimited supply of cells for experimentation and, since then, a vast number of immortalized cell lines have been established from a range of different

cancers. Decades of optimization have led to rapid and reproducible techniques employing cancer cell lines. Cells are typically either grown as an adherent monolayer or in suspension and, despite the profound impacts that these techniques have had on biological research, it has been noted that these simple biological systems do not truly represent the *in vivo* environment.<sup>[2]</sup> Monolayer culture conditions fail to capture the tumor microenvironment which involves the complex interaction between heterogeneous cell populations, extracellular matrix (ECM) components, and the influence of a host of secreted factors that are present in the tissue. Additionally, it has been shown that growing cells on ridged 2D structures, such as tissue culture plastics,

results in abnormal metabolism and protein expression.<sup>[2]</sup>

This highlights the need for *in vitro* models which more closely replicate the *in vivo* situation. Multicellular tumor spheroids (MCTS) are an *in vitro* model composed of cancer cells which have been allowed to grow as 3D aggregates. These structures replicate gas and nutrient diffusion, gene expression, protein abundance, cell–cell interactions and cell–ECM connections seen in primary tumors.<sup>[3–8]</sup> Mass spectrometry approaches hold great potential for elucidating the molecular organization of these structures and how MCTS respond to cancer therapeutics. Together these methods promise to provide insight into the complex molecular mechanisms underpinning cancer progression and response to therapy in a way which is rapid, reproducible, and closely replicates the *in vivo* conditions.

In the first part of this review we summarize the mass spectrometry approaches used to investigate MCTS as a model focusing on cancer progression and treatment response. There are a number of traditional LC-MS/MS approaches, which have been applied to the MCTS model, as well as other soluble techniques, which aim to provide information about the global abundance of proteins and other molecules. This includes gel and label based techniques such as 2D-PAGE and stable isotopic labeling of amino acids in culture (SILAC), respectively. These techniques have typically focused on identifying proteomic differences between the same cells grown as monolayers or as MCTS.<sup>[9,10]</sup>

One short coming of traditional mass spectrometry approaches in this context is that they require homogenization of the sample causing loss of spatially defined information. MCTS

M. Acland, P. Mittal, Dr. M. Klingler-Hoffmann, Prof. P. Hoffmann  
Adelaide Proteomics Centre  
School of Biological Sciences  
University of Adelaide  
Adelaide, South Australia, Australia  
E-mail: Peter.Hoffmann@unisa.edu.au

M. Acland, P. Mittal  
Institute of Photonics and Advanced Sensing (IPAS)  
University of Adelaide  
Adelaide, South Australia, Australia

Dr. N. A. Lokman, Dr. M. K. Oehler  
Discipline of Obstetrics and Gynaecology  
School of Medicine  
Robinson Research Institute  
University of Adelaide  
Adelaide, South Australia, Australia

Dr. M. Klingler-Hoffmann, Prof. Dr. P. Hoffmann  
Future Industries Institute  
University of South Australia  
Adelaide, South Australia, Australia

Dr. M. K. Oehler  
Department of Gynaecological Oncology  
Royal Adelaide Hospital  
Adelaide, South Australia, Australia

DOI: 10.1002/prca.201700124

formed from homotypic population of cancer cells develop layers of different proliferative capacities<sup>[11]</sup> making spatial localization of molecules important. In the second part of this review we summarize current methods for investigating spatially defined molecular information and therapeutics response such as mass spectrometry imaging (MSI). The publications summarised are listed in **Table 1**. Finally we outline a MSI approach established in our lab to investigate peptide abundance in primary ovarian cancer ascites derived spheroids (ADS) and discuss the future application of mass spectrometry to ADS in the pursuit of personalized cancer therapy.

## 2. MCTS as a Biological Model for Avascularized Tumors

### 2.1. MCTS Replicate Solid Tumor Structure and Tumorigenicity

MCTS are being used extensively in research and drug development, as they closely replicate avascularized solid tumors.<sup>[4,6–8]</sup> The cell–cell and cell–ECM connections seen in MCTS mimic the *in vivo* situation and have profound effects on cellular signaling.<sup>[3,5]</sup> Consequently, research utilizing this biologically relevant cellular model aims to bridge the gap between research employing monolayer culture and that of *in vivo* experimentation.<sup>[9]</sup>

When grown to diameters greater than 500  $\mu\text{m}$ , MCTS from a single cell lines form a core of necrotic cells. They are believed to be a result of the cells' response to gradients of oxygen, nutrients, pH, CO<sub>2</sub>, and metabolic waste within the MCTS structure.<sup>[11]</sup> The cells surrounding the necrotic core seem to have adapted to their challenging conditions, with a majority of cells in this region entering a quiescent state, while most of the cells in the outer regions of the MCTS continues to proliferate. This results in three physiological layers of different proliferative capacities<sup>[11]</sup> (**Figure 1**) and this heterogeneous cellular structure profoundly alters growth, survival, and response to treatment as compared to the same cells grown as monolayers.<sup>[12]</sup>

Furthermore, some cell lines have been shown to be more tumorigenic as MCTS when compared to single cell suspensions in the animal model,<sup>[13]</sup> supporting their relevance as a biological model. Interestingly, MCTS formed from co-cultures of cancer cells and normal fibroblasts have more tumorigenic properties than homotypic spheroids and both cell types in suspension<sup>[13]</sup> which correlated with increased spheroid density in cancer–fibroblast co-cultures. This is not surprising considering that signaling between cancer cells and cancer associated fibroblasts are important in cancer progression<sup>[14]</sup> and it again highlights the importance, and complexity, of heterotypic cell–cell interactions.

### 2.2. Chemotherapy Response in MCTS

Cells grown as MCTS have been demonstrated to be more resistant to the majority of traditional chemotherapy treatments when compared to the same cells cultured as monolayers.<sup>[15–18]</sup> The exact mechanism by which MCTS formation protects cells from chemotherapy has not been fully elucidated. However, inhibited diffusion of the drugs, the maintenance of a quiescent

population within the MCTS, expression of pro-survival genes as a result of cell–cell contact, and paracrine/autocrine signaling<sup>[19]</sup> have been suggested as possible mechanisms. This is supported by studies demonstrating that disruption of cell–cell contacts sensitizes MCTS to chemotherapy treatment.<sup>[16]</sup> One explanation for higher chemotherapy resistance in MCTS is that the inner quiescent layer is in a non-proliferative G0 cell cycle stage, providing resistance to therapies which target proliferating cells.<sup>[20]</sup> In melanoma MCTS, cells in G0 were localized to the inner layer of the MCTS with cycling cells on the periphery, which correlated with higher oxygen levels.<sup>[21]</sup> The cell cycle stages were shown to be similar to a mouse xenograft model with more cell cycle arrest observed distant from blood vessels.<sup>[21]</sup> Moreover, hypoxia in the central layers of MCTS has been shown to reduce the effectiveness of radiation and chemotherapy<sup>[22,23]</sup> as well as being a factor which promotes metastasis and progression.<sup>[24,25]</sup> Together, this suggests that the MCTS microenvironment mimics that of a solid tumor giving rise to microenvironment driven phenotypic changes which have vast influences on cancer progression and chemotherapy response.

### 2.3. Cancer Biomarkers are Present in MCTS

The biological relevance of the MCTS model has been demonstrated by the appearance of more relevant cancer biomarkers in cells grown as MCTS compared to cells grown as monolayers.<sup>[26,27]</sup> One example is the pancreatic cancer cell line PC3, which, in 3D culture conditions, exhibited a shift from E-cadherin to N-cadherin expression and increased CXCR4 and  $\beta 1$  integrin abundance at the cell membrane.<sup>[27]</sup> Expression of these proteins is similar to that observed in primary pancreatic cancer biopsies.

MCTS have also been shown to more closely resemble gene expression patterns observed in solid tumor.<sup>[28–31]</sup> In general, this includes an increase in cell adhesion and cell junction genes with a decreased expression of genes associated with DNA replication and progression of the cell cycle.<sup>[28,30,31]</sup> In the case of head and neck squamous cell carcinoma (HNSCC), increased expression of cytochrome P450 xenobiotic metabolism genes were observed in MCTS compared to monolayers.<sup>[28]</sup> This has also been reported in hepatocellular carcinomas<sup>[30]</sup> and more closely replicates the expression observed in cancer tissue.<sup>[31]</sup> The cytochrome P450 superfamily is thought to be responsible for up to 75% of all drug metabolism processes<sup>[32]</sup> and the upregulation of these genes in MCTS suggests increased drug resistance mechanisms in these structures compared to the same cells grown as monolayers.

### 2.4. Conclusion of MCTS as a Biological Model for Avascularized Tumors

MCTS represent a powerful biological model to further analyze and better understand the complex biology and drug response of avascularized tumors. They faithfully replicate the solid tumor in gene expression, protein biomarkers, drug response, gas and nutrient gradients, and the subsequent cellular layers of different proliferative capacities.<sup>[33]</sup> However, there are still a number of limitations associated with this *in vitro* model. For example, not all immortalized cells' lines are able to spontaneously

**Table 1.** Mass spectrometry approaches to investigating cancer spheroids.

Paper	Author	Analysis method	Spheroid growth method	Cell origin	Key findings
<b>Soluble based mass spectrometry approaches</b>					
Bottom-up proteomic analysis of single HCT 116 colon carcinoma multicellular spheroids	Feist et al. (2015). Hummon Lab	LC-MS/MS (DDA)	Agarose overlay	HCT116 colon cancer cell line	Established that, through the use of purification techniques, a single spheroid can be investigated with LC-MS/MS in a reproducible way.
Nutrient restriction of glucose or serum results in similar proteomic expression changes in 3D colon cancer cell lines	Schroll et al. (2016)	iTRAQ + LC-MS/MS (DDA)	Agarose overlay	HCT116 colon cancer cell line	↑SIRT1 (metabolic), ↑PIAS1 (signaling), ↓MRD1 (drug resistance), ↓ZBTB7 (oncogenic transcription factor). Showed that nutrient restriction increases cell viability but also increases effectiveness of chemotherapy.
Proteomic analysis reveals differences in protein expression in spheroid versus monolayer cultures of low-passage colon carcinoma cells	Gaedtke et al. (2007)	2D-PAGE + MALDI MS	Agarose overlay	Two newly made colon cancer cell lines used at a very low passage	Identified differentially regulated proteins in MCTS (↑Laminin A/C fragment, ↑P0 ribosomal component, ↑acidic calponin).
Metabolic alteration of HepG2 in scaffold based 3D culture: proteomic approach	Prusksakorn et al. (2010)	2D-PAGE + MALDI MS	Collagen type 1 scaffold	HepG2 colon cancer cell line	Increase in glycolytic, ECM and cytoskeletal proteins in MCTS compared to monolayers.
3D neuroblastoma cell culture: proteomic analysis between monolayer and multicellular tumor spheroids	Kumar et al. (2008)	2D-PAGE + MALDI MS	polyHEMA coated plates	Neuroblastoma cell lines: SK-N-AS, SK-N-DZ, and IMR32	Increase in glycolytic and heat shock proteins in MCTS compared to monolayers.
Comparative proteomics of ovarian cancer aggregate formation reveals an increased expression of calcium-activated chloride channel regulator 1 (CLCA1)	Musrap et al. (2015)	SILAC + LC-MS/MS	Hanging drop	Ovarian cancer cell lines: OV90, TOV-112D, and ES-2	Greatly increased expression of CLCA1 in MCTS (eightfold) in MCTS compared to monolayers. This ion channel is essential in MCTS formation in this context.
Proteomic comparison of 3D and 2D glioma models reveals increased HLA-E expression in 3D models is associated with resistance to NK cell mediated cytotoxicity	He et al. (2014)	Dimethyl labeling + LC-MS/MS	Rotary cell culture	Glioma cell line: U251	Decreased abundance of proteins involved in proteosomal degradation and antigen presentation in MCTS compared to monolayers. Observed decreased susceptibility to NK cell mediated apoptosis in MCTS.
Quantitative proteomic and phosphoproteomic comparison of 2D and 3D colon cancer cell culture models	Yue et al. (2016)	SILAC + LC-MS/MS	ULA (ultra low attachment) plates	Colon cancer cell line: HT29	Highly reproducible phosphoproteomic analysis of MCTS. Identified differentially abundant proteins and phosphoproteins involved in proliferation, cell cycle, and DNA repair.
Multicellular tumor spheroids combined with mass spectrometric histone analysis to evaluate epigenetic drugs	Feist et al. (2017)	Serial trypsinization, histone extraction, and DIA LC-MS/MS	Agarose overlay	HCT116 colon cancer cell line	Observed significantly different methylation patterns in MCTS compared to monolayers. Treated spheroids with UNC1999, which inhibits methylation of H3D27, and observed decreased H3D27 methylation in the outer layers of the spheroid. Established this as a platform for testing epigenetic targeting anti-cancer agents.
Proteomic approach toward molecular backgrounds of drug resistance of osteosarcoma cells in spheroid culture system	Arai et al. (2013)	2D-DIGE	NanoCulture plates (NCPs; 96-well, low-binding; SCIVAX Corporation, Kanagawa, Japan)	11 osteocarcinoma cell lines	Nine out of 11 osteocarcinoma cell lines were significantly more resistant as MCTS than as monolayers. This was correlated with cathepsin D, gelsolin and ferritin abundance.

(Continued)

Table 1. Continued.

Paper	Author	Analysis method	Spheroid growth method	Cell origin	Key findings
Plasma membrane proteomics of tumor spheres identify CD166 as a novel marker for cancer stem-like cells in head and neck squamous cell carcinoma	Yan et al. (2013)	Membrane fractionation + SDS-PAGE + LC-MS/MS	ULA plates	HNSCC cell lines: CAL27, HN6, HN12, HN13	Identified differential abundance of proteins involved in differentiation (CD44), cell adhesion (CD166), and numerous signaling pathways (Wnt, integrin, and TGF $\beta$ signaling pathways). They focused on CD166 as a protein which was required for spheroid formation and has been associated with malignant progression of a number of cancers.
Colorectal cancer derived organotypic spheroids maintain essential tissue characteristics but adapt their metabolism in culture	Rajcevic et al. (2014)	SDS-PAGE combined with LC-MS/MS	Agarose overlay	Primary tumor fragments from patients with colorectal carcinoma	Performed the first global proteomic analysis of "organotypic spheroids" (OS) formed from tumor biopsies. They observed an 86% similarity in protein abundance between OS and the tumors they were derived from demonstrating an in vitro method of tumor aggregate generation which directly replicates the primary tumor it was derived from.
3D neuroblastoma cell culture: proteomic analysis between monolayer and multicellular tumor spheroids	Kumar et al. (2008)	Nuclear and cytoplasmic protein enrichment, 2D electrophoresis and LC-MS/MS	ULA plates	Three neuroblastoma cell lines: SK-N, SK-N-DZ, and IMR-32.	Investigated differential protein abundance between monolayers and MCTS and identified proteins with altered abundance to be heat shock and glycolysis related.
<b>Mass spectrometry imaging</b>					
Imaging mass spectrometry of 3D cell culture systems	Li and Hummon (2011)	MALDI + LC-MS/MS	Agarose overlay	HCT116 colon cancer cell line	Established the work flow for MALDI imaging of MCTS. Found increased expression of various survival proteins.
Chemical imaging of platinum based drugs and their metabolites	Liu and Hummon (2016)	MALDI MSI	Agarose overlay	HCT116 colon cancer cell line	Were able to semiquantitatively track the distribution of the platinum based drug, oxaliplatin, and its metabolite in MCTS.
Drug penetration and metabolism in 3D cell cultures treated in a 3D printed fluidic device: assessment of irinotecan via MALDI imaging mass spectrometry	LaBonia et al. (2016)	MALDI MSI	Agarose overlay	HCT116 colon cancer cell line	Were able to track the penetration of irinotecan into MCTS delivered via a 3D printed fluidic device which better replicated the dynamic drug dosing which occurs in vivo.
Accumulation of arachidonic acid-containing phosphatidylinositol at the outer edge of colorectal cancer	Hiraide et al. (2016)	MALDI MSI	Cell matrix type 1 (gelatin based scaffold)	Primary colon cancer derived spheroids, and the colon cancer cell lines; HCT116 and DLD1	Identified high abundance of the phospholipid PI(18:0/20:4) on the periphery of primary cell derived MCTS. This was not present in cell line derived spheroid showing the shortcomings of the cell line MCTS model.
Quantitative bioimaging of platinum group elements in tumor spheroids	Neihoff et al. (2016)	LA-ICP-MS	Spinner Flask	TFK-1 bile duct carcinoma cell line	Were able to quantitatively track the distribution of platinum and palladium based drugs into cancer spheroids.
Analyzing liposomal drug delivery systems in 3D cell culture models using MALDI imaging mass spectrometry	Lukowski et al. (2017)	MALDI MSI	Agarose overlay	Colon cancer cell line: HCT116	Traced the penetration of liposomal doxorubicin into MCTS. Observed similar penetration between free drug and liposomal drug however there was slower metabolism of the liposomal drug. Strong precedence for using the MCTS model to investigate uptake of liposome encased compounds.

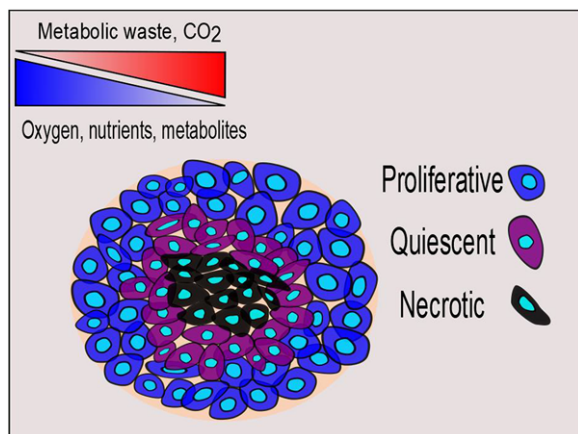


**Figure 1.** Graphical representation of a multicellular tumour spheroid formed from homotypic dissociated cells. The structure has proliferating cells on the outer layer (blue) a quiescent inner ring (purple) and a necrotic core (black). These layers are a result of limited diffusion of oxygen and nutrients in conjunction with increased waste and CO<sub>2</sub> in the centre of the structure. (Layers are drawn for illustration purposes only and are not drawn to scale)

form MCTS and those which do require extensive optimization and validation which limits the use of this model.<sup>[34]</sup> Additionally, these structures fail to replicate a number of aspects of the solid tumor such as heterogeneous cell populations, paracrine and endocrine signaling, and immune cell interactions all of which play a role in cancer progression. To address this, currently more complex in vitro systems are being evaluated, including methods to encourage MCTS formation by co-culturing with other cell types, such as fibroblasts,<sup>[13]</sup> and replication of the complex signaling which occurs in vivo.<sup>[35]</sup> These methods are an exciting avenue for the future development of the MCTS model.

### 3. Generating and Maintaining MCTS in Culture

MCTS were first documented in the 1970's<sup>[36]</sup> and have experienced a renaissance in the last 5 years,<sup>[37]</sup> likely due to advancements in culturing techniques. MCTS is an umbrella term describing 3D structures composed of cancer cells alone or co-cultured with other cell types with or without matrix or other scaffolds.<sup>[2]</sup> The simplest, and most widely used, means of generating MCTS consist of suspensions of homotypic cancer cells which are encouraged to aggregate by a range of methods. The best characterized include culturing on non-adhesive surfaces,<sup>[38,39]</sup> hanging drop,<sup>[40,41]</sup> and spinner flask (reviewed in<sup>[42]</sup>).

Establishing MCTS in non-adhesive tissue culture plates is the most common method of growing these structures. These techniques are rapid and inexpensive and can potentially be employed in high throughput drug testing. To standardize MCTS size with this method, cells can be seeded into 96 well round bottom plates,<sup>[34]</sup> but cultures usually still contain a mix of attached cells and MCTS.<sup>[2]</sup> The hanging drop method involves growing MCTS in drops of media on the underside of tissue culture plastic held by surface tension. This technique generates

consistent MCTS but is labor intensive and unsuitable for long term culturing.<sup>[2]</sup> Finally, the spinner flask method utilizes suspension culture, which is continuously stirred to encourage MCTS formation. This method is useful for large scale production of MCTS. However, the sheer force used to generate MCTS can result in phenotypic changes and heterogeneous distribution of cell numbers within the MCTS.<sup>[42]</sup>

There are also a number of more complex 3D culturing methods developed in order to more closely replicate the in vivo environment for any particular biological situation. These include co-culturing with other cell types,<sup>[5]</sup> culturing in matrices, such as hydrogels,<sup>[43]</sup> and in microfluidic devices<sup>[44]</sup> (reviewed in<sup>[35]</sup>).

#### 3.1. Primary Cell Derived Three Dimensional Cell Culture

In addition to being formed from dissociated cells in culture, 3D aggregates also appear as part of ovarian cancer malignant progression and will be defined here as "ADS."<sup>[45]</sup> Ovarian cancer is characterized by dissemination of tumor cells into the abdominal cavity causing the formation of malignant cancer-cell rich fluid called "ascites."<sup>[46,47]</sup> Within the ascites ovarian cancer cells exist as both single cells and spherical aggregates.<sup>[48]</sup> These structures are thought to be of importance in inherent and acquired chemo resistance,<sup>[49]</sup> which is a defining characteristic of ovarian cancer, and represents a reservoir of cancer cells which drive metastases.<sup>[50]</sup>

### 4. Analysis Techniques for Investigating MCTS

Despite many advances in culturing methods, there remains the barrier of analyzing these 3D structures in a way which maintains their biologically important structures. A range of techniques have been developed to investigate the morphology, topography, growth, cellular organization, gene expression, cell cycle patterns, and invasive and metastatic potential of MCTS (reviewed in<sup>[51]</sup>). This includes a range of microscopy based techniques, flow cytometry, traditional proteomic, genomic, metabolomic,<sup>[52]</sup> and transcriptomic techniques as well as the application of mathematical modeling.<sup>[51]</sup>

However, in this complex 3D context, many of these techniques are inadequate. For example, colorimetric dyes and lysate based techniques, such as flow cytometry and western blots, lose the spatial information during sample preparation. Additionally, fluorophore based techniques, such as microscopy and histology, require foreknowledge of molecules of interest limiting the potential of these techniques to discover novel molecular aspects of these structures.

To overcome the issues related to loss of spatial information, the MCTS can be separated into solubilized layers via serial trypsinization.<sup>[53]</sup> This technique was first applied and validated in the 1980's to characterize the different cell populations in MCTS formed from mouse mammary tumor cell line.<sup>[53]</sup> Briefly, it involves washing the MCTS with trypsin, removing the dissociated cells forming the outer layer, and repeating until the entire spheroid is separated.<sup>[53]</sup> Sutherland et al. (1980) demonstrated that this approach separated the MCTS consistently and went on to characterize an inner layer of cells as



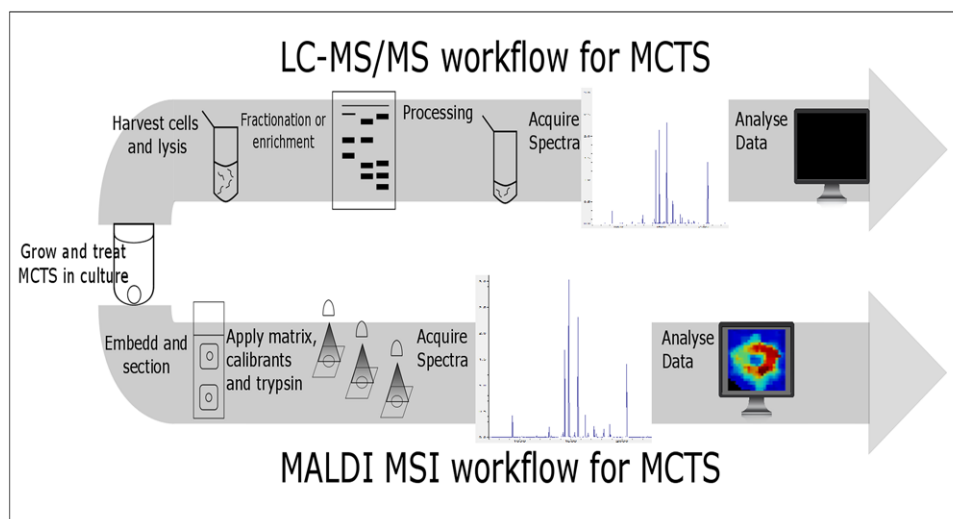


**Figure 2.** Workflow for LC–MS/MS and MALDI MSI analysis of MCTS. **LC–MS/MS:** Cells are harvested and lysed before specific fractionation techniques are applied. This is followed by processing including tryptic digest for investigation of peptides. The sample is loaded into the LC–MS/MS and spectra are acquired before data analysis to identify molecules and perform relative quantification of abundance. **MALDI MSI:** Spheroids are embedded and sectioned onto conductive slides. Matrix and calibrants are applied to the sections before spectra are acquired in a MALDI-TOF instrument. Spectra are co registered with images of the sections to acquire spatially localised molecular information.

quiescent while the outer layers were proliferative, however to a lower extent than the same cells grown as monolayers.<sup>[53]</sup> This technique is compatible with a range of analysis techniques, including mass spectrometry, and is discussed further in Section 4.2.1.

#### 4.1. Traditional Mass Spectrometry Techniques for Analyzing MCTS

One way to address some of the short comings of the techniques discussed above is to investigate the molecular underpinnings of these structures using mass spectrometry (Figure 2). Mass spectrometry analyses have the potential to identify vast numbers of proteins, post translational modifications (PTMs), lipids, metabolites, and other analytes with relative quantification. No fore-knowledge of the molecule of interest is required, making these techniques ideal for discovery approaches. These techniques have been used in cancer biology to identify biomarkers for cancer detection,<sup>[54–57]</sup> to predict chemotherapy response,<sup>[58–62]</sup> and to investigate the biology of cancer progression.<sup>[63]</sup> In the case of MCTS, mass spectrometry has been employed to identify molecules which are involved in MCTS formation or confer MCTS specific characteristics as well as tracing penetration of therapeutics into these structures.

One of the barriers to effective elucidation of the proteome using mass spectrometry is the great complexity of the sample. This complexity can result in higher abundance analytes suppressing the signals from less abundant, but no less biologically important, ones.<sup>[64]</sup> To overcome this, a range of fractionation techniques are employed in traditional mass spectrometry work flows in order to reduce the complexity of the sample.

Liquid chromatography (LC) techniques have become the standard approach for fractionation of analytes before mass

spectrometry analysis. The most commonly used LC technique is reverse phase liquid chromatography (RP-LC).<sup>[65]</sup> One limitation of RP-LC is that highly polar analytes are difficult to separate as they are not well retained on the column. This can be overcome through the use of hydrophilic interaction liquid chromatography (HILIC)<sup>[66]</sup> and this technique has been employed to separate carbohydrates,<sup>[67]</sup> peptides,<sup>[66]</sup> and polar pharmaceuticals.<sup>[68]</sup> It is yet to be widely applied for the analysis of MCTS, however holds potential and might result in a complementary data set. Together, these LC techniques provide effective fractionation of a range of complex samples allowing for effective identification and relative quantification in MS instruments.

Recently, label free proteomic analysis of MCTS was achieved for single MCTS formed from the colon cancer cell line: HCT116.<sup>[69]</sup> Initially, they established that a single MCTS (approximately 1 mm in diameter) contains an average of  $39 \pm 4 \mu\text{g}$  of protein. Through careful protein concentration, via acetone precipitation, and sample preparation the authors were able to minimize any protein losses resulting in the identification of more than 1350 proteins from a number of duplicate runs with high reproducibility and relative quantification. Through the application of Pearson's correlation they were able to show that variations in identified proteins between different single MCTS were purely due to random variations in spectra<sup>[69]</sup> supporting the high level of reproducibility in LC-MS/MS analysis of MCTS and the possible application with high throughput platforms.

In addition to being formed from dissociated cells in culture, spherical aggregates can also be grown directly from a tissue biopsy fragment<sup>[70]</sup> which has the advantage of maintaining more tissue-like characteristics such as ECM, capillaries, and tumor cell heterogeneity.<sup>[70]</sup> For example, Rajcevic et al. (2014) found that, when colorectal cancer biopsy fragments were grown as 3D aggregates, they formed a distinct organization with an outer layer of epithelial cells and an inner core of mesenchymal cells,

and a small number of infiltrating immune cells, showing the complex heterogeneity in tumors and how they can be replicated using these *in vitro* techniques.<sup>[71]</sup> They went on to perform the first global proteomic analysis of these “organotypic spheroids” (OS) using SDS-PAGE coupled with LC-MS/MS and comparing them to cancer tissue directly obtained from a biopsy. They were able to identify 1315 proteins with 35 upregulated and 70 downregulated in OS compared to cancer tissue. They highlighted an 86% similarity in proteins identified in OS and tumor biopsies with the proteins that were found to be differentially abundant being mostly ECM and cytoskeletal proteins, which is to be expected as the spatial organization of this cellular structure is changed *ex vivo*. Despite the small differences in proteomes in these organotypic spheroids compared to tumor biopsies, this method holds promise for further improving upon the biological relevance of these *in vitro* techniques.

#### 4.1.1. 2D Gel Based Fractionation Combined with MS Analysis

2D electrophoresis techniques, such as 2D-PAGE, are fractionation methods commonly employed in proteomic mass spectrometry workflows. It typically involves separating proteins based on their isoelectric point in the first dimension and by molecular weight in the second dimension<sup>[72]</sup> and is an effective method for separating proteins out of complex samples. Once a protein spot is separated it can be readily identified using mass spectrometry. However, one protein spot can contain a number of proteins, with the most abundant being the most likely to be identified.

An example of the use of 2D-PAGE coupled with LC-MS/MS compared HepG2 liver cancer cell lines grown as monolayers or as MCTS in collagen based scaffolds.<sup>[10]</sup> This approach identified more than  $823 \pm 45$  spots in monolayer culture and  $762 \pm 65$  in MCTS with 73 of these spots shown to be significantly differentially abundant between the two groups. This was followed up with in-gel tryptic digestion and LC-MS/MS identifying a number of proteins involved in cytoskeletal organization and indicative of a shift toward anaerobic glycolysis, which has been widely observed in MCTS.<sup>[69,73–76]</sup> The microenvironmental stresses on cancer, replicated through MCTS culture, are vital in the shift to glycolytic metabolism which mediates angiogenesis, tumor progression, and metastasis.<sup>[3]</sup>

Through immunoblotting for stabilized HIF-1 $\alpha$ , they identified increased levels of hypoxia in MCTS<sup>[10]</sup> and established that, when grown as MCTS, these cells could replicate a number of aspects of an avascularized tumor.<sup>[77]</sup> The role of hypoxia in driving tumor progression, and reducing the effectiveness of anti-cancer therapy, has been described in a number of contexts.<sup>[78,79]</sup> In addition to altered metabolism and hypoxia response, an increased abundance of ECM and cytoskeletal proteins were identified in MCTS, which both play a role in cancer progression, particularly in migration and metastasis.<sup>[80,81]</sup>

A similar approach was also applied to three neuroblastoma cell lines grown in low attachment plates.<sup>[9]</sup> Through combined nuclear and cytoplasmic enrichment followed by 2D electrophoresis, they identified 18 spots differentially abundant in MCTS compared to monolayer cells. These proteins were identified via in-gel tryptic digestion followed by LC-MS/MS and were characterized as heat shock and glycolysis related. The

altered metabolism and expression of heat shock proteins (HSPs), seen only in the MCTS, replicates protein expression in solid tumors<sup>[82,83]</sup> further establishing MCTS as a strong biological model. The increased abundance of stress response proteins, such as HSPs, have been associated with apoptosis resistance, angiogenesis, and chemo resistance<sup>[82]</sup> and are expected to arise in response to the stressful conditions in the inner layers of the MCTS.

2D electrophoresis, with MALDI MS mass fingerprint protein identification, was used to investigate the proteomic differences in primary colon cancer cell lines grown as MCTS or as monolayers.<sup>[73]</sup> Through the generation, and early passage analysis, of colorectal cancer cell lines they aimed to reduce the impact that long term culturing has on the phenotype of cancer cell lines. Four protein spots showed significantly altered abundance in MCTS compared to monolayer culture when analyzed via 2D electrophoresis. These were then identified by MALDI MS mass fingerprinting as acidic calponin, laminin A/C, 15-hydroxyprostaglandin dehydrogenase, and acidic ribosomal protein P0 which are associated with the cytoskeleton, prostaglandin metabolism, and ribosomal function, respectively. Laminin A/C was identified by MALDI MS, however in the 2D electrophoresis it was approximately 30 kDa smaller than the expected size of the full length protein. They concluded that this represented a truncated version of the proteins which was more abundant in MCTS compared to monolayers. This difference was more pronounced in more compact MCTS and coincided with high levels of apoptosis. The abundance of this protein in 2D cultures under hypoxia and/or serum deprivation was investigated to determine whether these particular stresses are responsible for the cleavage of this protein in MCTS. Hypoxia alone were not sufficient to alter the abundance of this protein fragment in 2D cultures, however serum deprivation alone, or combined hypoxia and serum deprivation, resulted in an increased abundance of this truncated protein. It was demonstrated that the truncated laminin A/C protein fragment is a product of caspase-6 activation through the use of a caspase-6 inhibitor. This supports early findings of caspase-6 activation and protein cleavage within the MCTS.<sup>[84]</sup> Interestingly, apoptosis and consequently caspase-6 activation, was present in localized areas throughout the spheroid. This is in contrast to the well characterized morphology of MCTS,<sup>[11]</sup> specifically the necrotic core, suggesting that these properties may not be universal.

#### 4.1.2. Label Based MS Approaches

Minute differences in sample preparation, sample injection, and between each MS run can have profound effects on the MS results. This is particularly true when attempting to quantify differential protein abundance between samples. This results in a large number of technical replicate runs being required before any quantitative difference can be confidently identified. To overcome this, mass tags, such as SILAC, iTRAQ, and dimethyl labeling, can be incorporated into the samples, typically labeling proteins or peptides, during tissue culture or after cell lysis. The addition of these mass tags to one of the comparative groups allows multiple samples to be mixed and prepared in an identical manner while facilitating their separation within the mass spectrometer.

Through the use of such labeling techniques, multiple samples can be investigated simultaneously facilitating accurate relative quantification, reducing bias, and increasing reproducibility.<sup>[64]</sup>

SILAC combined with LC-MS/MS, was applied by Musrap et al. (2015) to compare the proteome of the ovarian cancer cell line, OV90, grown adherently or as MCTS.<sup>[76]</sup> Through the use of this method 1533 proteins were identified with 13 more abundant in MCTS and 6 less abundant when compared to adherent cells. From this they focused on calcium-activated chloride channel regulator 1 (CLCA1) for further analysis. This protein was found to be eightfold more abundant in MCTS compared to adherently grown cells and has been implicated in a number of biological processes including cell–cell adhesion and apoptosis.<sup>[85]</sup> Chloride channels have previously been implicated in ovarian cancer–stroma interactions facilitating metastasis<sup>[86]</sup> and they observed that siRNA knockdown of CLCA1 or chemical inhibition of chloride channels inhibited aggregation of MCTS in these cell lines. From these findings they suggest that MCTS formation, and some aspects of cancer progression, may be dependent on chloride channels. However, further research is required to understand the importance of these results.

Dimethyl labeling combined with LC-MS/MS was employed by He et al. (2014) to investigate global protein abundance in U251 cells, a human glioma cell line, cultured as monolayers or MCTS.<sup>[74]</sup> They were able to identify 363 differentially abundant proteins between monolayers and MCTS with the majority of these involved in metabolic processes, particularly glycolysis, which supports previous findings regarding the altered metabolism in 3D culture.<sup>[87]</sup> Additionally, they highlight changes in the abundance of proteins involved in antigen presentation and proteasome function, which plays a vital role in antigen presentation,<sup>[88]</sup> in MCTS. This includes human leukocyte antigen E (HLA-E), a well-known ligand of CD94/NKG2A that inhibits natural killer cell function.<sup>[89]</sup> Its expression was further investigated with western blot, supported by RT-PCR and FACS, and found HLA-E to be significantly more abundant in MCTS compared to monolayers which was reflected in greater resistance of MCTS to NK mediated cytotoxicity in vitro and in animal models.

#### 4.1.3. Phosphoproteomic Analysis of MCTS

To reveal altered signaling pathways in MCTS, Yue et al. (2016) used SILAC, couple with LC-MS/MS, to compare the phosphoproteome of HT29 colon cancer cell lines grown in 2D or 3D cell culture conditions.<sup>[90]</sup> They identified 2245 quantifiable proteins with 225 showing increased abundance and 116 proteins with decreased abundance in MCTS compared to monolayers. Additionally, they identified 801 quantifiable phosphoproteins with 73 upregulated and 236 downregulated in MCTS compared to monolayers. This general decrease in phosphorylation rates observed in MCTS is suggested to be indicative of slowed growth. In particular, there was significantly altered phosphorylation of proteins involved in proliferation, cytoskeletal regulation, apoptosis, migration, and cell adhesion<sup>[90]</sup> showing that both the proteome and phosphoproteome are significantly altered in MCTS. After extensive network analysis they observed that proteins and phosphoproteins differentially abundant in MCTS compared to

monolayers were part of a complex network implicated in proliferation, cell cycle, DNA repair, and DNA replication. Although the importance of these findings is yet to be demonstrated, it is precedence for phosphoproteomic analyses of MCTS being performed with high levels of reproducibility.

#### 4.1.4. Conclusion of Traditional Mass Spectrometry Techniques for Analyzing MCTS

Traditional mass spectrometry techniques have proven to be a valuable tool for characterizing the molecular underpinnings of MCTS. In particular, they have identified many molecular differences conferred by growing cells in 3D conditions which, compared to monolayer culture, more closely replicates conditions found within solid tumors. Specifically, mass spectrometry techniques have revealed altered abundance of proteins involved in metabolism, stress responses, survival, cell–cell and cell–ECM interactions, decreased proliferation, and immune evasion. Additionally, a number of proteins involved in MCTS formation itself have been identified. For example, the importance of chloride channels in MCTS formation in ovarian cancer.<sup>[76]</sup> Although mass spectrometry has been able to elucidate the altered abundance of proteins in these various MCTS contexts, further experiments are required to determine the biological relevance of these results. Mass spectrometry approaches toward analyzing MCTS do, however, provide a powerful foundation for future research into the molecular underpinnings of cancer progression.

#### 4.2. Mass Spectrometry Techniques to Obtain Spatially Defined Information from MCTS

Cellular heterogeneity and cell–cell contacts play a large role in cancer progression and drug resistance.<sup>[91]</sup> With the advent of in vitro models which replicate this heterogeneity, such as MCTS, comes the need for analysis techniques which provide spatially defined molecular information in a manner which maintains the biologically relevant features of the model structure. This is seen in MCTS which are heterogeneously organized 3D structures and, in the case of MCTS formed from dispersed cultured cells, form three physiological layers as a result of oxygen, nutrient, and waste gradients (Figure 1).<sup>[11]</sup> The different conditions in different layers of the MCTS have significant influences on the molecular and phenotypic nature of the cells<sup>[75]</sup>; however, the mass spectrometry approaches described above have been limited to whole MCTS analysis. This may result in a loss of information, for example, high abundance proteins from the proliferative or necrotic regions may mask lower abundance proteins from the less translationally active quiescent region. This is of particular importance when investigating the impact of therapeutic agents on MCTS as therapeutic penetration and spatial accumulation of the therapeutic is of great importance.<sup>[19]</sup>

##### 4.2.1. Serial Trypsinization Followed by Mass Spectrometry

As discussed above (Section 4), serial trypsinization is a method which can provide spatially defined molecular information by

separating the MCTS into solubilized layers. This is ideal for LC-MS/MS analysis of different layers of the MCTS which can provide spatially defined information about peptide and PTM abundance as well as penetration and accumulation of therapeutic agents.

Serial trypsinization combined with LC-MS/MS has recently been applied to investigate the effect of the epigenetic drug UNC1999, a small molecule inhibitor of EZH1 and EZH2,<sup>[92]</sup> in a colon cancer MCTS model.<sup>[93]</sup> EZH1 and 2 are the catalytic subunit of the polycomb repressive complex 2<sup>[94]</sup> which controls the di- and trimethylation of histone H3 lysine 27 (H3D27).<sup>[95]</sup> Hypermethylation of this histone has been associated with cancer progression and identified as a possible therapeutic target.<sup>[96]</sup> Previously, the MCTS model has been shown to better replicate the epigenetic profile of primary cancer cells<sup>[97]</sup> making this a strong platform for testing of epigenetic drugs. Serial trypsinization followed by LC-MS/MS revealed vast differences in methylation patterns between monolayers and MCTS. Interestingly, there were also significant epigenetic differences between the different layers of the MCTS highlighting the biological heterogeneity of the structure. They followed this with an investigation into the influence of UNC1999 and found significant epigenetic changes, including a decrease in H3D27 trimethylation in the outer two layers of the treated MCTS. They did not observe this in the core component of the MCTS however, and attributed this to incomplete penetration of the drug. Phenotypically, this decreased H3D27 trimethylation in the treated MCTS resulted in decreased proliferation and deterioration of the MCTS structure in many cases, showing the importance of epigenetics in MCTS integrity.<sup>[93]</sup>

Serial trypsinization overcomes the spatial barriers to traditional mass spectrometry analysis of MCTS by separating the structure into sequential layers. However, it requires extensive optimization for each cell line. Although the above study has employed a number of techniques to confirm that the MCTS shrinks by consistent volumes with each trypsinization, this reproducibility has not been confirmed in terms of spatially defined molecular information.

#### 4.2.2. MALDI Mass Spectrometry Imaging

An alternative approach to analyzing these structures in a spatially relevant manner is through the use of MSI, typically MALDI MSI. The technique uses a matrix which co-crystallizes with the sample before directing a laser at a discrete region which facilitates ionization and sublimation. This produces a mass spectrum at each laser point which, when combined across a section, can provide spatially defined identification and relative quantification of analytes. This technique has been employed to investigate a vast range of analytes such as peptides,<sup>[98]</sup> and drugs<sup>[99]</sup> in MCTS. MALDI MSI also has the potential to investigate a number of PTMs, such as glycosylation<sup>[100]</sup> and has been widely utilized to investigate PTM profiles across tissue sections. While serial trypsinization followed by LC-MS/MS has been utilized to investigate PTMs in MCTS,<sup>[101]</sup> this is yet to be performed using MALDI MSI.

In addition to providing spatially defined molecular information, MALDI MSI also has the advantages of being able to

analyze multiple samples during one run (such as with a tissue microarray [TMA]) and to investigate hundreds of molecules including those from different classes (e.g., peptides and PTMs) in a single experiment.<sup>[102]</sup>

However, compared to other mass spectrometry approaches, MALDI MSI has lower sensitivity resulting from interference from the matrix and the small amount of material analyzed at each laser point.<sup>[103]</sup> While fractionation techniques can be used in conjunction with MALDI, this is not the case with MALDI MSI performed on tissue sections, which further reduces the sensitivity of the technique.<sup>[103]</sup> The complexity of the samples in MALDI MSI also impedes identification of biological analytes. Typical identification techniques include peptide mass fingerprinting<sup>[104]</sup> and sequencing via tandem MS,<sup>[105]</sup> both of which require isolation of the analyte. As a result, complementary mass spectrometry analyses, such as LC-MS/MS, are often required for accurate analyte identification. However, the advent of more sensitive MALDI MSI techniques, such as FT-MS, hold potential for direct identification of biological analytes on tissue.<sup>[106]</sup> Although MALDI MSI investigating peptides has been applied to the MCTS model, it is more commonly used to trace the penetration of pharmaceutical compounds within the structure as their chemical structure and molecular weight are known and are generally distinct from intrinsic analytes.

The first MALDI MSI investigation of MCTS was performed by the Hummon group in 2011<sup>[98]</sup> who investigated protein abundance in MCTS, derived from the colon cancer cell line HCT116, using MALDI MSI. By embedding the MCTS in gelatin followed by cryosectioning, they were able to perform MALDI MSI on these structures and demonstrated visualization of a number of proteins through consecutive sections. Some of these were localized to specific regions of the MCTS structure, specifically the necrotic core and proliferative outer layer. They performed protein identification by solubilizing MCTS, performing 1D gel electrophoresis and analyzing specific bands with LC-MS/MS before confirming protein identifications by comparing the mass identified by LC-MS/MS with the *m/z* values seen in the MALDI MSI. Through this process they were able to identify cytochrome C and histone H4 and map their distribution.

In addition to proteins and drugs, MALDI MSI is also able to analyze other biological molecules such as lipids<sup>[107]</sup> and glycans.<sup>[108]</sup> Hiraide et al. (2016) used MALDI MSI to characterize the lipid profile of primary tissue derived colon cancer MCTS<sup>[107]</sup> and identified high expression of a lipid mass on the periphery of the MCTS. Laser capture microdissection (LCD) of the outer regions of the MCTS followed by LC-MS/MS was used to identify this mass as phosphatidylinositol (18:0/20:4). This phospholipid can be converted to phosphatidylinositol 3,4,5-trisphosphate which triggers the Akt pathways and consequently activates various tumor promoting processes.<sup>[109]</sup> Interestingly, this phospholipid was not observed in MCTS formed from cultured cell lines which they suggest is due to heterogeneity of cancer cells within the primary tumor which would not be present in the highly homogenous cell lines.<sup>[110]</sup>

MALDI MSI was also utilized by Liu and Hummon (2016) to investigate the penetration of the platinum based chemotherapy, oxaliplatin. They performed an on tissue chemical derivatization using diethyldithiocarbamate to overcome platinum's low ionization efficiency in MALDI MSI.<sup>[111]</sup> They observed an

accumulation of platinum in the periphery and the core of the MCTS, as has been observed previously by LA-ICP-MS.<sup>[112]</sup> However they were also able to identify an inactive methionine bound metabolite localized to the core of the MCTS showing that MALDI can provide additional information about drug penetration into MCTS with appropriate sample preparation. They suggest that the localization of the inactive metabolite to the necrotic core is a product of increased detoxification in this area or an expulsion of this product from the quiescent layer. This quiescent layer is consistently devoid of platinum based chemotherapeutics,<sup>[99,111–113]</sup> despite complete penetration of the drugs, suggesting that these cells possess detoxification or drug efflux mechanisms.

Recently Lukowski et al. (2017)<sup>[114]</sup> have employed MALDI MSI to investigate the penetration of doxorubicin encased in a liposomal envelope in the first experiment of its kind. Liposomes are phospholipid structures which have low toxicity, can enhance drug delivery, and reduce clearance of the drug from the body.<sup>[115]</sup> Comparing penetration of free and liposome encased doxorubicin into the MCTS formed from the colon cancer cell line HCT116, they did not observe a significant difference in penetration efficiency. However, an increased accumulation of the free drug at the outer layers of the MCTS was observed at an earlier stage, suggesting that there is a delayed release of the drug from the liposome.

To further the pursuit of revealing spatially defined molecular information in MCTS, we have performed MALDI MSI on ADS, grown from primary ovarian cancer cells in what is, to the best of our knowledge, the first ever analysis of its kind performed on ADS. Ovarian cancer cells were isolated from the ascites (patient 1 (serous ovarian carcinoma, stage 3C)), and maintained as monolayers before being grown as ADS as per Li et al. (2011)<sup>[98]</sup> except polyHEMA coated plates were used in place of agarose during ADS formation. These structures reached a diameter of approximately 600  $\mu\text{m}$  after 9 d in culture after which they were formalin fixed and paraffin embedded (FFPE). In brief, ADS were isolated via centrifugation and washed in PBS before adding matrigel to encase the structures. Following incubation at 37 °C for 4 h, a 1 h formalin fixation was performed. This was followed by a shortened processing, to maintain ADS integrity, before they were embedded in paraffin and sectioned at 6  $\mu\text{m}$  thickness onto indium tin oxide (ITO) (Bruker Daltonics, Bremen, Germany) conductive glass slides for MALDI MSI analysis. These sections were then prepared for MALDI imaging as previously described.<sup>[116]</sup> Briefly, following deparaffinization and citric acid antigen retrieval (10 mM citric acid, pH = 6), ADS sections were digested with trypsin gold (Promega, Madison, WI), followed by incubation in a humidified chamber at 37 °C for 2 h. Internal calibrants<sup>[117]</sup> and  $\alpha$ -cyano-4-hydroxycinnamic acid matrix (CHCA, Bruker Daltonics) was then overlaid onto the ADS section using an ImagePrep station (Figure 2).

Mass spectra were acquired using an UltrafleXtreme MALDI-TOF/TOF instrument (Bruker Daltonics) with FlexControl (version 3.4) and FlexImaging software (version 4.0) in positive reflectron mode. The data was acquired at 50  $\mu\text{m}$  lateral resolution with a laser frequency of 2 kHz over an  $m/z$  range of 800–4500 Da (Figure 2). Following data acquisition, CHCA matrix was removed using 70% ethanol before the ADS sections were H&E stained and scanned using a Nanozoomer (Hamamatsu,

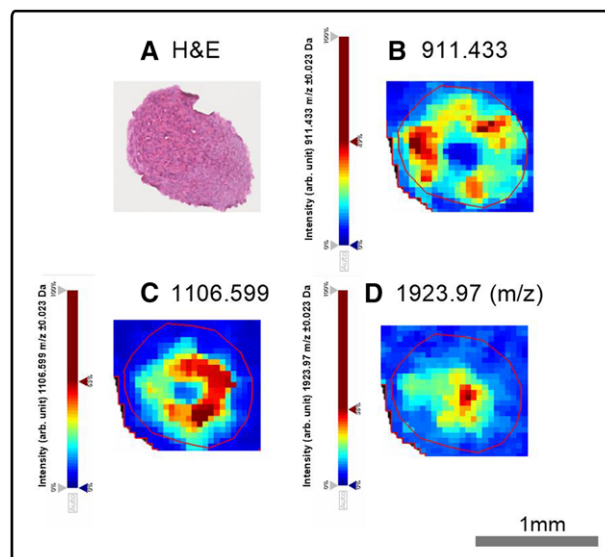


**Figure 3.** MALDI MSI analysis of peptide abundance in untreated ascites derived cancer spheroids. Specific  $m/z$  values, which correlate with distinguished regions of the ADS, were identified: A) H&E stain of ADS. B)  $m/z=911.433$ . C)  $m/z=1106.599$ . D)  $m/z=1923.97$

Shimadzu) (Figure 3). The spatial distribution of peptides was visualized using SCiLS lab software (version 2016a, GmbH, Bremen, Germany) in the form of ion intensity maps.

Using this approach, we were able to identify more than 200  $m/z$  values that were unique to the ADS structure. Of these, we identified 15  $m/z$  values whose intensity correlated with discriminative regions of the structure (proliferative, quiescent, and necrotic layers). We predict that this represents region specific protein abundance (Figure 3).

These preliminary experiments show that MALDI MSI can be effectively applied to ADS. However, this is with the caveat that these cells were maintained as monolayers before being encouraged to grow as 3D structures, which is expected to not accurately replicate pathological ADS. Into the future we aim to apply these techniques to a broader patient cohort, to investigate drug penetration in this context and to utilize this platform to investigate the molecular underpinnings of cancer progression and chemo response.

The techniques described above allow for spatially defined elucidation of analytes present in solubilized fractions of the MCTS or across slide mounted sections. Despite the limitations inherent with each of these techniques they have provided relevant information about protein expression, phospholipids, metabolism, and drug distribution in a spatially defined manner. Finally we have presented, for the first time, a MALDI MSI approach to investigate peptide abundance in aggregates formed from ascites derived primary ovarian cancer cells.

## 5. Outlook for Mass Spectrometry of Ovarian Cancer ADS

MCTS are typically used as a model of avascularized tumors, however, ovarian cancer is characterized by the presence of

spherical structures<sup>[45]</sup> suspended in ascites within the peritoneal cavity (ADS).<sup>[46,47]</sup> These structures represent an easily accessible source of primary cancer samples, which can provide information about a patient's individual disease. Ovarian cancer is characterized by initial response to chemotherapy<sup>[118]</sup> with high rates of relapse (above 50% within 5 years<sup>[119]</sup>). In addition to their role in metastasis,<sup>[120]</sup> ovarian cancer ADS have been shown to be more resistant to chemotherapy than monolayers in vitro<sup>[121,122]</sup> and therefore represent a chemo-resistant niche which can be the source of recurrence after chemotherapy.

The proteomic analysis of primary samples has the potential to provide vast amounts of information about progression, metastasis, and chemo response in this deadly gynecological malignancy. This represents an avenue to understanding the molecular underpinnings of a patient's individual disease facilitating a personalized approach to treatment and management of the disease.

In the pursuit of personalized cancer treatment, malignant ascites represent an easily accessible source of samples for the investigation of prognostic and predictive markers. Through analysis of the secretome of malignant ascites by 2D-DIGE coupled with MALDI MS, Huang et al. (2013)<sup>[123]</sup> found the protein ceruloplasmin to be significantly increased in the ascites of patients resistant to the first line treatment with platinum based chemotherapy. The identification of biomarkers which can predict chemotherapy response holds great potential for improving patient outcomes. However, this approach is yet to be applied to ovarian cancer ADS themselves despite predictions that these structures play a key role in the high rates of chemo resistance observed in this disease.<sup>[121,122]</sup> In addition to improving patient outcomes and reducing side effects, effectively predicting that a first line chemotherapy will be ineffective can facilitate the use of second line chemotherapies providing much needed information about the clinical effectiveness of these compounds.

## 6. Conclusion

Despite their discovery more than 40 years ago, MCTS models have only recently emerged as a powerful platform for in vitro research and drug testing. They have repeatedly been shown to better replicate and represent the avascularized tumors compared to the same cells grown as monolayers in regard to gene expression, antigen expression, proliferation, hypoxia, nutrient, waste, and gas diffusion gradients.<sup>[3–9,26,27,124–127]</sup>

The application of mass spectrometry analysis techniques to this biological model promises to provide new insight into cancer progression and treatment response. This includes identification of altered metabolism, cell–cell interactions and cell–ECM connections as well as antigen expression.<sup>[9,10,71,74,76,90,128]</sup> Although additional techniques are required to complement proteomics analysis of these structures, it represents a powerful foundation from which novel cancer research can be developed.

Recently, MSI has been used to investigate spatially defined peptide expression and drug penetration in MCTS.<sup>[99,111,113,129,130]</sup> The ability to image therapeutics and molecules in a spatially defined way provides a window into solid tumors and their response to therapy. This has the potential to lead to a

better understanding of cancer progression, pharmacokinetics, and the role of heterogeneous cell population in response to treatment.

In the context of ovarian cancer, being able to investigate the molecular underpinnings of a patient's individual disease in a rapid and informative manner through mass spectrometry analysis of ADS represents an avenue toward personalized cancer therapy. This platform has potential to identify effective treatments and/or molecular markers, which predict response to treatment. Personalized therapy is the way of the future for cancer treatment<sup>[131]</sup> and in particular in ovarian cancer, which is characterized by high recurrence rates and drug resistance, highlighting the need for better methods to inform appropriate treatment to improve patients outcome.

The development of novel and more sophisticated mass spectrometry techniques, including MSI, and their applications and implementation in clinical laboratories, will contribute significantly to making personal medicine a reality.

## Abbreviations

CLCA1, Calcium-activated chloride channel regulator 1; ECM, Extracellular matrix; H3D27, Histone 3 lysine 27; HNSCC, Head and neck squamous cell carcinoma; LCD, Laser capture microdissection; MALDI, Matrix assisted laser desorption/ionization; MCTS, Multicellular tumor spheroids; MSI, Mass spectrometry imaging; OS, Organotypic spheroids; PIP3, Phosphatidylinositol 3,4,5-trisphosphate; PRC2, Polychrome repressive complex 2

## Acknowledgements

M.K.O. and P.H. acknowledge the support provided by the OCRF and the NCRIS node for Tissue Imaging Mass Spectrometry.

## Conflict of Interest

The authors have declared no conflict of interest.

## Keywords

cancer, drug resistance, mass spectrometry-LC-MS/MS, mass spectrometry-MALDI-TOF, multicellular tumor spheroids, ovarian cancer

Received: August 28, 2017  
Revised: November 13, 2017

- [1] W. F. Scherer, J. T. Sylverson, G. O. Gey, *J. Exp. Med.* **1953**, 97, 695.
- [2] S. Nath, G. R. Devi, *Pharmacol. Ther.* **2016**, 163, 94.
- [3] G. Bergers, L. E. Benjamin, *Nat. Rev. Cancer* **2003**, 3, 401.
- [4] L. G. Griffith, M. A. Swartz, *Nat. Rev. Mol. Cell Biol.* **2006**, 7, 211.
- [5] J. B. Kim, *Semin. Cancer Biol.* **2005**, 15, 365.
- [6] F. Pampaloni, E. G. Reynaud, E. H. Stelzer, *Nat. Rev. Mol. Cell Biol.* **2007**, 8, 839.

- [7] R. M. Sutherland, *Science* **1988**, *240*, 177.
- [8] K. M. Yamada, E. Cukierman, *Cell* **2007**, *130*, 601.
- [9] H. R. Kumar, X. Zhong, D. J. Hoelz, F. J. Rescorla, R. J. Hickey, L. H. Malkas, J. A. Sandoval, *Pediatr. Surg. Int.* **2008**, *24*, 1229.
- [10] D. Pruksakorn, K. Lirdprapamongkol, D. Chokchaichamnankit, P. Subhasitanont, K. Chiablaem, J. Svasti, C. Srisomsap, *Proteomics* **2010**, *10*, 3896.
- [11] M. Vinci, S. Gowan, F. Boxall, L. Patterson, M. Zimmermann, W. Court, C. Lomas, M. Mendiola, D. Hardisson, S. A. Eccles, *BMC Biol.* **2012**, *10*, 29.
- [12] L. Bauer, *Applied Clinical Pharmacokinetics*, McGraw-Hill, New York **2014**.
- [13] J. I. Park, J. Lee, J. L. Kwon, H. B. Park, S. Y. Lee, J. Y. Kim, J. Sung, J. M. Kim, K. S. Song, K. H. Kim, *Transl. Oncol.* **2016**, *9*, 79.
- [14] C. M. Dowling, C. Herranz Ors, P. A. Kiely, *Biosci. Rep.* **2014**, *34*, e00126.
- [15] W. Mueller-Klieser, *Crit. Rev. Oncol. Hematol.* **2000**, *36*, 123.
- [16] B. Desoize, J. Jardillier, *Crit. Rev. Oncol. Hematol.* **2000**, *36*, 193.
- [17] W. Mueller-Klieser, *Am. J. Physiol.* **1997**, *273*, C1109.
- [18] K. Halfter, O. Hoffmann, N. Ditsch, M. Ahne, F. Arnold, S. Paepke, D. Grab, I. Bauerfeind, B. Mayer, *J. Transl. Med.* **2016**, *14*, 112.
- [19] A. Frankel, R. Buckman, R. S. Kerbel, *Cancer Res.* **1997**, *57*, 2388.
- [20] J. A. Aguirre-Chiso, *Nat. Rev. Cancer* **2007**, *7*, 834.
- [21] N. K. Haass, K. A. Beaumont, D. S. Hill, A. Anfosso, P. Mrass, M. A. Munoz, I. Kinjyo, W. Weninger, *Pigment Cell Melanoma Res.* **2014**, *27*, 764.
- [22] G. L. Semenza, *Crit. Rev. Biochem. Mol. Biol.* **2000**, *35*, 71.
- [23] P. Vaupel, F. Kallinowski, P. Okunieff, *Adv. Exp. Med. Biol.* **1990**, *277*, 895.
- [24] M. W. Dewhirst, Y. Cao, B. Moeller, *Nat. Rev. Cancer* **2008**, *8*, 425.
- [25] M. Tafani, L. Sansone, F. Limana, T. Arcangeli, E. De Santis, M. Polese, M. Fini, M. A. Russo, *Oxid. Med. Cell. Longev.* **2016**, 3907147.
- [26] P. Horan Hand, D. Colcher, D. Salomon, J. Ridge, P. Noguchi, J. Schlom, *Cancer Res.* **1985**, *45*, 833.
- [27] L. C. Windus, D. L. Kiss, T. Glover, V. M. Avery, *Exp. Cell Res.* **2012**, *318*, 2507.
- [28] M. Schmidt, C. J. Scholz, C. Polednik, J. Roller, *Oncol. Rep.* **2016**, *35*, 2431.
- [29] R. A. Davidowitz, L. M. Selfors, M. P. Iwanicki, K. M. Elias, A. Karst, H. Piao, T. A. Ince, M. G. Drage, J. Dering, G. E. Konecny, U. Matulonis, G. B. Mills, D. J. Slamon, R. Drapkin, J. S. Brugge, *J. Clin. Invest.* **2014**, *124*, 2611.
- [30] T. T. Chang, M. Hughes-Fulford, *Tissue Eng. Part A* **2009**, *15*, 559.
- [31] N. Masood, F. A. Malik, M. A. Kayani, *Asian Pac. J. Cancer Prev.* **2011**, *12*, 377.
- [32] F. P. Guengerich, *Chem. Res. Toxicol.* **2008**, *21*, 70.
- [33] F. Hirschhaeuser, H. Menne, C. Dittfeld, J. West, W. Mueller Klieser, L. A. Kunz Schughart, *J. Biotechnol.* **2010**, *148*, 3.
- [34] J. Friedrich, C. Seidel, R. Ebner, L. A. Kunz Schughart, *Nat. Protoc.* **2009**, *4*, 309.
- [35] X. Cui, Y. Hartanto, H. Zhang, *J. R. Soc. Interface* **2017**, *14*.
- [36] R. M. Sutherland, J. A. McCredie, W. R. Inch, *J. Natl. Cancer Inst.* **1971**, *46*, 113.
- [37] D. Antoni, H. Burckel, E. Josset, G. Noel, *Int. J. Mol. Sci.* **2015**, *16*, 5517.
- [38] H. L. Ma, Q. Jiang, S. Han, Y. Wu, J. Cui Tomshine, D. Wang, Y. Gan, G. Zou, X. J. Liang, *Mol. Imaging* **2012**, *11*, 487.
- [39] J. M. Yuhas, A. P. Li, A. O. Martinez, A. J. Ladman, *Cancer Res.* **1977**, *37*, 3639.
- [40] O. Schmal, J. Seifert, T. E. Schaffer, C. B. Walter, W. K. Aicher, G. Klein, *Stem Cells Int.* **2016**, 4148093.
- [41] A. I. Neto, C. R. Correia, M. B. Oliveira, M. I. Rial-Hermida, C. Alvarez-Lorenzo, R. L. Reis, J. F. Mano, *Biomater. Sci.* **2015**, *3*, 581.
- [42] J. W. Haycock, *Methods Mol. Biol.* **2011**, 695, 1.
- [43] F. Ruedinger, A. Lavrentieva, C. Blume, I. Pepelanova, T. Scheper, *Appl. Microbiol. Biotechnol.* **2015**, *99*, 623.
- [44] D. Gao, H. Liu, Y. Jiang, J. M. Lin, D. Gao, H. Liu, Y. Jiang, *TrAC Trends Analytical Chem.* **2012**, *35*, 150.
- [45] J. Liao, F. Qian, N. Tchabo, P. Mhawech-Fauceglia, A. Beck, Z. Qian, X. Wang, W. J. Huss, S. B. Lele, C. D. Morrison, K. Odunsi, *PLoS One* **2014**, *9*, e84941.
- [46] P. Holm-Nielsen, *Acta Pathol. Microbiol. Scand.* **1953**, *33*, 10.
- [47] A. T. Byrne, L. Ross, J. Holash, M. Nakanishi, L. Hu, J. I. Hofmann, G. D. Yancopoulos, R. B. Jaffe, *Clin. Cancer Res.* **2003**, *9*, 5721.
- [48] C. N. Landen, Jr., M. J. Birrer, A. K. Sood, *J. Clin. Oncol.* **2008**, *26*, 995.
- [49] J. M. Lee, P. Mhawech-Fauceglia, N. Lee, L. C. Parsanian, Y. G. Lin, S. A. Gayther, K. Lawrenson, *Lab. Invest.* **2013**, *93*, 528.
- [50] M. P. Iwanicki, R. A. Davidowitz, M. R. Ng, A. Besser, T. Muranen, M. Merritt, G. Danuser, T. A. Ince, J. S. Brugge, *Cancer Discov.* **2011**, *1*, 144.
- [51] E. C. Costa, A. F. Moreira, D. de Melo-Diogo, V. M. Gaspar, M. P. Carvalho, I. J. Correia, *Biotechnol. Adv.* **2016**, *34*, 1427.
- [52] A. Kalfe, A. Telfah, J. Lambert, R. Hergenroder, *Anal. Chem.* **2015**, *87*, 7402.
- [53] J. P. Freyer, R. M. Sutherland, *Cancer Res.* **1980**, *40*, 3956.
- [54] G. Mermelekas, J. Zoidakis, *Expert Rev. Mol. Diagn.* **2014**, *14*, 549.
- [55] A. Matta, R. Ralhan, L. V. DeSouza, K. W. Siu, *Mass Spectrom. Rev.* **2010**, *29*, 945.
- [56] P. Indovina, E. Marcelli, F. Pentimalli, P. Tanganelli, G. Tarro, A. Giordano, *Mass Spectrom. Rev.* **2013**, *32*, 129.
- [57] P. Alvarez-Chaver, O. Otero Estevez, M. Paez de la Cadena, F. J. Rodriguez-Berrocal, V. S. Martinez-Zorzano, *World J. Gastroenterol.* **2014**, *20*, 3804.
- [58] C. C. Yeh, C. H. Hsu, Y. Y. Shao, W. C. Ho, M. H. Tsai, W. C. Feng, L. P. Chow, *Mol. Cell. Proteomics* **2015**, *14*, 1527.
- [59] J. He, D. Shen, D. U. Chung, R. E. Saxton, J. P. Whitelegge, K. F. Faull, H. R. Chang, *Int. J. Oncol.* **2009**, *35*, 683.
- [60] M. Han, J. Dai, Y. Zhang, Q. Lin, M. Jiang, X. Xu, Q. Liu, J. Jia, *Oncol. Rep.* **2012**, *28*, 2233.
- [61] T. Akashi, Y. Nishimura, R. Wakatabe, M. Shiwa, T. Yamori, *Biochem. Biophys. Res. Commun.* **2007**, *352*, 514.
- [62] M. Aichler, B. Luber, F. Lordick, A. Walch, *World J. Gastroenterol.* **2014**, *20*, 13648.
- [63] C. R. Jimenez, H. M. Verheul, *Am. Soc. Clin. Oncol. Educ. Book* **2014**, e504.
- [64] R. Aebersold, M. Mann, *Nature* **2003**, *422*, 198.
- [65] W. M. A. Niessen, *Liquid Chromatography–Mass Spectrometry*, Taylor & Francis, Boca Raton, FL **2007**.
- [66] A. J. Alpert, *J. Chromatogr.* **1990**, *499*, 177.
- [67] A. J. Alpert, M. Shukla, A. K. Shukla, L. R. Zieske, S. W. Yuen, M. A. Ferguson, A. Mehlert, M. Pauly, R. Orlando, *J. Chromatogr. A* **1994**, *676*, 191.
- [68] R. Li, J. Huang, *J. Chromatogr. A* **2004**, *1041*, 163.
- [69] P. E. Feist, L. Sun, X. Liu, N. J. Dovichi, A. B. Hummon, *Rapid Commun. Mass Spectrom.* **2015**, *29*, 654.
- [70] R. Bjerkvig, A. Tonnesen, O. D. Laerum, E. O. Backlund, *J. Neurosurg.* **1990**, *72*, 463.
- [71] U. Rajcevic, J. C. Knol, S. Piersma, S. Bougnaud, F. Fack, E. Sundlisaeter, K. Sondenaa, R. Myklebust, T. V. Pham, S. P. Niclou, C. R. Jimenez, *Proteome Sci.* **2014**, *12*, 39.
- [72] S. Magdeldin, S. Enany, Y. Yoshida, B. Xu, Y. Zhang, Z. Zureena, I. Lokamani, E. Yaoita, T. Yamamoto, *Clin. proteomics* **2014**, *11*, 16.
- [73] L. Gaedtke, L. Thoenes, C. Culmsee, B. Mayer, E. Wagner, *J. Proteome Res.* **2007**, *6*, 4111.
- [74] W. He, Y. Kuang, X. Xing, R. J. Simpson, H. Huang, T. Yang, J. Chen, L. Yang, E. Liu, W. He, J. Gu, *J. Proteome Res.* **2014**, *13*, 2272.

- [75] K. M. McMahon, M. Volpato, H. Y. Chi, P. Musiwaro, K. Poterłowicz, Y. Peng, A. J. Scally, L. H. Patterson, R. M. Phillips, C. W. Sutton, *J. Proteome Res.* **2012**, *11*, 2863.
- [76] N. Musrap, A. Tuccitto, G. S. Karagiannis, P. Saraon, I. Batruch, E. P. Diamandis, *J. Biol. Chem.* **2015**, *290*, 17218.
- [77] R. H. Thomlinson, L. H. Gray, *Br. J. Cancer* **1955**, *9*, 539.
- [78] B. A. Teicher, *Cancer Metastasis Rev.* **1994**, *13*, 139.
- [79] P. Subarsky, R. P. Hill, *Clin. Exp. Metastasis* **2003**, *20*, 237.
- [80] S. Olk, G. Zoidl, R. Dermietzel, *Cell Motil. Cytoskeleton* **2009**, *66*, 1000.
- [81] T. Ohnishi, S. Hiraga, S. Izumoto, H. Matsumura, Y. Kanemura, N. Arita, T. Hayakawa, *Clin. Exp. Metastasis* **1998**, *16*, 729.
- [82] S. K. Calderwood, M. A. Khaleque, D. B. Sawyer, D. R. Ciocca, *Trends Biochem. Sci.* **2006**, *31*, 164.
- [83] M. V. Liberti, J. W. Locasale, *Trends Biochem. Sci.* **2016**, *41*, 211.
- [84] J. Poland, P. Sinha, A. Siegert, M. Schnolzer, U. Korf, S. Hauptmann, *Electrophoresis* **2002**, *23*, 1174.
- [85] M. E. Loewen, G. W. Forsyth, *Physiol. Rev.* **2005**, *85*, 1061.
- [86] J. Frede, S. P. Fraser, G. Oskay-Ozcelik, Y. Hong, E. Ioana Braicu, J. Sehouli, H. Gabra, M. B. Djamgoz, *Eur. J. Cancer* **2013**, *49*, 2331.
- [87] K. Fischer, P. Hoffmann, S. Voelkl, N. Meidenbauer, J. Ammer, M. Edinger, E. Gottfried, S. Schwarz, G. Rothe, S. Hoves, K. Renner, B. Timischl, A. Mackensen, L. Kunz-Schughart, R. Andreesen, S. W. Krause, M. Kreutz, *Blood* **2007**, *109*, 3812.
- [88] F. Ossendorp, M. Eggers, A. Neisig, T. Ruppert, M. Groettrup, A. Sijts, E. Mengede, P. M. Kloetzel, J. Neefjes, U. Koszinowski, C. Melief, *Immunity* **1996**, *5*, 115.
- [89] V. M. Braud, D. S. Allan, C. A. O'Callaghan, K. Soderstrom, A. D'Andrea, G. S. Ogg, S. Lazetic, N. T. Young, J. I. Bell, J. H. Phillips, L. L. Lanier, A. J. McMichael, *Nature* **1998**, *391*, 795.
- [90] X. Yue, J. K. Lukowski, E. M. Weaver, S. B. Skube, A. B. Hummon, *J. Proteome Res.* **2016**, *15*, 4265.
- [91] Y. Yuan, Y. C. Jiang, C. K. Sun, Q. M. Chen, *Oncol. Rep.* **2016**, *35*, 2499.
- [92] K. D. Konze, A. Ma, F. Li, D. Barsyte-Lovejoy, T. Parton, C. J. Macnevin, F. Liu, C. Gao, X. P. Huang, E. Kuznetsova, M. Rougie, A. Jiang, S. G. Pattenden, J. L. Norris, L. I. James, B. L. Roth, P. J. Brown, S. V. Frye, C. H. Arrowsmith, K. M. Hahn, G. G. Wang, M. Vedadi, J. Jin, *ACS Chem. Biol.* **2013**, *8*, 1324.
- [93] P. E. Feist, S. Sidoli, X. Liu, M. M. Schroll, S. Rahmy, R. Fujiwara, B. A. Garcia, A. B. Hummon, *Anal. Chem.* **2017**.
- [94] X. Shen, Y. Liu, Y. J. Hsu, Y. Fujiwara, J. Kim, X. Mao, G. C. Yuan, S. H. Orkin, *Mol. Cell* **2008**, *32*, 491.
- [95] K. J. Ferrari, A. Scelfo, S. Jammula, A. Cuomo, I. Barozzi, A. Stutzer, W. Fischle, T. Bonaldi, D. Pasini, *Mol. Cell* **2014**, *53*, 49.
- [96] K. H. Yoo, L. Hennighausen, *Int. J. Biol. Sci.* **2012**, *8*, 59.
- [97] S. A. Bapat, V. Jin, N. Berry, C. Balch, N. Sharma, N. Kurrey, S. Zhang, F. Fang, X. Lan, M. Li, B. Kennedy, R. M. Bigsby, T. H. Huang, K. P. Nephew, *Epigenetics* **2010**, *5*, 716.
- [98] H. Li, A. B. Hummon, *Anal. Chem.* **2011**, *83*, 8794.
- [99] X. Liu, E. M. Weaver, A. B. Hummon, *Anal. Chem.* **2013**, *85*, 6295.
- [100] O. J. Gustafsson, M. T. Briggs, M. R. Condina, L. J. Winderbaum, M. Pelzing, S. R. McColl, A. V. Everest-Dass, N. H. Packer, P. Hoffmann, *Anal. Bioanal. Chem.* **2015**, *407*, 2127.
- [101] P. E. Feist, S. Sidoli, X. Liu, M. M. Schroll, S. Rahmy, R. Fujiwara, B. A. Garcia, A. B. Hummon, *Anal. Chem.* **2017**, *89*, 2773.
- [102] J. O. Gustafsson, M. K. Oehler, A. Ruszkiewicz, S. R. McColl, P. Hoffmann, *Int. J. Mol. Sci.* **2011**, *12*, 773.
- [103] T. C. Rohner, D. Staab, M. Stoeckli, *Mech. Ageing Dev.* **2005**, *126*, 177.
- [104] J. Webster, D. Oxley, *Methods Mol. Biol.* **2012**, *800*, 227.
- [105] A. I. Nesvizhskii, *Methods Mol. Biol.* **2007**, *367*, 87.
- [106] J. H. Jungmann, R. M. Heeren, *J. Proteomics* **2012**, *75*, 5077.
- [107] T. Hiraide, K. Ikegami, T. Sakaguchi, Y. Morita, T. Hayasaka, N. Masaki, M. Waki, E. Sugiyama, S. Shinriki, M. Takeda, Y. Shibasaki, S. Miyazaki, H. Kikuchi, H. Okuyama, M. Inoue, M. Setou, H. Konno, *Sci. Rep.* **2016**, *6*, 29935.
- [108] M. T. Briggs, Y. Y. Ho, G. Kaur, M. K. Oehler, A. V. Everest-Dass, N. H. Packer, P. Hoffmann, *Rapid Commun. Mass Spectrom.* **2017**, *30*, 825.
- [109] Z. Gu, J. Wu, S. Wang, J. Suburu, H. Chen, M. J. Thomas, L. Shi, I. J. Edwards, I. M. Berquin, Y. Q. Chen, *Carcinogenesis* **2013**, *34*, 1968.
- [110] D. L. Holliday, V. Speirs, *Breast Cancer Res.* **2011**, *13*, 215.
- [111] X. Liu, A. B. Hummon, *Sci. Rep.* **2016**, *6*, 38507.
- [112] A. C. Niehoff, J. Grunebaum, A. Moosmann, D. Mulac, J. Sobbing, R. Niehaus, R. Buchholz, S. Kroger, A. Wiehe, S. Wagner, M. Sperling, H. von Briesen, K. Langer, U. Karst, *Anal. Chim. Acta* **2016**, *938*, 106.
- [113] G. J. LaBonia, S. Y. Lockwood, A. A. Heller, D. M. Spence, A. B. Hummon, *Proteomics* **2016**, *16*, 1814.
- [114] J. K. Lukowski, E. M. Weaver, A. B. Hummon, *Anal. Chem.* **2017**, *89*, 8453.
- [115] T. M. Allen, P. R. Cullis, *Adv. Drug Deliv. Rev.* **2013**, *65*, 36.
- [116] J. O. Gustafsson, M. K. Oehler, S. R. McColl, P. Hoffmann, *J. Proteome Res.* **2010**, *9*, 4315.
- [117] J. O. Gustafsson, J. S. Eddes, S. Meding, T. Koudelka, M. K. Oehler, S. R. McColl, P. Hoffmann, *J. Proteomics* **2012**, *75*, 5093.
- [118] M. Li, J. Yin, N. Mao, L. Pan, *Oncol. Rep.* **2013**, *29*, 58.
- [119] D. K. Armstrong, *Oncologist* **2002**, *7*, 20.
- [120] K. Shield, M. L. Ackland, N. Ahmed, G. E. Rice, *Gynecol. Oncol.* **2009**, *113*, 143.
- [121] S. Makhija, D. D. Taylor, R. K. Gibb, C. Gercel-Taylor, *Int. J. Oncol.* **1999**, *14*, 515.
- [122] S. L'Esperance, M. Bachvarova, B. Tetu, A. M. Mes-Masson, D. Bachvarov, *BMC Genomics* **2008**, *9*, 99.
- [123] H. Huang, Y. Li, J. Liu, M. Zheng, Y. Feng, K. Hu, Y. Huang, Q. Huang, *PLoS One* **2012**, *7*, e51256.
- [124] J. Friedrich, R. Ebner, L. A. Kunz-Schughart, *Int. J. Radiat. Biol.* **2007**, *83*, 849.
- [125] A. K. Ghosh, T. Hurd, F. Hildebrandt, *Am. J. Physiol. Renal. Physiol.* **2012**, *303*, F1225.
- [126] V. Harma, J. Virtanen, R. Makela, A. Happonen, J. P. Mpindi, M. Knuutila, P. Kohonen, J. Lotjonen, O. Kallioniemi, M. Nees, *PLoS One* **2010**, *5*, e10431.
- [127] J. Lopez, A. Poitevin, V. Mendoza-Martinez, C. Perez-Plasencia, A. Garcia-Carranca, *BMC Cancer* **2012**, *12*, 48.
- [128] M. M. Schroll, X. Liu, S. K. Herzog, S. B. Skube, A. B. Hummon, *Nutr. Res.* **2016**, *36*, 1068.
- [129] E. M. Weaver, A. B. Hummon, R. B. Keithley, *Anal. Methods* **2015**, *7*, 7208.
- [130] X. Liu, A. B. Hummon, *J. Am. Soc. Mass Spectrom.* **2015**, *26*, 577.
- [131] S. E. Jackson, J. D. Chester, *Int. J. Cancer* **2015**, *137*, 262.



1  
2  
3  
4  
5  
6  
7  
8  
9  
10  
11  
12  
13  
14  
15  
16  
17  
18  
19  
20  
21  
22  
23  
24  
25  
26  
27  
28  
29

This page is intentionally left blank

1  
2  
3  
4  
5  
6  
7  
8  
9  
10  
11  
12  
13  
14  
15  
16  
17  
18  
19  
20  
21  
22  
23  
24  
25

**CHAPTER 6: Monitoring Penetration  
and Accumulation of Novel CDK4/6  
Inhibitor in an Ovarian Cancer  
Multicellular Tumour Spheroid Model  
with MALDI Mass Spectrometry  
Imaging**

---

1       **Abstract:** The development of novel anti-cancer compounds represents an essential step in improving outcomes  
2       for patients. However, promising results in an *in vitro* setting often do not translate into effective patient  
3       treatment largely owing to *in vitro* models poorly replicating the *in vivo* environment. The multicellular tumour  
4       spheroid (MCTS) model seeks to overcome this issue in ovarian cancer by replicating several features of the solid  
5       tumour including inhibited penetration of some anti-cancer compounds. As the effectiveness of anti-cancer  
6       compounds is closely linked to its ability to reach all cells within the solid tumour, effective measurement of  
7       drug penetration into an *in vitro* model which replicates solid tumours represents an important step in  
8       demonstrating a novel compounds effectiveness. Here we utilise a novel sample preparation and MALDI mass  
9       spectrometry imaging approach to measure the penetration of a novel CDK4/6 inhibitor, CDDD2-94, into MCTS  
10      formed from ovarian cancer cells. Through this we demonstrate that this small molecule effectively penetrates,  
11      and accumulates, in the centre of the spheroid after 48 hours of exposure. This represents a powerful platform  
12      for relative quantification of drug penetration into a biologically relevant model of solid ovarian carcinomas.  
13

## 14   6.1. Introduction

15   For anticancer drugs to be effective they need to penetrate into the tumour mass and reach all  
16   tumour cells within [497]. Solid cancers, because of their rapid proliferation, distance themselves  
17   from vasculature resulting in significant barriers to drug delivery and efficacy. Increased  
18   tortuosity, restricted diffusion, high interstitial pressure, and acidic environmental pH can impact  
19   on drug delivery while hypoxia and other microenvironmental features influence cell death  
20   responses [498, 499].

21   Despite this, most studies on novel anticancer compounds are performed in two-dimensional cell  
22   culture, where high throughput analyses are easily performed [500], but numerous features of a  
23   solid tumour are not replicated. To overcome this, multicellular tumour spheroids (MCTS) have  
24   been employed extensively to investigate multiple features of cancer as they replicate several  
25   features of solid tumours [498, 499]. This *in vitro* model was first utilised in the 1980s [386] and  
26   has been used extensively in recent years to test a range of novel anti-cancer therapies [379, 498,  
27   501, 502].

28   Novel anticancer compounds which target molecular features of cancer have seen great interest in  
29   recent years [503]. However, while several are seen to be effective *in vitro*, significant reduction  
30   in effectiveness has been observed in *in vivo* and clinical settings [504]. The reasons for this are  
31   complex but, one contributing factor is inhibited penetration of molecular targeted treatments.

32   A recent publication investigated the penetration of a high molecular weight (mW) compound,  
33   DARPin-LoPE, which targeted HER2 [505]. This compound demonstrated cytotoxicity in two-  
34   dimensional cell culture of HER2 positive cells [506]. However, this compound only penetrated  
35   the outer layer of an ovarian cancer adenocarcinoma spheroid, while doxorubicin, a low mW anti-  
36   cancer compound, was seen to penetrate the entirety of the spheroid [505]. This correlated with  
37   significantly reduced anti-cancer activity of DAPRin-LoPE in HER2 positive spheroids compared  
38   to the same cell line grown in two-dimensional cell culture [505].

39   While complete penetration of a drug into a target tissue is essential for its efficacy, tracing the  
40   penetration into MCTS can represent a technical challenge. The paper discussed above utilised  
41   FITC labelled compounds to investigate penetration by microscopy, but such labelling has the  
42   potential to alter the action of the compound or impact its ability to enter the cell. Further, it

1 increases the mW of the compound which could be expected to reduce its penetration into a three-  
2 dimensional structure.

3 Here we have overcome this by utilising MALDI mass spectrometry imaging (MSI) to trace the  
4 penetration of a novel anti-cancer compound, CDDD2-94 [507], in ovarian cancer spheroids  
5 (Figure 4). The technique uses a matrix which co-crystallises with the sample before directing a  
6 laser at a discrete region facilitating ionisation and sublimation and results in a mass spectrum at  
7 each discrete location. When these mass spectra are analysed across a tissue section, they can  
8 provide spatially defined identification and relative quantification of analytes, including low mW  
9 anti-cancer compounds such as CDDD2-94.

10 CDDD2-94 is a 443.24Da small molecule inhibitor of cyclin independent kinase (CDK) 4 and  
11 CDK6, which has previously demonstrated efficacy against cancer cell growth [507]. CDK4 and  
12 CDK6 are essential proteins in the cell cycle which regulate the transition between G1 and S phase  
13 [508]. Treatments which inhibit CDK4/6 result in G1 cell cycle arrest [247] and inhibitors have  
14 been approved by the FDA for the treatment of metastatic breast cancer [509]. Despite the clinical  
15 success of this treatment approach in breast cancer, it has only been applied to a small number of  
16 other cancers, and its efficacy has not been comprehensively investigated in gynaecological  
17 cancers [508].

18 Here we present MALDI MSI data tracing the penetration of 2-94 into OV90 ovarian cancer  
19 spheroids derived from a poster presented at the 2017 Lorne Proteomics Symposium (Appendix  
20 X). OV90 spheroids were generated in culture and treated with 2-94 before being gelatine  
21 embedded, sectioned, and analysed using MALDI MSI. We observed time dependent penetration  
22 and accumulation of CDDD2-94 into the core of the spheroid section. This demonstrates  
23 techniques for the MALDI-MSI analysis of drug penetration of novel anti-cancer compounds into  
24 cancer spheroids and sets the foundation for further analysis of these compounds in this  
25 biologically relevant platform.

## 26 6.2. Methods and Materials

### 27 6.3.1. *PolyHEMA Coating*

28 PolyHEMA (Sigma-Aldrich) was prepared by adding 30mg/mL to 95% ethanol and incubating  
29 overnight at 37°C on a rotating platform in the dark. 50uL of this solution was added to each well  
30 of a 96 well round bottom plate (Corning) and left to dry with the lid off in a tissue culture hood  
31 with the fan, light, and UV off for 72 hours. Plates were then stored at 4°C for less than 3 months  
32 before use.

### 33 6.3.2. *Culturing OV90 Spheroids:*

34 OV90 cells were purchased from ATCC and used within 10 passages. They were cultured in RPMI  
35 media with 10% FCS and 1% penicillin/streptomycin. Once confluent they were transferred to  
36 PolyHEMA coated 96 well, round bottom plates at 4x10<sup>6</sup> cells per well. After 6 days one defined  
37 sphere formed in each well and was treated with the compound of interest.

1 **6.3.3. CDDD2-94 Treatment**

2 CDDD2-94, dissolved in DMSO, was prepared in RPMI media for a final treatment concentration  
3 of 5 $\mu$ M. For controls, an equal volume of DMSO alone was mixed with RPMI and added to cells.  
4 Spheroids were harvested after 8, 24 and 48 hours of treatment.

5 **6.3.4. Gelatine Embedding and Sectioning**

6 Spheroids were extracted from the well using a P100 pipette with the tip cut. Multiple spheroids  
7 from the same treatment group (5-10) were collected in a single Eppendorf tube and isolated in the  
8 bottom of the tube by a 5 second spin in a microcentrifuge. The media was removed, and spheroids  
9 were washed twice with PBS. Spheroids were collected in a P100 pipette with the tip cut off and  
10 placed onto a thin metal spatula. Paper tissue was used to carefully remove as much surrounding  
11 PBS as possible before spheroids were embedded in gelatine.

12 Gelatine was prepared at 350mg/mL and kept at 60°C on a heating block. 1mL of gelatine was  
13 added to the bottom of a 24 well plate well. The spatula with spheroids sitting on it was quickly  
14 dipped in the gelatine and the spheroids were transferred. An additional 500 $\mu$ L of melted gelatine  
15 was added to the top and allowed to solidify at room temperature. These gelatine blocks were then  
16 frozen at -80°C overnight before sectioning but could be stored for extended periods of time at -  
17 80°C.

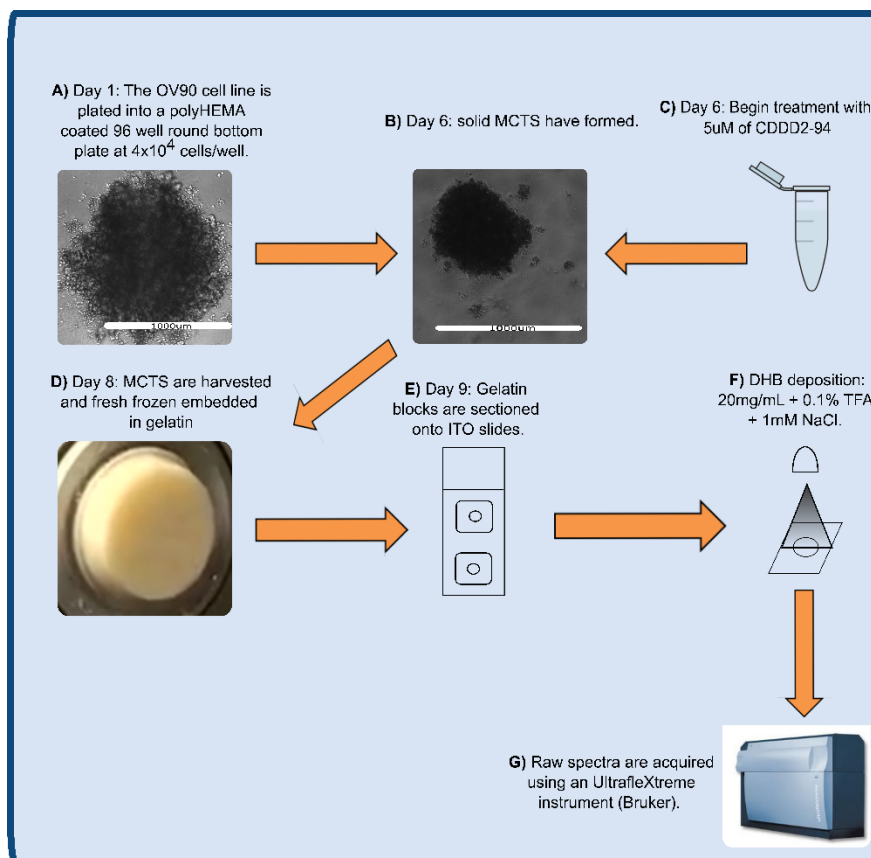
18 Frozen gelatine blocks containing spheroids were removed from their wells and mounted in a  
19 cryotome at -20°C. They were carefully sectioned at 5 $\mu$ M thickness onto glass slides and spheroid  
20 completeness was checked on a microscope. Once a spheroid was identified a full section was  
21 placed onto an ITO slide for subsequent MALDI-MSI analysis while consecutive sections were  
22 placed onto glass slides and underwent H&E staining [510].

23 **6.3.5. MALDI-MSI Data Acquisition**

24 Teach marks were applied to each corner of the ITO slide using a Tipp-Ex water based white out  
25 before scanning at 2400dpi (CanoScan 5600 F, Canon, Thailand). Following this, the matrix was  
26 applied to the tissue using an ImagePrep station (Bruker Daltonics) (20mg/mL 2,5-  
27 Dihydroxybenzoic acid (DHB), 0.1% trifluoroacetic acid (TFA), 1mM NaCl). Data was then  
28 acquired using a UltrafleXtreme MALDI TOF/TOF instrument (Bruker Daltonics) (This process  
29 is described in detail in M. Acland (2022) (Under Review)).

30 **6.3.6. MALDI-MSI Data Analysis**

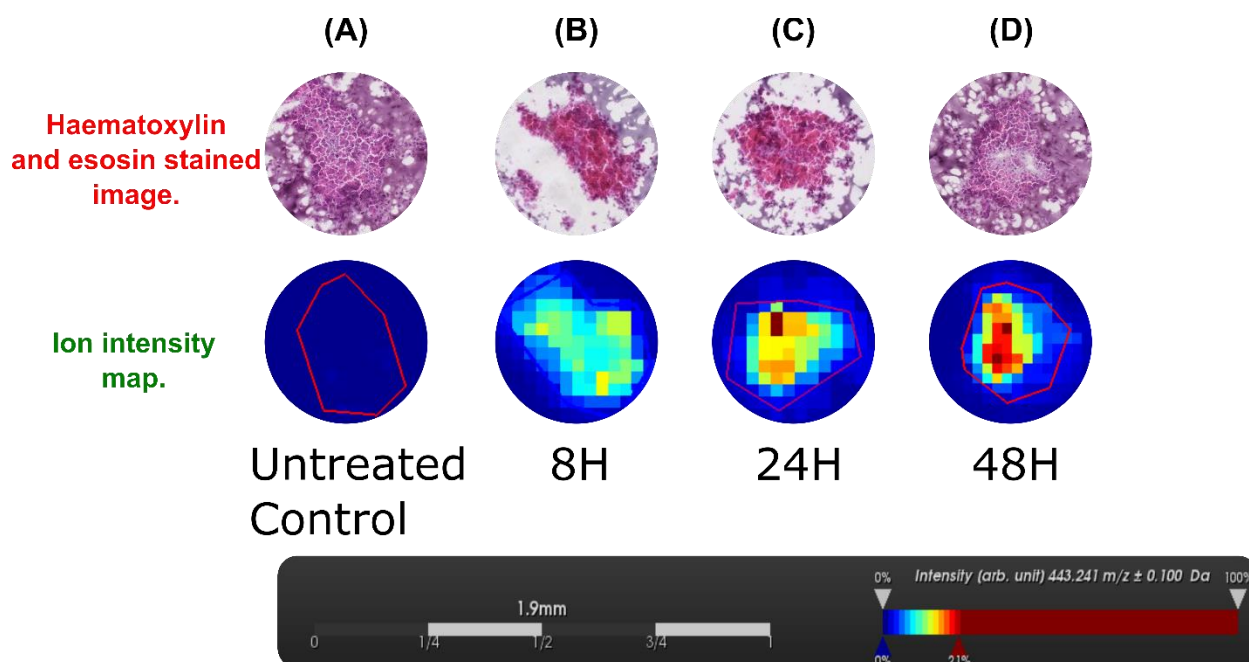
31 Once MALDI data was acquired, the slide was scanned at 20X objective using a Nanozoomer and  
32 Fleximaging software was used to co-register the identified spheroid regions with the MALDI  
33 spectra. The data was then imported into the SCiLs lab software and the  $m/z$  relating to CDDD2-  
34 94 (443.23Da) was selected to visualise the spatial distribution of our compound of interest. (This  
35 process is described in detail in Chapter 2)).



1  
 2 **Figure 4:** Workflow for MALDI MSI analysis of ovarian cancer MCTS. (A) OV90 cells are plated in  
 3 polyHEMA coated, 96 well, round bottom plates at  $4 \times 10^4$  cells/well. (B) After 6 days in culture solid  
 4 MCTS have formed. (C) MCTS are treated with  $5 \mu\text{M}$  of CDDD2-94. (D) After 2 days of treatment MCTS  
 5 are harvested and embedded into gelatine. (E) Gelatine blocks are sectioned onto ITO slides. (F) DHB  
 6 matrix is deposited onto gelatine sections containing MCTS. (G) Data was acquired on the UltrafleXtreme  
 7 (Bruker) MALDI instrument.

8 **6.3. Results**

9 MALDI-MSI analysis of the analyte relating to CDDD2-94 ( $443.23 \text{m/z}$ ) identified varying levels  
 10 of penetration of the compound into the spheroid over the treatment time course (Figure 5). In  
 11 untreated spheroids this analyte was not present. After 8 hours it can be visualised at the outer edge  
 12 of the spheroid while at 24 hours it has penetrated the centre of the structure. After 48 hours we  
 13 observed a significant accumulation of the analyte in the centre of the structure.



1  
2 **Figure 5:** MALDI MSI analysis of OV90 spheroids targeting the analyte at 443.24 Da which relates to the  
3 small molecule inhibitor of CDK4/6; CDDD2-94. The top row represents haematoxylin and eosin staining  
4 of OV90 Spheroids while the bottom row is consecutive sections of the same spheroid analysed by MALDI  
5 MSI. (A) Untreated control, (B) after 8 hours of treatment CDDD2-94 is seen to penetrate the entire  
6 spheroid, (C) after 24 hours 2-94 begins to accumulate in the centre of the spheroid, (D) after 48 hours  
7 CDDD2-94 has accumulated in the spheroids core.

8  
9 **6.4. Discussion**

10 Here we present data, which demonstrates our ability to trace the penetration of a novel anti-cancer  
11 compound into ovarian cancer spheroids using MALDI-MSI. This versatile method has potential  
12 for broader use as part of anti-cancer drug screening processes for tracing the penetration and  
13 accumulation of the compound in the biologically relevant MCTS model.

14 MALDI-MSI can visualise analytes across a wide mass range which has the potential to identify  
15 metabolic products of the compound in question. This includes active and inactive forms of the  
16 compound reflecting metabolism and inactivation processes in the cell respectively. Further,  
17 analytes relating to biological molecules, including proteins and metabolites, can also be identified  
18 with MALDI-MSI. This holds the potential to simultaneously visualise drug accumulation,  
19 metabolism/inactivation, and biological impact on the same tissue section.

20 This has been recently demonstrated by X. Tian, et al (2019) who investigated the metabolomic  
21 profile of HCT-116 colorectal cancer spheroids treated with irinotecan using a novel single probe  
22 MSI approach [511]. Through the application of machine learning algorithms, they demonstrated  
23 that they could divide MS signals into three distinct groups: outer layer, inner layer and background  
24 and use this approach to investigate altered metabolomic profiles in response to irinotecan  
25 treatment.

1 While MALDI-MSI investigations of MCTS, and their treatment with novel anti-cancer  
2 compounds, holds great potential there are several challenges which have prevented the  
3 widespread use of this technology. This includes difficulty in handling samples, limited resolution  
4 and mass accuracy of the technique compared to other MS approaches and the limited range of  
5 masses which can be investigated using this technique.

6 While MALDI-MSI is a versatile technique which can provide spatially defined molecular  
7 information, its application to MCTS is hampered by its limited resolution. In the above data we  
8 used a 50 $\mu$ m raster size which we have optimised to be as small as possible while still providing  
9 sufficient molecular information. However, in a spheroid which is, at most, 1mm in diameter, this  
10 limits the spatial details that we can acquire from this section.

11 Finally, due to the application of low molecular weight matrix to facilitate the ionisation and  
12 sublimation required for MALDI-MSI, there is significant interference in particular mass ranges  
13 depending on the matrix of choice. This can be overcome to some degree by selecting the  
14 appropriate matrix for purpose but prevents a truly holistic investigation of multiple classes of  
15 molecules on the same section.

16 Here we present a method for MALDI-MSI analysis of drug penetration into MCTS which has  
17 potential as part of novel drug testing platforms. This versatile technique could feasibly be used to  
18 incorporate the investigation of multiple molecular classes, including metabolites, drugs, drug  
19 products and proteins, on a single tissue section. However, challenges in sample preparation, image  
20 resolution and MS sensitivity remain significant barriers to the employment of MALDI-MSI in  
21 MCTS drug testing platforms more widely

22

23

24

25

26

27

28

29

30

31

32


33

34




1 6.1. Supplementary File


## MALDI mass spectrometry imaging of multicellular tumour spheroids: an improved platform for testing novel anti cancer compounds



THE UNIVERSITY  
of ADELAIDE



Future  
Industries  
Institute



LIFE  
PROTEOMICS

Mitchell Acland<sup>1,2</sup>, Noor Lokman<sup>3</sup>, Mark Condina<sup>4</sup>, Manuela Klingler-Hoffmann<sup>4</sup>, Shudong Wang<sup>5</sup>  
Martin Oehler<sup>3,6</sup>, Peter Hoffmann<sup>4</sup>

1. Adelaide Proteomics Centre, School of Biological Sciences, University of Adelaide, Adelaide, South Australia, Australia.  
2. Institute of Photonics and Advanced Sensing (IPAS), University of Adelaide, Adelaide, South Australia, Australia.  
3. Discipline of Obstetrics and Gynaecology, School of Medicine, Robinson Research Institute, University of Adelaide, Adelaide, Australia.  
4. Future Industries Institute, University of South Australia, Adelaide, South Australia, Australia.  
5. Centre for Drug Discovery and Development, University of South Australia, Adelaide, Australia  
6. Department of Gynaecological Oncology, Royal Adelaide Hospital, Adelaide, South Australia, Australia

### 1. Introduction

- Ovarian cancer is characterised by initial response to chemotherapy followed by relapse in 70% of cases.
- The testing of new anti cancer drugs is generally performed on adherent monolayer cell culture which has repeatedly shown to inadequately replicate the *in vivo* situation.
- Multicellular tumour spheroids (MCTS) are an *in vitro* model which replicates many aspects of the avascularised tumour including gas, waste and nutrient gradients (Figure 1), cell-cell and cell-matrix connections, gene expression and protein abundance.
- We have established an MCTS model which is compatible with MALDI imaging MS providing spatially defined information about drug penetration and accumulation in these structures.
- Here we investigate the penetration and accumulation of a novel anti cancer compound referred to here as 'compound A' into MCTS formed from the ovarian cancer cell line, OV90.

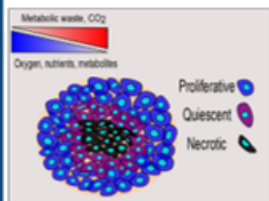
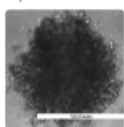


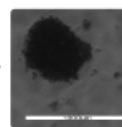
**Figure 1: A cross section of the MCTS showing waste, gas, nutrient and metabolite gradients.**  
These conditions give rise to different cellular states throughout the MCTS. The central core is comprised of microcirc cells, quiescent cells reside in the intermediate regions while cells on the periphery are proliferative. This has profound impacts on gene expression, protein abundance and response to treatment and replicates conditions present in avascularised tumour. This supports the MCTS model as a highly relevant model structure for testing anti cancer compounds and for cancer research in general.

### 2. Methods

**A) Day 1:** The OV90 cell line is plated into a polyHEMA coated 96 well round bottom plate at  $4 \times 10^4$  cells/well.

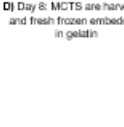


**B) Day 6:** solid MCTS have formed.




**C) Day 6:** Begin treatment with  $5 \mu\text{M}$  of compound A


**D) Day 8:** MCTS are harvested and fresh frozen embedded in gelatin



**E) Day 9:** Gelatin blocks are sectioned onto ITO slides.



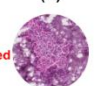
**F) DHB deposition:**  $20\text{mg/mL} + 0.1\% \text{ TFA} + 1\text{mM NaCl}$



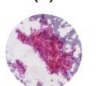
**G) Raw spectra are acquired** using an UltraflexXtreme instrument (Bruker).

### 3. Results


**(A) Untreated Control**




**(B) 8H**



**(C) 24H**

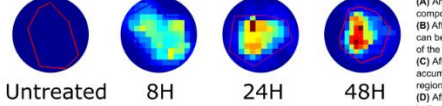



**(D) 48H**



**Figure 3: MALDI imaging MS tracing the penetration and accumulation of compound A ( $443.24 \pm 0.10\text{Da}$ ) into OV90 MCTS over 48 hours.**

Raw spectra were loaded into SCLIS lab (v2016b) and processed for baseline subtraction and normalization to total ion count. Ion intensity maps were generated for the peak at  $443.24 \pm 0.10\text{Da}$  which relates to the mass of the parent drug, 2-94. (A) An untreated control MCTS where no compound can be seen. (B) After 8 hours of treatment the compound can be seen to penetrate though the entirety of the MCTS. (C) After 24 hours there is some increased accumulation of the compound in distinct regions of the MCTS. (D) After 48 hours accumulation of the compound in the centre of the MCTS can be seen.





### 4. Summary

- MCTS are a biologically relevant model structure which replicates avascularised tumours.
- We have established a method for growing, treating and investigating the penetration and accumulation of a novel anti cancer compound in these structures using MALDI imaging MS.
- The compound is seen to fully penetrate the MCTS structure after 8 hours. After 48 hours an accumulation can be seen in the central region of the structure.


### 5. Future Directions

- To validate these results and quantify drug accumulation using microdissection followed by LC-MS/MS.
- To investigate the spectra for metabolites of the drug in order to trace their spatial localisation and accumulation.
- To apply these methods to other anti cancer compounds and to MCTS formed from primary cells to more closely replicate the *in vivo* situation.

**References**

- M. Acland, P. Mittal, N. Lokman, M. Klingler-Hoffmann, M. Oehler, P. Hoffmann, Mass Spectrometry Analyses of Multicellular Tumour Spheroids, Proteomics Clin Appl., accepted article.

adelaide.edu.au



2  
3  
4  
5

Supplementary Figure 1: Poster presented at the 2017 Lorne Proteomics Symposium.

1  
2  
3  
4  
5  
6  
7  
8  
9  
10  
11  
12  
13  
14  
15  
16  
17  
18  
19  
20  
21  
22  
23  
24  
25  
26  
27  
28

This page is intentionally left blank

1  
2  
3  
4  
5  
6  
7  
8  
9  
10  
11  
12  
13  
14  
15  
16  
17  
18  
19  
20  
21  
22  
23  
24  
25  
26

# CHAPTER 7: DISCUSSION

---

# 7. Discussion

Ovarian cancer is a complex and multifaceted disease which has, over the last four decades, resisted concerted efforts by the medical and scientific community to improve patient outcomes [209]. HGSOC, as the most common epithelial ovarian cancer, and the deadliest gynaecological malignancy, remains a major target of scientific investigation [2].

Here we present a comprehensive MS based investigation of the molecular features and characteristics of HGSOC. We focused our investigation on three key aspects of its HGSOC: precancerous development, resistance to standard CBP treatment, and the role of MCTS in malignant progression. Through the development of specialised samples preparation and MS techniques to investigate these key aspects of HGSOC, coupled with the identification of important proteins, metabolites and signalling pathways which underpin these events, this research sets the foundation for a greater understanding of the molecular features of HGSOC development, response to treatment and malignant progression.

## 7.1. Technical Limitations

MS based approaches have the power to identify, and relatively quantify, molecular features of ovarian cancer. This results in unbiased data, without the need for preselected molecular targets, which provides a deep coverage of the molecular class of interest. While proteomics remains the most employed MS based technology for investigating cancer, metabolomics and MSI are establishing themselves as powerful complimentary techniques. The flexibility of MS based technology to investigate multiple classes of molecules has the potential to provide a comprehensive picture of the molecular landscape of ovarian cancer.

However, the MS based investigation of HGSOC, and cancer in general, have several shortcomings and face challenges for their broad application into the future. This includes technical challenges, in sample preparation, data acquisition, data analysis and translating MS data into biologically relevant information.

### 7.1.1 *Molecules with Diverse Chemical Properties*

MS analysis required significant sample preparation steps to ensure that the sample is fractionated and able to be ionised; two essential steps in MS data acquisition [512]. This poses significant challenges in the measurement of molecules with diverse chemical properties. For example, it is very challenging to measure highly hydrophobic and highly hydrophilic molecules in a single experiment and, as a result, some proteins may be impossible to quantify by MS [513]. This is further exemplified in MALDI MSI which relies on interaction between the analyte and a matrix for effective ionisation and sublimation required for the acquisition of MS data with this technique.

The challenge associated with analysing molecules with diverse chemical properties is also seen in the MS based analysis of the metabolome.

MS based analysis of the metabolome faces challenges largely owing to the diverse range of chemical properties within the metabolome. While there are a diverse range of sample preparation

1 approaches to capture metabolites with different chemical features, there is no single method  
2 which can capture and analyse the entire metabolome at once [422].

### 3 **7.1.2 Data Acquisition**

4 One shortcoming which is common across MS analyses is that of ion suppression. This is a  
5 phenomenon where competition for ionisation efficiency in the ion source results in incomplete  
6 ionisation of some analytes. This results in the detected abundance being less than the absolute  
7 abundance and, in the case of already low abundance analytes, can result in the an analyte not  
8 being detected [512]. This is addressed through the, now standard, use of chromatography  
9 fractionation of the sample (as described above) to reduce complexity of the sample entering the  
10 ion source at any discrete time.

11 The major advantage of MALDI MSI is the ability to directly analyse samples in a spatially defined  
12 manner, such as tissue sections. However, this direct analysis without pre fractionation results in  
13 a less comprehensive analyte pattern challenged by multiple limitations including ion suppression  
14 [514, 515]. This is the major reason why MALDI MSI is not routinely used for comprehensive  
15 investigation of biological analytes. Instead, this technique can be effectively utilised for detection  
16 of a target molecule, such as a therapeutic agent, within a tissue section [516].

### 17 **7.1.3 Identification of Molecules of Interest**

18 MS analysis provides tens of thousands of data points reflecting the mass to charge ratio of analytes  
19 However, there are significant challenges in utilising this data to achieve confident identification  
20 of biological molecules. In the case of proteomics, this is further complicated by the  
21 incompatibility of full-length protein analysis on most MS platforms. To overcome this, proteins  
22 are treated with enzymes to digest them into peptides, most commonly using trypsin and lysozyme  
23 C. To fully characterise these peptides, tandem MS is employed. During this analysis selected  
24 peptides undergo further fractionation and subsequent MS analysis giving rise to amino acid level  
25 resolution, providing the sequence of the peptides. This requires complex data bases of known  
26 proteins and known fractionation patterns to accurately identify proteins. Progress in this space  
27 has been phenomenal and proteomics experiments now produce robust, reproducible, and  
28 standardised data [517].

29 While metabolites are typically much smaller than proteins, and do not require digestion, there is  
30 the further challenge of common metabolites having several isotopes with identical mass to charge  
31 ratios but significantly different structures, and subsequently, significantly different biological  
32 functions. As a result, it has been estimated that less than 2% of MS peaks observed in an  
33 untargeted MS metabolomics experiment are accurately identified [518]. This issue is further  
34 exacerbated by metabolomics data bases for identification from mass spectra being in their infancy  
35 in comparison to those for proteomics. These issues can be overcome through the use of reference  
36 standards spiked in during a metabolomics experiment [519]. However, this is a laborious process  
37 and is limited by the number of reference standards available for use. As a result, a standard  
38 metabolomics experiment identifies hundreds of metabolites from a human cell lysate while there  
39 are more than 100,000 predicted, expected and known human metabolites [420].

#### 1 **7.1.4 Deriving Biological Meaningful Data from Mass Spectrometry Data**

2 A standard global MS based proteomic experiment can routinely identify and quantify over 5,000  
3 proteins from a single sample. Translating this wealth of data into meaningful biological insights  
4 represents a major challenge and has been a limiting factor in the translation of proteomic  
5 investigations into biological insights and clinical impacts. When MS technology first facilitated  
6 the comprehensive investigation of a cellular proteome it was with the aim of identifying  
7 differentially abundant proteins of interest which were subsequently validated by other techniques,  
8 most commonly western blots. In modern proteomics investigations this has advanced to allow  
9 hypothesis generation and functional interpretation of proteomics results as explored throughout  
10 this thesis.

11 Primarily this is performed through the application of enrichment analysis where proteins  
12 differentially identified, or differentially abundant, between samples are associated with particular  
13 pathways to identify enriched pathways within the sample [520]. Shortcomings of this approach  
14 include the requirement for extensive data bases of proteins and their associated pathways to be  
15 developed for bioinformatic analysis. While there has been a concerted effort to achieve this in the  
16 case of proteomics over the last decade, similar data bases for metabolomics are in their infancy  
17 representing a barrier to understanding the biological relevance of metabolomic perturbations  
18 identified through MS analysis.

19 Further, as discussed above, identifying differentially abundant proteins is not sufficient to  
20 characterise the full complexity of molecular features of the cell. This represents a major barrier  
21 to functional analysis of MS data sets as a true picture can only be gained through the combination  
22 of several data sets including proteomics, metabolomics, genomics and the investigation of a range  
23 of post translational modifications [520]. More recently, the study of protein-protein interactions  
24 (interactomics) and proteolytic processing of proteins to create new isoforms (degradomics) have  
25 received greater attention and represent another layer of complexity to unravelling the molecular  
26 landscape of the cell or of disease [520].

27 In its current state, bioinformatics analyses face many challenges in combining the data from all  
28 these disparate sources to create an accurate and comprehensive picture of the molecular features  
29 of a cell or disease state. Overcoming this requires the development of extensive data bases and  
30 complex analysis platforms in conjunction with extensive meta-analysis of large numbers of  
31 studies to extract biologically meaningful information from this wealth of data.

#### 32 **7.2. Implications of the Paradigm Shift in the Origin of Ovarian Cancer**

33 First proposed in 2001, when dysplastic changes were observed in the fallopian tubes of women  
34 predisposed to developing ovarian cancer [100], that STIC represents the major precursor lesion  
35 of HGSOC is now widely accepted [75, 100, 521-523]. As discussed above, the demonstration that  
36 HGSOC arises from STIC in most cases [120, 121], and other precursors derived from the fallopian  
37 tube epithelium [122], represents a major paradigm shift in our understanding of the development  
38 of HGSOC. This goes some way to describe the striking difference in disease progress and  
39 treatment response observed between HGSOC and other cancers of the ovary [92]. This has  
40 implications for early detection, treatment, and our understanding of HGSOC development.

1 Despite the potential for MS to achieve molecular characterisation of precancerous lesions of  
2 HGSOC, there remain challenges in translating this into improved early detection and improving  
3 patient outcomes. This includes acquiring appropriate patient samples, accurately identifying the  
4 precancerous tissue regions, acquiring sufficient biological material for analysis, and correlating  
5 biological data from these lesions to cancer progression or clinical outcomes. In Chapter 3 we  
6 sought to overcome some of these challenges by performing global proteomic analysis on STIC  
7 derived from a patient without synchronous HGSOC. This type of sample is relatively rare, and  
8 our investigation provided novel molecular information about precancerous lesions in the early  
9 stages of their development. This has the potential to provide the foundation for deeper  
10 understanding of the early stages of STIC and how they transition from benign lesions in the  
11 fallopian tube into a deadly cancer. However, the small sample size and low protein identification,  
12 owing to the small amount of biological tissue available, makes it difficult to draw broad  
13 conclusions from this data alone. In Chapter 2 we outlined advances in sample preparation, LC-  
14 MS/MS and MALDI-MSI methodology which we hope to see utilised to effectively investigate  
15 these samples into the future. More recent work by Eckert, et al. (2019), combining similar sample  
16 preparation methodology with advanced LC-MS/MS technology, resulted in the identification of  
17 over 6000 proteins from STIC samples containing as little as 5000 cells [524].

18 One of the challenges relating to acquiring appropriate patient samples is the observation that many  
19 STIC identified in patients with established HGSOC represent metastatic implants rather than true  
20 precursor lesions [525]. This suggests that investigation of STIC in the absence of synchronous  
21 HGSOC is required to be confident of direct investigation of HGSOC origins. With this in mind,  
22 a multi-centre study was performed on 479 women with BRCA1/2 mutations who underwent  
23 bilateral risk reducing salpingo-oophorectomy [526]. This identified STIC in 11.9% of patients  
24 but did not identify any significant relationship between the presence of STIC and subsequent  
25 development of HGSOC. They hypothesise that this may be due to not all STIC developing into  
26 HGSOC, a theory which is supported by the observation that multiple, clonally independent, STIC  
27 lesions are often identified in an single patient [527]. In our own research it is also unclear if the  
28 STIC analysed in chapter 3 would go on to become HGSOC nor is there a reliable approach to  
29 predict this.

30 Another challenge to acquiring appropriate HGSOC precancerous samples is that STIC, and  
31 particularly their precursor, P53 lesions, are not easily identifiable, even by experienced  
32 pathologists and despite the advent of diagnostic criteria [528]. This was reflected in the  
33 multicentre study referenced above [526], which showed that extensive sampling of fallopian tubes  
34 identified double the number of STICs than identified by standard pathology sampling. We  
35 attempted to overcome this through annotation by an experienced pathologist, however, as  
36 described in the above publication [526], there is the potential for misidentification, or under  
37 identification, of STIC in these samples. In Chapter 2 we described a MALDI MSI based  
38 investigation of these samples to provide spatially defined molecular information. Through  
39 comparison of these samples, we identified over 70 analytes which were distinct between  
40 precancerous and healthy tissue representing preliminary results towards a MALDI MSI based  
41 identification of precancerous tissue in this context. Our lab has previously demonstrated the

1 efficacy of this approach in delineating between cancerous and non-cancerous endometrial tissue  
2 [529].

3 Other have identified molecular and genetic features of STIC which predict their likelihood of  
4 developing into HGSOE. For example, telomere shortening is observed in both STIC and P53  
5 signatures in the absence of HGSOE, and STIC genomically associated with HGSOE have been  
6 seen to have shorter telomeres [530]. Hypermethylation of histones is observed in STIC but not in  
7 P53 signatures suggesting that epigenetic alterations are an early event in the HGSOE  
8 carcinogenesis [531].

9 Further research is needed to better understand these structures and how HGSOE develops. This  
10 is particularly true for studies of the molecular features of STIC, including the proteome and post  
11 transcriptional modification relating to STIC development [115].

### 12 7.3. Overcoming Chemoresistance in Ovarian Cancer

13 Chemoresistance is a complex process which is still not fully understood. Further, the  
14 underpinning features of chemoresistance are heterogenous between patients, between tumours  
15 and over time. As discussed above, the temporal heterogeneity of chemoresistance is characterised  
16 by the concepts of inherent and acquired chemoresistance. For example, the formation of the  
17 MCTS structure, as investigated in Chapter 5, represents an inherent chemoresistant phenotype. In  
18 contrast, altered molecular features resulting from exposure to anti neoplastic agents, as explored  
19 in Chapter 4, represent examples of acquired chemoresistance. The observation that HGSOE  
20 typically responds to standard chemotherapy (CBP and Paclitaxel) before the patient relapses with  
21 resistant disease, shows that considering the molecular mechanisms of both inherent and acquired  
22 resistance, is essential for improving clinical outcomes in HGSOE.

23 While efforts continue to investigate the molecular and biological underpinnings of  
24 chemoresistance, there have been several advances in treatment approaches to overcome  
25 chemoresistance. This includes decades of optimising chemotherapy regimens and delivery  
26 methods (reviewed in [222]) and the development of novel anti-cancer agents. One such type of  
27 agent, CDK4/6 inhibitors, is discussed in chapter 6. As discussed above, targeted therapies  
28 represent an exciting avenue for treatment of ovarian cancer. However, there are several challenges  
29 including the requirement of the cancer in question to possess specific, targetable, characteristics  
30 [238], effective delivery of these compounds to cancer targets and inherent [242] and acquired  
31 resistance [238].

32 One example of an approach to identifying novel anti-cancer compounds utilised the TCGA  
33 ovarian cancer transcriptomics analysis of over 500 HGSOE samples [532]. By applying  
34 pRRophetic, a tool for correlating the drug sensitivity in cell lines with their related transcriptome  
35 for prediction of *in vivo* drug sensitivity [533, 534], to the TCGA data set they predicted the 50%  
36 inhibitory concentration (IC50) of 138 drugs for each of the 598 unique tumour transcriptomes in  
37 the dataset [532]. Through the comparison of predicted IC50 to survival time (utilised as a proxy  
38 for response to standard of care treatment with platinum and taxane standard chemotherapy), they  
39 identified 5 anti-cancer agents which were predicted to exhibit higher efficacy in standard of care  
40 resistant HGSOE. This was then validated in an independent *in vitro* and *in vivo* data set. The 5



1 compounds identified possessed a range of molecular targets and included 2 tyrosine kinase  
2 inhibitors, a PARP inhibitor, a MEK/ERK inhibitor and an anti-angiogenic agent. Many of these  
3 agents were already undergoing clinical trials, indicating the strength of this approach. One  
4 important shortcoming noted by the authors was the focus on single agent anti-cancer treatments  
5 and further work utilising similar predictive tools are expected to expand their investigation to  
6 include combination treatments.

7 In a second example of such an approach, researchers applied a bioinformatics approach to identify  
8 genes related to cisplatin chemoresistance in HGSOV [535] and identified the common thread of  
9 aberrant EGFR/ErbB2 signalling. This complex pathway has been seen to be involved in processes  
10 such as promoting cell survival, proliferation, differentiation, migration, invasion, adhesion and  
11 angiogenesis [536]. Sanguinarine inhibits these pathways and had not yet been investigated in  
12 ovarian cancer. They demonstrated, via immunohistochemistry, that, in a mouse xenograft model  
13 with cisplatin resistant ovarian cancer cells, combination treatment with Sanguinarine and cisplatin  
14 reduced signalling in the EGFR/ErbB2 pathway, and this correlated with decreased tumour mass  
15 [535].

16 One of the current, mostly unaddressed, challenges in treating cancer with targeted molecular  
17 therapies is intra tumoural heterogeneity (ITH), where cancers are made up of a heterogenous  
18 population of cells. This can result in resistance to treatment, particularly molecular targeted  
19 treatment [537-539].

#### 20 7.4. Mass Spectrometry Analyses of *in vitro* Models of Ovarian Cancer

21 To improve treatment of ovarian cancer research focuses on the discovery of diagnostic markers  
22 and the development of improved therapeutics. The continued development of pre-clinical models  
23 is essential to both avenues of research [540]. In chapter 5 we reviewed the MS-based analyses  
24 performed on MCTS, a commonly used *in vitro* model for ovarian cancer. Since the publication  
25 of this article in 2018, there have been significant advances in the field of pre-clinical models for  
26 ovarian cancer and mass spectrometry analysis of these structures.

27 It has been long established that ovarian cancer MCTS represent an effective *in vitro* model for  
28 replicating solid tumours. These structures are formed of mature cells, are self-assembling, free  
29 floating and form heterogenous layers resulting from oxygen and nutrient gradients [541]. These  
30 structures replicate numerous features of solid tumours including the tumour microenvironment  
31 [542, 543], greater resistance to treatment than cancer monolayers, and enrichment of tumour stem  
32 cells [544, 545].

33 There have been significant advances in the development of tumour spheroid models including  
34 ECM scaffolds [546] and co-culturing with diverse cell types [547]. These structures have been  
35 used to investigate how tumour features, which are replicated in MCTS, contribute to cancer  
36 progression and treatment resistance. This includes oxygen gradients, alterations in energy  
37 metabolism, an acidic microenvironment, decreased cell cycle progression, presence of CSCs, cell-  
38 cell and cell-ECM interactions (reviewed in [546]).

39 The application of microscopy techniques in conjunction with MSI has been utilised to provide  
40 greater biological context for the spatial identification of analytes. For example, J. Michalek, et al

1 (2019) combined MALDI MSI investigation of perifosine penetration into colon cancer spheroids  
2 with advanced microscopy targeting the proliferative marker Ki-67 [548]. By combining the  
3 results of these two different analysis techniques they identified alterations in proliferation which  
4 correlated with drug penetration. They built upon this by utilising markers for metastasis and  
5 apoptosis to demonstrate that inhibited penetration of perifosine contributed to tumour survival  
6 and increased expression of metastatic molecular markers [549].

7 While compounds such as perifosine can be detected using standard MALDI MSI, this is more  
8 difficult for platinum-based compounds such as CBP [550]. To overcome this, laser ablation ion  
9 coupled plasma mass spectrometry (LA-ICP-MS) is commonly utilised to provide high resolution  
10 images of elemental distribution in tissue sections [550]. Recently S. Markovic, et al. (2021)  
11 demonstrated that this technique is effective for tracing the penetration of CBP into MCTS derived  
12 from HT29 cells [551]. They demonstrated quantitative analysis of Pt accumulation using matrix  
13 matched gelatine standards. Further, in a single spheroid, Texas red coupled CBP was visualised  
14 via confocal fluorescence microscopy and LA-ICP-MS which demonstrated the accuracy of LA-  
15 ICP-MS for tracing penetration of CBP into this spheroid model.

16 Poorly vascularised solid tumours have distinct gradients of oxygen and nutrients where cells  
17 further from blood vessels have altered metabolic profiles. This has been seen to give rise to  
18 various pro cancer phenotypes including apoptosis resistance, adaptation to nutrient starvation,  
19 enhanced migration, invasion, and metastasis [552, 553]. This feature of solid tumours is clearly  
20 replicated in MCTS. H. Lulu, et al. (2019) utilised Fourier-transform ion cyclotron resonance (FT-  
21 ICR) MALDI MSI to investigate endogenous metabolites in breast cancer MCF-7 MCTS [554].  
22 They applied this technique to investigate the distribution of high energy adenosine phosphates  
23 and oxidized/reduced glutathione as these compounds are thought to be affected by nutrient and  
24 oxygen gradients [555]. They observed increased ATP in the outer regions while ADP and AMP  
25 were distributed uniformly across the spheroid. Further, the investigation of oxidised/reduced  
26 glutathione showed that both species existed predominantly in the centre of the MCTS, but their  
27 ratio was shifted toward the oxidised form in the centre of the spheroid indicating oxidative stress.

28 They expanded this analysis by identifying 5 metabolites (N-Acetyl-alpha-D-glucosamine 1-  
29 phosphate (GlcNAc-1-P), uridine monophosphate (UMP), uridine diphosphate (UDP), uridine  
30 triphosphate (UTP), uridine diphosphate N-acetylglucosamine (UDP-GlcNAc)) which most  
31 discriminated the outer layer (outer 50%) of the MCTS. Each of the identified metabolites are  
32 uridine phosphatases which agrees with the finding that hypoxia is associated with decreased  
33 abundance of uridine nucleosides [556, 557]. The 5 metabolites which most discriminate the  
34 inner layer of the spheroid (glucose-6-phosphate (G-6-P), cytidine 3', 5'-cyclic monophosphate  
35 (cCMP), cytidine monophosphate (CMP), cytidine diphosphate (CDP) and CDP-ethanolamine  
36 (CDP-Etn)) play a role in surface sialylation representing an adaptation to nutrient deprivation.

37 These studies show the utility of MALDI MSI, or complimentary MSI techniques for  
38 investigation drug penetration and biological features of MCTS, as explored in Chapters 5 and 6.  
39 Further, it demonstrates the power of combining multiple imaging techniques to better  
40 understand the biological impact of drug treatment on these structures.

## 1 7.5. Mass Spectrometry Analyses of Ascites Derived MCTS

2 In chapter 5 we demonstrated that ascites derived ovarian cancer spheroids could be investigated  
3 using MALDI MSI to reveal spatially defined proteomic features. In recent years there has been  
4 significant interest in analysing ovarian cancer ascites with mass spectrometry. This includes  
5 identifying ovarian cancer biomarkers within ascites [558-560], investigating the secretome of  
6 tumour associated macrophages in the ascites [561], correlation of ascites volume with sialylation  
7 [562] and the impact of ascites as a growth medium on the glycome of ovarian cancer cell lines  
8 [563]. However, there has been comparatively fewer investigations into the tumour spheroid  
9 structures contained within ovarian cancer ascites.

10 T. Worzfeld, et al. (2018) investigated ascites derived MCTS, tumour associated T-cells (TATs)  
11 and tumour associated macrophages (TAMs) from 8 patients with complimentary proteomic and  
12 transcriptomic analyses [560]. Their analysis of ascites derived MCTS revealed prominent  
13 expression of proteins involved in ECM remodelling. This includes synergistic actions of TAMs  
14 and MCTS to produce both structural ECM proteins and those which break down the ECM. They  
15 proposed that this is in line with the metastatic progression of ovarian cancer relying on sequential  
16 adhesion to mesothelial cells, invasion through the mesothelial layer and remodelling of the  
17 submesothelial matrix [559].

18 P. Mittal, et al. (2019) demonstrated a method for the isolation, FFPE embedding and MALDI  
19 MSI investigation of these MCTS acquired from patient ascites [564]. The ability to isolate these  
20 structures and embed them in a way which can be stored for extended periods of time with minimal  
21 impact of future analysis holds the potential for significant future research into these structures  
22 and their importance in ovarian cancer progression.

## 23 7.6. Importance of this work and future directions

24 Comprehensive MS based analyses of multiple molecular classes holds the potential to  
25 revolutionise diagnosis and treatment of HGSOE [418]. By developing a deeper understanding of  
26 the molecular underpinnings of ovarian cancer development, response to therapy and metastatic  
27 progression there is the potential to improve early detection, therapy and, ultimately, patient  
28 outcomes.

29 However, there remain several challenges to the MS based characterisation and investigation of  
30 the molecular features of HGSOE. This including access to relevant tissue, method development  
31 and integration of numerous molecular features. Currently there is a great focus in improving MS  
32 techniques, instrumentation, and data analysis methods [416] to overcome these challenges.

33 Here we have set the foundation for comprehensive MS based analyses of ovarian cancer through  
34 methods development and research insights. This includes the development of techniques for MS  
35 analysis of small, precancerous tissues and MCTS. Further to this, we provide insight into the  
36 molecular features of precancerous tissues and provide molecular characterisation of  
37 chemoresistance in ovarian cancer.

38 The methods described above outline how MS analysis of precancerous lesions of the fallopian  
39 tube can provide molecular insight into the development of HGSOE. Into the future this can be

1 built upon through the gathering of a large range of STIC samples from women who undergo risk  
2 reducing salpingo-oophorectomy. As outlined in the introduction, identification of STIC,  
3 especially at the early stages of development, remains challenging. We propose utilizing MALDI  
4 MSI to identify the molecular features which separate precancerous tissue from adjacent benign  
5 tissue to improve identification of STIC. Utilizing traditional genomic and histological methods  
6 for validation, this holds the potential to improve the accuracy of STIC identification for use in  
7 further studies. Further to this, through the application of longitudinal analyses of patient  
8 outcomes, the correlation of MS molecular analyses of STIC with the subsequent development of  
9 cancer has diagnostic potential in patients who undergo risk reducing salpingo-oophorectomy.

10 Chemoresistance remains the largest barrier to positive outcomes for patients with HGSOV. This  
11 highlights the need for diagnostic tools which can effectively characterise an individual's tumours  
12 with predictive power to advise treatment approaches. This is particularly true for ovarian cancer  
13 where a 'one size fits all' approach to treatment has been in place for over 30 years [208] and has  
14 resulted in only modest improvements in patient survival rates over that time. In Chapter 4 we set  
15 the foundation for molecular characterisation of a chemoresistant phenotype with the aim of  
16 predicting patient response to treatment. To expand upon this many samples are required from a  
17 range of tumour stages. It is imperative that samples are appropriately stratified to reflect the  
18 dynamic nature of HGSOV, particularly following initial chemotherapy treatment. Further to this,  
19 the combination of proteomics, metabolomics and other MS, and non-MS, techniques could be  
20 combined in a panomics approach to better capture the full complexity of the chemoresistant  
21 phenotype. This necessitates the further development of multi omic integrative data analysis  
22 platforms, such as 'omics analyst' [565], to consolidate these disparate data sources. Through this  
23 approach, it is hypothesised that a molecular pattern which is indicative of resistance to a particular  
24 treatment regime can be identified and utilised in the clinic to better advise treatment.

25 The search for a signature of chemoresistance is further complicated by structural features  
26 including MCTS located within the ascites. Identifying a molecular signature for chemoresistance  
27 must also extend to the molecular features inherent to these structures. For this reason, a panomics  
28 investigation of MCTS extracted from patients and directly investigated by MS holds the potential  
29 to provide deep molecular information about, what is proposed to be, a chemoresistant niche which  
30 can reseed ovarian cancer after chemotherapy treatment. Ascites are a readily available source of  
31 primary patient samples which, with the application of appropriate methodology, could be directly  
32 analysed after extraction to capture the molecular features inherent to the MCTS structure and the  
33 ascites in which they reside. While the clinical impact of this approach is limited by the observation  
34 that ascites only arise in advanced disease, it holds the potential to advise the use of novel anti-  
35 cancer compounds in patients who are identified as having a molecular signature indicative of  
36 resistance to standard treatment.

37 Finally, the future of ovarian cancer treatment is underpinned by the development of a vast number  
38 of novel anti-cancer compounds. This is being complimented by the development of complex and  
39 biologically relevant *in vitro* models against which a vast panel of compounds can be tested in a  
40 high throughput approach. This can be approached through the improvement of *in vitro* models  
41 such as MCTS. This includes incorporating more features of the *in vivo* environment including

1 multiple cell types, ECM, and appropriate chemical signals within the media. To achieve this, a  
2 deeper understanding of the molecular features of ovarian cancer, including features which are  
3 subtype and stage specific, is required to achieve the goal of a high throughput *in vitro* model  
4 which closely replicates the *in vivo* situation. It is hypothesised that this represents the pathway for  
5 improving the hit rate of new anti-cancer compounds and reinvigorating the development of new  
6 treatments for HGSOC.

7 Some of the challenges inherent to the above proposed approaches include heterogeneity between  
8 patients and between tumours in the same patient, acquiring sufficient information from small  
9 amounts of biological materials and combining the analysis of multiple molecular features into a  
10 single cohesive cellular molecular picture. MS based analyses seeks to overcome these challenges  
11 by providing rapid, deep, and clinically relevant information about an individual's cancer with  
12 sensitivity down to a single cell.

13 Improving outcomes for HGSOC patients requires nuanced surgical and pharmacological  
14 intervention advised by a comprehensive understanding of the biology and molecular features of  
15 this disease throughout its development and in response to treatment. The collection and analysis  
16 of vast amounts of MS data to identify the molecular features of this complex disease, subsequent  
17 patient stratification and development of anti-cancer compounds, facilitated through the  
18 development of advanced *in vitro* models, promises to unravel the intimidating complexity of  
19 ovarian cancer, and represents a powerful tool for improving outcomes for patients with this deadly  
20 disease.

21  
22  
23  
24  
25  
26  
27  
28  
29  
30  
31  
32  
33  
34

1  
2  
3  
4  
5  
6  
7  
8  
9  
10  
11  
12  
13  
14  
15  
16  
17  
18  
19  
20  
21  
22  
23  
24  
25  
26  
27

# Proteomic Analysis of Methylglyoxal Modifications Reveals Susceptibility of Glycolytic Enzymes to Dicarbonyl Stress

---



Article

# Proteomic Analysis of Methylglyoxal Modifications Reveals Susceptibility of Glycolytic Enzymes to Dicarbonyl Stress

Leigh Donnellan <sup>1</sup>, Clifford Young <sup>2</sup>, Bradley S. Simpson <sup>1</sup>, Mitchell Acland <sup>2</sup>, Varinderpal S. Dhillon <sup>1</sup>, Maurizio Costabile <sup>1,3</sup>, Michael Fenech <sup>1,4</sup>, Peter Hoffmann <sup>2</sup> and Permal Deo <sup>1,\*</sup> 

<sup>1</sup> Clinical and Health Sciences, Health and Biomedical Innovation, University of South Australia, Adelaide 5000, Australia; donly017@mymail.unisa.edu.au (L.D.); bradley.simpson@unisa.edu.au (B.S.S.); varinderpal.dhillon@unisa.edu.au (V.S.D.); maurizio.costabile@unisa.edu.au (M.C.); michael.fenech@unisa.edu.au (M.F.)

<sup>2</sup> Clinical and Health Sciences, University of South Australia, Adelaide 5000, Australia; clifford.young@unisa.edu.au (C.Y.); mitch.acland@gmail.com (M.A.); peter.hoffmann@unisa.edu.au (P.H.)

<sup>3</sup> Centre for Cancer Biology and SA Pathology, University of South Australia, Frome Road, Adelaide 5000, Australia

<sup>4</sup> Genome Health Foundation, North Brighton, Adelaide 5048, Australia

\* Correspondence: permal.deo@unisa.edu.au; Tel.: +61-8-83021189; Fax: +61-8-83022389

**Abstract:** Methylglyoxal (MGO) is a highly reactive cellular metabolite that glycates lysine and arginine residues to form post-translational modifications known as advanced glycation end products. Because of their low abundance and low stoichiometry, few studies have reported their occurrence and site-specific locations in proteins. Proteomic analysis of WIL2-NS B lymphoblastoid cells in the absence and presence of exogenous MGO was conducted to investigate the extent of MGO modifications. We found over 500 MGO modified proteins, revealing an over-representation of these modifications on many glycolytic enzymes, as well as ribosomal and spliceosome proteins. Moreover, MGO modifications were observed on the active site residues of glycolytic enzymes that could alter their activity. We similarly observed modification of glycolytic enzymes across several epithelial cell lines and peripheral blood lymphocytes, with modification of fructose biphosphate aldolase being observed in all samples. These results indicate that glycolytic proteins could be particularly prone to the formation of MGO adducts.

**Keywords:** methylglyoxal; glycation; post-translational modifications; MG-H1; CEL; CEA; proteomics; glycolysis



**Citation:** Donnellan, L.; Young, C.; Simpson, B.S.; Acland, M.; Dhillon, V.S.; Costabile, M.; Fenech, M.; Hoffmann, P.; Deo, P. Proteomic Analysis of Methylglyoxal Modifications Reveals Susceptibility of Glycolytic Enzymes to Dicarbonyl Stress. *Int. J. Mol. Sci.* **2022**, *23*, 3689. <https://doi.org/10.3390/ijms23073689>

Academic Editor: Bruno Pagano

Received: 17 February 2022

Accepted: 17 March 2022

Published: 28 March 2022

**Publisher's Note:** MDPI stays neutral with regard to jurisdictional claims in published maps and institutional affiliations.



**Copyright:** © 2022 by the authors. Licensee MDPI, Basel, Switzerland. This article is an open access article distributed under the terms and conditions of the Creative Commons Attribution (CC BY) license (<https://creativecommons.org/licenses/by/4.0/>).

## 1. Introduction

Post-translational modifications (PTMs) of proteins play an important role in biological events by regulating protein activity, interactions, stability and degradation [1]. PTMs can be derived through enzymatic processes via specific proteins responsible for the addition or removal of modifications including phosphorylation, methylation, acetylation and ubiquitination [1]. Moreover, PTMs can also be derived from non-enzymatic covalent modifications caused by electrophilic metabolites which react with the nucleophilic groups of arginine and lysine residues [2]. These electrophilic metabolites include acetyl-CoA, malonyl-CoA, 4-hydroxynonenal, glyoxal and methylglyoxal (MGO) [2,3]. MGO is a highly reactive 1,2-dicarbonyl compound formed as a by-product of glycolysis, in which intermediate triosephosphates (dihydroxyacetone phosphate and glyceraldehyde-3 phosphate) spontaneously degrade to generate MGO [4]. Because MGO is formed via glucose metabolism, it has been implicated in the pathogenesis of diabetic complications [5]. Moreover, MGO has been shown to be elevated in cancer cells following the metabolic rewiring from oxidative phosphorylation to glycolysis (Warburg effect) as their primary energy source [6]. Cellular MGO concentrations are maintained by the glyoxalase system.

MGO spontaneously reacts with glutathione, forming a hemithioacetal that is recognized by glyoxalase 1 (GLO1) and converted to S-D-lactoylglutathione. This is subsequently recognized by GLO2 and converted to the non-reactive D-lactate and glutathione [7]. MGO that is not sequestered by the glyoxalase system is able to react non-enzymatically to form methylglyoxal-hydroimidazolone (MG-H) isomers (1, 2 and 3) on arginine residues and carboxyethyl modifications on both arginine ( $N^{\epsilon}$ -carboxyethylarginine (CEA)) and lysine ( $N^{\epsilon}$ -carboxyethyllysine (CEL)) residues, amongst other less abundant modifications [8]. Collectively, these modifications, as well as those formed by other metabolites (glucose, glyoxal and 3-deoxyglucosone) are referred to as Advanced Glycation Endproducts (AGEs) [9].

Detection of MGO modifications has been largely achieved by measuring the total cellular contribution, rather than its presence on specific proteins [10]. This has primarily been performed utilising spectroscopic, immunochemical, chromatographic and mass spectrometric methods [11]. While these approaches are effective for detecting changes in the abundance of the modification which can be used to infer biological significance, it lacks the specificity to directly identify target proteins, which is crucial for elucidating underlying mechanisms. Unfortunately, measuring these modifications on specific proteins has proved challenging, due to their low abundance, low stoichiometry and heterogeneity, which makes their detection and characterisation difficult. Only a few studies have attempted to measure site-specific MGO modifications in mammalian cells with varying degrees of success [12–16]. Initial studies struggled to identify MGO modifications under control conditions, requiring the use of exogenous MGO to increase the concentration of these modifications [12–14,16]. While this is an effective approach for increasing the concentration of these modifications, these conditions may promote non-specific MGO modification of proteins or residues that would otherwise be unmodified under physiological or pathological conditions. Only recently has a comprehensive assessment of MGO modifications in HEK293T cells been applied. In this study, subcellular fractionation was applied to decrease sample complexity allowing for the identification of more than 600 MG-H modified proteins [14].

We recently applied bottom-up proteomics of whole WIL2-NS cell lysates to identify MGO modifications on mitotic proteins to gain a deeper understanding of the aneuploid activity of MGO (manuscript in preparation). While we were able to identify several mitotic proteins harbouring MGO modifications, we also identified an abundance of non-mitotic modified proteins. Therefore, using the entire inventory of MGO modified proteins identified from our previous study, we performed several types of enrichment analysis to identify proteins and/or pathways that are most susceptible to MGO. Samples were digested with ProAla (ProAla) or trypsin and analysed by LC-MS. In WIL2-NS cells, we identified over 500 proteins with MGO modifications. Enrichment analysis revealed glycolytic enzymes are targets for MGO modifications, several of which occur on residues involved in substrate interactions and are likely to affect their activity. Furthermore, we showed that the modification of glycolytic enzymes was not unique to WIL2-NS, but was also present in several epithelial cell lines and peripheral blood lymphocytes in vivo, with modification of fructose biphosphate aldolase being the most prevalent.

## 2. Results

### 2.1. Characterization of MGO Modified Proteins

To explore the potential impact of dicarbonyl stress (elevated MGO) on cellular function, we used a discovery proteomics approach on whole-cell extracts from WIL2-NS cells to investigate the modification of intracellular proteins following treatment with MGO. Cells were treated with 500  $\mu\text{mol/L}$  MGO for 24 h, which led to a 2.2- and 1.8-fold increase in MG-H1 and CEL, respectively, as shown by LC-MS analysis (Supplementary S1 Figure S1A,B). This relative increase is consistent with those observed in pathological conditions such as diabetes and thus less likely to cause non-specific modifications [8].

Preparation of whole-cell extracts for proteomics was performed using trypsin and ProAla in separate digests. Overall, we identified 519 modified proteins (Supplementary S2). The majority of modifications were identified in trypsin digests; however, the incorpora-



tion of ProAla in this study increased the number of identified MGO modification sites by approximately 25% (Supplementary S1 Figure S1C). Surprisingly, only 3.8% of the modification sites were detected in both ProAla and trypsin digested samples (Supplementary S1 Figure S1C). This was mostly due to ProAla modified peptides contributing to increased sequence coverage where the corresponding modification sites were undetected by trypsin; for example, as shown for CEL modification of K20 of Transgelin-2 and K496 of RNA-splicing ligase RtcB homolog (Figure 1A).

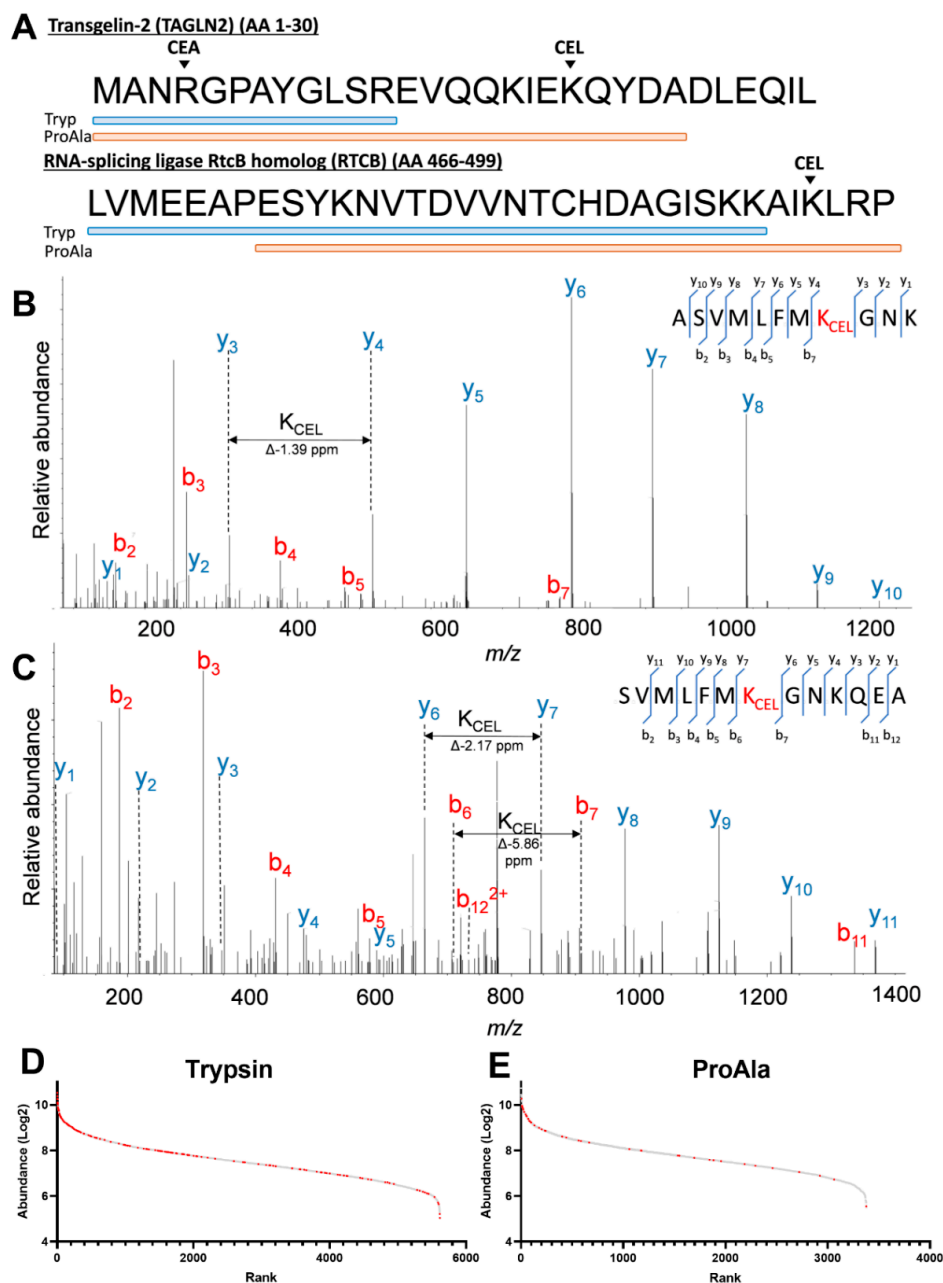


**Figure 1.** (A) Sequence coverage plot of Transgelin-2 (top) and RNA-splicing ligase RtcB homolog (bottom) protein sequences obtained from trypsin (blue) and ProAla (orange). (B,C) MS/MS spectra of a CEL modification on Glutaredoxin at K253 generated by trypsin digestion (B) and ProAla digestion (C) (see also Supplementary S1 Figure S2). (D,E) Abundance plot of proteins in trypsin digestion (D) and ProAla digestion (E) by rank. Grey spots represent unmodified proteins and red are those with MGO modifications.

Abundant y and b ions were observed for MGO-modified peptides produced in trypsin digested samples, which was particularly useful for identifying site-specific PTM residues (Figure 1B). Moreover, despite a C-terminus alanine or proline, abundant b and y ions could also be observed in ProAla digested samples (Figure 1C). Therefore, ProAla can be used in conjunction with trypsin to increase the identification rate of MGO modifications. To gain insight into what factors may influence the identification of MGO-modified proteins, we ranked the proteins from each digest based on their Log<sub>2</sub> abundance. In both digests, modification of proteins by MGO was more often observed in higher abundant proteins, with 45.8% and 61.9% of identifications occurring in the top 20% most abundant proteins for trypsin and ProAla, respectively (Figure 1D and Supplementary S1 Figure S1D). In the trypsin digest, 13 of the 20 most abundant proteins contained MGO modifications, consisting of 32 modification sites. A number of modifications per protein ranged from 1–19 sites, with beta-actin (ACTB) containing the highest number of MGO modification sites (Supplementary S1 Table S1 and Supplementary S1 Figure S1E).

## 2.2. Enrichment Analysis of MGO Modified Proteins

To explore the functional impact of MGO modifications in WIL2-NS cells, we performed enrichment analysis of biological processes, with the DAVID gene ontology tool using all MGO-modified proteins generated in this study. MGO-modified proteins showed over-representation in a diverse range of biological processes, including canonical glycolysis, translation initiation, regulation of cellular response to heat, mRNA splicing via spliceosome, amongst others (Table 1). Canonical glycolysis was the most enriched biological process (13.4-fold enrichment). Pathways with the largest number of MGO-modified proteins included cell-cell adhesion, mRNA splicing via spliceosome, translation initiation and protein folding, which all contained more than 20 modified proteins (Table 1). To further explore those pathways most impacted by MGO, we developed a protein–protein interaction network with STRING. KEGG pathway enrichment analysis was performed to determine pathways associated with the remaining clusters, which revealed glycolysis/gluconeogenesis, spliceosome and ribosome as the pathways most affected by MGO modifications (Figure 2). Glycolysis involves the conversion of glucose to pyruvate in ten enzyme-mediated steps. Remarkably, seven of the ten steps contained MGO-modified proteins, including glucose-6-phosphate isomerase (GPI), enolase 1/3 (ENO1/3), fructose bisphosphate aldolase A/C (ALDOA/C), triosephosphate isomerase (TPI), glyceraldehyde 3-phosphate dehydrogenase (GAPDH), phosphoglycerate kinase (PGK) and pyruvate kinase M (PKM) consisting of 20 modification sites in total (Figure 3A and Supplementary S3). The selective enrichment of glycolysis suggests MGO may modulate glucose metabolism by modifying enzymes involved in this pathway. To investigate the potential impact of MGO modifications on these proteins, we looked at the role of residues that were modified. ALDOA is a highly conserved glycolytic enzyme that catalyses the reaction that cleaves the aldol fructose 1,6-bisphosphate into triosephosphates dihydroxyacetone phosphate (DHAP) and glyceraldehyde 3-phosphate (G3P) [17]. Fructose 1,6-bisphosphate covalently binds to K229 followed by Schiff-base formation and carbon-carbon cleavage yielding triosephosphate formation [17]. K229, as well as K146 and R42, which non-covalently interact with the substrate in the active site, were modified by MGO, suggesting modification of these sites is likely to interfere with its interaction with fructose 1,6-bisphosphate (Figure 3B). All four modification sites observed on ALDOA were observed within the active site, despite the presence of numerous other lysine and arginine residing in the protein, suggesting modification of the active site residues was not random (Figure 3B). Strikingly, ENO1, another glycolytic enzyme that converts 2-phosphoglycerate to phosphoenolpyruvate [18], was shown to contain seven modification sites, three of which occurred on residues known to contain other PTMs (Figure 3C).

**Table 1.** Enrichment analysis for biological processes enriched with MGO modifications.

Biological Process	Count	Fold Enrichment	FDR	Genes
Canonical Glycolysis	9	13.4	$3.6 \times 10^{-5}$	<b>ALDOA, ALDOC, ENO1, ENO3, GPI, GAPDH, PGK1, PKM, TPI</b>
Gluconeogenesis	9	7.9	$1.6 \times 10^{-3}$	<b>ALDOA, ALDOC, ENO1, ENO3, GPI, GOT2, GAPDH, PGK1, TPI</b>
Translation initiation	22	6.2	$2.3 \times 10^{-8}$	<b>DDX3Y, DHX29, EIF3F, EIF4A1, PABPC1, PAIP1, RPL10, RPL13, RPL19, RPL21, RPL24, RPL31, RPL34, RPL4, RPS15, RPS2, RPS25, RPS26, RPS27A, RPS4X, RPS4Y1, RPS6</b>
Regulation of cellular response to heat	12	6.2	$4.7 \times 10^{-4}$	<b>FKBP4, HSP90AA1, HSP90AB1, HSPA8, HSPH1, NUP153, NUPL2, POM121C, POM121, RANBP2, RPA3, YWHAE</b>
Nucleosome assembly	17	5.5	$1.4 \times 10^{-5}$	<b>ATRX, H2AFX, ANP32A, ANP32B, DAXX, HMGB2, HIST1H1A, HIST1H2BB, HIST1H2BD, HIST1H2BK, HIST1H2BM, HIST1H3A, HIST1H4I, HIST2H2BE, HIST2H3PS2, H3F3A, NPM1</b>
Cell-cell adhesion	38	5.4	$1.3 \times 10^{-13}$	<b>ALDOA, AHNAK, CCT8, CKAP5, DDX6, DHX29, EEF1G, EEF2, EHD4, ENO1, FASN, FLNB, LASP1, HSP90AB1, HSPA8, HDLBP, HIST1H3A, HCFC1, LDHA, PARK7, PRDX1, PCBP1, PSMB6, PPME1, PKM, RAB1A, RANGAP1, RACK1, RPL24, RPL34, RPS2, RPS26, SPTAN1, SPTBN1, TAGLN2, YWHAB, YWHAE, YWHAZ</b>
mRNA splicing, via spliceosome	26	4.5	$2.4 \times 10^{-7}$	<b>ALYREF, CSTF2, DNAJC8, FUS, HSPA8, HNRNPC, HNRNPH1, HNRNPH2, HNRNPL, HNRNPM, HNRNPR, HNRNPU, NONO, PPIE, PABPC1, PCBP1, POLR2B, RBMX2, RBMX, SRSF2, SNRPB, SPEN, SF3B1, SF3B2, SYNCRIP, TRA2B</b>
Protein folding	21	4.5	$9.9 \times 10^{-6}$	<b>CANX, CCT2, CCT5, CCT8, FKBP4, FKBP5, GRPEL1, HSPE1-MOB4, HSP90AA1, HSP90AA2P, HSP90AB1, HSP90AB2P, HSP90B1, HSPA8, HSPA9, HSPE1, PPIA, PPIE, RANBP2, ST13, TXN</b>
Protein sumoylation	13	4.3	$5.2 \times 10^{-3}$	<b>BIRC5, HNRNPC, IFIH1, NUP153, NUPL2, POM121C, POM121, RAD21, RANBP2, RING1, SMC3, TRIM28</b>
G2/M transition of mitotic cell cycle	15	4.2	$1.5 \times 10^{-3}$	<b>ALMS1, BIRC5, CNTRL, CEP250, CKAP5, HAUS5, HSP90AA1, KHDRBS1, ODF2, PPP1CB, RPS27A, TUBA4A, TUBB4B, YWHAE</b>

Pathway enrichment analysis was performed using Database for Annotation, Visualization and Integrated Discovery (DAVID) v6.8 (<https://david.ncifcrf.gov/>, accessed on 9 December 2021) [21]. Biological Processes or proteins in **bold** were also observed in control (untreated) cells.

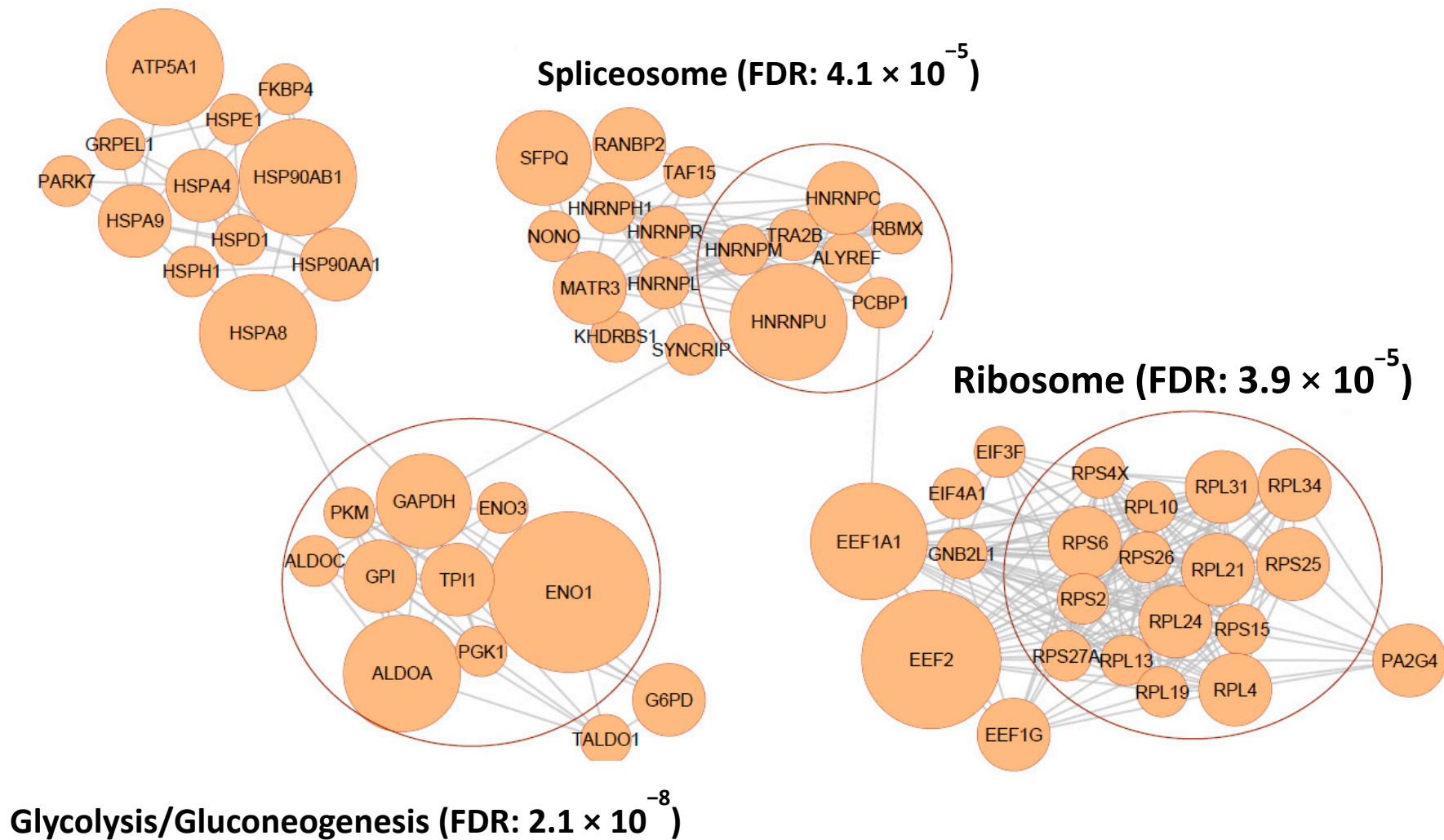


**Figure 2.** Protein–protein interaction network of MGO-modified proteins generated using STRING database v11.5 and Cytoscape v3.9.0 [19,20]. Size of the node (protein) reflects the number of MGO modifications found on that protein (ranging from 1–7). FDR; false discovery rate.

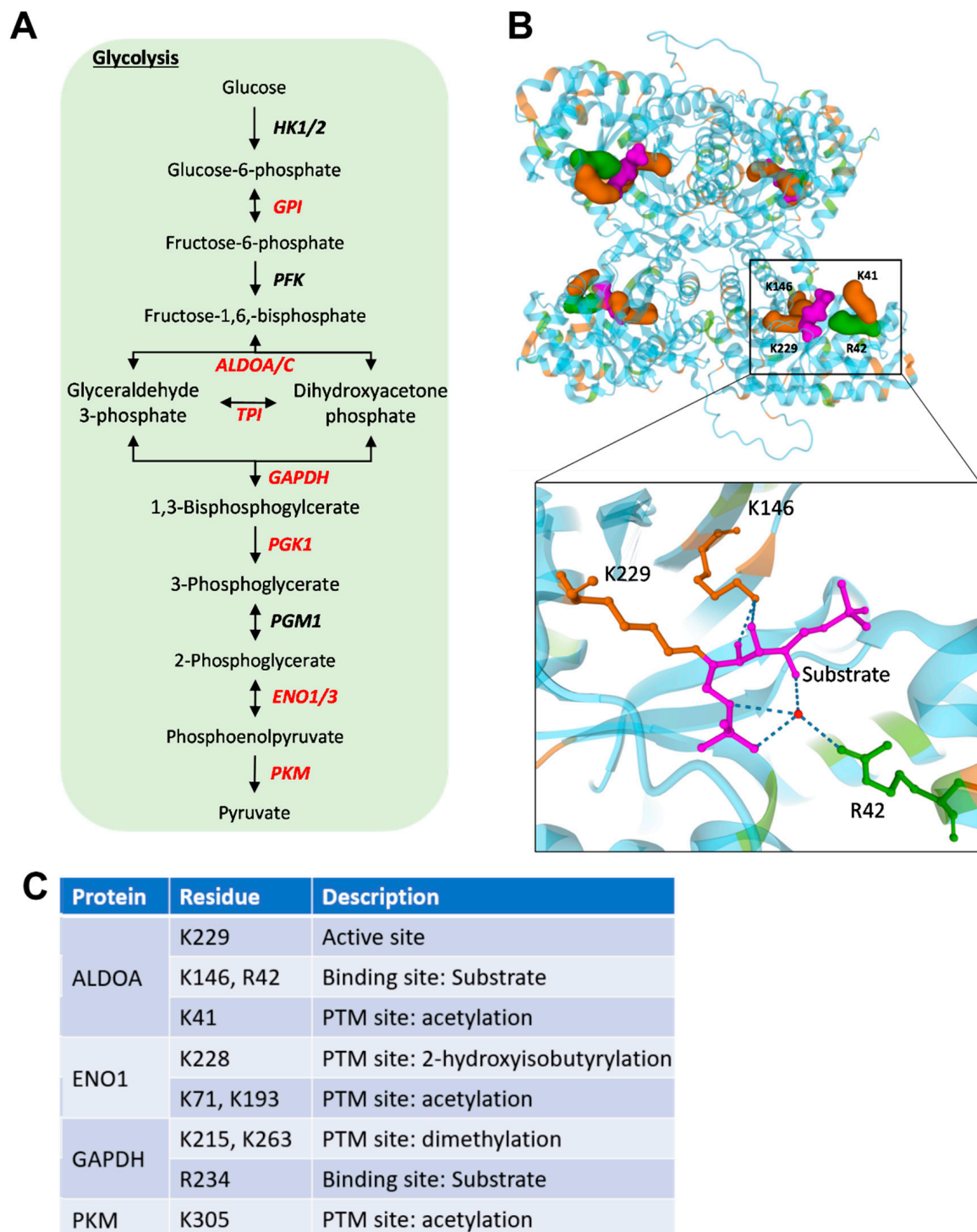


**Figure 3.** (A) Flow diagram showing glycolysis. Enzymes highlighted in red contain MGO modifications detected by LC-MS analysis. (B) Three-dimensional structure of fructose bisphosphate aldolase A (ALDOA, PDB entry 1ZAI). MGO-modified residues found in this study are labelled, and relevant arginine (green) and lysine (orange) residues are shown. Active site bound to intermediate Schiff-base substrate (purple) is enlarged. (C) Table of MGO modification sites that occur on residues involved in protein function. Features of each residue were obtained from UniProt. HK; hexokinase, GPI; glucose-6-phosphate, PFK; phosphofructokinase, ALDO; fructose bisphosphate aldolase, TPI; triosephosphate isomerase, GAPDH; glyceraldehyde 3-phosphate dehydrogenase, PGK; phosphoglycerate kinase, PGM; phosphoglucomutase, ENO; enolase, PKM; pyruvate kinase M.

### 2.3. Modification of Glycolytic Enzymes

Following the identification of glycolytic enzymes as primary targets for MGO modification in WIL2-NS cells, we examined if this was consistent across other cell types. Therefore, using previous data of epithelial cell lines, OV90 and Caov3 without (parental) and with chemoresistance to the chemotherapeutic drug carboplatin (CBPR) from our laboratory, raw data files were reprocessed for MGO modifications. As these cell lines were initially used for a different study, they were not treated with MGO and, therefore, modification sites represent those present under basal conditions. All cell lines, except for OV90 (parental), showed canonical glycolysis to be over-represented with MGO modifications (Figure 4A). Additionally, peripheral blood lymphocytes (PBL) isolated from three separate healthy male donors were similarly analysed for the occurrence of MGO modifications *in vivo*. As with the epithelial cell lines, analysis of MGO modification sites in PBL was performed without MGO treatment to detect modifications sites present under basal conditions only. Unfortunately, no significant enrichment was observed for MGO modifications on glycolytic enzymes in PBL, but modification of ALDOA was observed in PBL from all donors (Figure 4A,B). Furthermore, modification of ALDOA was observed in all epithelial cell lines (Figure 4B). We also investigated the modification of other proteins that occurred across multiple cell types, Histone H1.1 R57 (CEA), AT-rich interactive domain-containing protein 2 (Fragment) R277 (CEA) and Neuroblast differentiation-associated protein AHNAK K1333 (CEL) being the most commonly identified modification sites (Supplementary S1 Table S2).

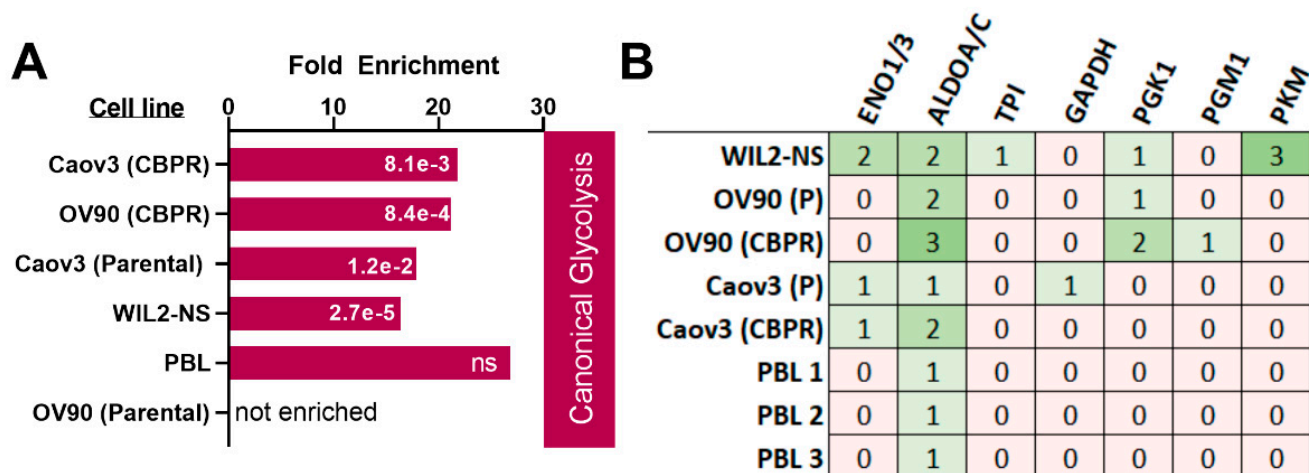


**Figure 4.** (A) Enrichment of MGO-modified glycolytic proteins in different cell types. For this analysis, all cells were untreated. For PBL, modified proteins from all three donors were collated into one list and enrichment analysis subsequently performed. FDR values are in white. (B) Occurrence of MGO-modified glycolytic enzymes in different cell types. CBPR; chemoresistance to the chemotherapeutic drug carboplatin, PBL; peripheral blood lymphocytes, ENO; enolase, ALDO; fructose biphosphate aldolase, TPI; triosephosphate isomerase, GAPDH; glyceraldehyde 3-phosphate dehydrogenase, PGK; phosphoglycerate kinase, PGM phosphoglucomutase, PKM; pyruvate kinase M, ns; not significant.

### 3. Discussion

Metabolite-driven PTMs have a diverse role in regulating protein function, by altering enzyme activity, obstructing protein–protein interactions and by forming covalent crosslinks between proteins [1]. To gain further insight into the role of PTMs, mapping of proteins and specific sites using proteomic techniques is an attractive approach. Therefore, we utilised LC-MS to explore intracellular MGO modifications. Detection of MGO modifications and other AGEs has remained difficult due to their low abundance, low stoichiometry and heterogeneity at modification sites and the lack of suitable enrichment techniques [22]. An ideal approach would utilise pan-specific antibodies to enrich native modifications at the peptide level. Only one previous study has reported this approach

for MGO modifications, using antibodies specific to each MG-H isomer and CEA to enrich MGO modified histone peptides; however, this yielded no enrichment [16]. Interestingly, an enrichment method using commercially available antibodies was applied to the AGE  $N^{\epsilon}$ -carboxymethyllysine, where a 10-fold increase in the identification of CML-modified peptides was observed [23]. Several commercially available antibodies exist for MGO modifications and potentially allow a more comprehensive picture of these modifications to be obtained. An alternative enrichment technique used an alkyne-labelled MGO analogue (alkMGO), which can be enriched by click-chemistry based techniques [24]. In this study, 71 MG-H, CEL and CEA modifications were identified in human serum incubated with 250  $\mu\text{mol/L}$  of alkMGO and more than 300 identified in erythrocyte lysates treated with 500  $\mu\text{mol/L}$  [24]. Unfortunately, the alkMGO analogue is not commercially available which limits its use by other researchers. The most common approach to increase the identification of MGO modified proteins is to increase their concentration using exogenous MGO, which was performed in our study. This approach has been used to study MGO modification sites in Human microvascular endothelial cells (HMEC-1), periodontal ligament fibroblasts (PDLF) and HEK293T cells [12–14]. In PDLF, only five proteins with MGO modifications were identified under control conditions [13]. This total increased to 172 proteins (consisting of 353 sites) following incubation of the cell lysate with 500  $\mu\text{M}$  MGO for 24 h. Furthermore, the same authors recently provided a comprehensive assessment of the dicarbonyl proteome in HEK293T cells by incubation with 131  $\mu\text{mol/L}$  of MGO followed by subcellular fractionation, which resulted in the identification of more than 600 MG-H modified proteins [14]. Similarly, Galligan et.al (2018) used exogenous MGO in GLO1 KO cells to study the site-specific MGO modifications on histone proteins, where they identified 21 sites across canonical histone proteins [16]. While the addition of exogenous MGO is useful for increasing the concentration and number of MGO modifications, several of the aforementioned studies have used concentrations likely to cause the non-specific modification of proteins beyond physiological or pathological conditions. To prevent excessive modification of proteins, we ensured the concentrations of MG-H1 and CEL following treatment was elevated by less than three-fold to reflect in vivo pathological conditions and minimise the occurrence of non-specific modifications [25]. We also utilised the non-standard protease ProAla, in addition to trypsin to increase total sequence coverage. ProAla has recently been shown to be more effective than trypsin at peptide mapping and identifying PTMs on more basic proteins such as histones, which are known targets for MGO [16,26]. Previous studies have also utilised other proteases, such as Lys-C and Glu-C, for the identification of various glycosylated proteins [12,23,24]. Therefore, the use of other proteases conjunction with trypsin may be useful in identifying additional MGO modification sites [27].

Enrichment analysis of our inventory of MGO modified proteins using DAVID and STRING revealed distinct networks which were enriched with these modifications. Most enriched was canonical glycolysis, where seven steps out of the ten-step process contained MGO modified proteins in WIL2-NS cells. Previous studies have shown various MGO modifications on arginine residues of glycolytic enzymes; however, in our study, the majority of modified sites resided on lysine residues [12,24]. This may be due to treatment durations, as MG-H modifications occur more rapidly than carboxyethylations, but also have a shorter half-life. Interestingly, glycolysis is the major pathway responsible for the formation of MGO by spontaneous degradation of intermediate triosephosphates [4]. Therefore, this may suggest a potential regulatory feedback mechanism whereby elevated MGO leads to modification of glycolytic proteins, decreasing their activity and lowering MGO back to a physiological concentration. Modification of fructose bisphosphate aldolase A at K229 or 146 was identified in all cell types analysed in this study, including PBL. Remarkably, all four modification sites of ALDOA were involved in its aldolase activity [28]. K229 acts as a nucleophile in the formation of the Schiff-base with the C2-carbonyl group of the substrate fructose 1,6-bisphosphate, followed by cleavage of the C3-C4 bond to release the glycolytic intermediates G3P and DHAP [28]. The charged form of K146 non-covalently interacts with

the substrate and intermediates to stabilise negative charges [28]. K41 and R42 have also been shown to interact with the 6-phosphate of the substrate [29]. All these interactions rely on the positively charged nucleophilic groups of the lysine or arginine residues which are lost following MGO modifications [30,31]. Therefore, it is highly likely that MGO modification of ALDOA at these residues, in particular K229, will affect substrate binding and its catalytic activity to interfere the progression of glycolysis. Moreover, modification of ENO1 was also shown to be a target of MGO, where seven modifications sites were detected following MGO treatment. Regulation of ENO1 activity has recently been shown to occur, at least in part by p300 mediated 2-hydroxyisobutyrylation of K228 [32], which was a site modified by MGO in our study. Knockdown of p300, which reduced the level of K228 2-hydroxyisobutyrylation, was shown to lower enzyme activity and the concentration of glycolytic intermediates [32]. Therefore, MGO modification of K228 could prevent p300 mediated 2-hydroxyisobutyrylation and cause a reduction in ENO1 glycolytic activity. MGO has been shown to decrease the activity of glycolytic enzymes in vitro and alter the abundance of glycolytic intermediates, specifically an increase in early stage (fructose 1,6 biphosphate, dihydroxyacetone phosphate, 3-phosphoglycerate) and a decrease in later stage intermediates (phosphoenolpyruvate and pyruvate) [33–36]. Unfortunately, most studies that have investigated the activity of specific glycolytic enzymes in response to MGO have used high concentrations (2.5–5 mM) that increase the likelihood of non-specific MGO modifications [33–36]. Therefore, further studies investigating the effects of site-specific MGO modifications on the activity of glycolytic enzymes (under normal or pathophysiological conditions) would provide valuable information and reveal clues to the mechanistic action displayed by MGO. A recent study showed that treatment of GLO2 knockout cells with 50  $\mu$ M MGO was able to decrease metabolic output through modification of the glycolytic enzymes by the glyoxalase intermediate S-D-lactoylglutathione, which produces lact(o)yllysine [37]. Interestingly, lact(o)yllysine and CEL are isomeric and may have similar signalling consequences. Both modifications produce identical mass shifts (+72) and can be difficult to differentiate by standard proteomics techniques. Nevertheless, both can be produced either directly (CEL) or indirectly (lact(o)yllysine) by MGO and therefore are associated with dicarbonyl stress.

Other cellular processes over-represented with MGO modifications included the spliceosome and ribosome. The spliceosome was previously shown to be enriched with MGO modifications and associated with a decrease in the abundance of proteins in this pathway [14]. The authors showed, using the Cancer Cell Line Encyclopedia (CCLE) that GLO1 mRNA expression positively correlated with the expression of spliceosome proteins (PPIL1 and CDC5L), suggesting increased GLO1 expression protects spliceosome proteins in tumour cells [14]. The spliceosome protein family serine and arginine-rich splicing factors (SRs), including SRSF2, which was modified with MGO in our study, are master regulators of pre-mRNA splicing. Dysregulation of this process can cause genomic instability and impede the normal expression pattern of proteins, resulting in aberrant biological function [38]. Loss of SRSF2 in mouse embryo fibroblasts cause cell cycle arrest in G2/M and double-strand break formation due in at least part to hyperphosphorylation and hyperacetylation of p53 [39]. Furthermore, mutations in SRSF2 and SF3B1, which also contained MGO modifications in this study, are observed in 5–75% of patients with various myeloid neoplasms, particularly chronic myelomonocytic leukemia and refractory anaemia with ring sideroblasts [40]. Therefore, protection of spliceosome pathway proteins may confer another role of GLO1 in tumour cells.

Our study reveals glycolysis/gluconeogenesis, spliceosome and ribosome as major STRING pathways enriched with MGO modifications. Although we were able to identify many MGO modified proteins, it is unlikely to be a comprehensive list. Further efforts to enrich those proteins which are modified by MGO are required, particularly in the identification of low abundant proteins that may harbour these modifications. Nevertheless, our study provided valuable insights into the potential impact MGO may have on cellular func-



tion. Furthermore, site-specific identification of MGO modification sites suggests they may have a role in regulating glycolytic output by altering the activity of glycolytic enzymes.

## 4. Materials and Methods

### 4.1. Materials

All reagents, chemicals and enzymes were purchased from Sigma unless indicated otherwise. Isotopically labelled and unlabelled MG-H1, CEL and Lysine were purchased from Iris Biotech (Marktredwitz, Germany). Trypsin Gold (Promega, V5280) and ProAlanase (Promega, VA2161) were purchased from Promega (Madison, WI, USA). Methylglyoxal solution was purchased from Sigma (St. Louis, MO, USA; M0252; Batch number BCBL7249V).

### 4.2. WIL2-NS Cell Culture

WIL2-NS cells (ATCC CRL-8155) was kindly gifted by Commonwealth Scientific Research Organisation (Adelaide, Australia). WIL2-NS cells were cultured in complete RPMI-1640 medium supplemented with 5% (*v/v*) fetal calf serum (FCS), L-glutamine (1% *v/v*) and penicillin/streptomycin (1% *v/v*) at 37 °C in a humidified atmosphere with 5% CO<sub>2</sub>. Cells were seeded at 5 × 10<sup>5</sup> cells/mL and incubated for 24 h before being treated with 500 µmol/L MGO for a further 24 h.

### 4.3. Whole-Cell Quantification of MG-H1 and CEL

WIL2-NS cells were lysed in ice-cold RIPA buffer with sonication over ice for two 10 s bursts (Misonix, NY, USA). Cellular debris was removed by centrifugation (17,000 × *g* for 10 min at RT). Protein was precipitated by the addition of ice-cold acetone (4:1 ratio of acetone: sample). Sample was left overnight at −20 °C before being centrifuged at 17,000 × *g* for 10 min at RT. Precipitated protein was washed twice with ice-cold acetone before being resuspended in 50 mM ammonium bicarbonate (pH 8). Samples were incubated at 37 °C for 4 h to aid protein solubilization. Undissolved protein was removed by centrifugation at 17,000 × *g* for 10 min (RT) and the protein concentration quantified using the Bicinchoninic acid (BCA; Sigma) assay following the manufacturer's instructions. Trypsin (TPCK treated, ≥10,000 BAEE units/mg protein) was added at a enzyme to protein ratio (1:50) and the sample incubated at 37 °C for 16 h. Following incubation, sample was heated to 95 °C for 10 min to denature the trypsin. Following this, sample was cooled to room temperature and Pronase E (≥3.5 units/mg protein) and Aminopeptidase (≥12 units/mg protein) were added at protein-to-enzyme ratio (1:50) for a further 24 h. Enzymes were removed by the addition of ice-cold acetone (4:1 ratio of acetone: sample) and the sample centrifuged at 17,000 × *g* for 10 min at RT. Supernatant was collected, dried under vacuum centrifugation and resuspended in 0.1% formic acid (*v/v*) containing the internal standard (100 nmol/L). Sample (2 µL) was injected and analytes were separated using a 150 × 4.6 mm, 4 µm Phenomenex C18 column (Phenomenex, Torrance, CA, USA) with a linear gradient of 0.1% formic acid in water (Buffer A) and 0.1% formic acid in acetonitrile (Buffer B) over 5 min at a flow rate of 0.6 mL/min. Multiple reaction monitoring (MRM) was conducted in positive mode using an AB Sciex 6500+ QTRAP mass spectrometer (Framingham, MA, USA) with the following transitions: *m/z* 147.4 > 83.9 (lysine), 151.2 > 87.9 (d<sub>4</sub> lysine), 219.2 > 130.2 (CEL), 222.2 > 134.2 (d<sub>4</sub>CEL), 229.2 > 116.1 (MG-H1) 232.2 > 116.1 (d<sub>3</sub> MG-H1). The ion source parameters were as follows: source temperature (450 °C), curtain gas (20 psi), collision gas (medium), ion spray voltage (5500 V) and ion source gas 1 and 2 (40 psi). The concentration of MG-H1 and CEL was normalized to lysine content and expressed as mmol analyte/mol lysine. Concentration of MG-H1 and CEL are expressed as mean ± SD (*n* = 3). Student *t*-test was conducted to determine any significant difference (*p* < 0.05) using GraphPad Prism (San Diego, CA, USA, Version 8.3.0).

### 4.4. Isolation and Purification of Peripheral Blood Lymphocytes

Venous blood was collected and lymphocytes isolated as previously described from three healthy male volunteers, aged 25–45 years by density gradient centrifugation [41].

Following isolation, PBL were stored in liquid nitrogen. The study was approved by the Human Research Ethics Committee of University of South Australia (Application ID: 203348) and written informed consent was obtained from all participants. For PBL, only cytoplasmic proteins were isolated by separation of cytoplasmic fraction from nuclear fraction by cell lysis with buffer containing 320 mM sucrose, 10 mM Tris-HCl, 5 mM MgCl<sub>2</sub> and 1% Triton-X100. Supernatant was collected and protein precipitated with three volumes of ice-cold acetone and washed three times. Protein was dissolved in 8 M urea/50 mM ammonium bicarbonate and the protein concentration determined by BCA assay.

#### 4.5. Proteomic Analysis of WIL2-NS and PBL

Cell lysis for and protein isolation for WIL2-NS was identical to whole-cell quantification of MG-H1 and CEL; however, following this, protein was resuspended in 50 mM ammonium bicarbonate/8 M urea. Protein concentration was measured by BCA assay. Preparation of WIL2-NS and PBL for proteomic analysis was identical, except that PBL was only digested with trypsin. Briefly, 100 µg of protein was reduced and alkylated with 10 mM dithiothreitol and 15 mM chloroacetamide, respectively. Sample was diluted with 50 mM ammonium bicarbonate to reduce urea concentration to 0.8 M. Trypsin (Trypsin Gold, Promega, V5280, 2 µg) was added and samples were incubated for 8 h at 37 °C at 500 rpm. Following incubation, 10.2 µL of formic acid was added to terminate the reaction and acidify the sample. For ProAla digestion, 20 µg of protein was reduced and alkylated with 10 mM dithiothreitol and 15 mM chloroacetamide, respectively. Sample was diluted with 33 mM HCl to reduce the urea concentration to 0.3 M and pH to ~1.5. ProAla enzyme (Promega, VA2161, 0.2 µg) was added, and samples were incubated for 4 h at 37 °C. All subsequent steps were the same for trypsin and ProAla digests. Peptides were purified using in-house packed C18 stage tips [42]. Stage tips were conditioned with 40 µL of acetonitrile and equilibrated with 80 µL of 0.1% (v/v) formic acid. Samples were loaded onto the stage tip and washed with 40 µL of 0.1% (v/v) formic acid. Samples were then eluted with 50% (v/v) acetonitrile in 0.1% (v/v) formic acid. Eluates were dried using a Speed-Vac and reconstituted in 20 µL of 0.1% (v/v) formic acid. Peptide concentration was determined by measuring tryptophan concentration of the peptides using an Agilent Cary Eclipse Fluorescence Spectrophotometer. Briefly, samples diluted 1:10 in 8 M urea/50 mM ammonium bicarbonate were loaded into a 50 µL Quartz cuvette and fluorescence was measured at excitation and emission of 295 nm and 350 nm, respectively. Concentration was determined by comparing against a standard curve generated using tryptophan. Protein concentration was deduced from tryptophan concentration assuming a tryptophan content of 1.17% in mammalian proteins [43].

OV90 and Caov3 cell lines were prepared as described above except that a mixture of Trypsin/Lys-C was used for the digestion and samples incubated overnight. These samples were prepared for another study, but raw data files were processed as described below for analysis of MGO modifications.

#### 4.6. High-Resolution Orbitrap Mass Spectrometry

LC-MS analysis was conducted on an EASY-nLC 1200 system coupled to an Orbitrap Exploris 480 mass spectrometer (Thermo Scientific, Bremen, Germany). Peptides from trypsin (1 µg) or ProAla (0.5 µg) digests were reconstituted in 0.1% formic acid and loaded onto a 25 cm fused silica column (75 µm inner diameter, 360 µm outer diameter) heated to 50 °C. The column was packed in-house with 1.9 µm ReproSil-Pur 120 C18-AQ particles (Dr. Maisch, Ammerbuch, Germany). Peptides were separated over a 70-min linear gradient (3 to 20% acetonitrile in 0.1% formic acid) at a flow rate of 300 nL/min. A FAIMS Pro interface (Thermo Scientific) generated compensation voltages at –50 and –70 V to regulate the entry of ionized peptides into the mass spectrometer. MS scans ( $m/z$  300 to 1500) were acquired at resolution 60,000 ( $m/z$  200) in positive ion mode. Peptide fragmentation (minimum threshold of  $1 \times 10^4$  precursor ions) was performed with 27.5% HCD collision energy, with

the resulting MS/MS scans (starting  $m/z$  85) measured at resolution 15,000. Cycle time was limited to 1.5 s, while the dynamic exclusion period was specified at 40 s.

#### 4.7. Data Analysis

Raw MS files were analysed using Proteome Discoverer 2.4 (Thermo Scientific, Bremen, Germany). Data were processed with the Sequest HT search engine against a concatenated database containing the 74,811 forward entries from the UniProt human database (1 December 2019) and their respective decoy counterparts. Trypsin or ProAlanase (cleaves C-terminal to proline and alanine residues) was specified as the enzyme and a maximum of five miscleavages was allowed. Precursor and fragment mass tolerances were 10 ppm and 0.02 Da, respectively. Arginine and lysine carboxyethylation (+72.021129), arginine methylglyoxal-hydroimidazolone (+54.010565), methionine oxidation (+15.994915), N-terminal acetylation (+42.010565), N-terminal methionine loss (−131.040485), N-terminal methionine loss and acetylation (−89.02992) were set as dynamic modifications, with cysteine carbamidomethylation (+57.021464) designated a static modification. Protein and peptide identification false discovery rates were both set at 1%.

Enrichment analysis was performed using the Database for Annotation, Visualization and Integrated Discovery (DAVID) v6.8 (<https://david.ncifcrf.gov/>) (accessed 9 December 2021) [19]. The STRING database v11.5 (Search Tool for the Retrieval of Interacting Genes, available at: <http://string-db.org/>, accessed 5 January 2022 [19]) was used for construction of the protein–protein interaction network. Only interactions with an interaction score greater than 0.95 were included and any disconnected nodes were removed. Remaining STRING network was exported to Cytoscape [20]. Cluster labels were assigned based on the KEGG analyses of pathways that were associated with the greatest number of proteins in that cluster. Venn diagrams were generated using <https://bioinformatics.psb.ugent.be/webtools/Venn/>, accessed 8 November 2021.

**Supplementary Materials:** The following supporting information can be downloaded at: <https://www.mdpi.com/article/10.3390/ijms23073689/s1>.

**Author Contributions:** L.D., C.Y. and P.D. contributed to the conceptualization of the study and design of experiments. L.D. performed the experiments and wrote the manuscript. L.D., M.A. and C.Y. performed the proteomics experiments. L.D., B.S.S., V.S.D., M.C., M.F., P.H. and P.D. contributed to the data analysis, discussion, review and editing of the article. All authors have read and agreed to the published version of the manuscript.

**Funding:** L.D. hold an Australian Institute of Health and Welfare, Government Research Training Program Scholarship.

**Institutional Review Board Statement:** The study was approved by the Human Research Ethics Committee of University of South Australia (Application ID: 203348 approved 03/02/2021).

**Informed Consent Statement:** Written informed consent was obtained from all participants.

**Data Availability Statement:** Raw MS files will be uploaded to a publicly available repository upon acceptance of the manuscript.

**Acknowledgments:** The authors acknowledge Bioplatforms Australia, and the State and Federal Governments, which co-fund the NCRIS-enabled Mass Spectrometry and Proteomics Facility at the University of South Australia. The authors would also like to thank Carmela Ricciardelli (University of Adelaide) for providing the OV90 and Caov3 cell lines used in this study.

**Conflicts of Interest:** The authors declare no conflict of interest.

## References

1. Walsh, C.T.; Garneau-Tsodikova, S.; Gatto, G.J., Jr. Protein posttranslational modifications: The chemistry of proteome diversifications. *Angew. Chem. Int. Ed. Engl.* **2005**, *44*, 7342–7372. [[CrossRef](#)] [[PubMed](#)]
2. Zheng, Q.; Maksimovic, I.; Upad, A.; David, Y. Non-enzymatic covalent modifications: A new link between metabolism and epigenetics. *Protein Cell* **2020**, *11*, 401–416. [[CrossRef](#)]

3. Harmel, R.; Fiedler, D. Features and regulation of non-enzymatic post-translational modifications. *Nat. Chem. Biol.* **2018**, *14*, 244–252. [[CrossRef](#)]
4. Phillips, S.A.; Thornalley, P.J. The formation of methylglyoxal from triose phosphates: Investigation using a specific assay for methylglyoxal. *Eur. J. Biochem.* **1993**, *212*, 101–105. [[CrossRef](#)] [[PubMed](#)]
5. Schalkwijk, C.G.; Stehouwer, C.D.A. Methylglyoxal, a Highly Reactive Dicarboxyl Compound, in Diabetes, Its Vascular Complications, and Other Age-Related Diseases. *Physiol. Rev.* **2020**, *100*, 407–461. [[CrossRef](#)] [[PubMed](#)]
6. Bellier, J.; Nokin, M.J.; Caprasse, M.; Tiamiou, A.; Blomme, A.; Scheijen, J.L.; Koopmansch, B.; MacKay, G.M.; Chiavarina, B.; Costanza, B.; et al. Methylglyoxal Scavengers Resensitize KRAS-Mutated Colorectal Tumors to Cetuximab. *Cell Rep.* **2020**, *30*, 1400–1416.e6. [[CrossRef](#)]
7. Rabbani, N.; Thornalley, P.J. Dicarboxyl stress in cell and tissue dysfunction contributing to ageing and disease. *Biochem. Biophys. Res. Commun.* **2015**, *458*, 221–226. [[CrossRef](#)] [[PubMed](#)]
8. Thornalley, P.J.; Battah, S.; Ahmed, N.; Karachalias, N.; Agalou, S.; Babaei-Jadidi, R.; Dawnay, A. Quantitative screening of advanced glycation endproducts in cellular and extracellular proteins by tandem mass spectrometry. *Biochem. J.* **2003**, *375*, 581–592. [[CrossRef](#)] [[PubMed](#)]
9. Rabbani, N.; Thornalley, P.J. Dicarboxyl proteome and genome damage in metabolic and vascular disease. *Biochem. Soc. Trans.* **2014**, *42*, 425–432. [[CrossRef](#)] [[PubMed](#)]
10. Rabbani, N.; Shaheen, F.; Anwar, A.; Masania, J.; Thornalley, P.J. Assay of methylglyoxal-derived protein and nucleotide AGEs. *Biochem. Soc. Trans.* **2014**, *42*, 511–517. [[CrossRef](#)] [[PubMed](#)]
11. Rabbani, N.; Thornalley, P.J. Glycation research in amino acids: A place to call home. *Amino Acids* **2012**, *42*, 1087–1096. [[CrossRef](#)]
12. Irshad, Z.; Xue, M.; Ashour, A.; Larkin, J.R.; Thornalley, P.J.; Rabbani, N. Activation of the unfolded protein response in high glucose treated endothelial cells is mediated by methylglyoxal. *Sci. Rep.* **2019**, *9*, 7889. [[CrossRef](#)]
13. Ashour, A.; Xue, M.; Al-Motawa, M.; Thornalley, P.J.; Rabbani, N. Glycolytic overload-driven dysfunction of periodontal ligament fibroblasts in high glucose concentration, corrected by glyoxalase 1 inducer. *BMJ Open Diabetes Res. Care* **2020**, *8*, e001458. [[CrossRef](#)] [[PubMed](#)]
14. Alhujaily, M.; Abbas, H.; Xue, M.; de la Fuente, A.; Rabbani, N.; Thornalley, P. Studies of Glyoxalase 1-Linked Multidrug Resistance Reveal Glycolysis-Derived Reactive Metabolite, Methylglyoxal, Is a Common Contributor in Cancer Chemotherapy Targeting the Spliceosome. *Front. Oncol.* **2021**, *11*, 4413. [[CrossRef](#)]
15. Keilhauer, E.C.; Geyer, P.E.; Mann, M. HCD Fragmentation of Glycated Peptides. *J. Proteome Res.* **2016**, *15*, 2881–2890. [[CrossRef](#)] [[PubMed](#)]
16. Galligan, J.J.; Wepy, J.A.; Streeter, M.D.; Kingsley, P.J.; Mitchener, M.M.; Wauchope, O.R.; Beavers, W.N.; Rose, K.L.; Wang, T.; Spiegel, D.A.; et al. Methylglyoxal-derived posttranslational arginine modifications are abundant histone marks. *Proc. Natl. Acad. Sci. USA* **2018**, *115*, 9228–9233. [[CrossRef](#)] [[PubMed](#)]
17. Lorentzen, E.; Siebers, B.; Hensel, R.; Pohl, E. Mechanism of the Schiff base forming fructose-1, 6-bisphosphate aldolase: Structural analysis of reaction intermediates. *Biochemistry* **2005**, *44*, 4222–4229. [[CrossRef](#)] [[PubMed](#)]
18. Pancholi, V. Multifunctional  $\alpha$ -enolase: Its role in diseases. *Cell. Mol. Life Sci. CMLS* **2001**, *58*, 902–920. [[CrossRef](#)] [[PubMed](#)]
19. Sibbersen, C.; Johannsen, M. Dicarboxyl derived post-translational modifications: Chemistry bridging biology and aging-related disease. *Essays Biochem.* **2020**, *64*, 97–110. [[CrossRef](#)] [[PubMed](#)]
20. Di Sanzo, S.; Spengler, K.; Leheis, A.; Kirkpatrick, J.M.; Rändler, T.L.; Baldensperger, T.; Dau, T.; Henning, C.; Parca, L.; Marx, C.; et al. Mapping protein carboxymethylation sites provides insights into their role in proteostasis and cell proliferation. *Nat. Commun.* **2021**, *12*, 6743. [[CrossRef](#)] [[PubMed](#)]
21. Sibbersen, C.; Schou Oxvig, A.M.; Bisgaard Olesen, S.; Nielsen, C.B.; Galligan, J.J.; Jørgensen, K.A.; Palmfeldt, J.; Johannsen, M. Profiling of Methylglyoxal Blood Metabolism and Advanced Glycation End-Product Proteome Using a Chemical Probe. *ACS Chem. Biol.* **2018**, *13*, 3294–3305. [[CrossRef](#)] [[PubMed](#)]
22. Ahmed, N.; Dobler, D.; Dean, M.; Thornalley, P. Peptide Mapping Identifies Hotspot Site of Modification in Human Serum Albumin by Methylglyoxal Involved in Ligand Binding and Esterase Activity. *J. Biol. Chem.* **2005**, *280*, 5724–5732. [[CrossRef](#)] [[PubMed](#)]
23. Samodova, D.; Hosfield, C.M.; Cramer, C.N.; Giuli, M.V.; Cappellini, E.; Franciosa, G.; Rosenblatt, M.M.; Kelstrup, C.D.; Olsen, J.V. ProAlanase is an Effective Alternative to Trypsin for Proteomics Applications and Disulfide Bond Mapping. *Mol. Cell. Proteom.* **2020**, *19*, 2139–2156. [[CrossRef](#)]
24. Priego-Capote, F.; Scherl, A.; Müller, M.; Waridel, P.; Lisacek, F.; Sanchez, J.-C. Glycation Isotopic Labeling with  $^{13}\text{C}$ -Reducing Sugars for Quantitative Analysis of Glycated Proteins in Human Plasma. *Mol. Cell. Proteom.* **2010**, *9*, 579–592. [[CrossRef](#)] [[PubMed](#)]
25. Bai, X.; Wang, Z.; Huang, C.; Wang, Z.; Chi, L. Investigation of Non-Enzymatic Glycosylation of Human Serum Albumin Using Ion Trap-Time of Flight Mass Spectrometry. *Molecules* **2012**, *17*, 8782–8794. [[CrossRef](#)]
26. Giansanti, P.; Tsiatsiani, L.; Low, T.Y.; Heck, A.J.R. Six alternative proteases for mass spectrometry-based proteomics beyond trypsin. *Nat. Protoc.* **2016**, *11*, 993–1006. [[CrossRef](#)] [[PubMed](#)]
27. Tittmann, K. Sweet siblings with different faces: The mechanisms of FBP and F6P aldolase, transaldolase, transketolase and phosphoketolase revisited in light of recent structural data. *Bioorganic Chem.* **2014**, *57*, 263–280. [[CrossRef](#)]

28. Dalby, A.; Dauter, Z.; Littlechild, J.A. Crystal structure of human muscle aldolase complexed with fructose 1,6-bisphosphate: Mechanistic implications. *Protein Sci.* **2008**, *8*, 291–297. [[CrossRef](#)] [[PubMed](#)]
29. Banerjee, S.; Chakraborti, A.S. In Vitro Study on Structural Alteration of Myoglobin by Methylglyoxal. *J. Protein Chem.* **2013**, *32*, 216–222. [[CrossRef](#)] [[PubMed](#)]
30. Mariño, L.; Ramis, R.; Casanovas, R.; Ortega-Castro, J.; Vilanova, B.; Frau, J.; Adrover, M. Unravelling the effect of N(epsilon)-(carboxyethyl)lysine on the conformation, dynamics and aggregation propensity of alpha-synuclein. *Chem. Sci.* **2020**, *11*, 3332–3344. [[CrossRef](#)] [[PubMed](#)]
31. Huang, H.; Tang, S.; Ji, M.; Tang, Z.; Shimada, M.; Liu, X.; Qi, S.; Locasale, J.W.; Roeder, R.G.; Zhao, Y.; et al. p300-Mediated Lysine 2-Hydroxyisobutyrylation Regulates Glycolysis. *Mol. Cell* **2018**, *70*, 663–678.e6. [[CrossRef](#)] [[PubMed](#)]
32. Leoncini, G.; Maresca, M.; Bonsignore, A. The effect of methylglyoxal on the glycolytic enzymes. *FEBS Lett.* **1980**, *117*, 17–18. [[CrossRef](#)]
33. Morgan, P.; Dean, R.T.; Davies, M.J. Inactivation of cellular enzymes by carbonyls and protein-bound glycation/glycooxidation products. *Arch. Biochem. Biophys.* **2002**, *403*, 259–269. [[CrossRef](#)]
34. Gomes, R.A.; Miranda, H.V.; Silva, M.S.; Graça, G.; Coelho, A.V.; Ferreira, A.E.; Cordeiro, C.; Freire, A.P. Yeast protein glycation in vivo by methylglyoxal. Molecular modification of glycolytic enzymes and heat shock proteins. *FEBS J.* **2006**, *273*, 5273–5287. [[PubMed](#)]
35. Leoncini, G.; Maresca, M.; Buzzi, E. Inhibition of the glycolytic pathway by methylglyoxal in human platelets. *Cell Biochem. Funct.* **1989**, *7*, 65–70. [[CrossRef](#)] [[PubMed](#)]
36. Gaffney, D.O.; Jennings, E.Q.; Anderson, C.C.; Marentette, J.O.; Shi, T.; Oxvig, A.-M.S.; Streeter, M.D.; Johannsen, M.; Spiegel, D.A.; Chapman, E.; et al. Non-enzymatic Lysine Lactoylation of Glycolytic Enzymes. *Cell Chem. Biol.* **2020**, *27*, 206–213.e6. [[CrossRef](#)] [[PubMed](#)]
37. Zheng, X.; Peng, Q.; Wang, L.; Zhang, X.; Huang, L.; Wang, J.; Qin, Z. Serine/arginine-rich splicing factors: The bridge linking alternative splicing and cancer. *Int. J. Biol. Sci.* **2020**, *16*, 2442–2453. [[CrossRef](#)] [[PubMed](#)]
38. Xiao, R.; Sun, Y.; Ding, J.-H.; Lin, S.; Rose, D.W.; Rosenfeld, M.G.; Fu, X.-D.; Li, X. Splicing Regulator SC35 Is Essential for Genomic Stability and Cell Proliferation during Mammalian Organogenesis. *Mol. Cell. Biol.* **2007**, *27*, 5393–5402. [[CrossRef](#)] [[PubMed](#)]
39. Yoshida, K.; Sanada, M.; Shiraiishi, Y.; Nowak, D.; Nagata, Y.; Yamamoto, R.; Sato, Y.; Sato-Otsubo, A.; Kon, A.; Nagasaki, M.; et al. Frequent pathway mutations of splicing machinery in myelodysplasia. *Nature* **2011**, *478*, 64–69. [[CrossRef](#)] [[PubMed](#)]
40. Donnellan, L.; Simpson, B.; Dhillon, V.S.; Costabile, M.; Fenech, M.; Deo, P. Methylglyoxal induces chromosomal instability and mitotic dysfunction in lymphocytes. *Mutagenesis* **2021**, *36*, 339–348. [[CrossRef](#)]
41. Wiśniewski, J.R.; Gaugaz, F.Z. Fast and Sensitive Total Protein and Peptide Assays for Proteomic Analysis. *Anal. Chem.* **2015**, *87*, 4110–4116. [[CrossRef](#)] [[PubMed](#)]
42. Huang, D.W.; Sherman, B.T.; Lempicki, R.A. Systematic and integrative analysis of large gene lists using DAVID bioinformatics resources. *Nat. Protoc.* **2009**, *4*, 44–57. [[CrossRef](#)]
43. Szklarczyk, D.; Gable, A.L.; Lyon, D.; Junge, A.; Wyder, S.; Huerta-Cepas, J.; Simonovic, M.; Doncheva, N.T.; Morris, J.H.; Bork, P.; et al. STRING v11: Protein-protein association networks with increased coverage, supporting functional discovery in genome-wide experimental datasets. *Nucleic Acids Res.* **2019**, *47*, D607–D613. [[CrossRef](#)]

# References

- 1
- 2 1. Bray, F., et al., *Global cancer statistics 2018: GLOBOCAN estimates of incidence and mortality worldwide for 36 cancers in 185 countries*. CA Cancer J Clin, 2018. **68**(6): p. 394-424.
- 3
- 4 2. Coburn, S.B., et al., *International patterns and trends in ovarian cancer incidence, overall and by histologic subtype*. Int J Cancer, 2017. **140**(11): p. 2451-2460.
- 5
- 6 3. Siegel, R.L., K.D. Miller, and A. Jemal, *Cancer statistics, 2020*. CA Cancer J Clin, 2020. **70**(1): p. 7-
- 7 30.
- 8 4. Siegel, R.L., K.D. Miller, and A. Jemal, *Cancer statistics, 2018*. CA Cancer J Clin, 2018. **68**(1): p. 7-
- 9 30.
- 10 5. Herzog, T.J., *Recurrent ovarian cancer: how important is it to treat to disease progression?* Clin Cancer Res, 2004. **10**(22): p. 7439-49.
- 11
- 12 6. Herzog, T.J. and B. Pothuri, *Ovarian cancer: a focus on management of recurrent disease*. Nat Clin Pract Oncol, 2006. **3**(11): p. 604-11.
- 13
- 14 7. Mohammadian, M., et al., *Variations in the incidence and mortality of ovarian cancer and their relationship with the human development index in European Countries in 2012*. Biomedical Research and Therapy, 2017. **4**(8): p. 1541-1557.
- 15
- 16
- 17 8. Tung, K.H., et al., *Reproductive factors and epithelial ovarian cancer risk by histologic type: a multiethnic case-control study*. Am J Epidemiol, 2003. **158**(7): p. 629-38.
- 18
- 19 9. Torre, L.A., et al., *Ovarian cancer statistics, 2018*. CA Cancer J Clin, 2018. **68**(4): p. 284-296.
- 20 10. Walsh, T., et al., *Mutations in 12 genes for inherited ovarian, fallopian tube, and peritoneal carcinoma identified by massively parallel sequencing*. Proc Natl Acad Sci U S A, 2011. **108**(44): p. 18032-7.
- 21
- 22
- 23 11. Toss, A., et al., *Hereditary ovarian cancer: not only BRCA 1 and 2 genes*. Biomed Res Int, 2015. **2015**: p. 341723.
- 24
- 25 12. Bandera, E.V., et al., *Impact of body mass index on ovarian cancer survival varies by stage*. Br J Cancer, 2017. **117**(2): p. 282-289.
- 26
- 27 13. Booth, C.M., et al., *The impact of socioeconomic status on stage of cancer at diagnosis and survival: a population-based study in Ontario, Canada*. Cancer, 2010. **116**(17): p. 4160-7.
- 28
- 29 14. Howlader, N., et al., *SEER cancer statistics review, 1975–2009 (vintage 2009 populations)*. Bethesda, MD: National Cancer Institute, 2012: p. 1975-2009.
- 30
- 31 15. Gaona-Luviano, P., L.A. Medina-Gaona, and K. Magaña-Pérez, *Epidemiology of ovarian cancer*. Chin Clin Oncol, 2020. **9**(4): p. 47.
- 32
- 33 16. Tewari, K., et al., *Malignant germ cell tumors of the ovary*. Obstet Gynecol, 2000. **95**(1): p. 128-33.
- 34
- 35 17. Nezhat, C., et al., *Familial cystic teratomas: four case reports and review of the literature*. J Minim Invasive Gynecol, 2010. **17**(6): p. 782-6.
- 36
- 37 18. Dimopoulos, M.A., et al., *Treatment of ovarian germ cell tumors with a 3-day bleomycin, etoposide, and cisplatin regimen: a prospective multicenter study*. Gynecol Oncol, 2004. **95**(3): p. 695-700.
- 38
- 39
- 40 19. Cushing, B., et al., *Randomized comparison of combination chemotherapy with etoposide, bleomycin, and either high-dose or standard-dose cisplatin in children and adolescents with high-risk malignant germ cell tumors: a pediatric intergroup study--Pediatric Oncology Group 9049 and Children's Cancer Group 8882*. J Clin Oncol, 2004. **22**(13): p. 2691-700.
- 41
- 42
- 43
- 44 20. Billmire, D., et al., *Outcome and staging evaluation in malignant germ cell tumors of the ovary in children and adolescents: an intergroup study*. J Pediatr Surg, 2004. **39**(3): p. 424-9; discussion 424-9.
- 45
- 46

- 1 21. Euscher, E.D., *Germ Cell Tumors of the Female Genital Tract*. Surg Pathol Clin, 2019. **12**(2): p. 621-649.
- 2
- 3 22. Gilks, C.B. and J. Prat, *Ovarian carcinoma pathology and genetics: recent advances*. Hum Pathol, 2009. **40**(9): p. 1213-23.
- 4
- 5 23. McCluggage, W.G., *Morphological subtypes of ovarian carcinoma: a review with emphasis on new developments and pathogenesis*. Pathology, 2011. **43**(5): p. 420-32.
- 6
- 7 24. Kurman, R.J. and M. Shih le, *Molecular pathogenesis and extraovarian origin of epithelial ovarian cancer--shifting the paradigm*. Hum Pathol, 2011. **42**(7): p. 918-31.
- 8
- 9 25. Shih le, M. and R.J. Kurman, *Ovarian tumorigenesis: a proposed model based on morphological and molecular genetic analysis*. Am J Pathol, 2004. **164**(5): p. 1511-8.
- 10
- 11 26. Wu, R., et al., *Type I to type II ovarian carcinoma progression: mutant Trp53 or Pik3ca confers a more aggressive tumor phenotype in a mouse model of ovarian cancer*. Am J Pathol, 2013. **182**(4): p. 1391-9.
- 12
- 13
- 14 27. Kossai, M., et al., *Ovarian Cancer: A Heterogeneous Disease*. Pathobiology, 2018. **85**(1-2): p. 41-49.
- 15
- 16 28. *Drugs of choice for cancer*. Treat Guidel Med Lett, 2003. **1**(7): p. 41-52.
- 17 29. Seidman, J.D., et al., *The histologic type and stage distribution of ovarian carcinomas of surface epithelial origin*. International journal of gynecological pathology, 2004. **23**(1): p. 41-44.
- 18
- 19 30. Ramalingam, P., *Morphologic, Immunophenotypic, and Molecular Features of Epithelial Ovarian Cancer*. Oncology (Williston Park), 2016. **30**(2): p. 166-76.
- 20
- 21 31. Catasús, L., et al., *Molecular genetic alterations in endometrioid carcinomas of the ovary: similar frequency of beta-catenin abnormalities but lower rate of microsatellite instability and PTEN alterations than in uterine endometrioid carcinomas*. Human pathology, 2004. **35**(11): p. 1360-1368.
- 22
- 23
- 24
- 25 32. Kline, R.C., et al., *Endometrioid carcinoma of the ovary: retrospective review of 145 cases*. Gynecologic oncology, 1990. **39**(3): p. 337-346.
- 26
- 27 33. Soliman, P.T., et al., *Synchronous primary cancers of the endometrium and ovary: a single institution review of 84 cases*. Gynecol Oncol, 2004. **94**(2): p. 456-62.
- 28
- 29 34. Anglesio, M.S., et al., *Synchronous Endometrial and Ovarian Carcinomas: Evidence of Clonality*. J Natl Cancer Inst, 2016. **108**(6): p. djv428.
- 30
- 31 35. Catasús, L., et al., *Molecular genetic alterations in endometrioid carcinomas of the ovary: similar frequency of beta-catenin abnormalities but lower rate of microsatellite instability and PTEN alterations than in uterine endometrioid carcinomas*. Hum Pathol, 2004. **35**(11): p. 1360-8.
- 32
- 33
- 34 36. Kandoth, C., et al., *Integrated genomic characterization of endometrial carcinoma*. Nature, 2013. **497**(7447): p. 67-73.
- 35
- 36 37. Cybulska, P., et al., *Molecular profiling and molecular classification of endometrioid ovarian carcinomas*. Gynecol Oncol, 2019. **154**(3): p. 516-523.
- 37
- 38 38. Soovares, P., et al., *L1CAM expression associates with poor outcome in endometrioid, but not in clear cell ovarian carcinoma*. Gynecol Oncol, 2017. **146**(3): p. 615-622.
- 39
- 40 39. Okamoto, A., et al., *Gynecologic Cancer InterGroup (GCIg) consensus review for clear cell carcinoma of the ovary*. 2014. **24**(Supp 3).
- 41
- 42 40. Yamaguchi, K., et al., *Identification of an ovarian clear cell carcinoma gene signature that reflects inherent disease biology and the carcinogenic processes*. 2010. **29**(12): p. 1741-1752.
- 43
- 44 41. Sugiyama, T., et al., *Clinical characteristics of clear cell carcinoma of the ovary: a distinct histologic type with poor prognosis and resistance to platinum-based chemotherapy*. 2000. **88**(11): p. 2584-2589.
- 45
- 46
- 47 42. Okamoto, A., et al., *Randomized phase III trial of paclitaxel/carboplatin (PC) versus cisplatin/irinotecan (CPT-P) as first-line chemotherapy in patients with clear cell carcinoma (CCC)*
- 48

- 1 *of the ovary: A Japanese Gynecologic Oncology Group (JGOG)/GCIG study.* 2014, American  
2 Society of Clinical Oncology.
- 3 43. Yamamoto, S., et al., *Clear-cell adenofibroma can be a clonal precursor for clear-cell*  
4 *adenocarcinoma of the ovary: a possible alternative ovarian clear-cell carcinogenic pathway.*  
5 2008. **216**(1): p. 103-110.
- 6 44. Kobayashi, H., et al., *Risk of developing ovarian cancer among women with ovarian*  
7 *endometrioma: a cohort study in Shizuoka, Japan.* 2007. **17**(1).
- 8 45. Vergote, I., et al., *Treatment algorithm in patients with ovarian cancer.* Facts Views Vis Obgyn,  
9 2020. **12**(3): p. 227-239.
- 10 46. Fujiwara, K., D. Shintani, and T. Nishikawa, *Clear-cell carcinoma of the ovary.* Ann Oncol, 2016.  
11 **27 Suppl 1**: p. i50-i52.
- 12 47. Sato, N., et al., *Loss of heterozygosity on 10q23. 3 and mutation of the tumor suppressor gene*  
13 *PTEN in benign endometrial cyst of the ovary: possible sequence progression from benign*  
14 *endometrial cyst to endometrioid carcinoma and clear cell carcinoma of the ovary.* 2000. **60**(24):  
15 p. 7052-7056.
- 16 48. Takano, M., et al., *Less impact of adjuvant chemotherapy for stage I clear cell carcinoma of the*  
17 *ovary: a retrospective Japan Clear Cell Carcinoma Study.* 2010. **20**(9).
- 18 49. Seidman, J.D., R.J. Kurman, and B.M. Ronnett, *Primary and metastatic mucinous*  
19 *adenocarcinomas in the ovaries: incidence in routine practice with a new approach to improve*  
20 *intraoperative diagnosis.* Am J Surg Pathol, 2003. **27**(7): p. 985-93.
- 21 50. Lheureux, S., M. Braunstein, and A.M. Oza, *Epithelial ovarian cancer: Evolution of management*  
22 *in the era of precision medicine.* CA Cancer J Clin, 2019. **69**(4): p. 280-304.
- 23 51. Shappell, H.W., et al., *Diagnostic criteria and behavior of ovarian seromucinous (endocervical-*  
24 *type mucinous and mixed cell-type) tumors: atypical proliferative (borderline) tumors,*  
25 *intraepithelial, microinvasive, and invasive carcinomas.* Am J Surg Pathol, 2002. **26**(12): p. 1529-  
26 41.
- 27 52. Lee, K.R. and M.R. Nucci, *Ovarian mucinous and mixed epithelial carcinomas of mullerian*  
28 *(endocervical-like) type: a clinicopathologic analysis of four cases of an uncommon variant*  
29 *associated with endometriosis.* Int J Gynecol Pathol, 2003. **22**(1): p. 42-51.
- 30 53. Taylor, J. and W.G. McCluggage, *Ovarian seromucinous carcinoma: report of a series of a newly*  
31 *categorized and uncommon neoplasm.* Am J Surg Pathol, 2015. **39**(7): p. 983-92.
- 32 54. Mackay, H.J., et al., *Prognostic relevance of uncommon ovarian histology in women with stage*  
33 *III/IV epithelial ovarian cancer.* International Journal of Gynecologic Cancer, 2010. **20**(6).
- 34 55. Pectasides, D., et al., *Advanced stage mucinous epithelial ovarian cancer: the Hellenic*  
35 *Cooperative Oncology Group experience.* Gynecol Oncol, 2005. **97**(2): p. 436-41.
- 36 56. Hess, V., et al., *Mucinous epithelial ovarian cancer: a separate entity requiring specific*  
37 *treatment.* J Clin Oncol, 2004. **22**(6): p. 1040-4.
- 38 57. Scott, M. and W.G. McCluggage, *Current concepts in ovarian epithelial tumorigenesis:*  
39 *correlation between morphological and molecular data.* Histol Histopathol, 2006. **21**(1): p. 81-  
40 92.
- 41 58. Gemignani, M.L., et al., *Role of KRAS and BRAF gene mutations in mucinous ovarian carcinoma.*  
42 Gynecol Oncol, 2003. **90**(2): p. 378-81.
- 43 59. Cuatrecasas, M., et al., *K-ras mutations in nonmucinous ovarian epithelial tumors: a molecular*  
44 *analysis and clinicopathologic study of 144 patients.* Cancer, 1998. **82**(6): p. 1088-95.
- 45 60. Seidman, J.D., et al., *The histologic type and stage distribution of ovarian carcinomas of surface*  
46 *epithelial origin.* 2004. **23**(1): p. 41-44.
- 47 61. Chen, M., et al., *A survival analysis comparing women with ovarian low-grade serous carcinoma*  
48 *to those with high-grade histology.* 2014. **7**: p. 1891.



1 62. Van Leeuwen, F., et al., *Risk of borderline and invasive ovarian tumours after ovarian stimulation*  
2 *for in vitro fertilization in a large Dutch cohort.* 2011. **26**(12): p. 3456-3465.

3 63. Vang, R., I.-M. Shih, and R.J.J.A.i.a.p. Kurman, *Ovarian low-grade and high-grade serous*  
4 *carcinoma: pathogenesis, clinicopathologic and molecular biologic features, and diagnostic*  
5 *problems.* 2009. **16**(5): p. 267.

6 64. Malpica, A., et al., *Grading ovarian serous carcinoma using a two-tier system.* *Am J Surg Pathol,*  
7 2004. **28**(4): p. 496-504.

8 65. Bonome, T., et al., *Expression profiling of serous low malignant potential, low-grade, and high-*  
9 *grade tumors of the ovary.* 2005. **65**(22): p. 10602-10612.

10 66. Crispens, M.A., et al., *Response and survival in patients with progressive or recurrent serous*  
11 *ovarian tumors of low malignant potential.* 2002. **99**(1): p. 3-10.

12 67. Gershenson, D.M.J.A.S.o.C.O.E.B., *The life and times of low-grade serous carcinoma of the ovary.*  
13 2013. **33**(1): p. e195-e199.

14 68. Romero, I., et al., *Low-grade serous carcinoma: new concepts and emerging therapies.* 2013.  
15 **130**(3): p. 660-666.

16 69. Wong, K.-K., et al., *BRAF mutation is rare in advanced-stage low-grade ovarian serous*  
17 *carcinomas.* 2010. **177**(4): p. 1611-1617.

18 70. Gershenson, D.M., et al., *Recurrent low-grade serous ovarian carcinoma is relatively*  
19 *chemoresistant.* 2009. **114**(1): p. 48-52.

20 71. Malpica, A., et al., *Grading ovarian serous carcinoma using a two-tier system.* 2004. **28**(4): p.  
21 496-504.

22 72. Plaxe, S.C.J.A.j.o.o. and gynecology, *Epidemiology of low-grade serous ovarian cancer.* 2008.  
23 **198**(4): p. 459. e1-459. e9.

24 73. Grabowski, J.P., et al., *Operability and chemotherapy responsiveness in advanced low-grade*  
25 *serous ovarian cancer. An analysis of the AGO Study Group metadatabase.* 2016. **140**(3): p. 457-  
26 462.

27 74. Ahmed, A.A., et al., *Driver mutations in TP53 are ubiquitous in high grade serous carcinoma of*  
28 *the ovary.* *J Pathol,* 2010. **221**(1): p. 49-56.

29 75. Bowtell, D.D., *The genesis and evolution of high-grade serous ovarian cancer.* *Nat Rev Cancer,*  
30 2010. **10**(11): p. 803-8.

31 76. Kurman, R.J., M.L. Carcangiu, and C.S. Herrington, *World Health Organisation classification of*  
32 *tumours of the female reproductive organs.* 2014: International Agency for Research on Cancer.

33 77. Kaldawy, A., et al., *Low-grade serous ovarian cancer: A review.* *Gynecol Oncol,* 2016. **143**(2): p.  
34 433-438.

35 78. Konstantinopoulos, P.A., et al., *Homologous Recombination Deficiency: Exploiting the*  
36 *Fundamental Vulnerability of Ovarian Cancer.* *Cancer Discov,* 2015. **5**(11): p. 1137-54.

37 79. Malek, J.A., et al., *Copy number variation analysis of matched ovarian primary tumors and*  
38 *peritoneal metastasis.* *PLoS One,* 2011. **6**(12): p. e28561.

39 80. McBride, D.J., et al., *Tandem duplication of chromosomal segments is common in ovarian and*  
40 *breast cancer genomes.* *J Pathol,* 2012. **227**(4): p. 446-55.

41 81. *Integrated genomic analyses of ovarian carcinoma.* *Nature,* 2011. **474**(7353): p. 609-15.

42 82. Konecny, G.E., et al., *Prognostic and therapeutic relevance of molecular subtypes in high-grade*  
43 *serous ovarian cancer.* *J Natl Cancer Inst,* 2014. **106**(10).

44 83. Verhaak, R.G., et al., *Prognostically relevant gene signatures of high-grade serous ovarian*  
45 *carcinoma.* *J Clin Invest,* 2013. **123**(1): p. 517-25.

46 84. Winterhoff, B., et al., *Molecular classification of high grade endometrioid and clear cell ovarian*  
47 *cancer using TCGA gene expression signatures.* *Gynecol Oncol,* 2016. **141**(1): p. 95-100.

- 1 85. Narod, S., *Can advanced-stage ovarian cancer be cured?* Nat Rev Clin Oncol, 2016. **13**(4): p. 255-  
2 61.
- 3 86. Matulonis, U.A., et al., *Ovarian cancer*. Nat Rev Dis Primers, 2016. **2**: p. 16061.
- 4 87. González-Martín, A., et al., *First-line and maintenance therapy for ovarian cancer: current status  
5 and future directions*. Drugs, 2014. **74**(8): p. 879-89.
- 6 88. Markman, M., *Optimizing primary chemotherapy in ovarian cancer*. Hematol Oncol Clin North  
7 Am, 2003. **17**(4): p. 957-68, viii.
- 8 89. Bast, R.C., Jr., B. Hennessy, and G.B. Mills, *The biology of ovarian cancer: new opportunities for  
9 translation*. Nat Rev Cancer, 2009. **9**(6): p. 415-28.
- 10 90. Bowtell, D.D., et al., *Rethinking ovarian cancer II: reducing mortality from high-grade serous  
11 ovarian cancer*. Nat Rev Cancer, 2015. **15**(11): p. 668-79.
- 12 91. Klotz, D.M. and P. Wimberger, *Cells of origin of ovarian cancer: ovarian surface epithelium or  
13 fallopian tube?* Arch Gynecol Obstet, 2017. **296**(6): p. 1055-1062.
- 14 92. Lisio, M.A., et al., *High-Grade Serous Ovarian Cancer: Basic Sciences, Clinical and Therapeutic  
15 Standpoints*. Int J Mol Sci, 2019. **20**(4).
- 16 93. Fathalla, M.F., *Incessant ovulation--a factor in ovarian neoplasia?* Lancet, 1971. **2**(7716): p. 163.
- 17 94. Ahmed, N., et al., *Cancerous ovarian stem cells: obscure targets for therapy but relevant to  
18 chemoresistance*. J Cell Biochem, 2013. **114**(1): p. 21-34.
- 19 95. Kuhn, E., R.J. Kurman, and I.M. Shih, *Ovarian Cancer Is an Imported Disease: Fact or Fiction?* Curr  
20 Obstet Gynecol Rep, 2012. **1**(1): p. 1-9.
- 21 96. Kurman, R.J. and M. Shih, *The origin and pathogenesis of epithelial ovarian cancer: a proposed  
22 unifying theory*. Am J Surg Pathol, 2010. **34**(3): p. 433-43.
- 23 97. Lengyel, E., *Ovarian cancer development and metastasis*. Am J Pathol, 2010. **177**(3): p. 1053-64.
- 24 98. Cheng, W., et al., *Lineage infidelity of epithelial ovarian cancers is controlled by HOX genes that  
25 specify regional identity in the reproductive tract*. Nat Med, 2005. **11**(5): p. 531-7.
- 26 99. Dubeau, L., *The cell of origin of ovarian epithelial tumors and the ovarian surface epithelium  
27 dogma: does the emperor have no clothes?* Gynecol Oncol, 1999. **72**(3): p. 437-42.
- 28 100. Piek, J.M., et al., *Dysplastic changes in prophylactically removed Fallopian tubes of women  
29 predisposed to developing ovarian cancer*. J Pathol, 2001. **195**(4): p. 451-6.
- 30 101. Lee, Y., et al., *A candidate precursor to serous carcinoma that originates in the distal fallopian  
31 tube*. J Pathol, 2007. **211**(1): p. 26-35.
- 32 102. Seidman, J.D., P. Zhao, and A. Yemelyanova, *"Primary peritoneal" high-grade serous carcinoma  
33 is very likely metastatic from serous tubal intraepithelial carcinoma: assessing the new paradigm  
34 of ovarian and pelvic serous carcinogenesis and its implications for screening for ovarian cancer*.  
35 Gynecol Oncol, 2011. **120**(3): p. 470-3.
- 36 103. Przybycin, C.G., et al., *Are all pelvic (nonuterine) serous carcinomas of tubal origin?* Am J Surg  
37 Pathol, 2010. **34**(10): p. 1407-16.
- 38 104. Kurman, R.J. and M. Shih, *Pathogenesis of ovarian cancer: lessons from morphology and  
39 molecular biology and their clinical implications*. Int J Gynecol Pathol, 2008. **27**(2): p. 151-60.
- 40 105. Visvanathan, K., et al., *Fallopian Tube Lesions in Women at High Risk for Ovarian Cancer: A  
41 Multicenter Study*. Cancer Prev Res (Phila), 2018. **11**(11): p. 697-706.
- 42 106. Folkins, A.K., et al., *A candidate precursor to pelvic serous cancer (p53 signature) and its  
43 prevalence in ovaries and fallopian tubes from women with BRCA mutations*. Gynecol Oncol,  
44 2008. **109**(2): p. 168-73.
- 45 107. Kuhn, E., et al., *TP53 mutations in serous tubal intraepithelial carcinoma and concurrent pelvic  
46 high-grade serous carcinoma--evidence supporting the clonal relationship of the two lesions*. J  
47 Pathol, 2012. **226**(3): p. 421-6.

- 1 108. Salvador, S., et al., *Chromosomal instability in fallopian tube precursor lesions of serous*  
2 *carcinoma and frequent monoclonality of synchronous ovarian and fallopian tube mucosal*  
3 *serous carcinoma*. *Gynecol Oncol*, 2008. **110**(3): p. 408-17.
- 4 109. Labidi-Galy, S.I., et al., *High grade serous ovarian carcinomas originate in the fallopian tube*. *Nat*  
5 *Commun*, 2017. **8**(1): p. 1093.
- 6 110. Marquez, R.T., et al., *Patterns of gene expression in different histotypes of epithelial ovarian*  
7 *cancer correlate with those in normal fallopian tube, endometrium, and colon*. *Clin Cancer Res*,  
8 2005. **11**(17): p. 6116-26.
- 9 111. Levanon, K., et al., *Primary ex vivo cultures of human fallopian tube epithelium as a model for*  
10 *serous ovarian carcinogenesis*. *Oncogene*, 2010. **29**(8): p. 1103-13.
- 11 112. Kindelberger, D.W., et al., *Intraepithelial carcinoma of the fimbria and pelvic serous carcinoma:*  
12 *Evidence for a causal relationship*. *Am J Surg Pathol*, 2007. **31**(2): p. 161-9.
- 13 113. Bijron, J.G., et al., *Fallopian tube intraluminal tumor spread from noninvasive precursor lesions: a*  
14 *novel metastatic route in early pelvic carcinogenesis*. *Am J Surg Pathol*, 2013. **37**(8): p. 1123-30.
- 15 114. Falconer, H., et al., *Ovarian cancer risk after salpingectomy: a nationwide population-based*  
16 *study*. *J Natl Cancer Inst*, 2015. **107**(2).
- 17 115. Shih, I.M., Y. Wang, and T.L. Wang, *The Origin of Ovarian Cancer Species and Precancerous*  
18 *Landscape*. *Am J Pathol*, 2021. **191**(1): p. 26-39.
- 19 116. Huang, H.S., et al., *Mutagenic, surviving and tumorigenic effects of follicular fluid in the context*  
20 *of p53 loss: initiation of fimbria carcinogenesis*. *Carcinogenesis*, 2015. **36**(11): p. 1419-28.
- 21 117. Huang, D., et al., *Deep Metabolomics of a High-Grade Serous Ovarian Cancer Triple-Knockout*  
22 *Mouse Model*. *J Proteome Res*, 2019. **18**(8): p. 3184-3194.
- 23 118. Kim, J., et al., *The ovary is an alternative site of origin for high-grade serous ovarian cancer in*  
24 *mice*. *Endocrinology*, 2015. **156**(6): p. 1975-81.
- 25 119. Tolcher, M.C., et al., *Characterization of precursor lesions in the endometrium and fallopian tube*  
26 *epithelium of early-stage uterine serous carcinoma*. *Int J Gynecol Pathol*, 2015. **34**(1): p. 57-64.
- 27 120. Chui, M.H., et al., *Clinicopathologic and molecular features of paired cases of metachronous*  
28 *ovarian serous borderline tumor and subsequent serous carcinoma*. 2019. **43**(11): p. 1462.
- 29 121. Murali, R., et al., *Somatic genetic alterations in synchronous and metachronous low-grade serous*  
30 *tumours and high-grade carcinomas of the adnexa*. 2019. **74**(4): p. 638-650.
- 31 122. Vang, R., I.M. Shih, and R.J.J.H. Kurman, *Fallopian tube precursors of ovarian low-and high-grade*  
32 *serous neoplasms*. 2013. **62**(1): p. 44-58.
- 33 123. Wang, Y., et al., *Tubal Origin of "Ovarian" Low-Grade Serous Carcinoma: A Gene Expression*  
34 *Profile Study*. *Journal of Oncology*, 2019. **2019**: p. 8659754.
- 35 124. Ducie, J., et al., *Molecular analysis of high-grade serous ovarian carcinoma with and without*  
36 *associated serous tubal intra-epithelial carcinoma*. 2017. **8**(1): p. 1-9.
- 37 125. Elias, K.M., J. Guo, and R.C. Bast, Jr., *Early Detection of Ovarian Cancer*. *Hematol Oncol Clin*  
38 *North Am*, 2018. **32**(6): p. 903-914.
- 39 126. Siegel, R.L., K.D. Miller, and A. Jemal, *Cancer Statistics, 2017*. *CA Cancer J Clin*, 2017. **67**(1): p. 7-  
40 30.
- 41 127. Chornokur, G., et al., *Global ovarian cancer health disparities*. *Gynecol Oncol*, 2013. **129**(1): p. 1-  
42 258-64.
- 43 128. Chan, J.K., et al., *Ovarian cancer in younger vs older women: a population-based analysis*. *Br J*  
44 *Cancer*, 2006. **95**(10): p. 1314-20.
- 45 129. Poole, E.M., et al., *Hormonal and reproductive risk factors for epithelial ovarian cancer by tumor*  
46 *aggressiveness*. *Cancer Epidemiol Biomarkers Prev*, 2013. **22**(3): p. 429-37.
- 47 130. Ørskov, M., et al., *Predictors of mortality within 1 year after primary ovarian cancer surgery: a*  
48 *nationwide cohort study*. *BMJ Open*, 2016. **6**(4): p. e010123.

- 1 131. Mori, M., et al., *Reproductive, genetic, and dietary risk factors for ovarian cancer*. Am J  
2 Epidemiol, 1988. **128**(4): p. 771-7.
- 3 132. Kim, S.J., et al., *Epidemiologic factors that predict long-term survival following a diagnosis of*  
4 *epithelial ovarian cancer*. Br J Cancer, 2017. **116**(7): p. 964-971.
- 5 133. Hankinson, S.E., et al., *A prospective study of reproductive factors and risk of epithelial ovarian*  
6 *cancer*. Cancer, 1995. **76**(2): p. 284-290.
- 7 134. Kvåle, G., et al., *Reproductive factors and risk of ovarian cancer: a prospective study*. Int J Cancer,  
8 1988. **42**(2): p. 246-51.
- 9 135. Huusom, L.D., et al., *Association of reproductive factors, oral contraceptive use and selected*  
10 *lifestyle factors with the risk of ovarian borderline tumors: a Danish case-control study*. Cancer  
11 Causes & Control, 2006. **17**(6): p. 821-829.
- 12 136. Soegaard, M., et al., *Different risk factor profiles for mucinous and nonmucinous ovarian cancer:*  
13 *results from the Danish MALOVA study*. Cancer Epidemiology and Prevention Biomarkers, 2007.  
14 **16**(6): p. 1160-1166.
- 15 137. Riman, T., et al., *Risk factors for epithelial borderline ovarian tumors: results of a Swedish case-*  
16 *control study*. Gynecologic oncology, 2001. **83**(3): p. 575-585.
- 17 138. Royar, J., H. Becher, and J. Chang-Claude, *Low-dose oral contraceptives: protective effect on*  
18 *ovarian cancer risk*. Int J Cancer, 2001. **95**(6): p. 370-4.
- 19 139. Tsilidis, K.K., et al., *Oral contraceptive use and reproductive factors and risk of ovarian cancer in*  
20 *the European Prospective Investigation into Cancer and Nutrition*. Br J Cancer, 2011. **105**(9): p.  
21 1436-42.
- 22 140. Soegaard, M., et al., *Different risk factor profiles for mucinous and nonmucinous ovarian cancer:*  
23 *results from the Danish MALOVA study*. Cancer Epidemiol Biomarkers Prev, 2007. **16**(6): p. 1160-  
24 6.
- 25 141. Hillier, S.G., M.T. Rae, and O. Gubbay, *Ovulation and ovarian cancer*. Adv Exp Med Biol, 2008.  
26 **617**: p. 171-8.
- 27 142. Moorman, P.G., et al., *Ovulation and ovarian cancer: a comparison of two methods for*  
28 *calculating lifetime ovulatory cycles (United States)*. Cancer Causes Control, 2002. **13**(9): p. 807-  
29 11.
- 30 143. Macciò, A. and C. Madeddu, *Inflammation and ovarian cancer*. Cytokine, 2012. **58**(2): p. 133-47.
- 31 144. Pearce, C.L., et al., *Association between endometriosis and risk of histological subtypes of*  
32 *ovarian cancer: a pooled analysis of case-control studies*. Lancet Oncol, 2012. **13**(4): p. 385-94.
- 33 145. Wiegand, K.C., et al., *ARID1A mutations in endometriosis-associated ovarian carcinomas*. N Engl  
34 J Med, 2010. **363**(16): p. 1532-43.
- 35 146. Risch, H.A. and G.R. Howe, *Pelvic inflammatory disease and the risk of epithelial ovarian cancer*.  
36 Cancer Epidemiol Biomarkers Prev, 1995. **4**(5): p. 447-51.
- 37 147. Leitzmann, M.F., et al., *Body mass index and risk of ovarian cancer*. Cancer, 2009. **115**(4): p. 812-  
38 22.
- 39 148. Berg, J.M., J.L. Tymoczko, and L. Stryer, *Biochemistry: International Version*. 2002, WH Freeman.
- 40 149. Ogura, K., et al., *Effects of leptin on secretion of LH and FSH from primary cultured female rat*  
41 *pituitary cells*. 2001. **144**(6): p. 653-658.
- 42 150. Dunneram, Y., D.C. Greenwood, and J.E. Cade, *Diet, menopause and the risk of ovarian,*  
43 *endometrial and breast cancer*. Proc Nutr Soc, 2019. **78**(3): p. 438-448.
- 44 151. Jervis, S., et al., *Ovarian cancer familial relative risks by tumour subtypes and by known ovarian*  
45 *cancer genetic susceptibility variants*. 2014. **51**(2): p. 108-113.
- 46 152. Stratton, J.F., et al., *A systematic review and meta-analysis of family history and risk of ovarian*  
47 *cancer*. 1998. **105**(5): p. 493-499.

- 1 153. Alsop, K., et al., *BRCA mutation frequency and patterns of treatment response in BRCA*  
2 *mutation–positive women with ovarian cancer: a report from the Australian Ovarian Cancer*  
3 *Study Group*. 2012. **30**(21): p. 2654.
- 4 154. Antoniou, A., et al., *Average risks of breast and ovarian cancer associated with BRCA1 or BRCA2*  
5 *mutations detected in case series unselected for family history: a combined analysis of 22*  
6 *studies*. 2003. **72**(5): p. 1117-1130.
- 7 155. Chen, S. and G.J.J.o.c.o.o.j.o.t.A.S.o.C.O. Parmigiani, *Meta-analysis of BRCA1 and BRCA2*  
8 *penetrance*. 2007. **25**(11): p. 1329.
- 9 156. Lakhani, S.R., et al., *Pathology of ovarian cancers in BRCA1 and BRCA2 carriers*. 2004. **10**(7): p.  
10 2473-2481.
- 11 157. Yoshida, K. and Y. Miki, *Role of BRCA1 and BRCA2 as regulators of DNA repair, transcription, and*  
12 *cell cycle in response to DNA damage*. *Cancer Sci*, 2004. **95**(11): p. 866-71.
- 13 158. Bolton, K.L., et al., *Association between BRCA1 and BRCA2 mutations and survival in women with*  
14 *invasive epithelial ovarian cancer*. 2012. **307**(4): p. 382-389.
- 15 159. Patch, A.-M., et al., *Whole–genome characterization of chemoresistant ovarian cancer*. 2015.  
16 **521**(7553): p. 489-494.
- 17 160. Patel, P.S., A. Algouneh, and R. Hakem, *Exploiting synthetic lethality to target BRCA1/2-deficient*  
18 *tumors: where we stand*. *Oncogene*, 2021. **40**(17): p. 3001-3014.
- 19 161. Morris, C.R., M.T. Sands, and L.H. Smith, *Ovarian cancer: predictors of early-stage diagnosis*.  
20 *Cancer Causes Control*, 2010. **21**(8): p. 1203-11.
- 21 162. Præstegaard, C., et al., *The association between socioeconomic status and tumour stage at*  
22 *diagnosis of ovarian cancer: A pooled analysis of 18 case-control studies*. *Cancer Epidemiol*,  
23 2016. **41**: p. 71-9.
- 24 163. Alberg, A.J., et al., *Socioeconomic Status in Relation to the Risk of Ovarian Cancer in African-*  
25 *American Women: A Population-Based Case-Control Study*. *Am J Epidemiol*, 2016. **184**(4): p. 274-  
26 83.
- 27 164. *SEER. Cancer Stat Facts: ovarian cancer*. Available at  
28 <https://seer.cancer.gov/statfacts/html/ovary.html>. Retrieved December 2021.
- 29 165. Beral, V., et al., *Ovarian cancer and oral contraceptives: collaborative reanalysis of data from 45*  
30 *epidemiological studies including 23,257 women with ovarian cancer and 87,303 controls*. 2019.
- 31 166. Andrews, L. and D.G. Mutch, *Hereditary Ovarian Cancer and Risk Reduction*. *Best Pract Res Clin*  
32 *Obstet Gynaecol*, 2017. **41**: p. 31-48.
- 33 167. Rebbeck, T.R., N.D. Kauff, and S.M. Domchek, *Meta-analysis of risk reduction estimates*  
34 *associated with risk-reducing salpingo-oophorectomy in BRCA1 or BRCA2 mutation carriers*. *J*  
35 *Natl Cancer Inst*, 2009. **101**(2): p. 80-7.
- 36 168. Kauff, N.D., et al., *Risk-reducing salpingo-oophorectomy in women with a BRCA1 or BRCA2*  
37 *mutation*. *N Engl J Med*, 2002. **346**(21): p. 1609-15.
- 38 169. Koukoura, O., et al., *DNA methylation profiles in ovarian cancer: implication in diagnosis and*  
39 *therapy*. 2014. **10**(1): p. 3-9.
- 40 170. Doubeni, C.A., A.R. Doubeni, and A.E. Myers, *Diagnosis and Management of Ovarian Cancer*. *Am*  
41 *Fam Physician*, 2016. **93**(11): p. 937-44.
- 42 171. Ebell, M.H., M.B. Culp, and T.J. Radke, *A Systematic Review of Symptoms for the Diagnosis of*  
43 *Ovarian Cancer*. *Am J Prev Med*, 2016. **50**(3): p. 384-394.
- 44 172. Liu, J.H. and K.M. Zanotti, *Management of the adnexal mass*. *Obstet Gynecol*, 2011. **117**(6): p.  
45 1413-1428.
- 46 173. Cannistra, S.A., *Cancer of the ovary*. *N Engl J Med*, 2004. **351**(24): p. 2519-29.
- 47 174. Bodelon, C., et al., *Analysis of serial ovarian volume measurements and incidence of ovarian*  
48 *cancer: implications for pathogenesis*. 2014. **106**(10): p. dju262.

- 1 175. Sharma, A., et al., *Quality assurance and its impact on ovarian visualization rates in the*  
2 *multicenter United Kingdom Collaborative Trial of Ovarian Cancer Screening (UKCTOCS)*. 2016.  
3 **47**(2): p. 228-235.
- 4 176. Mathieu, K.B., et al., *Screening for ovarian cancer: imaging challenges and opportunities for*  
5 *improvement*. 2018. **51**(3): p. 293.
- 6 177. Aalipour, A., et al., *Engineered immune cells as highly sensitive cancer diagnostics*. 2019. **37**(5):  
7 p. 531-539.
- 8 178. Pal, S., et al., *DNA-enabled rational design of fluorescence-Raman bimodal nanoprobes for*  
9 *cancer imaging and therapy*. 2019. **10**(1): p. 1-13.
- 10 179. Bast, R.C., Jr., et al., *Reactivity of a monoclonal antibody with human ovarian carcinoma*. J Clin  
11 Invest, 1981. **68**(5): p. 1331-7.
- 12 180. Dochez, V., et al., *Biomarkers and algorithms for diagnosis of ovarian cancer: CA125, HE4, RMI*  
13 *and ROMA, a review*. J Ovarian Res, 2019. **12**(1): p. 28.
- 14 181. Clarke-Pearson, D.L., *Clinical practice. Screening for ovarian cancer*. N Engl J Med, 2009. **361**(2):  
15 p. 170-7.
- 16 182. Stewart, C., C. Ralyea, and S. Lockwood, *Ovarian Cancer: An Integrated Review*. Semin Oncol  
17 Nurs, 2019. **35**(2): p. 151-156.
- 18 183. Javadi, S., et al., *Ovarian Cancer, the Revised FIGO Staging System, and the Role of Imaging*. AJR  
19 Am J Roentgenol, 2016. **206**(6): p. 1351-60.
- 20 184. Duska, L.R. and E.C. Kohn, *The new classifications of ovarian, fallopian tube, and primary*  
21 *peritoneal cancer and their clinical implications*. Ann Oncol, 2017. **28**(suppl\_8): p. viii8-viii12.
- 22 185. Prat, J., *Abridged republication of FIGO's staging classification for cancer of the ovary, fallopian*  
23 *tube, and peritoneum*. Cancer, 2015. **121**(19): p. 3452-4.
- 24 186. Peres, L.C., et al., *Invasive Epithelial Ovarian Cancer Survival by Histotype and Disease Stage*. J  
25 Natl Cancer Inst, 2019. **111**(1): p. 60-68.
- 26 187. Prat, J., *FIGO's staging classification for cancer of the ovary, fallopian tube, and peritoneum:*  
27 *abridged republication*. J Gynecol Oncol, 2015. **26**(2): p. 87-9.
- 28 188. Brown, P.O. and C.J.P.m. Palmer, *The preclinical natural history of serous ovarian cancer:*  
29 *defining the target for early detection*. 2009. **6**(7): p. e1000114.
- 30 189. Nash, Z. and U. Menon, *Ovarian cancer screening: Current status and future directions*. Best  
31 Pract Res Clin Obstet Gynaecol, 2020. **65**: p. 32-45.
- 32 190. Stirling, D., et al., *Screening for familial ovarian cancer: failure of current protocols to detect*  
33 *ovarian cancer at an early stage according to the international Federation of gynecology and*  
34 *obstetrics system*. 2005. **23**(24): p. 5588-5596.
- 35 191. Jervis, S., et al., *A risk prediction algorithm for ovarian cancer incorporating BRCA1, BRCA2,*  
36 *common alleles and other familial effects*. 2015. **52**(7): p. 465-475.
- 37 192. Carver, T., et al., *CanRisk Tool-A Web Interface for the Prediction of Breast and Ovarian Cancer*  
38 *Risk and the Likelihood of Carrying Genetic Pathogenic Variants*. Cancer Epidemiol Biomarkers  
39 Prev, 2021. **30**(3): p. 469-473.
- 40 193. PI, M.W., et al., *FORECEE-Female cancer prediction using cervical omics to individualise*  
41 *screening and prevention*. 2017.
- 42 194. Nené, N.R., et al., *Association between the cervicovaginal microbiome, BRCA1 mutation status,*  
43 *and risk of ovarian cancer: a case-control study*. Lancet Oncol, 2019. **20**(8): p. 1171-1182.
- 44 195. Jacobs, I.J., et al., *Ovarian cancer screening and mortality in the UK Collaborative Trial of Ovarian*  
45 *Cancer Screening (UKCTOCS): a randomised controlled trial*. 2016. **387**(10022): p. 945-956.
- 46 196. Russell, M.R., et al., *Protein Z: A putative novel biomarker for early detection of ovarian cancer*.  
47 2016. **138**(12): p. 2984-2992.

- 1 197. Blyuss, O., et al., *Serial patterns of ovarian cancer biomarkers in a prediagnosis longitudinal*  
2 *dataset*. 2015. **2015**.
- 3 198. Yang, W.-L., et al., *Elevation of TP53 autoantibody before CA125 in preclinical invasive epithelial*  
4 *ovarian cancer*. 2017. **23**(19): p. 5912-5922.
- 5 199. Drescher, C.W., et al., *Longitudinal screening algorithm that incorporates change over time in*  
6 *CA125 levels identifies ovarian cancer earlier than a single-threshold rule*. 2013. **31**(3): p. 387.
- 7 200. Grossman, D.C., et al., *Screening for ovarian cancer: US preventive services task force*  
8 *recommendation statement*. 2018. **319**(6): p. 588-594.
- 9 201. UK National Screening Committee - Online at [https://view-health-screening-](https://view-health-screening-recommendations.service.gov.uk/?name=ovarian+cancer)  
10 [recommendations.service.gov.uk/?name=ovarian+cancer](https://view-health-screening-recommendations.service.gov.uk/?name=ovarian+cancer). Retrieved, December 2021.
- 11 202. Cohen, J.D., et al., *Detection and localization of surgically resectable cancers with a multi-analyte*  
12 *blood test*. 2018. **359**(6378): p. 926-930.
- 13 203. Kinde, I., et al., *Evaluation of DNA from the Papanicolaou test to detect ovarian and endometrial*  
14 *cancers*. 2013. **5**(167): p. 167ra4-167ra4.
- 15 204. Erickson, B.K., et al., *Detection of somatic TP53 mutations in tampons of patients with high-*  
16 *grade serous ovarian cancer*. 2014. **124**(5): p. 881.
- 17 205. Maritschnegg, E., et al., *Lavage of the uterine cavity for molecular detection of müllerian duct*  
18 *carcinomas: a proof-of-concept study*. 2015. **33**(36): p. 4293.
- 19 206. du Bois, A., et al., *Role of surgical outcome as prognostic factor in advanced epithelial ovarian*  
20 *cancer: a combined exploratory analysis of 3 prospectively randomized phase 3 multicenter*  
21 *trials: by the Arbeitsgemeinschaft Gynaekologische Onkologie Studiengruppe Ovarialkarzinom*  
22 *(AGO-OVAR) and the Groupe d'Investigateurs Nationaux Pour les Etudes des Cancers de l'Ovaire*  
23 *(GINECO)*. *Cancer*, 2009. **115**(6): p. 1234-44.
- 24 207. Karam, A., et al., *Fifth ovarian Cancer consensus conference of the gynecologic Cancer*  
25 *InterGroup: first-line interventions*. 2017. **28**(4): p. 711-717.
- 26 208. Griffiths, C.T. and A.F.J.T.S.c.o.N.A. Fuller, *Intensive surgical and chemotherapeutic management*  
27 *of advanced ovarian cancer*. 1978. **58**(1): p. 131-142.
- 28 209. Vaughan, S., et al., *Rethinking ovarian cancer: recommendations for improving outcomes*. *Nat*  
29 *Rev Cancer*, 2011. **11**(10): p. 719-25.
- 30 210. Trzaska, S.J.C. and e. news, *Cisplatin*. 2005. **83**(25): p. 52-52.
- 31 211. Karasawa, T. and P.S.J.T.I. Steyger, *An integrated view of cisplatin-induced nephrotoxicity and*  
32 *ototoxicity*. 2015. **237**(3): p. 219-227.
- 33 212. Bukowska, B., A. Gajek, and A. Marczak, *Two drugs are better than one. A short history of*  
34 *combined therapy of ovarian cancer*. *Contemp Oncol (Pozn)*, 2015. **19**(5): p. 350-3.
- 35 213. McGuire, W.P., et al., *Taxol: a unique antineoplastic agent with significant activity in advanced*  
36 *ovarian epithelial neoplasms*. *Ann Intern Med*, 1989. **111**(4): p. 273-9.
- 37 214. Thigpen, J.T., et al., *Phase II trial of paclitaxel in patients with progressive ovarian carcinoma*  
38 *after platinum-based chemotherapy: a Gynecologic Oncology Group study*. *J Clin Oncol*, 1994.  
39 **12**(9): p. 1748-53.
- 40 215. McGuire, W.P., et al., *Cyclophosphamide and cisplatin compared with paclitaxel and cisplatin in*  
41 *patients with stage III and stage IV ovarian cancer*. *N Engl J Med*, 1996. **334**(1): p. 1-6.
- 42 216. Bookman, M.A., B.E. Greer, and R.F. Ozols, *Optimal therapy of advanced ovarian cancer:*  
43 *carboplatin and paclitaxel versus cisplatin and paclitaxel (GOG158) and an update on GOG0182-*  
44 *ICON5*. *Int J Gynecol Cancer*, 2003. **13** **Suppl 2**: p. 149-55.
- 45 217. Neijt, J.P., et al., *Exploratory phase III study of paclitaxel and cisplatin versus paclitaxel and*  
46 *carboplatin in advanced ovarian cancer*. *J Clin Oncol*, 2000. **18**(17): p. 3084-92.
- 47 218. du Bois, A., et al., *A randomized clinical trial of cisplatin/paclitaxel versus carboplatin/paclitaxel*  
48 *as first-line treatment of ovarian cancer*. *J Natl Cancer Inst*, 2003. **95**(17): p. 1320-9.

- 1 219. Chan, J.K., et al., *Weekly vs. Every-3-Week Paclitaxel and Carboplatin for Ovarian Cancer*. N Engl  
2 J Med, 2016. **374**(8): p. 738-48.
- 3 220. Katsumata, N., et al., *Long-term follow-up of a randomized trial comparing conventional  
4 paclitaxel and carboplatin with dose-dense weekly paclitaxel and carboplatin in women with  
5 advanced epithelial ovarian, fallopian tube, or primary peritoneal cancer: JGOG 3016 trial*. 2012,  
6 American Society of Clinical Oncology.
- 7 221. Pignata, S., et al., *Carboplatin plus paclitaxel once a week versus every 3 weeks in patients with  
8 advanced ovarian cancer (MITO-7): a randomised, multicentre, open-label, phase 3 trial*. Lancet  
9 Oncol, 2014. **15**(4): p. 396-405.
- 10 222. Monk, B.J. and J.K. Chan, *Is intraperitoneal chemotherapy still an acceptable option in primary  
11 adjuvant chemotherapy for advanced ovarian cancer?* Ann Oncol, 2017. **28**(suppl\_8): p. viii40-  
12 viii45.
- 13 223. Jayson, G.C., et al., *Ovarian cancer*. Lancet, 2014. **384**(9951): p. 1376-88.
- 14 224. Gill, S.E., et al., *Optimizing the treatment of ovarian cancer: Neoadjuvant chemotherapy and  
15 interval debulking versus primary debulking surgery for epithelial ovarian cancers likely to have  
16 suboptimal resection*. Gynecol Oncol, 2017. **144**(2): p. 266-273.
- 17 225. Damia, G. and M. Broggini, *Platinum Resistance in Ovarian Cancer: Role of DNA Repair*. Cancers  
18 (Basel), 2019. **11**(1).
- 19 226. Pilié, P.G., et al., *State-of-the-art strategies for targeting the DNA damage response in cancer*.  
20 Nat Rev Clin Oncol, 2019. **16**(2): p. 81-104.
- 21 227. Zhao, H. and H. Piwnicka-Worms, *ATR-mediated checkpoint pathways regulate phosphorylation  
22 and activation of human Chk1*. Mol Cell Biol, 2001. **21**(13): p. 4129-39.
- 23 228. Galluzzi, L., et al., *Mitochondrial liaisons of p53*. Antioxid Redox Signal, 2011. **15**(6): p. 1691-714.
- 24 229. Kroemer, G., L. Galluzzi, and C. Brenner, *Mitochondrial membrane permeabilization in cell death*.  
25 Physiol Rev, 2007. **87**(1): p. 99-163.
- 26 230. Gupta, S.C., et al., *Upsides and downsides of reactive oxygen species for cancer: the roles of  
27 reactive oxygen species in tumorigenesis, prevention, and therapy*. Antioxid Redox Signal, 2012.  
28 **16**(11): p. 1295-322.
- 29 231. Martindale, J.L. and N.J. Holbrook, *Cellular response to oxidative stress: signaling for suicide and  
30 survival*. J Cell Physiol, 2002. **192**(1): p. 1-15.
- 31 232. Joybari, A.Y., et al., *Oxaliplatin-induced renal tubular vacuolization*. Ann Pharmacother, 2014.  
32 **48**(6): p. 796-800.
- 33 233. Dasari, S. and P.B. Tchounwou, *Cisplatin in cancer therapy: molecular mechanisms of action*. Eur  
34 J Pharmacol, 2014. **740**: p. 364-78.
- 35 234. Ozben, T., *Oxidative stress and apoptosis: impact on cancer therapy*. J Pharm Sci, 2007. **96**(9): p.  
36 2181-96.
- 37 235. Shrivastava, A., et al., *Cannabidiol induces programmed cell death in breast cancer cells by  
38 coordinating the cross-talk between apoptosis and autophagy*. Mol Cancer Ther, 2011. **10**(7): p.  
39 1161-72.
- 40 236. Hosnedlova, B., et al., *Nano-selenium and its nanomedicine applications: a critical review*. Int J  
41 Nanomedicine, 2018. **13**: p. 2107-2128.
- 42 237. Boulikas, T., et al., *Systemic Lipoplatin infusion results in preferential tumor uptake in human  
43 studies*. Anticancer Res, 2005. **25**(4): p. 3031-9.
- 44 238. Lee, Y.T., Y.J. Tan, and C.E. Oon, *Molecular targeted therapy: Treating cancer with specificity*. Eur  
45 J Pharmacol, 2018. **834**: p. 188-196.
- 46 239. Padma, V.V., *An overview of targeted cancer therapy*. BioMedicine, 2015. **5**(4): p. 1-6.
- 47 240. Amer, M.H., *Gene therapy for cancer: present status and future perspective*. Molecular and  
48 cellular therapies, 2014. **2**(1): p. 1-19.



- 1 241. Tsai, M.-J., et al., *Tumor microenvironment: a new treatment target for cancer*. International  
2 Scholarly Research Notices, 2014. **2014**.
- 3 242. Saijo, N., *Progress in cancer chemotherapy with special stress on molecular-targeted therapy*.  
4 Japanese journal of clinical oncology, 2010. **40**(9): p. 855-862.
- 5 243. Sherr, C.J., D. Beach, and G.I. Shapiro, *Targeting CDK4 and CDK6: From Discovery to Therapy*.  
6 Cancer Discov, 2016. **6**(4): p. 353-67.
- 7 244. Vaughn, D.J., et al., *Phase 2 trial of the cyclin-dependent kinase 4/6 inhibitor palbociclib in*  
8 *patients with retinoblastoma protein-expressing germ cell tumors*. Cancer, 2015. **121**(9): p.  
9 1463-8.
- 10 245. Gopalan, P.K., et al., *A phase II clinical trial of the CDK 4/6 inhibitor palbociclib (PD 0332991) in*  
11 *previously treated, advanced non-small cell lung cancer (NSCLC) patients with inactivated*  
12 *CDKN2A*. 2014, American Society of Clinical Oncology.
- 13 246. Leonard, J.P., et al., *Selective CDK4/6 inhibition with tumor responses by PD0332991 in patients*  
14 *with mantle cell lymphoma*. Blood, 2012. **119**(20): p. 4597-607.
- 15 247. Finn, R.S., et al., *PD 0332991, a selective cyclin D kinase 4/6 inhibitor, preferentially inhibits*  
16 *proliferation of luminal estrogen receptor-positive human breast cancer cell lines in vitro*. Breast  
17 Cancer Res, 2009. **11**(5): p. R77.
- 18 248. Zhang, Y.X., et al., *Antiproliferative effects of CDK4/6 inhibition in CDK4-amplified human*  
19 *liposarcoma in vitro and in vivo*. Mol Cancer Ther, 2014. **13**(9): p. 2184-93.
- 20 249. Rader, J., et al., *Dual CDK4/CDK6 inhibition induces cell-cycle arrest and senescence in*  
21 *neuroblastoma*. Clin Cancer Res, 2013. **19**(22): p. 6173-82.
- 22 250. Hortobagyi, G.N., et al., *Ribociclib as First-Line Therapy for HR-Positive, Advanced Breast Cancer*.  
23 N Engl J Med, 2016. **375**(18): p. 1738-1748.
- 24 251. Finn, R.S., et al., *Palbociclib and Letrozole in Advanced Breast Cancer*. N Engl J Med, 2016.  
25 **375**(20): p. 1925-1936.
- 26 252. Taylor-Harding, B., et al., *Cyclin E1 and RTK/RAS signaling drive CDK inhibitor resistance via*  
27 *activation of E2F and ETS*. Oncotarget, 2015. **6**(2): p. 696-714.
- 28 253. Iyengar, M., et al., *CDK4/6 inhibition as maintenance and combination therapy for high grade*  
29 *serous ovarian cancer*. Oncotarget, 2018. **9**(21): p. 15658-15672.
- 30 254. Basu, A. and S. Krishnamurthy, *Cellular responses to Cisplatin-induced DNA damage*. J Nucleic  
31 Acids, 2010. **2010**.
- 32 255. Konecny, G.E., *Combining PARP and CDK4/6 inhibitors in MYC driven ovarian cancer*.  
33 EBioMedicine, 2019. **43**: p. 9-10.
- 34 256. Zhang, Q.F., et al., *CDK4/6 inhibition promotes immune infiltration in ovarian cancer and*  
35 *synergizes with PD-1 blockade in a B cell-dependent manner*. Theranostics, 2020. **10**(23): p.  
36 10619-10633.
- 37 257. Yi, J., et al., *MYC status as a determinant of synergistic response to Olaparib and Palbociclib in*  
38 *ovarian cancer*. EBioMedicine, 2019. **43**: p. 225-237.
- 39 258. Goel, S., et al., *CDK4/6 inhibition triggers anti-tumour immunity*. Nature, 2017. **548**(7668): p.  
40 471-475.
- 41 259. Schaer, D.A., et al., *The CDK4/6 Inhibitor Abemaciclib Induces a T Cell Inflamed Tumor*  
42 *Microenvironment and Enhances the Efficacy of PD-L1 Checkpoint Blockade*. Cell Rep, 2018.  
43 **22**(11): p. 2978-2994.
- 44 260. Morgan, R.J., et al., *Ovarian cancer, version 1.2016, NCCN clinical practice guidelines in oncology*.  
45 Journal of the National Comprehensive Cancer Network, 2016. **14**(9): p. 1134-1163.
- 46 261. Xu, X.L., et al., *A novel nomogram based on LODDS to predict the prognosis of epithelial ovarian*  
47 *cancer*. Oncotarget, 2017. **8**(5): p. 8120-8130.

- 1 262. Pfisterer, J., et al., *Gemcitabine plus carboplatin compared with carboplatin in patients with*  
2 *platinum-sensitive recurrent ovarian cancer: an intergroup trial of the AGO-OVAR, the NCIC CTG,*  
3 *and the EORTC GCG.* Journal of Clinical Oncology, 2006. **24**(29): p. 4699-4707.
- 4 263. Abdullah, L.N. and E.K. Chow, *Mechanisms of chemoresistance in cancer stem cells.* Clin Transl  
5 Med, 2013. **2**(1): p. 3.
- 6 264. Tapia, G. and I. Diaz-Padilla, *Molecular mechanisms of platinum resistance in ovarian cancer.*  
7 Ovarian Cancer-A clinical and translational update, 2013.
- 8 265. Ling, K.-S., et al., *Mechanisms involved in chemoresistance in ovarian cancer.* Taiwanese Journal  
9 of Obstetrics and Gynecology, 2005. **44**(3): p. 209-217.
- 10 266. Salomon-Perzyński, A., et al., *High-grade serous ovarian cancer: the clone wars.* Arch Gynecol  
11 Obstet, 2017. **295**(3): p. 569-576.
- 12 267. Cooke, S.L. and J.D. Brenton, *Evolution of platinum resistance in high-grade serous ovarian*  
13 *cancer.* Lancet Oncol, 2011. **12**(12): p. 1169-74.
- 14 268. Sagggar, J.K., et al., *The tumor microenvironment and strategies to improve drug distribution.*  
15 Front Oncol, 2013. **3**: p. 154.
- 16 269. Meads, M.B., R.A. Gatenby, and W.S. Dalton, *Environment-mediated drug resistance: a major*  
17 *contributor to minimal residual disease.* Nat Rev Cancer, 2009. **9**(9): p. 665-74.
- 18 270. Cornelison, R., D.C. Llana, and C.N. Landen, *Emerging Therapeutics to Overcome*  
19 *Chemoresistance in Epithelial Ovarian Cancer: A Mini-Review.* Int J Mol Sci, 2017. **18**(10).
- 20 271. Freimund, A.E., et al., *Mechanisms of Drug Resistance in High-Grade Serous Ovarian Cancer.*  
21 Hematol Oncol Clin North Am, 2018. **32**(6): p. 983-996.
- 22 272. Matsumoto, S., et al., *Effect of copper and role of the copper transporters ATP7A and CTR1 in*  
23 *intracellular accumulation of cisplatin.* Anticancer Res, 2007. **27**(4b): p. 2209-16.
- 24 273. Kim, E.S., et al., *Copper transporter CTR1 expression and tissue platinum concentration in non-*  
25 *small cell lung cancer.* Lung Cancer, 2014. **85**(1): p. 88-93.
- 26 274. Sun, S., et al., *The association between copper transporters and the prognosis of cancer patients*  
27 *undergoing chemotherapy: a meta-analysis of literatures and datasets.* Oncotarget, 2017. **8**(9):  
28 p. 16036-16051.
- 29 275. Hall, M.D., et al., *The role of cellular accumulation in determining sensitivity to platinum-based*  
30 *chemotherapy.* Annu Rev Pharmacol Toxicol, 2008. **48**: p. 495-535.
- 31 276. Ishida, S., et al., *Uptake of the anticancer drug cisplatin mediated by the copper transporter Ctr1*  
32 *in yeast and mammals.* Proc Natl Acad Sci U S A, 2002. **99**(22): p. 14298-302.
- 33 277. Petris, M.J., et al., *Copper-stimulated endocytosis and degradation of the human copper*  
34 *transporter, hCtr1.* J Biol Chem, 2003. **278**(11): p. 9639-46.
- 35 278. Katano, K., et al., *Acquisition of resistance to cisplatin is accompanied by changes in the cellular*  
36 *pharmacology of copper.* Cancer Res, 2002. **62**(22): p. 6559-65.
- 37 279. Ishida, S., et al., *Enhancing tumor-specific uptake of the anticancer drug cisplatin with a copper*  
38 *chelator.* Cancer Cell, 2010. **17**(6): p. 574-83.
- 39 280. Fu, S., et al., *Exploratory study of carboplatin plus the copper-lowering agent trientine in patients*  
40 *with advanced malignancies.* Invest New Drugs, 2014. **32**(3): p. 465-72.
- 41 281. Holzer, A.K., et al., *Cisplatin rapidly down-regulates its own influx transporter hCTR1 in cultured*  
42 *human ovarian carcinoma cells.* Clin Cancer Res, 2004. **10**(19): p. 6744-9.
- 43 282. Lee, J., M.J. Petris, and D.J. Thiele, *Characterization of mouse embryonic cells deficient in the ctr1*  
44 *high affinity copper transporter. Identification of a Ctr1-independent copper transport system.* J  
45 Biol Chem, 2002. **277**(43): p. 40253-9.
- 46 283. Holzer, A.K., G.H. Manorek, and S.B. Howell, *Contribution of the major copper influx transporter*  
47 *CTR1 to the cellular accumulation of cisplatin, carboplatin, and oxaliplatin.* Mol Pharmacol, 2006.  
48 **70**(4): p. 1390-4.

- 1 284. Yoshizawa, K., et al., *Copper efflux transporter (ATP7B) contributes to the acquisition of cisplatin-*  
2 *resistance in human oral squamous cell lines.* Oncol Rep, 2007. **18**(4): p. 987-91.
- 3 285. Samimi, G., et al., *Increased expression of the copper efflux transporter ATP7A mediates*  
4 *resistance to cisplatin, carboplatin, and oxaliplatin in ovarian cancer cells.* Clin Cancer Res, 2004.  
5 **10**(14): p. 4661-9.
- 6 286. Samimi, G., et al., *Increased expression of the copper efflux transporter ATP7A mediates*  
7 *resistance to cisplatin, carboplatin, and oxaliplatin in ovarian cancer cells.* Clinical Cancer  
8 Research, 2004. **10**(14): p. 4661-4669.
- 9 287. Katano, K., et al., *Confocal microscopic analysis of the interaction between cisplatin and the*  
10 *copper transporter ATP7B in human ovarian carcinoma cells.* Clinical cancer research, 2004.  
11 **10**(13): p. 4578-4588.
- 12 288. Katano, K., et al., *The copper export pump ATP7B modulates the cellular pharmacology of*  
13 *carboplatin in ovarian carcinoma cells.* Molecular pharmacology, 2003. **64**(2): p. 466-473.
- 14 289. Katano, K., et al., *Acquisition of resistance to cisplatin is accompanied by changes in the cellular*  
15 *pharmacology of copper.* Cancer research, 2002. **62**(22): p. 6559-6565.
- 16 290. Lutsenko, S., et al., *Function and regulation of human copper-transporting ATPases.* Physiol Rev,  
17 2007. **87**(3): p. 1011-46.
- 18 291. Konkimalla, V.B., B. Kaina, and T. Efferth, *Role of transporter genes in cisplatin resistance.* In  
19 *Vivo*, 2008. **22**(3): p. 279-283.
- 20 292. Mangala, L.S., et al., *Therapeutic Targeting of ATP7B in Ovarian Carcinoma.* Clin Cancer Res,  
21 2009. **15**(11): p. 3770-80.
- 22 293. Lukanović, D., et al., *The contribution of copper efflux transporters ATP7A and ATP7B to*  
23 *chemoresistance and personalized medicine in ovarian cancer.* Biomed Pharmacother, 2020.  
24 **129**: p. 110401.
- 25 294. Zhou, J., et al., *The Drug-Resistance Mechanisms of Five Platinum-Based Antitumor Agents.* Front  
26 *Pharmacol*, 2020. **11**: p. 343.
- 27 295. Brozovic, A., A. Ambriović-Ristov, and M. Osmak, *The relationship between cisplatin-induced*  
28 *reactive oxygen species, glutathione, and BCL-2 and resistance to cisplatin.* Crit Rev Toxicol,  
29 2010. **40**(4): p. 347-59.
- 30 296. Zimmermann, T. and J.V. Burda, *Cisplatin interaction with amino acids cysteine and methionine*  
31 *from gas phase to solutions with constant pH.* Interdiscip Sci, 2010. **2**(1): p. 98-114.
- 32 297. Byun, S.S., et al., *Augmentation of cisplatin sensitivity in cisplatin-resistant human bladder*  
33 *cancer cells by modulating glutathione concentrations and glutathione-related enzyme activities.*  
34 *BJU Int*, 2005. **95**(7): p. 1086-90.
- 35 298. Masters, J.R., et al., *Sensitivity of testis tumour cells to chemotherapeutic drugs: role of*  
36 *detoxifying pathways.* Eur J Cancer, 1996. **32a**(7): p. 1248-53.
- 37 299. Cadoni, E., et al., *Competitive reactions among glutathione, cisplatin and copper-phenanthroline*  
38 *complexes.* J Inorg Biochem, 2017. **173**: p. 126-133.
- 39 300. Rocha, C.R., et al., *Glutathione depletion sensitizes cisplatin- and temozolomide-resistant glioma*  
40 *cells in vitro and in vivo.* Cell Death Dis, 2015. **6**(4): p. e1727.
- 41 301. Estrela, J.M., A. Ortega, and E. Obrador, *Glutathione in cancer biology and therapy.* Crit Rev Clin  
42 *Lab Sci*, 2006. **43**(2): p. 143-81.
- 43 302. Kimura, T. and T. Kambe, *The Functions of Metallothionein and ZIP and ZnT Transporters: An*  
44 *Overview and Perspective.* Int J Mol Sci, 2016. **17**(3): p. 336.
- 45 303. Krizkova, S., et al., *An adsorptive transfer technique coupled with brdicka reaction to reveal the*  
46 *importance of metallothionein in chemotherapy with platinum based cytostatics.* Int J Mol Sci,  
47 2010. **11**(12): p. 4826-42.

- 1 304. Habel, N., et al., *Zinc chelation: a metallothionein 2A's mechanism of action involved in*  
2 *osteosarcoma cell death and chemotherapy resistance*. Cell Death Dis, 2013. **4**(10): p. e874.
- 3 305. Pekarik, V., et al., *Prostate cancer, miRNAs, metallothioneins and resistance to cytostatic drugs*.  
4 Curr Med Chem, 2013. **20**(4): p. 534-44.
- 5 306. Dabholkar, M., et al., *Messenger RNA levels of XPAC and ERCC1 in ovarian cancer tissue correlate*  
6 *with response to platinum-based chemotherapy*. J Clin Invest, 1994. **94**(2): p. 703-8.
- 7 307. Reed, E., *Platinum-DNA adduct, nucleotide excision repair and platinum based anti-cancer*  
8 *chemotherapy*. Cancer Treat Rev, 1998. **24**(5): p. 331-44.
- 9 308. Spivak, G., *Nucleotide excision repair in humans*. DNA Repair (Amst), 2015. **36**: p. 13-18.
- 10 309. Wright, W.D., S.S. Shah, and W.D. Heyer, *Homologous recombination and the repair of DNA*  
11 *double-strand breaks*. J Biol Chem, 2018. **293**(27): p. 10524-10535.
- 12 310. Edwards, S.L., et al., *Resistance to therapy caused by intragenic deletion in BRCA2*. Nature, 2008.  
13 **451**(7182): p. 1111-5.
- 14 311. Wawryk-Gawda, E., et al., *P53 protein in proliferation, repair and apoptosis of cells*.  
15 Protoplasma, 2014. **251**(3): p. 525-33.
- 16 312. Oda, E., et al., *Noxa, a BH3-only member of the Bcl-2 family and candidate mediator of p53-*  
17 *induced apoptosis*. Science, 2000. **288**(5468): p. 1053-8.
- 18 313. Nakano, K. and K.H. Vousden, *PUMA, a novel proapoptotic gene, is induced by p53*. Mol Cell,  
19 2001. **7**(3): p. 683-94.
- 20 314. Kigawa, J., et al., *p53 gene status and chemosensitivity in ovarian cancer*. Hum Cell, 2001. **14**(3):  
21 p. 165-71.
- 22 315. Asada, N., H. Tsuchiya, and K. Tomita, *De novo deletions of p53 gene and wild-type p53 correlate*  
23 *with acquired cisplatin-resistance in human osteosarcoma OST cell line*. Anticancer Res, 1999.  
24 **19**(6b): p. 5131-7.
- 25 316. Sznarkowska, A., R. Olszewski, and J. Zawacka-Pankau, *[Pharmacological activation of tumor*  
26 *suppressor, wild-type p53 as a promising strategy to fight cancer]*. Postepy Hig Med Dosw  
27 (Online), 2010. **64**: p. 396-407.
- 28 317. Abel, F., et al., *Imbalance of the mitochondrial pro-and anti-apoptotic mediators in*  
29 *neuroblastoma tumours with unfavourable biology*. 2005. **41**(4): p. 635-646.
- 30 318. Plas, D.R. and C.B. Thompson, *Akt-dependent transformation: there is more to growth than just*  
31 *surviving*. Oncogene, 2005. **24**(50): p. 7435-42.
- 32 319. Pommier, Y., et al., *Apoptosis defects and chemotherapy resistance: molecular interaction maps*  
33 *and networks*. Oncogene, 2004. **23**(16): p. 2934-49.
- 34 320. Norouzi-Barough, L., et al., *Molecular mechanisms of drug resistance in ovarian cancer*. J Cell  
35 Physiol, 2018. **233**(6): p. 4546-4562.
- 36 321. Peracchio, C., et al., *Involvement of autophagy in ovarian cancer: a working hypothesis*. J  
37 Ovarian Res, 2012. **5**(1): p. 22.
- 38 322. Dahiya, N. and P.J. Morin, *MicroRNAs in ovarian carcinomas*. Endocr Relat Cancer, 2010. **17**(1):  
39 p. F77-89.
- 40 323. Shen, D.W., et al., *Cisplatin resistance: a cellular self-defense mechanism resulting from multiple*  
41 *epigenetic and genetic changes*. Pharmacol Rev, 2012. **64**(3): p. 706-21.
- 42 324. Kato, K., et al., *Structure and functional analysis of the human STAT3 gene promoter: alteration*  
43 *of chromatin structure as a possible mechanism for the upregulation in cisplatin-resistant cells*.  
44 Biochim Biophys Acta, 2000. **1493**(1-2): p. 91-100.
- 45 325. Chang, X., et al., *Identification of hypermethylated genes associated with cisplatin resistance in*  
46 *human cancers*. Cancer Res, 2010. **70**(7): p. 2870-9.
- 47 326. Steele, N., et al., *Combined inhibition of DNA methylation and histone acetylation enhances gene*  
48 *re-expression and drug sensitivity in vivo*. Br J Cancer, 2009. **100**(5): p. 758-63.

- 1 327. Warburg, O., *On the origin of cancer cells*. Science, 1956. **123**(3191): p. 309-14.
- 2 328. Hui, S., et al., *Glucose feeds the TCA cycle via circulating lactate*. Nature, 2017. **551**(7678): p.
- 3 115-118.
- 4 329. Gillies, R.J., I. Robey, and R.A. Gatenby, *Causes and consequences of increased glucose*
- 5 *metabolism of cancers*. J Nucl Med, 2008. **49 Suppl 2**: p. 24s-42s.
- 6 330. Gatenby, R.A. and E.T. Gawlinski, *The glycolytic phenotype in carcinogenesis and tumor invasion:*
- 7 *insights through mathematical models*. Cancer Res, 2003. **63**(14): p. 3847-54.
- 8 331. Greijer, A. and E.J.J.o.c.p. Van der Wall, *The role of hypoxia inducible factor 1 (HIF-1) in hypoxia*
- 9 *induced apoptosis*. 2004. **57**(10): p. 1009-1014.
- 10 332. Elstrom, R.L., et al., *Akt stimulates aerobic glycolysis in cancer cells*. 2004. **64**(11): p. 3892-3899.
- 11 333. Matoba, S., et al., *p53 regulates mitochondrial respiration*. 2006. **312**(5780): p. 1650-1653.
- 12 334. Lunt, S.Y. and M.G. Vander Heiden, *Aerobic glycolysis: meeting the metabolic requirements of*
- 13 *cell proliferation*. Annu Rev Cell Dev Biol, 2011. **27**: p. 441-64.
- 14 335. Pelicano, H., et al., *Mitochondrial respiration defects in cancer cells cause activation of Akt*
- 15 *survival pathway through a redox-mediated mechanism*. 2006. **175**(6): p. 913-923.
- 16 336. Gottlieb, E. and I.P.J.N.R.C. Tomlinson, *Mitochondrial tumour suppressors: a genetic and*
- 17 *biochemical update*. 2005. **5**(11): p. 857-866.
- 18 337. Klawitter, J., et al., *Metabolic characteristics of imatinib resistance in chronic myeloid leukaemia*
- 19 *cells*. Br J Pharmacol, 2009. **158**(2): p. 588-600.
- 20 338. Merz, A.L. and N.J. Serkova, *Use of nuclear magnetic resonance-based metabolomics in*
- 21 *detecting drug resistance in cancer*. Biomark Med, 2009. **3**(3): p. 289-306.
- 22 339. Kao, K.K. and M.P. Fink, *The biochemical basis for the anti-inflammatory and cytoprotective*
- 23 *actions of ethyl pyruvate and related compounds*. Biochem Pharmacol, 2010. **80**(2): p. 151-9.
- 24 340. Huang, C.Y., et al., *Distinct cytoprotective roles of pyruvate and ATP by glucose metabolism on*
- 25 *epithelial necroptosis and crypt proliferation in ischaemic gut*. J Physiol, 2017. **595**(2): p. 505-
- 26 521.
- 27 341. Liu, X., et al., *Acetate Production from Glucose and Coupling to Mitochondrial Metabolism in*
- 28 *Mammals*. Cell, 2018. **175**(2): p. 502-513.e13.
- 29 342. Moloney, J.N. and T.G. Cotter, *ROS signalling in the biology of cancer*. Semin Cell Dev Biol, 2018.
- 30 **80**: p. 50-64.
- 31 343. Semenza, G.L.J.B.J., *Oxygen-dependent regulation of mitochondrial respiration by hypoxia-*
- 32 *inducible factor 1*. 2007. **405**(1): p. 1-9.
- 33 344. Bustamente, E., H.P. Morris, and P.L. Pedersen, *Hexokinase: the direct link between*
- 34 *mitochondrial and glycolytic reactions in rapidly growing cancer cells*. Adv Exp Med Biol, 1977.
- 35 **92**: p. 363-80.
- 36 345. Mathupala, S.P., Y.H. Ko, and P.L. Pedersen, *Hexokinase II: cancer's double-edged sword acting*
- 37 *as both facilitator and gatekeeper of malignancy when bound to mitochondria*. Oncogene, 2006.
- 38 **25**(34): p. 4777-86.
- 39 346. Pastorino, J.G., N. Shulga, and J.B. Hoek, *Mitochondrial binding of hexokinase II inhibits Bax-*
- 40 *induced cytochrome c release and apoptosis*. J Biol Chem, 2002. **277**(9): p. 7610-8.
- 41 347. Wallace, D.C., *Mitochondria and cancer*. Nat Rev Cancer, 2012. **12**(10): p. 685-98.
- 42 348. Weinberg, S.E. and N.S. Chandel, *Targeting mitochondria metabolism for cancer therapy*. Nat
- 43 Chem Biol, 2015. **11**(1): p. 9-15.
- 44 349. Emmings, E., et al., *Targeting Mitochondria for Treatment of Chemoresistant Ovarian Cancer*. Int
- 45 J Mol Sci, 2019. **20**(1).
- 46 350. DeBerardinis, R.J., et al., *The biology of cancer: metabolic reprogramming fuels cell growth and*
- 47 *proliferation*. Cell Metab, 2008. **7**(1): p. 11-20.

- 1 351. Yousefi, M., et al., *Current insights into the metastasis of epithelial ovarian cancer - hopes and*  
2 *hurdles*. Cell Oncol (Dordr), 2020. **43**(4): p. 515-538.
- 3 352. Hess, K.R., et al., *Metastatic patterns in adenocarcinoma*. Cancer, 2006. **106**(7): p. 1624-1633.
- 4 353. Chaffer, C.L. and R.A. Weinberg, *A perspective on cancer cell metastasis*. science, 2011.  
5 **331**(6024): p. 1559-1564.
- 6 354. Eisenkop, S.M. and N.M. Spirtos, *The clinical significance of occult macroscopically positive*  
7 *retroperitoneal nodes in patients with epithelial ovarian cancer*. Gynecol Oncol, 2001. **82**(1): p.  
8 143-9.
- 9 355. Tan, D.S., R. Agarwal, and S.B. Kaye, *Mechanisms of transcoelomic metastasis in ovarian cancer*.  
10 The lancet oncology, 2006. **7**(11): p. 925-934.
- 11 356. Xu, L., et al., *Inhibition of malignant ascites and growth of human ovarian carcinoma by oral*  
12 *administration of a potent inhibitor of the vascular endothelial growth factor receptor tyrosine*  
13 *kinases*. International journal of oncology, 2000. **16**(3): p. 445-499.
- 14 357. Kipps, E., D.S. Tan, and S.B. Kaye, *Meeting the challenge of ascites in ovarian cancer: new*  
15 *avenues for therapy and research*. Nat Rev Cancer, 2013. **13**(4): p. 273-82.
- 16 358. Kim, S., et al., *Malignant ascites enhances migratory and invasive properties of ovarian cancer*  
17 *cells with membrane bound IL-6R in vitro*. Oncotarget, 2016. **7**(50): p. 83148-83159.
- 18 359. Kim, S., B. Kim, and Y.S. Song, *Ascites modulates cancer cell behavior, contributing to tumor*  
19 *heterogeneity in ovarian cancer*. Cancer Sci, 2016. **107**(9): p. 1173-8.
- 20 360. Kim, K.S., et al., *Hypoxia enhances lysophosphatidic acid responsiveness in ovarian cancer cells*  
21 *and lysophosphatidic acid induces ovarian tumor metastasis in vivo*. Cancer Res, 2006. **66**(16): p.  
22 7983-90.
- 23 361. Runyon, B.A., J.C. Hoefs, and T.R. Morgan, *Ascitic fluid analysis in malignancy-related ascites*.  
24 Hepatology, 1988. **8**(5): p. 1104-9.
- 25 362. Ahmed, N. and K. Stenvers, *Getting to know ovarian cancer ascites: opportunities for targeted*  
26 *therapy-based translational research*. Frontiers in oncology, 2013. **3**: p. 256.
- 27 363. Carmignani, C.P., et al., *Intraperitoneal cancer dissemination: mechanisms of the patterns of*  
28 *spread*. Cancer and Metastasis Reviews, 2003. **22**(4): p. 465.
- 29 364. Lopez, R.I., et al., *Prognostic factor analysis, for patients with no evidence of disease after initial*  
30 *chemotherapy for advanced epithelial ovarian carcinoma*. International Journal of Gynecological  
31 Cancer, 1996. **6**(1): p. 8-14.
- 32 365. Tan, D.S., R. Agarwal, and S.B. Kaye, *Mechanisms of transcoelomic metastasis in ovarian cancer*.  
33 Lancet Oncol, 2006. **7**(11): p. 925-34.
- 34 366. Landen, C.N., Jr., M.J. Birrer, and A.K. Sood, *Early events in the pathogenesis of epithelial ovarian*  
35 *cancer*. J Clin Oncol, 2008. **26**(6): p. 995-1005.
- 36 367. Sher, I., et al., *Autocrine VEGF-A/KDR loop protects epithelial ovarian carcinoma cells from*  
37 *anoikis*. Int J Cancer, 2009. **124**(3): p. 553-61.
- 38 368. Makhija, S., et al., *Taxol-induced bcl-2 phosphorylation in ovarian cancer cell monolayer and*  
39 *spheroids*. Int J Oncol, 1999. **14**(3): p. 515-21.
- 40 369. L'Esperance, S., et al., *Global gene expression analysis of early response to chemotherapy*  
41 *treatment in ovarian cancer spheroids*. BMC Genomics, 2008. **9**: p. 99.
- 42 370. House, C.D., L. Hernandez, and C.M. Annunziata, *In vitro enrichment of ovarian cancer tumor-*  
43 *initiating cells*. J Vis Exp, 2015(96).
- 44 371. Burleson, K.M., et al., *Ovarian carcinoma ascites spheroids adhere to extracellular matrix*  
45 *components and mesothelial cell monolayers*. Gynecol Oncol, 2004. **93**(1): p. 170-81.
- 46 372. Burleson, K.M., L.K. Hansen, and A.P. Skubitz, *Ovarian carcinoma spheroids disaggregate on type*  
47 *I collagen and invade live human mesothelial cell monolayers*. Clin Exp Metastasis, 2004. **21**(8):  
48 p. 685-97.

- 1 373. Shield, K., et al., *Multicellular spheroids in ovarian cancer metastases: Biology and pathology*.  
2 Gynecol Oncol, 2009. **113**(1): p. 143-8.
- 3 374. Burleson, K.M., et al., *Ovarian carcinoma ascites spheroids adhere to extracellular matrix*  
4 *components and mesothelial cell monolayers*. Gynecologic oncology, 2004. **93**(1): p. 170-181.
- 5 375. Colvin, E.K., *Tumor-associated macrophages contribute to tumor progression in ovarian cancer*.  
6 Front Oncol, 2014. **4**: p. 137.
- 7 376. Davidson, B., C.G. Trope, and R. Reich, *The role of the tumor stroma in ovarian cancer*. Front  
8 Oncol, 2014. **4**: p. 104.
- 9 377. Abrahams, V.M., et al., *Epithelial ovarian cancer cells secrete functional Fas ligand*. Cancer Res,  
10 2003. **63**(17): p. 5573-81.
- 11 378. Frankel, A., R. Buckman, and R.S. Kerbel, *Abrogation of taxol-induced G2-M arrest and apoptosis*  
12 *in human ovarian cancer cells grown as multicellular tumor spheroids*. Cancer Res, 1997. **57**(12):  
13 p. 2388-93.
- 14 379. Vinci, M., et al., *Advances in establishment and analysis of three-dimensional tumor spheroid-*  
15 *based functional assays for target validation and drug evaluation*. BMC Biol, 2012. **10**: p. 29.
- 16 380. Al Habyan, S., et al., *Multicellular detachment generates metastatic spheroids during intra-*  
17 *abdominal dissemination in epithelial ovarian cancer*. Oncogene, 2018. **37**(37): p. 5127-5135.
- 18 381. Desoize, B. and J. Jardillier, *Multicellular resistance: a paradigm for clinical resistance?* Crit Rev  
19 Oncol Hematol, 2000. **36**(2-3): p. 193-207.
- 20 382. Pease, J.C., M. Brewer, and J.S. Tirnauer, *Spontaneous spheroid budding from monolayers: a*  
21 *potential contribution to ovarian cancer dissemination*. Biol Open, 2012. **1**(7): p. 622-8.
- 22 383. Acland, M., et al., *Mass Spectrometry Analyses of Multicellular Tumor Spheroids*. Proteomics Clin  
23 Appl, 2018. **12**(3): p. e1700124.
- 24 384. Griffith, L.G. and M.A. Swartz, *Capturing complex 3D tissue physiology in vitro*. Nat Rev Mol Cell  
25 Biol, 2006. **7**(3): p. 211-24.
- 26 385. Pampaloni, F., E.G. Reynaud, and E.H. Stelzer, *The third dimension bridges the gap between cell*  
27 *culture and live tissue*. Nat Rev Mol Cell Biol, 2007. **8**(10): p. 839-45.
- 28 386. Sutherland, R.M., *Cell and environment interactions in tumor microregions: the multicell*  
29 *spheroid model*. Science, 1988. **240**(4849): p. 177-84.
- 30 387. Yamada, K.M. and E. Cukierman, *Modeling tissue morphogenesis and cancer in 3D*. Cell, 2007.  
31 **130**(4): p. 601-10.
- 32 388. Kim, J.B., *Three-dimensional tissue culture models in cancer biology*. Semin Cancer Biol, 2005.  
33 **15**(5): p. 365-77.
- 34 389. Bergers, G. and L.E. Benjamin, *Tumorigenesis and the angiogenic switch*. Nat Rev Cancer, 2003.  
35 **3**(6): p. 401-10.
- 36 390. Park, J.I., et al., *Scaffold-Free Coculture Spheroids of Human Colonic Adenocarcinoma Cells and*  
37 *Normal Colonic Fibroblasts Promote Tumorigenicity in Nude Mice*. Transl Oncol, 2016. **9**(1): p.  
38 79-88.
- 39 391. Mueller-Klieser, W., *Tumor biology and experimental therapeutics*. Crit Rev Oncol Hematol,  
40 2000. **36**(2-3): p. 123-39.
- 41 392. Mueller-Klieser, W., *Three-dimensional cell cultures: from molecular mechanisms to clinical*  
42 *applications*. Am J Physiol, 1997. **273**(4 Pt 1): p. C1109-23.
- 43 393. Halfter, K., et al., *Testing chemotherapy efficacy in HER2 negative breast cancer using patient-*  
44 *derived spheroids*. J Transl Med, 2016. **14**(1): p. 112.
- 45 394. Horan Hand, P., et al., *Influence of spatial configuration of carcinoma cell populations on the*  
46 *expression of a tumor-associated glycoprotein*. Cancer Res, 1985. **45**(2): p. 833-40.
- 47 395. Windus, L.C., et al., *In vivo biomarker expression patterns are preserved in 3D cultures of*  
48 *Prostate Cancer*. Exp Cell Res, 2012. **318**(19): p. 2507-19.

- 1 396. Schmidt, M., et al., *Spheroid-based 3-dimensional culture models: Gene expression and*  
2 *functionality in head and neck cancer*. *Oncol Rep*, 2016. **35**(4): p. 2431-40.
- 3 397. Davidowitz, R.A., et al., *Mesenchymal gene program-expressing ovarian cancer spheroids exhibit*  
4 *enhanced mesothelial clearance*. *J Clin Invest*, 2014. **124**(6): p. 2611-25.
- 5 398. Chang, T.T. and M. Hughes-Fulford, *Monolayer and spheroid culture of human liver*  
6 *hepatocellular carcinoma cell line cells demonstrate distinct global gene expression patterns and*  
7 *functional phenotypes*. *Tissue Eng Part A*, 2009. **15**(3): p. 559-67.
- 8 399. Masood, N., F.A. Malik, and M.A. Kayani, *Expression of xenobiotic metabolizing genes in head*  
9 *and neck cancer tissues*. *Asian Pac J Cancer Prev*, 2011. **12**(2): p. 377-82.
- 10 400. Cui, X., Y. Hartanto, and H. Zhang, *Advances in multicellular spheroids formation*. *Journal of The*  
11 *Royal Society Interface*, 2017. **14**(127).
- 12 401. Aslam, B., et al., *Proteomics: Technologies and Their Applications*. *J Chromatogr Sci*, 2017. **55**(2):  
13 p. 182-196.
- 14 402. Mermelekas, G. and J. Zoidakis, *Mass spectrometry-based membrane proteomics in cancer*  
15 *biomarker discovery*. *Expert Rev Mol Diagn*, 2014. **14**(5): p. 549-63.
- 16 403. Matta, A., et al., *Mass spectrometry-based clinical proteomics: head-and-neck cancer biomarkers*  
17 *and drug-targets discovery*. *Mass Spectrom Rev*, 2010. **29**(6): p. 945-61.
- 18 404. Indovina, P., et al., *Mass spectrometry-based proteomics: the road to lung cancer biomarker*  
19 *discovery*. *Mass Spectrom Rev*, 2013. **32**(2): p. 129-42.
- 20 405. Alvarez-Chaver, P., et al., *Proteomics for discovery of candidate colorectal cancer biomarkers*.  
21 *World J Gastroenterol*, 2014. **20**(14): p. 3804-24.
- 22 406. Yeh, C.C., et al., *Integrated Stable Isotope Labeling by Amino Acids in Cell Culture (SILAC) and*  
23 *Isobaric Tags for Relative and Absolute Quantitation (iTRAQ) Quantitative Proteomic Analysis*  
24 *Identifies Galectin-1 as a Potential Biomarker for Predicting Sorafenib Resistance in Liver Cancer*.  
25 *Mol Cell Proteomics*, 2015. **14**(6): p. 1527-45.
- 26 407. He, J., et al., *Tumor proteomic profiling predicts the susceptibility of breast cancer to*  
27 *chemotherapy*. *Int J Oncol*, 2009. **35**(4): p. 683-92.
- 28 408. Han, M., et al., *Support vector machines coupled with proteomics approaches for detecting*  
29 *biomarkers predicting chemotherapy resistance in small cell lung cancer*. *Oncol Rep*, 2012. **28**(6):  
30 p. 2233-8.
- 31 409. Akashi, T., et al., *Proteomics-based identification of biomarkers for predicting sensitivity to a PI3-*  
32 *kinase inhibitor in cancer*. *Biochem Biophys Res Commun*, 2007. **352**(2): p. 514-21.
- 33 410. Aichler, M., et al., *Proteomic and metabolic prediction of response to therapy in gastric cancer*.  
34 *World J Gastroenterol*, 2014. **20**(38): p. 13648-57.
- 35 411. Jimenez, C.R. and H.M. Verheul, *Mass spectrometry-based proteomics: from cancer biology to*  
36 *protein biomarkers, drug targets, and clinical applications*. *Am Soc Clin Oncol Educ Book*, 2014:  
37 p. e504-10.
- 38 412. Silva, A.M.N., et al., *Post-translational modifications and mass spectrometry detection*. *Free*  
39 *Radic Biol Med*, 2013. **65**: p. 925-941.
- 40 413. Li, X., W. Wang, and J. Chen, *Recent progress in mass spectrometry proteomics for biomedical*  
41 *research*. *Sci China Life Sci*, 2017. **60**(10): p. 1093-1113.
- 42 414. Liu, Y., A. Beyer, and R. Aebersold, *On the Dependency of Cellular Protein Levels on mRNA*  
43 *Abundance*. *Cell*, 2016. **165**(3): p. 535-50.
- 44 415. Nagaraj, N., et al., *Deep proteome and transcriptome mapping of a human cancer cell line*. *Mol*  
45 *Syst Biol*, 2011. **7**: p. 548.
- 46 416. Aebersold, R. and M. Mann, *Mass-spectrometric exploration of proteome structure and function*.  
47 *Nature*, 2016. **537**(7620): p. 347-55.



- 1 417. Zhu, Y., et al., *Nanodroplet processing platform for deep and quantitative proteome profiling of*  
2 *10-100 mammalian cells*. Nat Commun, 2018. **9**(1): p. 882.
- 3 418. Doll, S., F. Gnad, and M. Mann, *The Case for Proteomics and Phospho-Proteomics in Personalized*  
4 *Cancer Medicine*. Proteomics Clin Appl, 2019. **13**(2): p. e1800113.
- 5 419. Dettmer, K., P.A. Aronov, and B.D. Hammock, *Mass spectrometry-based metabolomics*. Mass  
6 Spectrom Rev, 2007. **26**(1): p. 51-78.
- 7 420. Wishart, D.S., et al., *HMDB 4.0: the human metabolome database for 2018*. Nucleic Acids Res,  
8 2018. **46**(D1): p. D608-d617.
- 9 421. Kuehnbaum, N.L. and P. Britz-McKibbin, *New advances in separation science for metabolomics:*  
10 *resolving chemical diversity in a post-genomic era*. Chem Rev, 2013. **113**(4): p. 2437-68.
- 11 422. Aretz, I. and D. Meierhofer, *Advantages and Pitfalls of Mass Spectrometry Based Metabolome*  
12 *Profiling in Systems Biology*. Int J Mol Sci, 2016. **17**(5).
- 13 423. Wiśniewski, J.R. and M.J.A.c. Mann, *Consecutive proteolytic digestion in an enzyme reactor*  
14 *increases depth of proteomic and phosphoproteomic analysis*. 2012. **84**(6): p. 2631-2637.
- 15 424. Savaryn, J.P., T.K. Toby, and N.L. Kelleher, *A researcher's guide to mass spectrometry-based*  
16 *proteomics*. Proteomics, 2016. **16**(18): p. 2435-43.
- 17 425. Pitt, J.J., *Principles and applications of liquid chromatography-mass spectrometry in clinical*  
18 *biochemistry*. Clin Biochem Rev, 2009. **30**(1): p. 19-34.
- 19 426. Hanai, T. and T.T. Hanai, *HPLC: a practical guide*. Vol. 6. 1999: Royal Society of Chemistry.
- 20 427. Yates III, J.R.J.n.m., *A century of mass spectrometry: from atoms to proteomes*. 2011. **8**(8): p.  
21 633-637.
- 22 428. Kanehisa, M., et al., *KEGG for integration and interpretation of large-scale molecular data sets*.  
23 2012. **40**(D1): p. D109-D114.
- 24 429. Pang, Z., et al., *MetaboAnalyst 5.0: narrowing the gap between raw spectra and functional*  
25 *insights*. Nucleic Acids Res, 2021. **49**(W1): p. W388-w396.
- 26 430. Li, H. and A.B. Hummon, *Imaging mass spectrometry of three-dimensional cell culture systems*.  
27 Anal Chem, 2011. **83**(22): p. 8794-801.
- 28 431. Balluff, B. and L.A. McDonnell, *Mass Spectrometry Imaging of Metabolites*. Methods Mol Biol,  
29 2018. **1730**: p. 345-357.
- 30 432. Gustafsson, J.O., et al., *MALDI Imaging Mass Spectrometry (MALDI-IMS)-application of spatial*  
31 *proteomics for ovarian cancer classification and diagnosis*. Int J Mol Sci, 2011. **12**(1): p. 773-94.
- 32 433. Liu, X., E.M. Weaver, and A.B. Hummon, *Evaluation of therapeutics in three-dimensional cell*  
33 *culture systems by MALDI imaging mass spectrometry*. Anal Chem, 2013. **85**(13): p. 6295-302.
- 34 434. Tan, M., et al., *Overexpression of adenylate cyclase-associated protein 1 is associated with*  
35 *metastasis of lung cancer*. Oncol Rep, 2013. **30**(4): p. 1639-44.
- 36 435. Zhang, H. and G.L. Zhou, *CAP1 (Cyclase-Associated Protein 1) Exerts Distinct Functions in the*  
37 *Proliferation and Metastatic Potential of Breast Cancer Cells Mediated by ERK*. Sci Rep, 2016. **6**:  
38 p. 25933.
- 39 436. Chen, Q., et al., *Poly r(C) binding protein-1 is central to maintenance of cancer stem cells in*  
40 *prostate cancer cells*. Cell Physiol Biochem, 2015. **35**(3): p. 1052-61.
- 41 437. Kim, H.-J., et al., *LAP2 Is Widely Overexpressed in Diverse Digestive Tract Cancers and Regulates*  
42 *Motility of Cancer Cells*. PLoS ONE, 2012. **7**(6): p. e39482.
- 43 438. Chen, N., et al., *Quantitative proteome analysis of HCC cell lines with different metastatic*  
44 *potentials by SILAC*. Proteomics, 2008. **8**(23-24): p. 5108-18.
- 45 439. Ricciardelli, C., et al., *Transketolase is upregulated in metastatic peritoneal implants and*  
46 *promotes ovarian cancer cell proliferation*. Clin Exp Metastasis, 2015. **32**(5): p. 441-55.

- 1 440. Liu, S., et al., *Annexin A11 knockdown inhibits in vitro proliferation and enhances survival of Hca-F cell via Akt2/FoxO1 pathway and MMP-9 expression*. Biomed Pharmacother, 2015. **70**: p. 58-63.
- 2  
3
- 4 441. Liu, S., et al., *ANXA11 regulates the tumorigenesis, lymph node metastasis and 5-fluorouracil sensitivity of murine hepatocarcinoma Hca-P cells by targeting c-Jun*. Oncotarget, 2016. **7**(13): p. 16297-310.
- 5  
6
- 7 442. Li, M.H., et al., *Expression of cytoskeleton-associated protein 4 is related to lymphatic metastasis and indicates prognosis of intrahepatic cholangiocarcinoma patients after surgery resection*. Cancer Lett, 2013. **337**(2): p. 248-53.
- 8  
9
- 10 443. Volakis, L.I., et al., *Loss of myoferlin redirects breast cancer cell motility towards collective migration*. PLoS One, 2014. **9**(2): p. e86110.
- 11
- 12 444. Liu, G., et al., *Glutamate dehydrogenase is a novel prognostic marker and predicts metastases in colorectal cancer patients*. J Transl Med, 2015. **13**: p. 144.
- 13
- 14 445. Yoshida, Y., et al., *Clinical usefulness of mitochondrial transcription factor A expression as a predictive marker in colorectal cancer patients treated with FOLFOX*. Cancer Sci, 2011. **102**(3): p. 578-82.
- 15  
16
- 17 446. Ogawa, K., et al., *Clinical significance of elongation factor-1 delta mRNA expression in oesophageal carcinoma*. Br J Cancer, 2004. **91**(2): p. 282-6.
- 18
- 19 447. Kawahara, R., et al., *Agrin and perlecan mediate tumorigenic processes in oral squamous cell carcinoma*. PLoS One, 2014. **9**(12): p. e115004.
- 20
- 21 448. Lallemand, D. and M. Arpin, *Moesin/ezrin: a specific role in cell metastasis?* Pigment Cell Melanoma Res, 2010. **23**(1): p. 6-7.
- 22
- 23 449. Zhang, X., et al., *Kinectin-mediated endoplasmic reticulum dynamics supports focal adhesion growth in the cellular lamella*. Journal of Cell Science, 2010. **123**(22): p. 3901-3912.
- 24
- 25 450. Zhang, M., et al., *Human biliverdin reductase promotes EMT through the ERK1/2 signal pathway in breast cancer*. Eur J Pharmacol, 2016. **788**: p. 45-53.
- 26
- 27 451. Wang, P., et al., *Chloride intracellular channel 1 regulates colon cancer cell migration and invasion through ROS/ERK pathway*. World Journal of Gastroenterology : WJG, 2014. **20**(8): p. 2071-2078.
- 28  
29
- 30 452. Wang, L., et al., *Elevated expression of chloride intracellular channel 1 is correlated with poor prognosis in human gliomas*. J Exp Clin Cancer Res, 2012. **31**: p. 44.
- 31
- 32 453. Mori, M., et al., *Zyxin Mediates Actin Fiber Reorganization in Epithelial–Mesenchymal Transition and Contributes to Endocardial Morphogenesis*. Molecular Biology of the Cell, 2009. **20**(13): p. 3115-3124.
- 33  
34
- 35 454. Todd, M.C., et al., *Overexpression and delocalization of claudin-3 protein in MCF-7 and MDA-MB-415 breast cancer cell lines*. Oncology Letters, 2015. **10**(1): p. 156-162.
- 36
- 37 455. Cui, X., et al., *High expression of osteoglycin decreases the metastatic capability of mouse hepatocarcinoma Hca-F cells to lymph nodes*. Acta Biochim Biophys Sin (Shanghai), 2008. **40**(4): p. 349-55.
- 38  
39
- 40 456. Cui, X.-N., et al., *High expression of osteoglycin decreases gelatinase activity of murine hepatocarcinoma Hca-F cells*. World Journal of Gastroenterology : WJG, 2009. **15**(48): p. 6117-6122.
- 41  
42
- 43 457. Chen, W., et al., *Overexpression of annexin A4 indicates poor prognosis and promotes tumor metastasis of hepatocellular carcinoma*. Tumour Biol, 2016.
- 44
- 45 458. Liu, Z.H., et al., *Far upstream element-binding protein 1 is a prognostic biomarker and promotes nasopharyngeal carcinoma progression*. Cell Death Dis, 2015. **6**: p. e1920.
- 46
- 47 459. Zhang, J. and Q.M. Chen, *Far upstream element binding protein 1: a commander of transcription, translation and beyond*. Oncogene, 2013. **32**(24): p. 2907-16.
- 48

- 1 460. Nobumoto, A., et al., *Galectin-9 suppresses tumor metastasis by blocking adhesion to*  
2 *endothelium and extracellular matrices*. *Glycobiology*, 2008. **18**(9): p. 735-44.
- 3 461. Fujihara, S., et al., *Galectin-9 in cancer therapy*. *Recent Pat Endocr Metab Immune Drug Discov*,  
4 2013. **7**(2): p. 130-7.
- 5 462. Yamashita, T., et al., *Rho GDP-dissociation inhibitor alpha is associated with cancer metastasis in*  
6 *colon and prostate cancer*. *Pharmazie*, 2012. **67**(3): p. 253-5.
- 7 463. Liu, Z., et al., *PDZ and LIM domain protein 1(PDLIM1)/CLP36 promotes breast cancer cell*  
8 *migration, invasion and metastasis through interaction with alpha-actinin*. *Oncogene*, 2015.  
9 **34**(10): p. 1300-11.
- 10 464. Su, D., et al., *ADP-ribosylation factor-like 4C (ARL4C), a novel ovarian cancer metastasis*  
11 *suppressor, identified by integrated genomics*. *Am J Transl Res*, 2015. **7**(2): p. 242-56.
- 12 465. Zhang, C., et al., *Glucose-6-phosphate dehydrogenase: a biomarker and potential therapeutic*  
13 *target for cancer*. *Anticancer Agents Med Chem*, 2014. **14**(2): p. 280-9.
- 14 466. Rodriguez-Torres, M. and A.L. Allan, *Aldehyde dehydrogenase as a marker and functional*  
15 *mediator of metastasis in solid tumors*. *Clinical & Experimental Metastasis*, 2016. **33**: p. 97-113.
- 16 467. Tan, G.-J., et al., *Cathepsins mediate tumor metastasis*. *World Journal of Biological Chemistry*,  
17 2013. **4**(4): p. 91-101.
- 18 468. Shiozawa, T., et al., *Dimethylarginine dimethylaminohydrolase 2 promotes tumor angiogenesis in*  
19 *lung adenocarcinoma*. *Virchows Archiv*, 2016. **468**: p. 179-190.
- 20 469. Schapira, D.V. and M. Schapira, *Use of ceruloplasmin levels to monitor response to therapy and*  
21 *predict recurrence of breast cancer*. *Breast Cancer Res Treat*, 1983. **3**(2): p. 221-4.
- 22 470. Jiang, Y.Y., et al., *Microtubule-associated protein 4 is an important regulator of cell*  
23 *invasion/migration and a potential therapeutic target in esophageal squamous cell carcinoma*.  
24 *Oncogene*, 2016.
- 25 471. Yoshida, R., et al., *The loss of E-cadherin, alpha- and beta-catenin expression is associated with*  
26 *metastasis and poor prognosis in invasive breast cancer*. *Int J Oncol*, 2001. **18**(3): p. 513-20.
- 27 472. Beavon, I.R., *The E-cadherin-catenin complex in tumour metastasis: structure, function and*  
28 *regulation*. *Eur J Cancer*, 2000. **36**(13 Spec No): p. 1607-20.
- 29 473. Li, Y., et al., *Knockdown of Tubulin Polymerization Promoting Protein Family Member 3*  
30 *Suppresses Proliferation and Induces Apoptosis in Non-Small-Cell Lung Cancer*. *Journal of Cancer*,  
31 2016. **7**(10): p. 1189-1196.
- 32 474. Zhou, W., et al., *Stable knockdown of TPPP3 by RNA interference in Lewis lung carcinoma cell*  
33 *inhibits tumor growth and metastasis*. *Mol Cell Biochem*, 2010. **343**(1-2): p. 231-8.
- 34 475. Ahmed, I.S., et al., *Pgrmc1 (progesterone receptor membrane component 1) associates with*  
35 *epidermal growth factor receptor and regulates erlotinib sensitivity*. *J Biol Chem*, 2010. **285**(32):  
36 p. 24775-82.
- 37 476. Friel, A.M., et al., *Progesterone receptor membrane component 1 deficiency attenuates growth*  
38 *while promoting chemosensitivity of human endometrial xenograft tumors*. *Cancer letters*, 2015.  
39 **356**(2 0 0): p. 434-442.
- 40 477. Chen, C.H., et al., *A peptide that inhibits function of Myristoylated Alanine-Rich C Kinase*  
41 *Substrate (MARCKS) reduces lung cancer metastasis*. *Oncogene*, 2014. **33**(28): p. 3696-706.
- 42 478. Chen, C.H., et al., *Targeting myristoylated alanine-rich C kinase substrate phosphorylation site*  
43 *domain in lung cancer. Mechanisms and therapeutic implications*. *Am J Respir Crit Care Med*,  
44 2014. **190**(10): p. 1127-38.
- 45 479. Techasen, A., et al., *Myristoylated alanine-rich C kinase substrate phosphorylation promotes*  
46 *cholangiocarcinoma cell migration and metastasis via the protein kinase C-dependent pathway*.  
47 *Cancer Sci*, 2010. **101**(3): p. 658-65.

- 1 480. Clark, J.W., et al., *The potential role for prolactin-inducible protein (PIP) as a marker of human*  
2 *breast cancer micrometastasis*. British Journal of Cancer, 1999. **81**(6): p. 1002-1008.
- 3 481. Hassan, M.I., et al., *Prolactin inducible protein in cancer, fertility and immunoregulation:*  
4 *structure, function and its clinical implications*. Cell Mol Life Sci, 2009. **66**(3): p. 447-59.
- 5 482. Guetschow, E.D., et al., *Detection of prolactin inducible protein mRNA, a biomarker for breast*  
6 *cancer metastasis, using a molecular beacon-based assay*. Anal Bioanal Chem, 2012. **404**(2): p.  
7 399-406.
- 8 483. Hempel, N., P.M. Carrico, and J.A. Melendez, *Manganese superoxide dismutase (Sod2) and*  
9 *redox-control of signaling events that drive metastasis*. Anti-cancer agents in medicinal  
10 chemistry, 2011. **11**(2): p. 191-201.
- 11 484. Van Impe, K., et al., *A nanobody targeting the F-actin capping protein CapG restrains breast*  
12 *cancer metastasis*. Breast Cancer Res, 2013. **15**(6): p. R116.
- 13 485. Charafe-Jauffret, E., et al., *Aldehyde dehydrogenase 1-positive cancer stem cells mediate*  
14 *metastasis and poor clinical outcome in inflammatory breast cancer*. Clin Cancer Res, 2010.  
15 **16**(1): p. 45-55.
- 16 486. Dong, Y., et al., *The expression of aldehyde dehydrogenase 1 in invasive primary breast tumors*  
17 *and axillary lymph node metastases is associated with poor clinical prognosis*. Pathol Res Pract,  
18 2013. **209**(9): p. 555-61.
- 19 487. Wu, Z., et al., *An immunohistochemical study of thioredoxin domain-containing 5 expression in*  
20 *gastric adenocarcinoma*. Oncology Letters, 2015. **9**(3): p. 1154-1158.
- 21 488. Shao, C., et al., *Suprabasin is hypomethylated and associated with metastasis in salivary adenoid*  
22 *cystic carcinoma*. PLoS One, 2012. **7**(11): p. e48582.
- 23 489. Zhu, J., et al., *Overexpression of Suprabasin is Associated with Proliferation and Tumorigenicity*  
24 *of Esophageal Squamous Cell Carcinoma*. Scientific Reports, 2016. **6**: p. 21549.
- 25 490. Liu, L., et al., *Carnitine palmitoyltransferase 1A (CPT1A): a transcriptional target of PAX3-FKHR*  
26 *and mediates PAX3-FKHR-dependent motility in alveolar rhabdomyosarcoma cells*. BMC Cancer,  
27 2012. **12**: p. 154.
- 28 491. Lowy, C.M. and T. Oskarsson, *Tenascin C in metastasis: A view from the invasive front*. Cell Adh  
29 Migr, 2015. **9**(1-2): p. 112-24.
- 30 492. Najm, P. and M. El-Sibai, *Palladin regulation of the actin structures needed for cancer invasion*.  
31 Cell Adhesion & Migration, 2014. **8**(1): p. 29-35.
- 32 493. Goicoechea, S.M., et al., *Palladin promotes invasion of pancreatic cancer cells by enhancing*  
33 *invadopodia formation in cancer-associated fibroblasts*. Oncogene, 2014. **33**(10): p. 1265-73.
- 34 494. Goicoechea, S.M., et al., *Palladin contributes to invasive motility in human breast cancer cells*.  
35 Oncogene, 2009. **28**(4): p. 587-98.
- 36 495. Kleeff, J., et al., *Altered expression and localization of the tight junction protein ZO-1 in primary*  
37 *and metastatic pancreatic cancer*. Pancreas, 2001. **23**(3): p. 259-65.
- 38 496. Orban, E., et al., *Different expression of occludin and ZO-1 in primary and metastatic liver*  
39 *tumors*. Pathol Oncol Res, 2008. **14**(3): p. 299-306.
- 40 497. Minchinton, A.I. and I.F. Tannock, *Drug penetration in solid tumours*. Nat Rev Cancer, 2006. **6**(8):  
41 p. 583-92.
- 42 498. Jacobi, N., et al., *Organotypic three-dimensional cancer cell cultures mirror drug responses in*  
43 *vivo: lessons learned from the inhibition of EGFR signaling*. Oncotarget, 2017. **8**(64): p. 107423-  
44 107440.
- 45 499. Santini, M.T., G. Rainaldi, and P.L. Indovina, *Apoptosis, cell adhesion and the extracellular matrix*  
46 *in the three-dimensional growth of multicellular tumor spheroids*. Crit Rev Oncol Hematol, 2000.  
47 **36**(2-3): p. 75-87.

- 1 500. Rolver, M.G., L.O. Elingaard-Larsen, and S.F. Pedersen, *Assessing Cell Viability and Death in 3D Spheroid Cultures of Cancer Cells*. J Vis Exp, 2019(148).
- 2
- 3 501. Wong, C., et al., *Human neuroendocrine tumor cell lines as a three-dimensional model for the*
- 4 *study of human neuroendocrine tumor therapy*. J Vis Exp, 2012(66): p. e4218.
- 5 502. Pickl, M. and C.H. Ries, *Comparison of 3D and 2D tumor models reveals enhanced HER2*
- 6 *activation in 3D associated with an increased response to trastuzumab*. Oncogene, 2009. **28**(3):
- 7 p. 461-8.
- 8 503. Guan, L.Y. and Y. Lu, *New developments in molecular targeted therapy of ovarian cancer*. Discov
- 9 Med, 2018. **26**(144): p. 219-229.
- 10 504. Kutova, O.M., et al., *Targeted Delivery to Tumors: Multidirectional Strategies to Improve*
- 11 *Treatment Efficiency*. Cancers (Basel), 2019. **11**(1).
- 12 505. Sokolova, E., et al., *Penetration Efficiency of Antitumor Agents in Ovarian Cancer Spheroids: The*
- 13 *Case of Recombinant Targeted Toxin DARPIn-LoPE and the Chemotherapy Drug, Doxorubicin*.
- 14 Pharmaceuticals, 2019. **11**(5).
- 15 506. Proshkina, G.M., et al., *[Bifunctional Toxin DARP-LoPE Based on the HER2-Specific Innovative*
- 16 *Module of a Non-Immunoglobulin Scaffold as a Promising Agent for Theranostics]*. Mol Biol
- 17 (Mosk), 2017. **51**(6): p. 997-1007.
- 18 507. Bantie, L., et al., *A first-in-class CDK4 inhibitor demonstrates in vitro, ex-vivo and in vivo efficacy*
- 19 *against ovarian cancer*. Gynecol Oncol, 2020. **159**(3): p. 827-838.
- 20 508. Goel, S., et al., *CDK4/6 Inhibition in Cancer: Beyond Cell Cycle Arrest*. Trends Cell Biol, 2018.
- 21 **28**(11): p. 911-925.
- 22 509. O'Leary, B., R.S. Finn, and N.C. Turner, *Treating cancer with selective CDK4/6 inhibitors*. Nat Rev
- 23 Clin Oncol, 2016. **13**(7): p. 417-30.
- 24 510. Fischer, A.H., et al., *Hematoxylin and Eosin Staining of Tissue and Cell Sections*. Cold Spring
- 25 Harbor Protocols, 2008. **2008**(5): p. pdb.prot4986.
- 26 511. Tian, X., et al., *Anticancer Drug Affects Metabolomic Profiles in Multicellular Spheroids: Studies*
- 27 *Using Mass Spectrometry Imaging Combined with Machine Learning*. Anal Chem, 2019. **91**(9): p.
- 28 5802-5809.
- 29 512. Annesley, T.M.J.C.c., *Ion suppression in mass spectrometry*. 2003. **49**(7): p. 1041-1044.
- 30 513. Zhang, H., et al., *Integrated Proteogenomic Characterization of Human High-Grade Serous*
- 31 *Ovarian Cancer*. Cell, 2016. **166**(3): p. 755-765.
- 32 514. Pirman, D.A., et al., *Identifying tissue-specific signal variation in MALDI mass spectrometric*
- 33 *imaging by use of an internal standard*. 2013. **85**(2): p. 1090-1096.
- 34 515. Taylor, A.J., A. Dexter, and J.J.A.c. Bunch, *Exploring ion suppression in mass spectrometry*
- 35 *imaging of a heterogeneous tissue*. 2018. **90**(9): p. 5637-5645.
- 36 516. Schulz, S., et al., *Advanced MALDI mass spectrometry imaging in pharmaceutical research and*
- 37 *drug development*. Curr Opin Biotechnol, 2019. **55**: p. 51-59.
- 38 517. Hood, L.E., et al., *New and improved proteomics technologies for understanding complex*
- 39 *biological systems: addressing a grand challenge in the life sciences*. Proteomics, 2012. **12**(18): p.
- 40 2773-83.
- 41 518. da Silva, R.R., P.C. Dorrestein, and R.A. Quinn, *Illuminating the dark matter in metabolomics*.
- 42 Proc Natl Acad Sci U S A, 2015. **112**(41): p. 12549-50.
- 43 519. Xiao, J.F., B. Zhou, and H.W. Ransom, *Metabolite identification and quantitation in LC-MS/MS-*
- 44 *based metabolomics*. Trends Analyt Chem, 2012. **32**: p. 1-14.
- 45 520. Monti, C., et al., *Proteomics turns functional*. J Proteomics, 2019. **198**: p. 36-44.
- 46 521. George, S.H. and P. Shaw, *BRCA and Early Events in the Development of Serous Ovarian Cancer*.
- 47 Front Oncol, 2014. **4**: p. 5.

1 522. Crum, C.P., et al., *Lessons from BRCA: the tubal fimbria emerges as an origin for pelvic serous*  
2 *cancer*. Clin Med Res, 2007. **5**(1): p. 35-44.

3 523. Crum, C.P., et al., *Through the glass darkly: intraepithelial neoplasia, top-down differentiation,*  
4 *and the road to ovarian cancer*. J Pathol, 2013. **231**(4): p. 402-12.

5 524. Eckert, M.A., et al., *Proteomics reveals NNMT as a master metabolic regulator of cancer-*  
6 *associated fibroblasts*. Nature, 2019. **569**(7758): p. 723-728.

7 525. Eckert, M.A., et al., *Genomics of ovarian cancer progression reveals diverse metastatic*  
8 *trajectories including intraepithelial metastasis to the fallopian tube*. 2016. **6**(12): p. 1342-1351.

9 526. Visvanathan, K., et al., *Fallopian tube lesions in women at high risk for ovarian cancer: a*  
10 *multicenter study*. 2018. **11**(11): p. 697-706.

11 527. Wu, R.C., et al., *Genomic landscape and evolutionary trajectories of ovarian cancer precursor*  
12 *lesions*. 2019. **248**(1): p. 41-50.

13 528. Visvanathan, K., et al., *Diagnosis of serous tubal intraepithelial carcinoma based on morphologic*  
14 *and immunohistochemical features: a reproducibility study*. 2011. **35**(12): p. 1766.

15 529. Mittal, P., et al., *Proteomics of endometrial cancer diagnosis, treatment, and prognosis*.  
16 Proteomics Clin Appl, 2016. **10**(3): p. 217-29.

17 530. Asaka, S., et al., *Analysis of telomere lengths in p53 signatures and incidental serous tubal*  
18 *intraepithelial carcinomas without concurrent ovarian cancer*. 2019. **43**(8): p. 1083.

19 531. Pisanic, T.R., et al., *The methylomic landscape of fallopian tube lesions associated with ovarian*  
20 *high-grade serous carcinoma*. 2020.

21 532. Wang, F., et al., *Discovering drugs to overcome chemoresistance in ovarian cancers based on the*  
22 *cancer genome atlas tumor transcriptome profile*. Oncotarget, 2017. **8**(70): p. 115102-115113.

23 533. Geeleher, P., N.J. Cox, and R.S. Huang, *Clinical drug response can be predicted using baseline*  
24 *gene expression levels and in vitro drug sensitivity in cell lines*. Genome Biol, 2014. **15**(3): p. R47.

25 534. Geeleher, P., N. Cox, and R.S. Huang, *pRRophetic: an R package for prediction of clinical*  
26 *chemotherapeutic response from tumor gene expression levels*. PLoS One, 2014. **9**(9): p.  
27 e107468.

28 535. Yang, L., et al., *Exploring cisplatin resistance in ovarian cancer through integrated bioinformatics*  
29 *approach and overcoming chemoresistance with sanguinarine*. Am J Transl Res, 2020. **12**(3): p.  
30 923-939.

31 536. Yarden, Y. and M.X. Sliwkowski, *Untangling the ErbB signalling network*. Nat Rev Mol Cell Biol,  
32 2001. **2**(2): p. 127-37.

33 537. Oxnard, G.R., et al., *Association Between Plasma Genotyping and Outcomes of Treatment With*  
34 *Osimertinib (AZD9291) in Advanced Non-Small-Cell Lung Cancer*. J Clin Oncol, 2016. **34**(28): p.  
35 3375-82.

36 538. Piotrowska, Z., et al., *Heterogeneity Underlies the Emergence of EGFR T790M Wild-Type Clones*  
37 *Following Treatment of T790M-Positive Cancers with a Third-Generation EGFR Inhibitor*. Cancer  
38 Discov, 2015. **5**(7): p. 713-22.

39 539. Suda, K., et al., *Heterogeneity in resistance mechanisms causes shorter duration of epidermal*  
40 *growth factor receptor kinase inhibitor treatment in lung cancer*. Lung Cancer, 2016. **91**: p. 36-  
41 40.

42 540. Liu, H.D., et al., *Organoid of ovarian cancer: genomic analysis and drug screening*. Clin Transl  
43 Oncol, 2020. **22**(8): p. 1240-1251.

44 541. Gunti, S., et al., *Organoid and Spheroid Tumor Models: Techniques and Applications*. Cancers  
45 (Basel), 2021. **13**(4).

46 542. Stewart, J.M., et al., *Phenotypic heterogeneity and instability of human ovarian tumor-initiating*  
47 *cells*. Proc Natl Acad Sci U S A, 2011. **108**(16): p. 6468-73.

- 1 543. Kryczek, I., et al., *Expression of aldehyde dehydrogenase and CD133 defines ovarian cancer stem*  
2 *cells*. Int J Cancer, 2012. **130**(1): p. 29-39.
- 3 544. Bapat, S.A., et al., *Stem and progenitor-like cells contribute to the aggressive behavior of human*  
4 *epithelial ovarian cancer*. Cancer Res, 2005. **65**(8): p. 3025-9.
- 5 545. Mo, L., et al., *Ascites Increases Expression/Function of Multidrug Resistance Proteins in Ovarian*  
6 *Cancer Cells*. PLoS One, 2015. **10**(7): p. e0131579.
- 7 546. Nunes, A.S., et al., *3D tumor spheroids as in vitro models to mimic in vivo human solid tumors*  
8 *resistance to therapeutic drugs*. Biotechnol Bioeng, 2019. **116**(1): p. 206-226.
- 9 547. Tofani, L.B., et al., *Generation of a Three-Dimensional in Vitro Ovarian Cancer Co-Culture Model*  
10 *for Drug Screening Assays*. J Pharm Sci, 2021. **110**(7): p. 2629-2636.
- 11 548. Michálek, J., et al., *Quantitative Assessment of Anti-Cancer Drug Efficacy From Coregistered*  
12 *Mass Spectrometry and Fluorescence Microscopy Images of Multicellular Tumor Spheroids*.  
13 *Microsc Microanal*, 2019. **25**(6): p. 1311-1322.
- 14 549. Machálková, M., et al., *Drug Penetration Analysis in 3D Cell Cultures Using Fiducial-Based*  
15 *Semiautomatic Coregistration of MALDI MSI and Immunofluorescence Images*. Anal Chem, 2019.  
16 **91**(21): p. 13475-13484.
- 17 550. Bianga, J., et al., *Complementarity of MALDI and LA ICP mass spectrometry for platinum*  
18 *anticancer imaging in human tumor*. Metallomics, 2014. **6**(8): p. 1382-6.
- 19 551. Marković, S., et al., *High spatial resolution imaging of cisplatin and Texas Red cisplatin in tumour*  
20 *spheroids using laser ablation isotope dilution inductively coupled plasma mass spectrometry*  
21 *and confocal fluorescence microscopy*. Anal Chim Acta, 2021. **1162**: p. 338424.
- 22 552. Lee, S.L., et al., *Hypoxia-induced pathological angiogenesis mediates tumor cell dissemination,*  
23 *invasion, and metastasis in a zebrafish tumor model*. Proc Natl Acad Sci U S A, 2009. **106**(46): p.  
24 19485-90.
- 25 553. Rohwer, N. and T. Cramer, *Hypoxia-mediated drug resistance: novel insights on the functional*  
26 *interaction of HIFs and cell death pathways*. Drug Resist Updat, 2011. **14**(3): p. 191-201.
- 27 554. Tucker, L.H., et al., *Untargeted Metabolite Mapping in 3D Cell Culture Models Using High*  
28 *Spectral Resolution FT-ICR Mass Spectrometry Imaging*. Anal Chem, 2019. **91**(15): p. 9522-9529.
- 29 555. Jamieson, L.E., D.J. Harrison, and C.J. Campbell, *Chemical analysis of multicellular tumour*  
30 *spheroids*. Analyst, 2015. **140**(12): p. 3910-20.
- 31 556. Nagana Gowda, G., et al., *A metabolomics study of BPTES altered metabolism in human breast*  
32 *cancer cell lines*. 2018. **5**: p. 49.
- 33 557. Shirato, K., et al., *Hypoxic regulation of glycosylation via the N-acetylglucosamine cycle*. J Clin  
34 *Biochem Nutr*, 2011. **48**(1): p. 20-5.
- 35 558. Schuster-Little, N., et al., *Affinity-free enrichment and mass spectrometry analysis of the ovarian*  
36 *cancer biomarker CA125 (MUC16) from patient-derived ascites*. Analyst, 2021. **146**(1): p. 85-94.
- 37 559. Worzfeld, T., et al., *The Unique Molecular and Cellular Microenvironment of Ovarian Cancer*.  
38 *Front Oncol*, 2017. **7**: p. 24.
- 39 560. Worzfeld, T., et al., *Proteotranscriptomics Reveal Signaling Networks in the Ovarian Cancer*  
40 *Microenvironment*. Mol Cell Proteomics, 2018. **17**(2): p. 270-289.
- 41 561. Steitz, A.M., et al., *Tumor-associated macrophages promote ovarian cancer cell migration by*  
42 *secreting transforming growth factor beta induced (TGFBI) and tenascin C*. Cell Death Dis, 2020.  
43 **11**(4): p. 249.
- 44 562. Biskup, K., et al., *The ascites N-glycome of epithelial ovarian cancer patients*. J Proteomics, 2017.  
45 **157**: p. 33-39.
- 46 563. Alberto-Aguilar, D.R., et al., *Ascites from Ovarian Cancer Induces Novel Fucosylated Proteins*.  
47 *Cancer Microenviron*, 2019. **12**(2-3): p. 181-195.

- 1 564. Mittal, P., et al., *Matrix Assisted Laser Desorption/Ionization Mass Spectrometry Imaging (MALDI*
- 2 *MSI) for Monitoring of Drug Response in Primary Cancer Spheroids*. *Proteomics*, 2019. **19**(21-22):
- 3 p. e1900146.
- 4 565. Zhou, G., J. Ewald, and J. Xia, *OmicsAnalyst: a comprehensive web-based platform for visual*
- 5 *analytics of multi-omics data*. *Nucleic Acids Res*, 2021. **49**(W1): p. W476-w482.
- 6